National Library
of Canada

Bibliothèque nationale
du Canada

Canadian Theses Service

Service des thèses canadiennes

Ottawa, Canada
K1A 0N4

NOTICE

The quality of this microform is heavily dependent upon the quality of the original thesis submitted for microfilming. Every effort has been made to ensure the highest quality of reproduction possible.

If pages are missing, contact the university which granted the degree.

Some pages may have indistinct print especially if the original pages were typed with a poor typewriter ribbon or if the university sent us an inferior photocopy.

Previously copyrighted materials (journal articles, published tests, etc.) are not filmed.

Reproduction in full or in part of this microform is governed by the Canadian Copyright Act, R.S.C. 1970, c. C-30.

AVIS

La qualité de cette microforme dépend grandement de la qualité de la thèse soumise au microfilmage. Nous avons tout fait pour assurer une qualité supérieure de reproduction.

S'il manque des pages, veuillez communiquer avec l'université qui a conféré le grade.

La qualité d'impression de certaines pages peut laisser à désirer, surtout si les pages originales ont été dactylographiées à l'aide d'un ruban usé ou si l'université nous a fait parvenir une photocopie de qualité inférieure.

Les documents qui font déjà l'objet d'un droit d'auteur (articles de revue, tests publiés, etc.) ne sont pas microfilmés.

La reproduction, même partielle, de cette microforme est soumise à la Loi canadienne sur le droit d'auteur, SRC 1970, c. C-30.

NL-339 (r. 88/04)

Canada

THE UNIVERSITY OF ALBERTA

CHARACTERIZATION OF INDUCTIVELY COUPLED PLASMA-MASS SPECTROMETRY USING MIXED GAS PLASMAS

by

© JOSEPH W. H. LAM

A THESIS

SUBMITTED TO THE FACULTY OF GRADUATE STUDIES AND RESEARCH
IN PARTIAL FULFILMENT OF THE REQUIREMENTS FOR THE DEGREE
OF DOCTOR OF PHILOSOPHY

DEPARTMENT OF CHEMISTRY

EDMONTON, ALBERTA

FALL 1988

Permission has been granted to the National Library of Canada to microfilm this thesis and to lend or sell copies of the film.

L'autorisation a été accordée à la Bibliothèque nationale du Canada de microfilmer cette thèse et de prêter ou de vendre des exemplaires du film.

The author (copyright owner) has reserved other publication rights, and neither the thesis nor extensive extracts from it may be printed or otherwise reproduced without his/her written permission.

L'auteur (titulaire du droit d'auteur) se réserve les autres droits de publication; ni la thèse ni de longs extraits de celle-ci ne doivent être imprimés ou autrement reproduits sans son autorisation écrite.

ISBN 0-315-45840-2

THE UNIVERSITY OF ALBERTA

RELEASE FORM

NAME OF AUTHOR: JOSEPH W. H. LAM

TITLE OF THESIS: CHARACTERIZATION OF INDUCTIVELY COUPLED PLASMA-MASS SPECTROMETERY USING MIXED GAS PLASMAS.

DEGREE FOR WHICH THESIS WAS PRESENTED: Ph. D.

YEAR THIS DEGREE GRANTED: 1988

Permission is hereby granted to THE UNIVERSITY OF ALBERTA LIBRARY to reproduce single copies of this thesis and to lend or sell such copies for private, scholarly or scientific research purposes only.

The author reserves other publication rights, and neither the thesis nor extensive extracts from it may be printed or otherwise reproduced without the author's written permission.

....
(Student's signature)

Permanent address:
9407-52 Street,
Edmonton, Alberta
Canada. T6B 1G5

Date : 1988

THE UNIVERSITY OF ALBERTA

FACULTY OF GRADUATE STUDIES AND RESEARCH

The undersigned certify that they have read, and recommend to the Faculty of Graduate Studies and Research for acceptance, a thesis entitled CHARACTERIZATION OF INDUCTIVELY COUPLED PLASMA-MASS SPECTROMETRY USING MIXED GAS PLASMAS submitted by Joseph W. H. Lam in partial fulfilment of the requirements for the degree of Doctor of Philosophy.

Gary Horlick
Dr. G. Horlick (supervisor)

Byron Kratochvil
Dr. B. Kratochvil

Dr. N. Dovichi

George Kotovych
Dr. G. Kotovych

Dr. S. Sheinin

R.M. Barnes
Dr. R. Barnes

Date: July, 21, 1988

To my father and mother

ABSTRACT

Inductively coupled plasma-mass spectrometry (ICP-MS) is a relatively new analytical technique for trace and ultra-trace element analysis. The popularity and interest it generates stems from its relative ease of operation, simple sample preparation and a detection limit for most elements of about one to two orders of magnitude better than its counter-part, inductively coupled plasma-atomic emission spectrometry (ICP-AES). Yet, the technique itself has several limitations; interferences caused by spectral overlap from oxide, hydroxide and other poly-atomic ions and the difficulty in running organic matrixes are all part of the problem challenging the analyst.

In this thesis, the capability and performance of mixed gas plasmas in ICP-MS is evaluated. Typical analyte behaviour as a function of nebuliser flow rate, plasma power and sampling depth is compared between normal ICP's and mixed gas plasmas. It is observed that the behaviour and signal responses of analytes in different plasma types are dependent on properties of the analyte species. The excitation mechanisms for ion generation in ICP-MS are postulated.

Further, the role of the aqueous aerosol delivery system (solvent load and aerosol particle size) and its effect on ion signal is also studied. In fact, several signal characteristics, oxide levels and background features all depend to some extent on solvent load. The simultaneous use of mixed gas ICP's and aerosol processing has a synergic effect on reducing oxide levels and some background species.

The running of organic solvent based analytes in ICP-MS is most difficult because a 100% argon plasma is incapable of total decomposition of hydrocarbons. In this study, the capabilities of various low percentage mixed gas plasmas in the handling of organics are evaluated. An air mixed gas plasma has distinct advantages over oxygen mixed gas plasma

because it is able to combust the organic without affecting the signal sensitivity of refractory elements.

Finally, in order to gain some insight to the origin of oxides and background species in ICP-MS, the effects of sampler-skimmer separation along with mixed gas plasmas and aerosol processing techniques, on species level populations are also investigated.

ACKNOWLEDGEMENTS

I would like to extend my sincere thanks and appreciation to Professor Gary Horlick for making this research work possible. Also, I would like to thank my fellow colleages who made carrying out this work a pleasure.

My thanks also go to the technical support staff of the Chemistry Department for their expert advice throughout this thesis work.

I would also like to thank every member of my family for their understanding and tolerance during the course of my studies.

Finally, I also acknowledge the financial support from the Department of Chemistry, University of Alberta.

TABLE OF CONTENTS

CHAPTER PAGE

1. INTRODUCTION

A. Inductively Coupled Plasma-Mass Spectrometry 1
B. Ion Generation in an ICP 2
C. Role of Mixed Gas and Molecular Gas in ICP's 6
D. Formation of Mixed Gas ICP Discharge 9
   a. Mixed Gases in the Nebuliser Gas 10
   b. Mixed Gases in the Plasma Gas 10
E. Role of Mixed Gas in ICP-MS 11
F. Thesis Objectives 11
REFERENCES 14

2. EXPERIMENTAL CONDITIONS AND EQUIPMENT SET-UP

A. ICP-MS Instrumentation 17
B. Mixed Gas Plasmas 20
   a. Gas Mixing 20
   b. Procedure for Lighting a Mixed Gas ICP 21
C. Preparation of Chemical Solutions 21
   a. Aqueous Solutions 21
   b. Non-aqueous Solutions 22
REFERENCES 23

3. ANALYTE SIGNAL CHARACTERISTICS IN ICP-MS:- A COMPARISON OF ARGON AND MIXED GAS PLASMAS

A. Introduction 24
B. Nitrogen Mixed Gas Plasma 28

a. Effects of Nebuliser Flow Rate and RF Power 28
b. Effect of Sampling Depth 36
c. Effect of Percent Nitrogen in the Outer Gas 44
d. Effect of Percent Nitrogen in the Nebulising Gas 53
e. Discussion 59
C. Oxygen and Air Mixed Gas Plasmas 71
a. Effect of Percent Oxygen in the Outer Gas 74
b. Effect of Percent Air in the Outer Gas 79
c. Discussion 79
D. Effect of Mixed Gas Plasmas on Analyte and Analyte Oxide Signals 89
a. Effect of Percent Nitrogen in the Outer Gas on La and LaO 89
b. Effect of Percent Oxygen and Air in the Outer Gas on Analyte and Analyte Oxide Signals 92
c. Effect of Percent Nitrogen in the Nebulising Gas on La and LaO 99
E. Conclusion 102
REFERENCES 104

4. THE EFFECTS OF AEROSOL PROCESSING AND PLASMA GAS COMPOSITION ON ANALYTE AND ANALYTE MONO-OXIDE RESPONSE IN ICP-MS

A. Introduction 106
B. Oxide Behaviour in ICP-MS 107
C. Experimental 112
D. Effects of Aerosol Processing on Analyte Signals 115
a. Direct versus Condensed Aerosol Introduction 115
b. Effect of Heating Chamber Temperature 124
E. Effect of Aerosol Processing on La and LaO Ions 129

a. Direct, Condensed and Uncondensed Aerosol Introduction 129
b. Effect of Heating Chamber Temperature 130
c. Discussion 133
F. Effect of Nitrogen Mixed Gas Plasma and Aerosol Processing on La and LaO 144
a. Direct, Condensed and Uncondensed Aerosol Introduction 144
b. Effect of Heating Chamber Temperature 148
c. Discussion 151
G. Conclusion 152
REFERENCES 156

5. CHARACTERIZATION OF SOME MAJOR BACKGROUND SPECIES IN ICP-MS

A. Introduction 159
a. Non-structured Background 160
b. Structured Background 160
i) Primary Species 160
ii) Matrix Induced Molecular Species 161
iii) Argon Related Matrix Induced Species 161
iv) Matrix Element itself (isobaric) and/or its Oxide 161
B. Behaviour of some Primary Background Species 162
a. 100% Argon Plasma 162
i) Introduction 162
ii) Experimental Conditions 169
b. Nitrogen Mixed Gas Plasma 174
i) Introduction 174
ii) Experimental Conditions 176

c. Effect of Desolvation on Background Species 184
i) Introduction 184
ii) Experimental Conditions 184
iii) Results and Discussion 184
d. Conclusion 193
C. Behaviour of some Matrix Induced Molecular Species 196
a. Introduction 196
b. Experimental Conditions 200
c. Conclusion 200
D. Behaviour of some Argon Related Matrix Induced Species 204
a. Introduction 204
b. Experimental Conditions and Results 205
i) Effect of Plasma Operating Parameters on Ar-Na Species 205
ii) Effect of Nitrogen Mixed Gas Plasma on Ar-Cr and Ar-Cu Species 207
iii) Effect of Analyte Species on ArX levels 213
c. Conclusion 217
REFERENCES 219

6. AN EVALUATION OF MIXED GAS ICP's FOR THE RUNNING OF ORGANIC MATRIXES IN ICP-MS

A. Introduction 221
B. Preparation of Organo-metallic Standard Solutions 223
C. Performance of a Nitrogen-argon Mixed Gas Plasma 223
D. Performance of an Oxygen-argon Mixed Gas Plasma 226
E. Performance of an Air-argon Mixed Gas Plasma 229
F. Discussion 232
REFERENCES 233

7. A PRELIMINARY STUDY ON THE EFFECT OF SAMPLER-SKIMMER SEPARATION IN ICP-MS

A. Introduction 234
B. The Physical Arrangement of the Interface 239
C. Effect of Sampler-Skimmer Separation on Analytes and their corresponding Oxides 240
  a. Introduction 240
  b. Experimental Conditions 242
  c. Results and Discussion 242
D. Effect of Sampler-Skimmer Separation on some Background Species.......... 251
  a. Introduction 251
  b. Behaviour of some Primary Background Species 251
  c. Behaviour of Analyte Induced Argon Background Species 262
E. Effect of Sampler-Skimmer Separation on Analyte Matrix Effects 265
  a. Introduction 265
  b. Experimental Conditions 266
  c. Results and Discussion 266
F. Conclusions 270
REFERENCES 275

8. CONCLUSION AND FURTHER WORK

a. Sample Delivery System 277
b. Non-Spectroscopic Interelement Interference 278
c. Interface Design 279
d. Improvement of the Plasma Source 279
REFERENCES 282

LIST OF TABLES

TABLE PAGE

1-1. Degree of ionization for the elements in an argon ICP assuming local thermodynamic equilibrium, T_{ion} (Ar) = 6680 K and $n_e = 1.475 \times 10^{14}$ cm^{-3} as in reference [23] 4

3-1. Physical properties of some of the chosen elements used in this study....... 27

3-2. The signal intensity ratio for analytes obtained as a function of sampling depths using a 5% nitrogen cooled plasma to a 100% argon plasma. All comparisons were made at respective optimum nebuliser gas flow rates..... 45

3-3. Ion signal intensity ratio for analytes obtained as a function of percent nitrogen in the outer gas to a pure argon plasma. Data were obtained at individual optimum nebuliser gas flow rates at 10 mm sampling depth 54

3-4. Physical properties of some chosen elements as well as the ion sensitivity ratio from a 20% nitrogen mixed nebulising gas to the argon plasma. The ion intensity ratio was acquired at the individual optimum nebuliser flow rate 60

3-5. The calculated "Apparent Degree of Ionization, α" for analytes obtained with a 100% argon plasma as well as with a 5% nitrogen cooled discharge at sampling depths from 8 to 12 mm.................................. 63

3-6. The effect of mixed gas plasmas on oxide/metal ion ratios, each obtained at its respective peak metal ion sensitivity.. 98

5-1. Normalized ion populations of some argon related matrix induced species, expressed in ion counts/mMol... 214

7-1. The sensitivity ratio for ion species with and without the 0.23 cm spacer, each at its optimum nebuliser flow rate... 245

7-2. The sensitivity ratio for ion species with and without the 0.23 cm spacer, each at its optimum nebuliser flow rate 249

7-3. The normalized signal ratio for ion species at sampler-skimmer separations using 0.23 cm and 0.57 cm spacers. The signals were acquired each at its optimum nebuliser flow rate 255

7-4. The normalized signal ratio for ion species at sampler-skimmer separations using 0.23 cm and 0.57 cm spacers. The signals were acquired each at its optimum nebuliser flow rate 261

LIST OF FIGURES

FIGURE PAGE

1-1. Schematic diagram of the ICP source.. 7

2-1. Schematic diagram of the SCIEX Elan 250 ICP-MS 18

3-1. a) Dependence of Zn signal on nebuliser flow rate and plasma powers in a pure argon discharge. b) Dependence of Zn signal on nebuliser flow rate and plasma powers in a 5% nitrogen cooled discharge..................... 29

3-2. a) Dependence of Ge signal on nebuliser flow rate and plasma powers in a pure argon discharge (at 10 mm sampling depth). b) Dependence of Ge signal on nebuliser flow rate and plasma powers in a 5% nitrogen cooled discharge (at 10 mm sampling depth)... 30

3-3. a) Dependence of As signal on nebuliser flow rate and plasma powers in a pure argon discharge (at 10 mm sampling depth). b) Dependence of As signal on nebuliser flow rate and plasma powers in a 5% nitrogen cooled discharge (at 10 mm sampling depth)... 31

3-4. a) Dependence of Sr signal on nebuliser flow rate and plasma powers in a pure argon discharge (at 10 mm sampling depth). b) Dependence of Sr signal on nebuliser flow rate and plasma powers in a 5% nitrogen cooled discharge (at 10 mm sampling depth)... 32

3-5. a) Dependence of Y signal on nebuliser flow rate and plasma powers in a pure argon discharge (at 10 mm sampling depth). b) Dependence of Y signal on nebuliser flow rate and plasma powers in a 5% nitrogen cooled discharge (at 10 mm sampling depth)... 33

3-6. a) Dependence of Zr signal on nebuliser flow rate and plasma powers in a pure argon discharge (at 10 mm sampling depth). b) Dependence of Zr signal on nebuliser flow rate and plasma powers in a 5% nitrogen cooled discharge (at 10 mm sampling depth) 34

3-7. a) Dependence of Ru signal on nebuliser flow rate and plasma powers in a pure argon discharge (at 10 mm sampling depth). b) Dependence of Ru signal on nebuliser flow rate and plasma powers in a 5% nitrogen cooled discharge (at 10 mm sampling depth) 35

3-8. a) Dependence of Zn signal on nebuliser flow rate for a range of sampling depths in a pure argon discharge (at 1.50 kW). b) Dependence of Zn signal on nebuliser flow rate for a range of sampling depths in a 5% nitrogen cooled discharge (at 1.50 kW) 37

3-9. a) Dependence of Ge signal on nebuliser flow rate for a range of sampling depths in a pure argon discharge (at 1.50 kW). b) Dependence of Ge signal on nebuliser flow rate for a range of sampling depths in a 5% nitrogen cooled discharge (at 1.50 kW) 38

3-10. a) Dependence of As signal on nebuliser flow rate for a range of sampling depths in a pure argon discharge (at 1.50 kW). b) Dependence of As signal on nebuliser flow rate for a range of sampling depths in a 5% nitrogen cooled discharge (at 1.50 kW) 39

3-11. a) Dependence of Sr signal on nebuliser flow rate for a range of sampling depths in a pure argon discharge (at 1.50 kW). b) Dependence of Sr signal on nebuliser flow rate for a range of sampling depths in a 5% nitrogen cooled discharge (at 1.50 kW) 40

3-12. a) Dependence of Y signal on nebuliser flow rate for a range of sampling depths in a pure argon discharge (at 1.50 kW). b) Dependence of Y signal on nebuliser flow rate for a range of sampling depths in a 5% nitrogen cooled discharge (at 1.50 kW) 41

3-13. a) Dependence of Zr signal on nebuliser flow rate for a range of sampling depths in a pure argon discharge (at 1.50 kW). b) Dependence of Zr signal on nebuliser flow rate for a range of sampling depths in a 5% nitrogen cooled discharge (at 1.50 kW) 42

3-14. a) Dependence of Ru signal on nebuliser flow rate for a range of sampling depths in a pure argon discharge (at 1.50 kW). b) Dependence of Ru signal on nebuliser flow rate for a range of sampling depths in a 5% nitrogen cooled discharge (at 1.50 kW) 43

3-15. Dependence of Zn signal on nebuliser flow rate for a range of nitrogen mixed into the outer gas (at 1.50 kW and 10 mm sampling depth) 46

3-16. Dependence of Ge signal on nebuliser flow rate for a range of nitrogen mixed into the outer gas (at 1.50 kW and 10 mm sampling depth) 47

3-17. Dependence of As signal on nebuliser flow rate for a range of nitrogen mixed into the outer gas (at 1.50 kW and 10 mm sampling depth) 48

3-18. Dependence of Sr signal on nebuliser flow rate for a range of nitrogen mixed into the outer gas (at 1.50 kW and 10 mm sampling depth) 49

3-19. Dependence of Y signal on nebuliser flow rate for a range of nitrogen mixed into the outer gas (at 1.50 kW and 10 mm sampling depth) 50

3-20. Dependence of Zr signal on nebuliser flow rate for a range of nitrogen mixed into the outer gas (at 1.50 kW and 10 mm sampling depth) 51

3-21. Dependence of Ru signal on nebuliser flow rate for a range of nitrogen mixed into the outer gas (at 1.50 kW and 10 mm sampling depth) 52

3-22. Effect of 20% nitrogen mixed nebuliser gas on Te at 15 mm sampling depth (at 1.50 kW).. 55

3-23. Effect of 20% nitrogen mixed nebuliser gas on Cs at 15 mm sampling depth (at 1.50 kW).. 56

3-24. Effect of 20% nitrogen mixed nebuliser gas on Ba at 15 mm sampling depth (at 1.50 kW).. 57

3-25. Effect of 20% nitrogen mixed nebuliser gas on La at 15 mm sampling depth (at 1.50 kW) 58

3-26. a) Figure to illustrate the degree of element ionization in ICP (from Table 3-1). b) Figure to illustrate elemental ionization energy. c) Figure to illustrate the degree of signal enhancements from a 5% nitrogen cooled plasma at the sampling depth of 8 mm 61

3-27. a) Figure to illustrate the degree of element ionization in ICP (from Table 3-1). b) Figure to demonstrate the "apparent degree of element ionization" obtained from an argon plasma at 12 mm sampling depth. c) Figure to demonstrate the "apparent degree of element ionization" obtained from a 5% nitrogen cooled plasma at 8 mm sampling depth 64

3-28. Bar graphs to correlate the metal oxide bond energy for elements to signal enhancements observed with a 5% nitrogen cooled plasma at 8 mm sampling depth (in the order of increasing ionization potentials) 65

3-29. Bar graphs to correlate the metal oxide bond energy for elements to signal enhancements observed with a 5% nitrogen cooled plasma at 8 mm sampling depth (in the order of increasing metal oxide bond energies)....... 67

3-30. Diagram to demonstrate the relationship between signal enhancements from nitrogen mixed gas plasma to metal oxide bond energies 68

3-31. Bar graphs to illustrate the correlation between metal oxide bond energy to "optimum nebuliser flow rate" for species in an argon plasma 70

3-32. Bar graphs to demonstrate the lack of correlation between optimum nebuliser flow rate and metal oxide bond energy in a 5% nitrogen plasma .. 72

3-33. Bar graphs to demonstrate the correlation between species ionization potential to optimum nebuliser flow rate in a 5% nitrogen plasma 73

3-34. a) Dependence of Te signal on nebuliser flow rate and percentage of oxygen in the plasma gas (at 1.50 kW and 10 mm sampling depth). b) Dependence of Te signal on nebuliser flow rate and percentage of nitrogen in the plasma gas (at 1.50 kW and 10 mm sampling depth) 75

3-35. a) Dependence of Cs signal on nebuliser flow rate and percentage of oxygen in the plasma gas (at 1.50 kW and 10 mm sampling depth). b) Dependence of Cs signal on nebuliser flow rate and percentage of nitrogen in the plasma gas (at 1.50 kW and 10 mm sampling depth)......... 76

3-36. a) Dependence of Ba signal on nebuliser flow rate and percentage of oxygen in the plasma gas (at 1.50 kW and 10 mm sampling depth). b) Dependence of Ba signal on nebuliser flow rate and percentage of nitrogen in the plasma gas (at 1.50 kW and 10 mm sampling depth)......... 77

3-37. a) Dependence of Ce signal on nebuliser flow rate and percentage of oxygen in the plasma gas (at 1.50 kW and 10 mm sampling depth). b) Dependence of Ce signal on nebuliser flow rate and percentage of nitrogen in the plasma gas (at 1.50 kW and 10 mm sampling depth)......... 78

3-38. a) Dependence of Te signal on nebuliser flow rate and percentage of air in the plasma gas (at 1.50 kW and 10 mm sampling depth). b) Dependence of Te signal on nebuliser flow rate and percentage of nitrogen in the plasma gas (at 1.50 kW and 10 mm sampling depth)........................... 80

3-39. a) Dependence of Cs signal on nebuliser flow rate and percentage of air in the plasma gas (at 1.50 kW and 10 mm sampling depth). b) Dependence of Cs signal on nebuliser flow rate and percentage of nitrogen in the plasma gas (at 1.50 kW and 10 mm sampling depth)........................... 81

3-40. a) Dependence of Ba signal on nebuliser flow rate and percentage of air in the plasma gas (at 1.50 kW and 10 mm sampling depth). b) Dependence of Ba signal on nebuliser flow rate and percentage of nitrogen in the plasma gas (at 1.50 kW and 10 mm sampling depth)........................... 82

3-41. a) Dependence of Ce signal on nebuliser flow rate and percentage of air in the plasma gas (at 1.50 kW and 10 mm sampling depth). b) Dependence of Ce signal on nebuliser flow rate and percentage of nitrogen in the plasma gas (at 1.50 kW and 10 mm sampling depth)........................... 83

3-42. Bar graphs to demonstrate the different signal enhancement effects by 5% nitrogen, oxygen, and air mixed gas plasmas on Te, Cs, Ba and Ce at rf power of 1.50 kW and 10 mm sampling depth.................................. 84

3-43. a) Dependence of La signal on nebuliser flow rate and percentage of nitrogen in the plasma gas (at 1.50 kW and 10 mm sampling depth). b) Dependence of LaO signal on nebuliser flow rate and percentage of nitrogen in the plasma gas (at 1.50 kW and 10 mm sampling depth)......... 91

3-44. a) Dependence of BaO signal on nebuliser flow rate and percentage of oxygen in the plasma gas (at 1.50 kW and 10 mm sampling depth). b) Dependence of BaO signal on nebuliser flow rate and percentage of nitrogen in the plasma gas (at 1.50 kW and 10 mm sampling depth)......... 94

3-45. a) Dependence of CeO signal on nebuliser flow rate and percentage of oxygen in the plasma gas (at 1.50 kW and 10 mm sampling depth). b) Dependence of CeO signal on nebuliser flow rate and percentage of nitrogen in the plasma gas (at 1.50 kW and 10 mm sampling depth)......... 95

3-46. a) Dependence of BaO signal on nebuliser flow rate and percentage of air in the plasma gas (at 1.50 kW and 10 mm sampling depth). b) Dependence of BaO signal on nebuliser flow rate and percentage of nitrogen in the plasma gas (at 1.50 kW and 10 mm sampling depth)......... 96

3-47. a) Dependence of CeO signal on nebuliser flow rate and percentage of air in the plasma gas (at 1.50 kW and 10 mm sampling depth). b) Dependence of CeO signal on nebuliser flow rate and percentage of nitrogen in the plasma gas (at 1.50 kW and 10 mm sampling depth)......... 97

3-48. The effect of 20% nitrogen nebulising gas on La and LaO signals at sampling depth of 15 mm (rf power 1.50 kW)................................. 100

3-49. The effect of 20% nitrogen nebulising gas on LaO signal at 15 mm sampling depth 101

4-1. Diagram to show typical responses for La and LaO to nebuliser flow rate... 110

4-2. Schematic diagram of the aerosol processing set-up (for condensed and desolvated nebulisations).......... 113

4-3. Schematic diagram of the uncondensed aerosol nebulisation 114

4-4. Dependence of As signal on nebuliser flow rate in "direct" and condensed aerosol nebulisations.......... 116

4-5. Dependence of Sr signal on nebuliser flow rate in "direct" and condensed aerosol nebulisations.......... 117

4-6. Dependence of Ru signal on nebuliser flow rate in "direct" and condensed aerosol nebulisations.......... 118

4-7. a) Bar graph to compare the relationship between signal intensity difference in direct and condensed nebulisations to analytes ionization potential. b) The lack of correlation between signal intensity changed and metal oxide bond energy 120

4-8. Diagram to show the effect of chamber heating temperature and nebuliser flow rate on Sr signal in an argon plasma.......... 126

4-9. Diagram to show the effect of chamber heating temperature and nebuliser flow rate on Y signal in an argon plasma.......... 127

4-10. Diagram to show the effect of chamber heating temperature and nebuliser flow rate on As signal in an argon plasma 128

4-11. a) Diagram to show the signal responses of La in direct and condensed aerosol nebulisations. b) Diagram to show the signal responses of LaO in direct and condensed aerosol nebulisations 131

4-12. a) Diagram to show the signal responses of La in direct and uncondensed aerosol nebulisations. b) Diagram to show the signal responses of LaO in direct and uncondensed aerosol nebulisations 132

4-13. a) Diagram to show the effect of chamber heating temperature and nebuliser flow rate on La signal in desolvated nebulisation. b) Diagram to show the effect of chamber heating temperature and nebuliser flow rate on LaO signal in desolvated nebulisation.. 134

4-14. a) Diagram to show the effect of chamber heating temperature and nebuliser flow rate on La signal in uncondensed nebulisation. b) Diagram to show the effect of chamber heating temperature and nebuliser flow rate on LaO signal in uncondensed nebulisation.. 135

4-15. Bar graph to demonstrate the effect of chamber temperature on the percentage of LaO in desolvated nebulisation.. 136

4-16. Bar graph to demonstrate the effect of chamber temperature on the percentage of LaO in uncondensed nebulisation.. 137

4-17. Diagram to show the different degrees of signal overlap in direct and condensed aerosol nebulisation for La and LaO.. 141

4-18. Diagram to show the different degrees of signal overlap in direct and uncondensed aerosol nebulisation for La and LaO.. 142

4-19. a) Diagram to show the signal responses of La in direct and condensed aerosol nebulisations. b) Diagram to show the signal responses of LaO in direct and condensed aerosol nebulisations 146

4-20. a) Diagram to show the signal responses of La in direct and uncondensed aerosol nebulisations. b) Diagram to show the signal responses of LaO in direct and uncondensed aerosol nebulisations 147

4-21. Bar graph to demonstrate the different effect of chamber temperature on the percentage of LaO in an argon and a nitrogen mixed gas plasma (desolvated aerosol nebulisation).. 149

4-22. Bar graph to demonstrate the different effect of chamber temperature on the percentage of LaO in an argon and a nitrogen mixed gas plasma (uncondensed aerosol nebulisation).. 150

4-23. a) Diagram to illustrate the effect of aerosol processing and nitrogen mixed gas plasma on the signal profiles of La. b) Diagram to demonstrate the effect of aerosol processing and nitrogen mixed gas plasma on the signal profiles of LaO.. 153

4-24. Diagram to show the different degrees of signal overlap by aerosol processing and nitrogen mixed gas plasma for La and LaO.................... 154

5-1. Background mass spectra for distilled water (1-84 amu)........................ 163

5-2. Background spectra for distilled water (1-50 amu) at amplification levels of 100 (top), 10 (middle) and 1 (bottom) 164

5-3. Background spectra for distilled water (44-84 amu) at amplification levels of 100 (top), 10 (middle) and 1 (bottom) 165

5-4. a) Background spectrum for distilled water at 1 to 50 amu. b) Background spectrum for deuterium oxide (heavy water) at 1 to 50 amu ... 167

5-5. a) Background spectrum for distilled water at 44 to 84 amu. b) Background spectrum for deuterium oxide at 44 to 84 amu 168

5-6. Dependence of $^{36}Ar^+$ and $^{36}ArH^+$ signals on nebuliser flow rate for a range of rf powers and sampling depths 170

5-7. Dependence of $^{40}ArO^+$ and $^{40}ArOH^+$ signals on nebuliser flow rate for a range of rf powers and sampling depths 171

5-8. Dependence of $^{40}Ar_2^+$ and $^{40}Ar_2H^+$ signals on nebuliser flow rate for a range of rf powers and sampling depths 172

5-9. Dependence of $^{40}ArN^+$ and $^{63}Cu^+$ signals on nebuliser flow rate for a range of rf powers and sampling depths 173

5-10. Dependence of $^{36}Ar^+$, $^{36}ArH^+$, $^{40}ArN^+$, $^{40}ArO^+$, $^{40}ArOH^+$, $^{63}Cu^+$, $^{40}Ar_2^+$ and $^{40}Ar_2H^+$ signals on nebuliser flow rate for a range of sampling depths and at 1.50 kW rf power 175

5-11. a) The effect of nebuliser flow rate and 0, 5, 12 and 20% nitrogen cooled plasmas on ArO species (2% nitric acid "Blank" solution). b) The effect of nebuliser flow rate and 0, 5, 12 and 20% nitrogen cooled plasmas on mass 56 (Fe and ArO) from a solution containing 0.2 ppm Fe in 2% nitric acid 177

5-12. a) The effect of nebuliser flow rate and 0, 5, 12 and 20% nitrogen cooled plasmas on ArOH species (2% nitric acid "Blank" solution). b) The effect of nebuliser flow rate and 0, 5, 12 and 20% nitrogen cooled plasmas on mass 57 (Fe and ArOH) from a solution containing 0.2 ppm Fe in 2% nitric acid 178

5-13. a) The effect of nebuliser flow rate and 0, 5, 12 and 20% nitrogen cooled plasmas on argon dimer (2% nitric acid "Blank" solution). b) The effect of nebuliser flow rate and 0, 5, 12 and 20% nitrogen cooled plasmas on mass 80 (Se and Ar_2) from a solution containing 5 ppm Se in 2% nitric acid 179

5-14. a) The net signal responses for ^{56}Fe (after blank subtracted) in 0, 5, 12 and 20% nitrogen cooled plasmas. b) The BEC values for ArO to Fe signals (each at peak Fe intensity) 181

5-15. a) The net signal responses for ^{57}Fe (after blank subtracted) in 0, 5, 12 and 20% nitrogen cooled plasmas. b) The BEC values for ArOH to Fe signals (each at peak Fe intensity) 182

5-16. a) The net signal responses for ^{80}Se (after blank subtracted) in 0, 5, 12 and 20% nitrogen cooled plasmas. b) The BEC values for Ar_2 to Se signals (each at peak Se intensity) 183

5-17. The effects of desolvated nebulisation on ArO, ArOH, Cu, ArN, Ar_2 and Ar_2H ion species in a 100% argon plasma and a 5% nitrogen cooled discharge 186

5-18. The effects of aerosol processing on mass 17 (OH) in a 100% argon plasma and in a 5% nitrogen cooled discharge 188

5-19. The effects of aerosol processing on mass 18 (OH_2) in a 100% argon plasma and in a 5% nitrogen cooled discharge 189

5-20. The effects of aerosol processing on mass 19 (OH_3) in a 100% argon plasma and in a 5% nitrogen cooled discharge 190

5-21. The effects of aerosol processing on mass 32 (O_2) in a 100% argon plasma and in a 5% nitrogen cooled discharge 191

5-22. a) The effects of aerosol processing on mass 36 (^{36}Ar) in a 100% argon plasma and in a 5% nitrogen cooled discharge. b) The effects of aerosol processing on mass 37 (^{36}ArH) in a 100% argon plasma and in a 5% nitrogen cooled discharge 192

5-23. Background mass spectrum for distilled water (43 to 90 amu) obtained using a 5% nitrogen cooled plasma 195

5-24. a) Background mass spectrum for 2% hydrochloric acid (43 to 90 amu) b) Background mass spectrum for 2% hydrochloric acid in a 50% v/v deuterium oxide solution 197

5-25. a) Background mass spectrum for 2% sulphuric acid (43 to 90 amu). b) Background mass spectrum for 2% sulphuric acid in a 50% v/v deuterium oxide solution 198

5-26. a) The effect of nebuliser flow rate and 0, 5, 12 and 20% nitrogen cooled plasmas on ClO species (2% hydrochloric acid "Blank" solution). b) The effect of nebuliser flow rate and 0, 5, 12 and 20% nitrogen cooled plasmas on mass 51 (V and ClO) from a solution containing 0.5 ppm V in 2% HCl.. 201

5-27. The effect of nebuliser flow rate and 0, 5, 12 and 20% nitrogen cooled plasmas on ArCl species (2% hydrochloric acid "Blank" solution) 202

5-28. a) The net signal responses for ^{51}V (after blank subtracted) in 0, 5, 12 and 20% nitrogen cooled plasmas. b) The BEC values for ClO to V signals (each at peak V intensity) 203

5-29. a) Dependence of ArNa signals on rf powers and nebuliser flow rate in an argon plasma and in a 5% nitrogen cooled plasma at 10 mm sampling depth. b) Dependence of ArNa signals on nebuliser flow rate and rf powers at 15 mm sampling depth 206

5-30. Dependence of ArCr signals on nebuliser flow rate and different percentage of nitrogen mixed gas plasmas 208

5-31. Dependence of ArCu signals on nebuliser flow rate and different percentage of nitrogen mixed gas plasmas 209

5-32. a) Effect of 20% nitrogen mixed nebuliser gas on ArCr at 10 mm sampling depth. b) Effect of 20% nitrogen mixed nebuliser gas on ArCr at 15 mm sampling depth 211

5-33. a) Effect of 20% nitrogen mixed nebuliser gas on ArCu at 10 mm sampling depth. b) Effect of 20% nitrogen mixed nebuliser gas on ArCu at 15 mm sampling depth 212

5-34. a) Bar graph to show the normalized ArX ion signal for elements detected in an argon ICP. b) Ionic radii of element species as provided in reference [15] 216

6-1. Diagram to illustrate the solvent condensation system 225

6-2. a) Dependence of Cd signal in xylene on nebuliser flow rate in a 20% nitrogen mixed nebulising gas plasma. b) Dependence of Cd signal in xylene on nebuliser flow rate in a 20% nitrogen mixed nebulising gas and a 2% nitrogen cooled plasma 227

6-3. a) Dependence of Cd signal in xylene on nebuliser flow rate in a 20%

oxygen mixed nebulising gas plasma. b) Dependence of Cd signal in xylene on nebuliser flow rate in a 2.5% oxygen mixed gas plasma........... 228

6-4. a) Dependence of Cd signal in xylene on nebuliser flow rate in a 20% air mixed nebulising gas plasma. b) Dependence of Cd signal in xylene on nebuliser flow rate in a 5% air mixed gas plasma 231

7-1. a) Skimmer cone sampling at Mach disc. b) Skimmer cone sampling after Mach disc. c) Skimmer cone sampling before Mach disc 237

7-2. Schematic layout of the sampler-skimmer interface with the spacer insert... 241

7-3. Effect of a 0.23 cm spacer insert on Ce and CeO signals in a 100% argon plasma 244

7-4. Effect of a 0.23 cm spacer insert on Ce and CeO signals in a 5% nitrogen cooled plasma.. 248

7-5. Effect of sampler-skimmer separation distances on some background ion species in a pure argon plasma 253

7-6. Effect of sampler-skimmer separations on peak background ion signals in a 100% argon plasma.. 254

7-7. The effect of sampler-skimmer separations on $^{40}ArN^+$, $^{40}ArO^+$, $^{40}ArOH^+$, $^{63}Cu^+$, $^{40}Ar_2^+$ and $^{40}Ar_2H^+$ species in a 5% nitrogen cooled plasma 258

7-8. Effect of sampler-skimmer separations on peak $^{40}ArN^+$, $^{40}ArO^+$, $^{40}ArOH^+$, $^{63}Cu^+$, $^{40}Ar_2^+$ and $^{40}Ar_2H^+$ ion signals in a 5% nitrogen cooled plasma.. 260

7-9. Ion signal dependence for Ar-Na on nebuliser flow rate in a 5% nitrogen cooled plasma and its responses to spacer inserts in a pure argon plasma ... 263

7-10. Effect of sampler-skimmer separations on peak Ar-Na signals in a pure argon plasma.. 264

7-11. a) Effect of sampler-skimmer separations on normalized peak Mn ion signals. b) Degree of signal suppression by 1000 ppm U on peak Mn signal as a function of sampler-skimmer separations. c) Degree of signal suppression by 1000 ppm Na on peak Mn ion signal as a function of sampler-skimmer separations.. 267

7-12. a) Effect of sampler-skimmer separations on normalized peak ArO ion signals. b) Degree of signal suppression by 1000 ppm U on peak ArO ion signal as a function of sampler-skimmer separations. c) Degree of signal suppression by 1000 ppm Na on ArO ion signal as a function of sampler-skimmer separations.. 268

7-13. a) Effect of sampler-skimmer separations on normalized peak Ar_2 ion signals. b) Degree of signal suppression by 1000 ppm U on peak Ar_2 ion signal as a function of sampler-skimmer separations. c) Degree of signal suppression by 1000 ppm Na on peak Ar_2 ion signal as a function of sampler-skimmer separations.. 269

7-14. Mass spectrum of Ce obtained using a 5% nitrogen cooled plasma.......... 272

7-15. Mass spectrum of Ce obtained using a 5% nitrogen cooled plasma with a 0.23 cm spacer insert.. 273

Chapter 1

Introduction

A. Inductively Coupled Plasma-Mass Spectrometry

Inductively coupled plasma-mass spectrometry (ICP-MS) is a relatively new analytical technique for trace element analysis. The original concept evolved from the direct coupling of a d.c. capillary arc plasma to a quadrupole mass spectrometer [1]. However, this source exhibited serious matrix effects and it was subsequently replaced by sources such as the microwave induced plasma (MIP) [2] and finally the inductively coupled plasma (ICP). In particular, development work with an ICP coupled to a quadrupole mass spectrometer was carried out by three research groups; the SCIEX group at Toronto [2, 3], the Ames Laboratory of the Iowa State University headed by Fassel [4-6] and by Gray from the University of Surrey with Date from the British Geological Survey and VG Instruments [7-12]. Since the first scientific publication on ICP-MS in 1980 [4], development of the technique has been rapid. The first commercial instrument was available in 1984 and since then, there have been over 150 instruments sold world wide.

The technique has important key features that make it one of the best for trace and ultra-trace elemental analysis. In particular, the detection limits for most elements are about 100 times superior to those achieved by inductively coupled plasma-atomic emission spectrometry (ICP-AES) under similar conditions. These detection limits are achieved while maintaining a wide linear dynamic range (10^6) with respect to the measurement of concentration. Also, the mass spectra of the elements are considerably simpler than their optical emission spectra. Thus spectral overlap is less severe when compared to the spectra obtained with optical emission spectrometry. Furthermore, the mass spectrum for each element is simple and governed by the natural abundance of its isotopes, making qualitative determination of an unknown sample relatively easy. For more information regarding the technique, several excellent review articles have been published [11, 13-20].

B. Ion Generation in an ICP

The concept of ICP-MS is based on the use of the ICP as an elemental ion source which is directly sampled into a quadrupole mass spectrometer.

Theoretically, the degree of ionization (α) of an element in an ICP can be calculated as follows [21]:

$$\alpha = \frac{n_i}{n_a + n_i} = \frac{\dfrac{n_i\ n_e}{n_a}}{n_e + \dfrac{n_i\ n_e}{n_a}} = \frac{S_n}{n_e + S_n} \qquad (1\text{-}1)$$

where:

n_i, n_a, n_e = number densities for ions, atoms and electrons respectively.

S_n = Saha equilibrium constant.

$$\text{and} \quad S_n = \frac{n_i\, n_e}{n_a} \qquad (1\text{-}2)$$

$$= \frac{(2\,\pi\, m\, k\, T)^{3/2}}{h^3} \times \frac{2\, Z_i}{Z_a} \times \exp(-\, V_i / k\, T) \qquad (1\text{-}3)$$

where:

m = mass of the electron.

k = Boltzmann constant.

T = ionization temperature.

h = Planck constant.

Z_i, Z_a = partition functions of the ions and atom respectively.

V_i = ionization potential of the element (eV).

Therefore, the degree of ionization for the element can be calculated if the electron density and Ionization Temperature of the plasma is known. Using values of $n_e = 1.475 \times 10^{14}$ cm^{-3} and T_{ion} (Ar) at 6680 K, Furuta [22, 23] calculated the degree of ionization for most of the elements (see Table 1-1). Indeed, for elements with ionization potentials less than 9 eV, the degree of ionization is calculated to be over 80%. Similar data has also been reported by other workers using the same approach [14].

A question remains as to the validity of the calculated results since the basis of the calculation relies on the plasma being at local thermodynamic equilibrium (LTE), and it was widely believed that thermodynamic equilibrium was not attained in the ICP. However, Caughlin and Blades [24] had compared experimental and LTE ion-atom emission line intensity ratios for five elements recently and concluded that the experimental values are within a factor of five of LTE. They also compared the degree of ionization α values between experimental results and LTE calculated values. For elements with low ionization energy, the α values were comparable, however, they begin to deviate for elements with high ionization energy. Using ICP-MS, Gray and Date [9] monitored signal responses for several elements at 10 mm and 1.2 kW and they observed a fit of $T = 9000$ K and $n_e = 4.5 \times 10^{15}$ cm^{-3} from the Saha equation. Although their results were a bit too high, they confirm that the marriage of the two techniques did not affect the ICP source too badly.

The initial work carried out in ICP-MS at Alberta was to characterize the ion signal response to plasma operating parameters [25], background features [26], oxide and hydroxide behaviour [27] and matrix effects [28]. The initial results indicated that the

Table 1-1. Degree of ionization for the elements in an argon ICP assuming local thermodynamic equilibrium, T_{ion} (Ar) = 6680 K and $n_e = 1.475 \times 10^{14}$ cm^{-3} as in reference [23].

Element	IP (eV)	Degree of Ionization
Cs	3.894	99.98
Rb	4.177	99.98
K	4.341	99.97
Na	5.139	99.91
Ba	5.212	99.96
Ra	5.279	99.95
Li	5.392	99.85
La	5.577	99.91
Sr	5.695	99.92
In	5.786	99.42
Al	5.986	98.92
Ga	5.999	99.00
Tl	6.108	99.38
Ca	6.113	99.86
Y	6.38	98.99
Sc	6.54	99.71
V	6.74	99.23
Cr	6.766	98.89
Ti	6.82	99.49
Zr	6.84	99.31
Nb	6.88	98.94
Hf	7.0	98.89
Mo	7.099	98.54
Tc	7.28	97.50
Bi	7.289	94.14
Sn	7.344	96.72
Ru	7.37	96.99
Pb	7.416	97.93
Mn	7.435	97.10
Rh	7.46	95.87
Ag	7.576	94.45
Ni	7.635	92.55
Mg	7.646	98.25
Cu	7.726	91.59
Co	7.86	94.83
Fe	7.870	96.77
Re	7.88	94.54
Ta	7.89	96.04
Ge	7.899	91.64
W	7.98	94.86
Si	8.151	87.90
B	8.298	62.03
Pd	8.34	94.21
Sb	8.641	81.07

Os	8.7	79.96
Cd	8.993	85.43
Pt	9.0	61.83
Te	9.009	66.74
Au	9.225	48.87
Be	9.322	75.36
Zn	9.394	74.50
Se	9.752	30.53
As	9.81	48.87
S	10.360	11.47
Hg	10.437	32.31
I	10.451	24.65
P	10.486	28.79
Rn	10.748	35.74
Br	11.814	3.183
C	11.260	3.451
Xe	12.130	5.039
Cl	12.967	0.4558
O	13.618	0.04245
Kr	13.999	0.2263
N	14.534	0.04186
Ar	15.759	0.01341
F	17.422	0.0001919
Ne	21.564	0.0000005468
He	24.587	0.000000001007

dependence of the ion signal on plasma operating condition was a great deal more complicated than in ICP-AES. Also, significant level of oxides, hydroxides and to an extent some doubly ionized species, not normally observed using optical detection systems, were also recorded. In addition, the background spectrum was found to be more complicated than originally thought. Not only affected by the analyte matrix, but it also is highly dependent on the solvent medium. A 5% (volume/volume) mineral acid solution (HCl, H_2SO_4) gives a very complicated background spectrum, with nitric acid causing the least complication [26].

C. Role of Mixed Gas and Molecular Gas in ICP's

The ICP is formed in an assembly called a "plasma torch" consisting of three concentric quartz tubes. A schematic drawing of the assembly is shown in Figure 1-1. The three tubes are termed as "outer tube", "intermediate tube" and "central tube". The torch assembly is placed inside a 3 to 4 turn water-cooled induction coil, termed the load coil, which in turn is connected to a high power radio frequency (rf) generator. Typically, argon gas is introduced through these tubes. Due to their different functions, they are also commonly labeled as plasma gas, auxiliary gas and nebuliser gas corresponding to gas introduction through the outer tube, intermediate tube and central tube respectively. The main function of the plasma gas is to maintain the plasma, stabilize it and also prevent the outer tube from melting. This role gave the traditional name of coolant to this outer gas as well. The auxiliary gas is to position the plasma along the axis in order that it does not fall and subsequently melt the rim of the inner or intermediate tubing. The nebuliser gas is used to generate and carry the sample aerosol to the plasma and at the same time confine the sample to the central channel of the plasma.

After the rf supply is turned on, the gas in the coil region is made electrically conductive (partially ionized) by a Tesla coil spark. The plasma is sustained by the rf current flowing

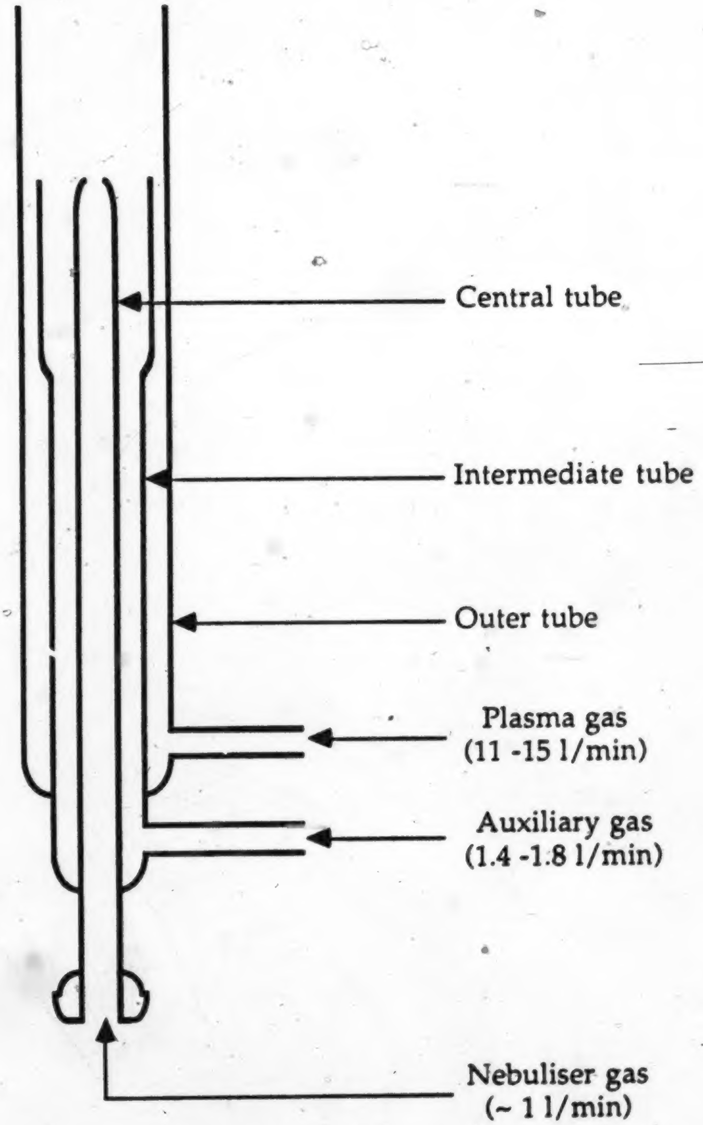

Figure 1-1. **Schematic diagram of the ICP source.**

in the coil. This is achieved by inducing magnetic fields oscillating axially inside the coil which in turn generate annular electric currents in the ionized conductor gas. It is then heated as a result of its ohmic resistance.

As the sample is carried through the central channel of the plasma, aerosol droplets are desolvated, vaporized, atomized, excited and ionized [29]. The popularity of ICP as a source for atomic spectrometry is partly due to the efficient interaction between the sample and the plasma source as well as to the high temperature (~ 6000 K) in the axial channel of the plasma. As a result, this technique gives low detection limits (in the range of ng/ml) for most elements, wide dynamic ranges in concentration, minimal matrix effects and the capability of multi-element determinations.

Argon is routinely used as the operating gas for analytical plasma spectrometry. Despite the numerous advantages for using the argon supported ICP (ICAP) mentioned above and its inert chemical behaviour, there are some practical advantages in using alternate supporting gases such as air, hydrogen, nitrogen and oxygen, particularly as mixed gases along with argon. Greenfield and his coworkers [30] were the first to use molecular gases to replace argon either wholly or partly in the ICP and to study the plasma behaviour as well as their effect on spectrochemical analysis. Details regarding the historic evolution of the technique have been discussed by Lau [31] and Choot [32]. For economic reasons, a main objective in using mixed gas ICP-AES is to reduce the cost of expensive argon gas in ICP facilities. However, this has been partly offset by the development of low-gas-flow ICP torches. Currently there are at least three types of commercial "low-flow" torch available: Sherritt Gordon Mines, Applied Research Laboratories, and Lab-test Equipment Company, Ltd. They decrease the normal consumption of argon by more than half. In a different approach, Kornblum et al. [33] developed a water-cooled jacketed plasma torch which could effectively reduce the consumption of argon to 2 l/min. Similarly, Ripson and coworkers [34, 35] claimed better results are achieved when the external cooling is replaced with air.

For analytical considerations, the complex background spectrum of the ICAP in the near-IR region has been improved with the use of nitrogen mixed gas plasma [36, 37]. Also, with the better ability of energy transfer, molecular gases are superior for the decomposition of refractory elements. In addition, the introduction of chemically reactive species such as oxygen and nitrogen has been demonstrated to be more suitable in the decomposition of organic based sample solutions. Further, mixed gas plasmas are particularly useful in understanding and studying transport properties and fundamental principles of the ICP [6, 38-41].

D. Formation of a Mixed Gas ICP Discharge

A mixed gas ICP discharge cannot normally be generated directly, but rather, the molecular gas is introduced and mixed slowly into the argon gas flow after an argon ICP has been stabilized. Gases such as nitrogen and oxygen (5-15% in the outer argon flow), provide a more intense plasma discharge compared with a 100% argon ICP. The plasma is not only brighter, it is much smaller (25 to 50% smaller) than that of the argon discharge. This volume reduction is a consequence of a thermal pinch effect. This is due to the dissociation of molecular gas, resulting in the diffusion of molecules from colder (outside) to hotter (inside) regions of the plasma. This process requires energy. At the same time, the dissociated products diffuse back out to the colder region and they subsequently associate and release energy. The overall process results in a net transport of energy from the hotter region to the colder region. This also explains the better efficiency of mixed gas plasma discharges in the handling of refractory elements. However, it is generally observed that higher rf power and gas flow rates are necessary to operate the mixed gas discharge. In practice, mixed gases are normally introduced into the nebuliser gas and/or the plasma gas and there does not seem to be any practical advantage in the use of a mixed auxiliary gas.

a. Mixed Gases in the Nebuliser Gas

The introduction of nitrogen into the nebuliser gas flow resulted in a more diffused larger central region while the length of the plasma becomes smaller as the percentage of nitrogen is increased [32, 42]. On the other hand, the intensity of the plasma is lowered and the plasma is less stable.

Apart from some specific applications, the use of a mixed gas as the nebulising gas is not favourable. This is probably a result of the diffuse analyte channel, giving rise to poorer plasma-sample interaction, lower analyte signal sensitivity, higher element detection limits and a poor plasma stability.

b. Mixed Gases in the Plasma Gas

When a molecular gas is introduced into the argon discharge as a fraction of the plasma gas, it changes the physical appearance of the plasma discharge. The changes are dependent on the nature as well as on the amount of foreign gas present in the plasma. For the case of nitrogen mixed gas plasma, it has been observed that the use of nitrogen gas results in a reduction of the plasma volume [43]. The decrease is a function of the amount of nitrogen present in the plasma; the larger the amount of nitrogen, the smaller the resultant volume. With a 100% replacement of the plasma gas with nitrogen, the discharge is about a quarter of its original size. When other foreign gases such as oxygen or air are introduced, similar trends have also been reported. However, under similar operating conditions, it is observed that while the physical size of oxygen and air mixed gas discharges are smaller than that of the argon plasma, they are larger than the nitrogen mixed gas plasma. The reduction in size is considered to effect better analyte-plasma interaction and reduce interference effects caused by solute vaporization due to the formation of refractory compounds [44].

To all intents and purposes, this is only meant to be a brief introduction to mixed gas plasma discharges. For a more detailed overview, the reader should consult a recent article by Montaser and Van Hoven [45].

E. Role of Mixed Gas in ICP-MS

The use of foreign gases in ICP-MS has not been extensive. In the area of fundamental studies, Houk et al. [6] were the first to make use of a 100% nitrogen cooled plasma discharge to investigate the behaviour of some background species using a laboratory constructed instrument. Montaser et al. [46] used a slightly modified VG PlasmaQuad ICP-MS system to briefly study a helium plasma. It was successful towards the elimination of some of the argon related background species as well as for the determination of halogens. On the practical side, low percentage oxygen mixed gas plasmas have been introduced for the combustion or decomposition of organics [47] as well as drug metabolites [48].

F. Thesis Objectives

The aim of this work is to study the potential utilization of mixed gases in ICP-MS. In the determination of spectroscopic temperatures for nitrogen mixed gas plasmas and argon plasma discharges, it has been observed that while the excitation temperatures (T_{ex}) were lower with nitrogen mixed gas plasma, the ionization temperatures (T_{ion}) were higher with the introduction of a low percentage of nitrogen as the plasma gas. The typical T_{ion} value was found to be 9000 K as compared with the 7000 K calculated for the argon discharge [49]. Therefore, it is expected that the introduction of nitrogen gas into the plasma discharge could provide a better source of ion population (i.e. stronger signals), especially in the case of hard to ionize species.

The ion signal response in ICP-MS has been found to be very dependent on plasma operating parameters [25]. Some of the signal behaviour were explained in terms of a spatial shift of the initial radiation zone (IRZ) [27]. The introduction of foreign gases into the plasma discharge results in a dramatic change in the physical structure of the discharge; hence, a study of species behaviours using mixed gas plasmas may help to elucidate the overall behaviour.

In addition, the interferences caused by spectral overlap from oxide, hydroxide and other poly-atomic ions in ICP-MS are more complex than was expected from a high temperature source such as the ICP. Another goal of this study is to establish the origin and, perhaps, methodology for the eventual removal of these interferences.

In the regime of routine analysis using ICP-MS, the handling of organic solvent based analytes is found to be most tedious. Generally, a 100% argon plasma is not capable of total decomposition of the hydrocarbon. Thus the unreacted organic material as well as carbon condenses out on the cooler surface of the sampler cone. In an extreme situation, the uncombusted hydrocarbon travels through to the interface inside the mass spectrometer where it condenses on the electrostatic lenses, quadrupole rods and eventually to the ion detector. The most efficient method in the removal of hydrocarbon is the introduction of oxygen into the plasma. However, the use of oxygen has to be well balanced as any excess amount of oxygen results in the corrosion of the copper sampler. One subject of this study is to search for an alternate source of foreign gas that could make routine organic analysis less troublesome.

Another major theme for the thesis is the role of the aqueous aerosol delivery system in determining the ultimate signal characteristics in ICP-MS. Several signal characteristics, oxide levels and background features depend to some extent on solvent load (the amount of solvent vapour delivered to the plasma) and aerosol particle size. Several aerosol processing approaches are studied and it will be seen that some of the observed effects are similar to those that occur with mixed gas ICP's. In fact, the simultaneous use of mixed gas ICP's and aerosol pre-processing has a synergic effect on reducing oxide levels and some background species. Finally, in order to gain some insight as to the origin of oxides and background species in ICP-MS, some preliminary results of sampler-skimmer spacer studies are reported. In this work the effect of sampler-skimmer separation on analyte, oxide and background species is investigated along with mixed gas plasmas and aerosol processing techniques as probes of performance.

REFERENCES

1. A. L. Gray, Analyst, 100, 289 (1975).
2. D. J. Douglas, Can. Research, 16, 55 (1983).
3. D. J. Douglas, E. S. K. Quan and R. G. Smith, Spectrochim. Acta, 38B, 39 (1983).
4. R. S. Houk, V. A. Fassel, G. D. Flesch, H. J. Svec, A. L. Gray and C. E. Taylor, Anal. Chem., 52, 2283 (1980).
5. R. S. Houk, H. J. Svec and V. A. Fassel, Appl. Spectrosc., 35, 380 (1981).
6. R. S. Houk, A. Montaser and V. A. Fassel, Appl. Spectrosc., 37, 425 (1983).
7. A. R. Date and A. L. Gray, Analyst, 106, 1255 (1981).
8. A. R. Date and A. L. Gray, Analyst, 108, 159 (1983).
9. A. L. Gray and A. R. Date, Analyst, 108, 1033 (1983).
10. A. R. Date and A. L. Gray, Spectrochim. Acta, 38B, 29 (1983).
11. A. L. Gray, Spectrochim. Acta, 40B, 1525 (1985)
12. A. L. Gray, Spectrochim. Acta, 41B, 151 (1986).
13. G. Horlick, S. H. Tan, M. A. Vaughan and Y. Shao, Inductively Coupled Plasmas in Analytical Atomic Spectrometry, Ed. A. Montaser and D. W. Golightly, VCH Publishers, Inc., N. Y. (1987) Chapter 10.
14. R. S. Houk, Anal. Chem., 58, 97A (1986).
15. D. J. Douglas and R. S. Houk, Prog. Anal. At. Spectrosc., 8, 1 (1985).
16. R. S. Houk, ICP Information Newslett., 10, 194 (1984).
17. D. J. Douglas, ICP Information Newslett., 10, 196 (1984).
18. A. L. Gray, ICP Information Newslett., 10, 200 (1984).
19. A. R. Date, ICP Information Newslett., 10, 202 (1984).
20. J. E. Cantle, ICP Information Newslett., 10, 206 (1984).

21. P. W. J. M. Boumans, Theory of Spectrochemical Excitation, Hilger and Watts, London (1966).

22. N. Furuta, Spectrochim. Acta, 40B, 1013 (1985).

23. N. Furuta, Spectrochim. Acta, 40B, 1115 (1985).

24. B. L. Caughlin, M. W. Blades, Spectrochim. Acta, 40B, 1539 (1985).

25. G. Horlick, S. H. Tan, M. A. Vaughan and C. A. Rose, Spectrochim. Acta, 40B, 1555 (1985).

26. S. H. Tan and G. Horlick, Appl. Spectrosc., 40, 445 (1986).

27. M. A. Vaughan, G. Horlick, Appl. Spectrosc., 40, 434 (1986).

28. S. H. Tan and G. Horlick, J. Anal. At. Spectrom., 2, 745 (1987).

29. M. W. Blades, B. L. Caughlin, Z. H. Walker and L. L. Burton, Prog. Anal. At. Spectrosc., 10, 57 (1987).

30. S. Greenfield, I. L. W. Jones, C. T. Berry and L. G. Bunch, Proc. Soc. Anal. Chem., 2, 111 (1965).

31. M. P. Lau, Dissertation, Dept. of Chem., Univ. of Alberta, Edm. AB., (1981).

32. E. H. Choot, Dissertation, Dept. of Chem., Univ. of Alberta, Edm. AB., (1983).

33. G. R. Kornblum, W. van der Waa and L. de Galan, Anal. Chem., 51, 2378 (1980).

34. P. A. M. Ripson, L. de Galan and J. W. Ruiter, Spectrochim. Acta, 37B, 733 (1982).

35. P. A. M. Ripson, E. B. M. Jansen and L. de Galan, Anal. Chem., 56, 2329 (1984).

36. R. C. L. Ng and G. Horlick, Appl. Spectrosc., 39, 834 (1985).

37. E. A. Stubley and G. Horlick, Appl. Spectrosc., 38, 162 (1984).

38. A. Batal, J. Jarosz and J. M. Mermet, Spectrochim. Acta, 37B, 511 (1982).

39. A. Montaser and V. A. Fassel, Appl. Spectrosc., 36, 613 (1982).

40. V. M. Goldfarb and H. V. Goldfarb, Spectrochim. Acta, 40B, 177 (1985).

41. E. H. Choot and G. Horlick, Spectrochim. Acta, 41B, 935 (1986).

42. A. Montaser, V. A. Fassel and J. Zalewski, Appl. Spectrosc., 35, 292 (1981).

43. E. H. Choot and G. Horlick, Spectrochim. Acta, 41B, 889 (1986).

44. E. H. Choot and G. Horlick, Spectrochim. Acta, 41B, 925 (1986).

45. A. Montaser and R. L. Van Hoven, CRC Critical Reviews in Analytical Chemistry, 18, 45 (1987).

46. A. Montaser, S-K Chan and D. W. Koppenaal, Anal. Chem., 59, 1240 (1987).

47. D. Hausler, Spectrochim. Acta, 42B, 63 (1987).

48. K. G. Tepperman and R. C. Elder, poster presented at ICP-MS Symposium, Muskoka Sands, Canada (1987).

49. J. Lam, Unpublished results.

Chapter 2

Experimental Conditions and Equipment Set-up

A. ICP-MS Instrumentation

A SCIEX ELAN Model 250 was used throughout this study. A schematic diagram of the instrument is shown in Figure 2-1. The ICP is a standard Plasma-Therm 2.5 kW system. The torch supplied with the instrument was replaced with a low-gas-flow torch manufactured by Sherritt Gordon Mines Ltd. (the so called MAK torch). The nebuliser (Meinhard) and spray chamber (Scott type) are all standard components. The load coil (4-turn) is centre tap grounded to prevent the formation of an arc discharge while undergoing the continuum mode of plasma extraction [1]. The location of the plasma box can be manually adjusted to provide three axes of movement, thus enabling alignment of the ion-path as well as relocation of the sampling depth (distance from the top of the load coil to the sampling orifice). The only modification to this assembly was the reconfiguration of the load coil in order that it extended out by about 1 cm, thus enabling sampling depth measurements to be made to within 5 mm of the load coil. The solution uptake to the nebuliser was controlled with the use of a Rabbit™ peristaltic pump by Rainin Instrument Co. Inc. This allowed a constant flow of sample at ~ 1 ml/min. The plasma gas was regulated using the provided gas flow controller while the nebuliser and auxiliary gas flow rates were controlled by Matheson Model 8240-0423 mass flow controllers.

Sampling of the plasma discharge into the mass spectrometer is achieved through a set of metallic cones. The first cone, termed the sampler, is made of copper and fabricated in the U of A machine shop. The second cone, the skimmer, is made of stainless steel and is supplied by the manufacturer. The space between the sampler and skimmer, the interface

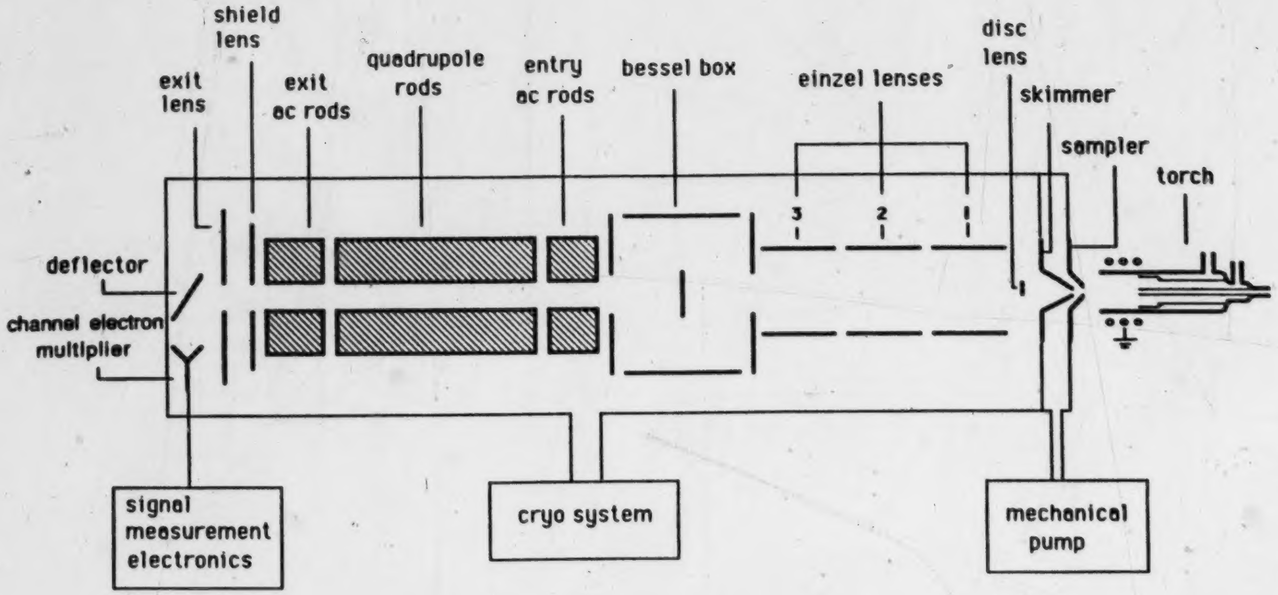

Figure 2-1. Schematic diagram of the SCIEX Elan 250 ICP-MS.

region, is evacuated by an Edward mechanical pump to maintain a pressure of about 1-2 torr during operation.

The mass spectrometer consists of 4 sets of electrostatic lenses* to direct and focus ions into the quadrupole mass filter [2]. The transmitted ions, selected according to their mass-to-charge ratios, are deflected by a high voltage deflector and detected by the off-axis channel electron multiplier (CEM). The pressure inside the mass spectrometer is maintained by a helium cooled cryo pump to provide a background pressure of about 10^{-7} torr and a temperature of 14 K when on stand-by mode and an operating pressure of about 10^{-5} torr when the plasma is running.

When in operation, the data acquisition is controlled by a turn-key Intel 16-bit microprocessor with the data stored automatically onto a 10 Mbyte Winchester hard disc. The raw data can then be transferred to a Macintosh personal computer where they can be reconfigured and manipulated using commercially available spreadsheet or graphic programs.

As reported by Vaughan and Horlick [2], the optimum voltage settings of the electrostatic lenses are a function of the mass-to-charge ratio of the ion species. The manufacturer recommends a standard optimisation procedure in order to obtain a somewhat uniform signal response for the whole mass spectrum. This tedious approach was not carried out to overcome the non-uniformity of the instrument response. Instead, the ion species chosen for each study were kept to a reasonably narrow mass range and the ion lenses were optimised with respect to a chosen isotopic mass at about the middle of the group of species chosen.

---

* Data obtained in this work, unless otherwise stated, were through a set of "retro-fit commercial quality" lenses supplied by the manufacturer.

Ion signals from the ICP can be acquired in either Elemental Mode or Range Mode. In the regime of quantitative analysis, the mass filter is set to function in Elemental Mode, in which the identities of the species have to be pre-determined. Under this condition, the mass filter acts like a programmable slew-scanning spectrometer by peak hopping to those pre-selected elemental masses. On the other hand, when qualitative information is desired, the mass filter is programmed to function in a Range Mode where the mass unit is set to increment sequentially per unit point until the full pre-set mass range is covered. The mass resolution obtained from the instrument can be High (H), Low (L) or somewhere in between (M). In the high resolution mode, the width of the peak is equivalent to 0.6 amu (atomic mass unit) at 10% peak height and the low resolution is considered to give an equivalent of 1 amu peak width at 10% from the base of the peak. In addition, the instrument is set-up to require 20 points and 10 points to define a peak under high and low resolution mode, respectively.

Unless otherwise stated, in the Elemental Mode, the ion signals were determined in the high resolution mode where each mass was sampled with 7 data points at the centre of the peak at 0.1 sec per point. Finally, the signal was averaged after 6 repeat measurements were taken. In the Range Mode, under which mass spectra were acquired, the resolution was set at High with measurement time taken at 1.0 sec/point.

B. Mixed Gas Plasmas

a. Gas Mixing

The mixing of argon with foreign gases (nitrogen, oxygen or air) was done prior to their introduction into the plasma discharge. Two rotameters (Matheson, East Rutherford, N. J.) were used to facilitate the gas mixing. For the introduction of a low percentage of mixed gas into the plasma gas stream, Matheson Model 605 and Model 603 flow tubes were used to regulate the gas flow for argon and the foreign gas respectively. The gas mixture was then fed to the flow controller of the SCIEX instrument in the usual way. In a similar fashion, a mixed nebuliser gas was accomplished using two Matheson 603 flow tubes and the resultant gas mixture was then fed to the Matheson mass flow controller.

b. Procedure for Lighting a Mixed Gas ICP

The plasma discharge was lit initially in a 100% argon environment. It was then allowed to settle down for about 20 minutes (arbitrary) after its initial generation. The foreign gas was then slowly introduced into the gas stream of the plasma discharge. Initially, the plasma was unstable due to a change in impedance of the plasma as a result of foreign gas introduction. The power coupled to the load coil was adjusted automatically by the servo-driven automatic matching network. Once the system had stabilized, an additional amount of foreign gas could be easily introduced into the plasma discharge. Despite the presence of the automatic matching network, the reflected power also increased with increasing amount of foreign gas. This was reduced by manual fine tuning of the capacitor.

C. Preparation of Chemical Solutions

a. Aqueous Solutions

The low concentration (parts per million 'ppm' or lower) standards were diluted from commercially available standard stock solutions (Spex Industries Inc., Edison, N. Y.). These were either standards for Plasma Emission Spectroscopy or Atomic Absorption Spectroscopy quality grades. The distilled/deionised water used in this work was obtained by feeding 'house' distilled water through a Millipore Mill-Q water purification system. For analyte solutions with concentrations more than 1000 ppm, they were prepared by the dissolution of analytical grade salts of individual elements in distilled/deionised water. Unless otherwise stated, each individual solution was made up into 2% (v/v) nitric acid (BDH Chemicals, Toronto and branches).

The acid spectra obtained in Chapter 5 were made up individually from concentrated acid that was doubly distilled from Vycor (purchased from Pfaitz and Bauer). Final concentrations were 2% (v/v), diluted by distilled water aforementioned.

Deuterium oxide was obtained from MSD Isotopes, Merck Frosst Canada Inc.

b. Non-aqueous Solutions

The organic standard solution of cadmium in xylene was in the form of cyclohexanebutyrate obtained from the U. S. Department of Commerce National Bureau of Standard SRM 1053a. Chemical reagents 2-ethylhexanoic acid was from Eastman Kodak Company, (Rochester N. Y. 14650) and 1-methylhexylamine was from Eastman Organic Chemical. The organic solvent xylene was from Terochem Laboratories Ltd., (Edmonton, Canada).

The solutions were prepared as directed in the instructions from NBS.

REFERENCES

1. D. J. Douglas and J. B. French, Spectrochim. Acta, 41B, 197 (1986).
2. M. A. Vaughan, G. Horlick and S. H. Tan, J. Anal. At. Spectrom., 2, 765 (1987).

Chapter 3

Analyte Signal Characteristics in ICP-MS:-

A Comparison of Argon and Mixed Gas Plasmas

A. Introduction

In spectrometric analysis using the ICP, argon has been almost exclusively used as the operating gas. However, this choice has several inherent limitations. From the stand-point of economic considerations, running an ICP on a regular basis consumes a large amount of this rather expensive gas. Although part of this operating cost has recently been offset by the availability of the so call "low-flow-torch", still, the replacement of argon with a less costly supporting gas would be beneficial. The utilization of argon is also restricted in specific applications where the spectral features originating from argon interfere with the species of interest. In the beginning, the reason for choosing argon as the operating gas was brought about by its relatively inert properties thereby avoiding the formation of undesirable by-products through side-reactions during the analysis. However, because of its inert behaviour, argon does not interact and destroy complicated non-aqueous type matrixes. Hence, this is generally not the gas of choice in the running of organic based media. Rather, a more combustible molecular gas such as oxygen is often used in this situation. For a comprehensive overview regarding the historical development and the performance of ICPs using foreign gases, several excellent review articles have been written on this subject [1-3].

The idea of utilizing molecular gases as part of the supporting gas in ICP analyses was initiated by Greenfield and coworkers. In fact, during his early development work with the

ICP [4], he used nitrogen solely as the cooling (outer) gas. However, this type of early generation design typically required high rf powers and high gas flow rates: 64 l/min nitrogen along with 20 l/min of argon. Due to this high demand for operating gases, the technique was costly to operate, and it did not receive proper recognition among the early ICP researchers. Also, the analytical performance from this type of ICP did not show any substantial improvement over the more economical design developed by other research groups [5, 6]. However, as early as 1970, Truitt and Robinson [7, 8] demonstrated that a nitrogen cooled ICP running at a rather modest rf power of 2 kW could be sustained at a much lower gas flow rate (22 l/min). By the late 1970's, other researchers were able to utilize mixed gas or pure molecular discharges with running conditions at comparable plasma powers and flow rates to those of the conventional argon discharge [9-20].

Some controversy regarding the overall analytical performance of mixed gas plasmas as compared to the standard argon discharge still remains. A summary has been documented by Boumans [21]. However, the general consensus is: when a low percentage of a foreign gas such as nitrogen, oxygen or air is mixed with argon as the outer gas, it not only provides a better signal to noise ratio but it also enhances the analyte sensitivity over the conventional argon discharge. These advantages, however, deteriorate rapidly with an increasing amount of foreign gas introduced into the plasma, that is, if the outer argon gas flow is completely replaced by the foreign gas.

In general, when foreign gases (nitrogen, oxygen, air) are introduced into the argon discharge, the physical volume of the plasma changes drastically. This physical transformation is understood to be mainly a result of the difference in the chemical nature of the foreign gas and gives rise to a net change in the thermal conductivity of the system. As a result, a strong temperature gradient develops. The establishment of this gradient enhances the migration of species from the colder to the hotter zone of the ICP and as a consequence, results in a net change in the physical volume of the plasma discharge.

Because of this additional driving force encouraging the migration of particles inside the plasma, better plasma-analyte interaction than is commonly observed in a pure argon ICP is enabled. In fact, in optical emission work using a 5-10% nitrogen mixed gas ICP, significant sensitivity enhancement has been observed especially in the case of ionic emission [10, 11, 20]. Since the fundamental basis of ICP-MS is the detection of charged ions, therefore the utilization of a low percent nitrogen mixed gas could be particularly attractive.

It has been observed, in ICP-MS, that analyte ion signals are strongly dependent on certain plasma operating parameters such as nebuliser flow rate, plasma power and sampling depth [22, 23]. An effective way to illustrate the dependence of ion signal on changes in the values of these parameters is to plot the ion signal versus nebuliser flow rate for a set of power or sampling depth values. In this study, these types of plots will be used to compare the ion signal obtained from 100% argon ICP's to the ion signals from ICP's based on mixed gases. For the most part, comparison will be made to 100% argon and nitrogen-argon mixed gas ICP's in which the outer (coolant) gas is 5 to 20% nitrogen. Some data will also be presented for oxygen and air mixed gas ICP's where 2.5 to 8% of the foreign gas is mixed into the outer argon gas flow and where nitrogen is added to the nebulising gas of an otherwise argon ICP.

A range of species was chosen for this study based on the following considerations. The elements studied were chosen to be relatively close in atomic mass in order to minimize mass discrimination effects, to have a wide range of ionization energies and to have a range of metal-oxide bond strengths. The elements chosen were Zn, Ge, As, Sr, Y, Zr and Ru (see Table 3-1). Most data were taken using a multi-element solution containing 0.2 ppm of each element in 2% nitric acid. Unless otherwise stated, the outer gas (argon or mixed gas) flow rate was 15 l/min, and the auxiliary gas (argon) flow rate was 1.80 l/min.

Table 3-1 Physical properties of some chosen elements used in this study.

Element	Mass	First IP (eV) [30]	D° (X-O) [30]	Calculated α[*1] [24]
Zn	64	9.39	2.91	0.745
Ge	73	7.9	6.78	0.9164
As	75	9.81	4.95	0.4887
Sr	88	5.69	4.27	0.9992
Y	89	6.38	7.37	0.9899
Zr	90	6.84	7.84	0.9931
Ru	99	7.37	4.95	0.9699
Te	128	9.009	4.01	0.6674
Cs	133	3.894	3.04	0.9998
Ba	137	5.212	5.62	0.9996
Ce	140	5.477	8.20	0.98[*2]

[*1] α Degree of ionization from reference [24] calculated using Ionization Temperature, T_{ion} = 6680 K and electron density, $n_e = 1.475 \times 10^{14}$ cm^{-3}.

[*2] α Degree of ionization from reference [38] calculated using T_{ion} = 7500 K and $n_e = 1.0 \times 10^{15}$ cm^{-3}.

B. Nitrogen Mixed Gas Plasma

a. Effects of Nebuliser Flow Rate and RF Power

Previous work in ICP-MS [22, 23] has illustrated the strong dependence of analyte ion signals on plasma operating conditions, in particular the dependence of the analyte ion signals on nebuliser gas flow rate and plasma power. As shown in Figure 3-1a, the signal profile acquired for Zn in a normal 100% argon ICP and at a sampling depth of 10 mm has a peak response at one particular nebuliser gas flow rate. As power is increased, the peak signal response shifts to a higher nebuliser gas flow rate. Vaughan and Horlick [23] related this shift to a spatial shift of the zone of maximum ion density in the ICP. This zone is situated 2-5 mm above the so called initial radiation zone (IRZ). The IRZ [25] is the zone low in the analyte channel at which neutral atom emission first appears and is known to retract into the analyte channel when rf power is increased. Thus, in ICP-MS, as power is increased, the nebuliser flow rate must also be increased to maintain the plasma ion zone at an optimal position with respect to the sampling cone.

The effect of adding 5% nitrogen to the argon outer gas of the ICP on the analyte signal response of Zn is shown in Figure 3-1b. Now a considerably higher flow rate is required to achieve peak signal intensity.

As mentioned in the introduction, one of the effects of the addition of nitrogen to the outer argon gas flow of the ICP is a reduction in the physical size of the plasma. As little as 5% N_2 in the outer gas results in about a 25% decrease in the size of the discharge. Thus, it is not really surprising that it takes a higher nebuliser flow rate to move the ion zone to the sampling cone which still is set at 10 mm from the top of the load coil.

Very similar trends and data have been observed for the other analytes studied. These data are shown in Figures 3-2 to 3-7 for Ge, As, Sr, Y, Zr and Ru. In addition, it should

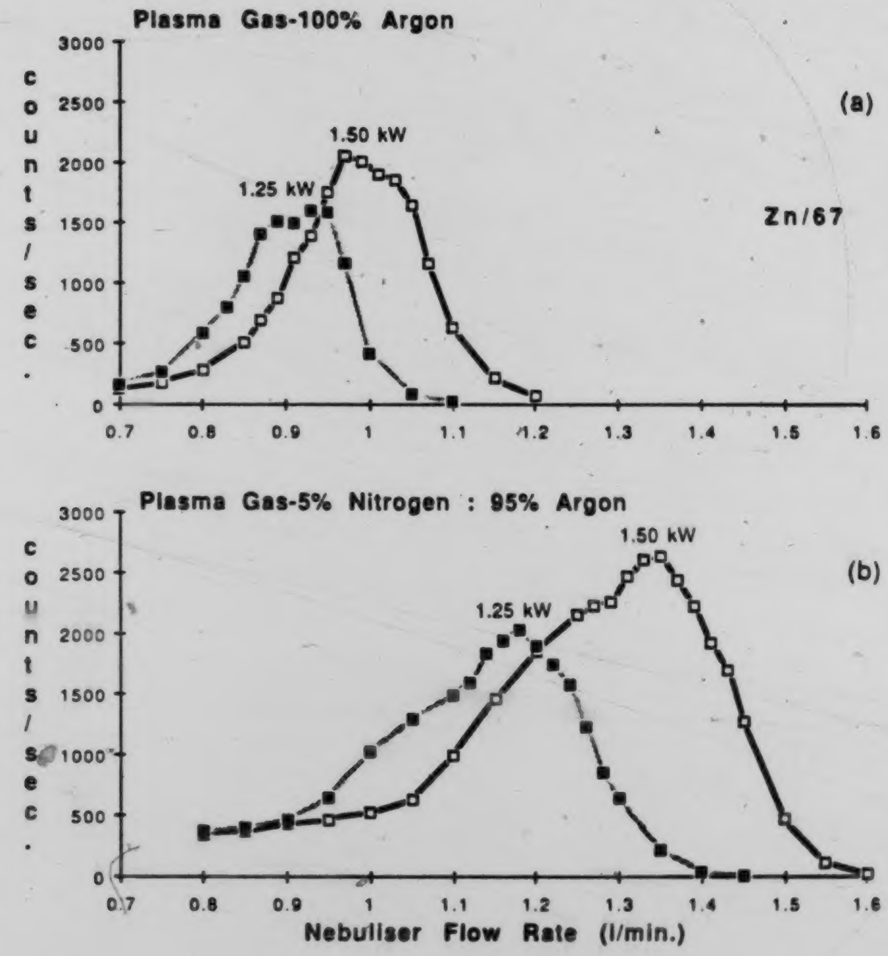

Figure 3-1. a) Dependence of Zn signal on nebuliser flow rate and plasma powers in a pure argon discharge. b) Dependence of Zn signal on nebuliser flow rate and plasma powers in a 5% nitrogen cooled discharge.

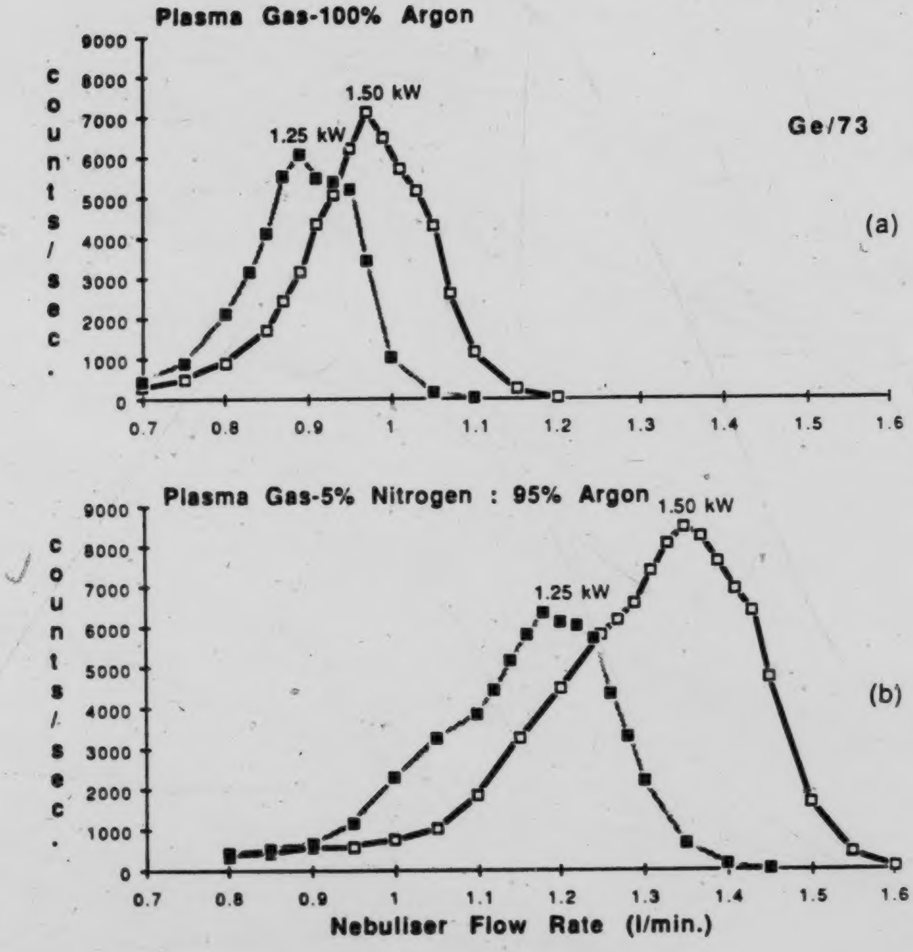

Figure 3-2. a) Dependence of Ge signal on nebuliser flow rate and plasma powers in a pure argon discharge (at 10 mm sampling depth). b) Dependence of Ge signal on nebuliser flow rate and plasma powers in a 5% nitrogen cooled discharge (at 10 mm sampling depth).

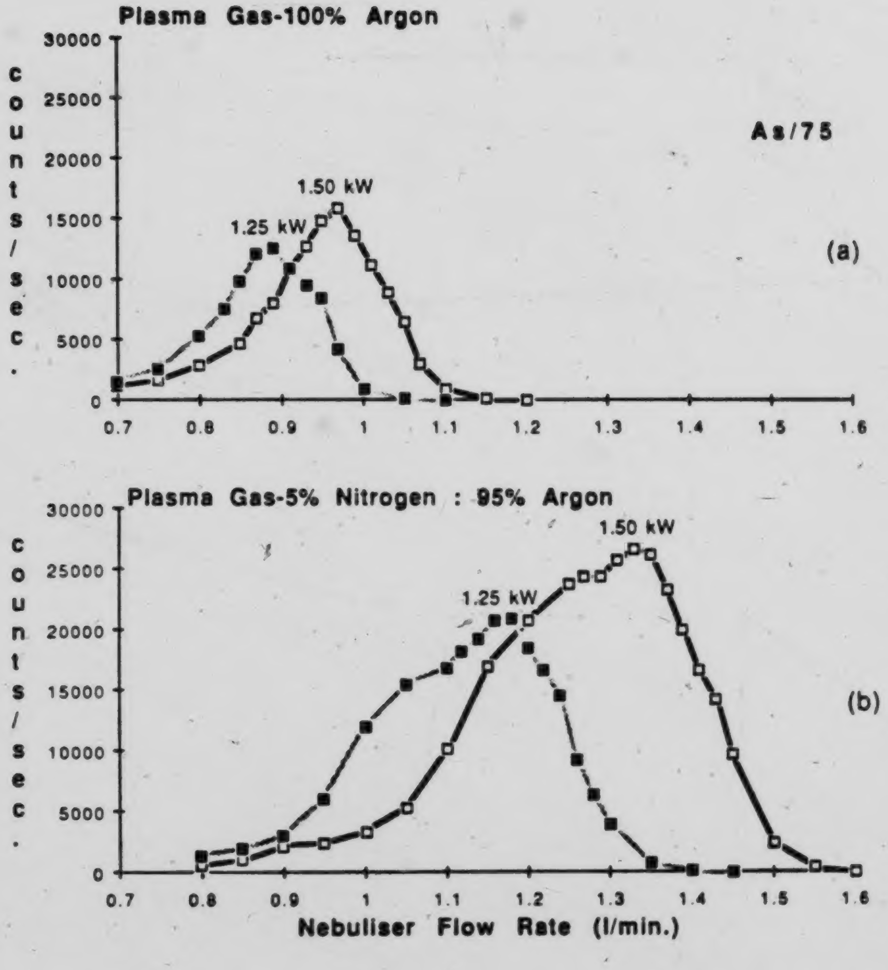

Figure 3-3. a) Dependence of As signal on nebuliser flow rate and plasma powers in a pure argon discharge (at 10 mm sampling depth).b) Dependence of As signal on nebuliser flow rate and plasma powers in a 5% nitrogen cooled discharge (at 10 mm sampling depth).

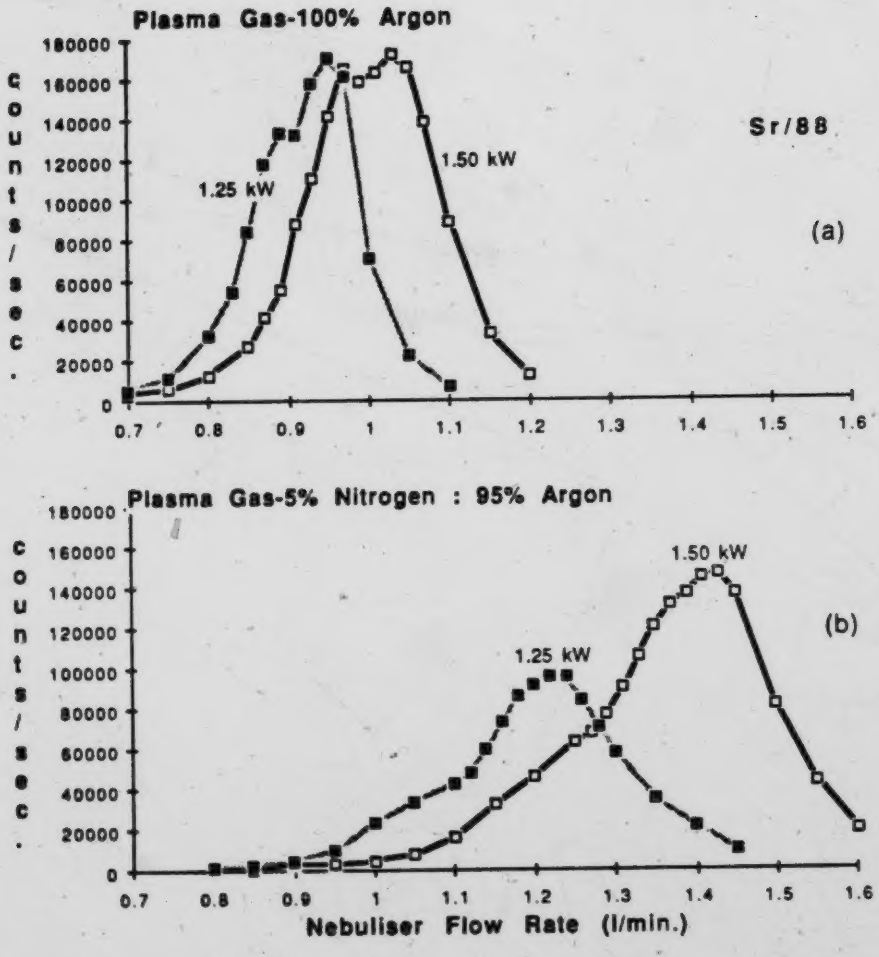

Figure 3-4. a) Dependence of Sr signal on nebuliser flow rate and plasma powers in a pure argon discharge (at 10 mm sampling depth). b) Dependence of Sr signal on nebuliser flow rate and plasma powers in a 5% nitrogen cooled discharge (at 10 mm sampling depth).

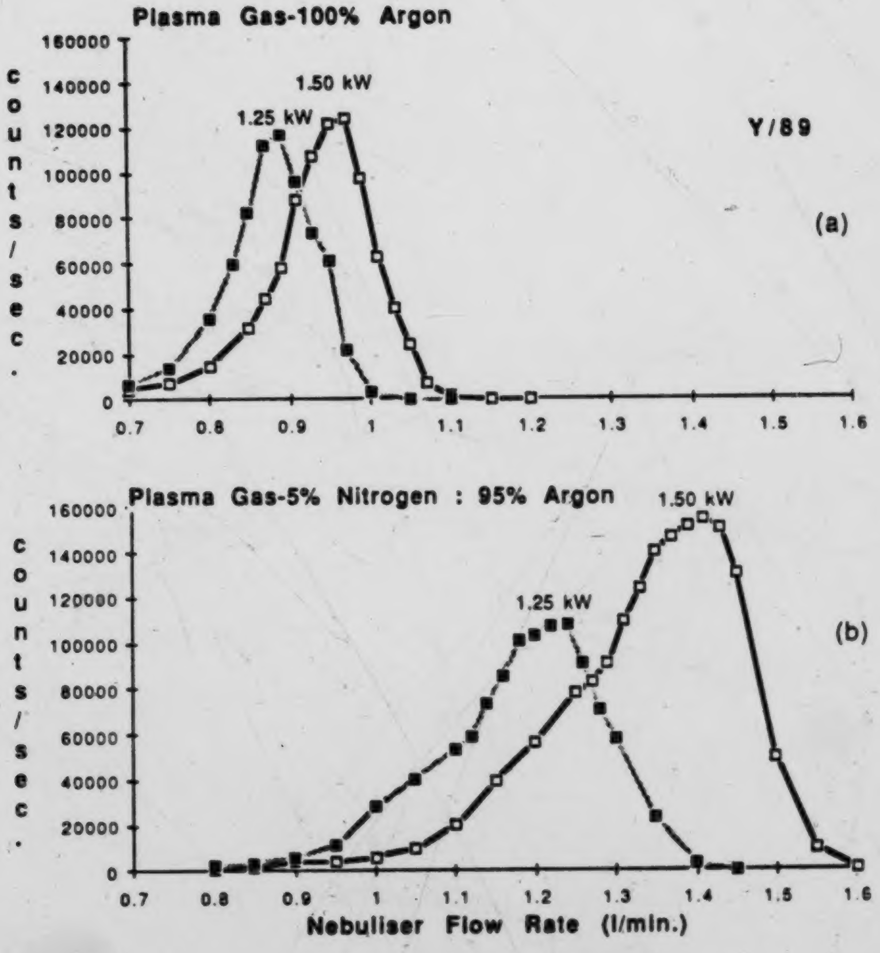

Figure 3-5. a) Dependence of Y signal on nebuliser flow rate and plasma powers in a pure argon discharge (at 10 mm sampling depth). b) Dependence of Y signal on nebuliser flow rate and plasma powers in a 5% nitrogen cooled discharge (at 10 mm sampling depth).

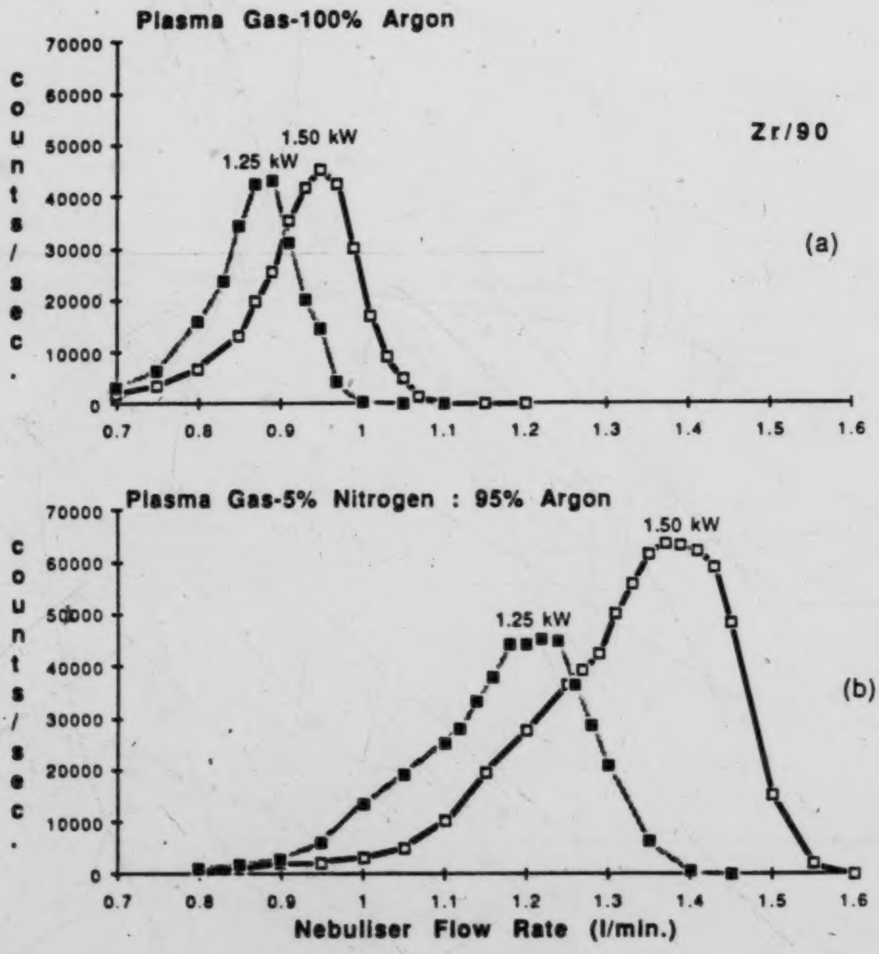

Figure 3-6. a) Dependence of Zr signal on nebuliser flow rate and plasma powers in a pure argon discharge (at 10 mm sampling depth). b) Dependence of Zr signal on nebuliser flow rate and plasma powers in a 5% nitrogen cooled discharge (at 10 mm sampling depth).

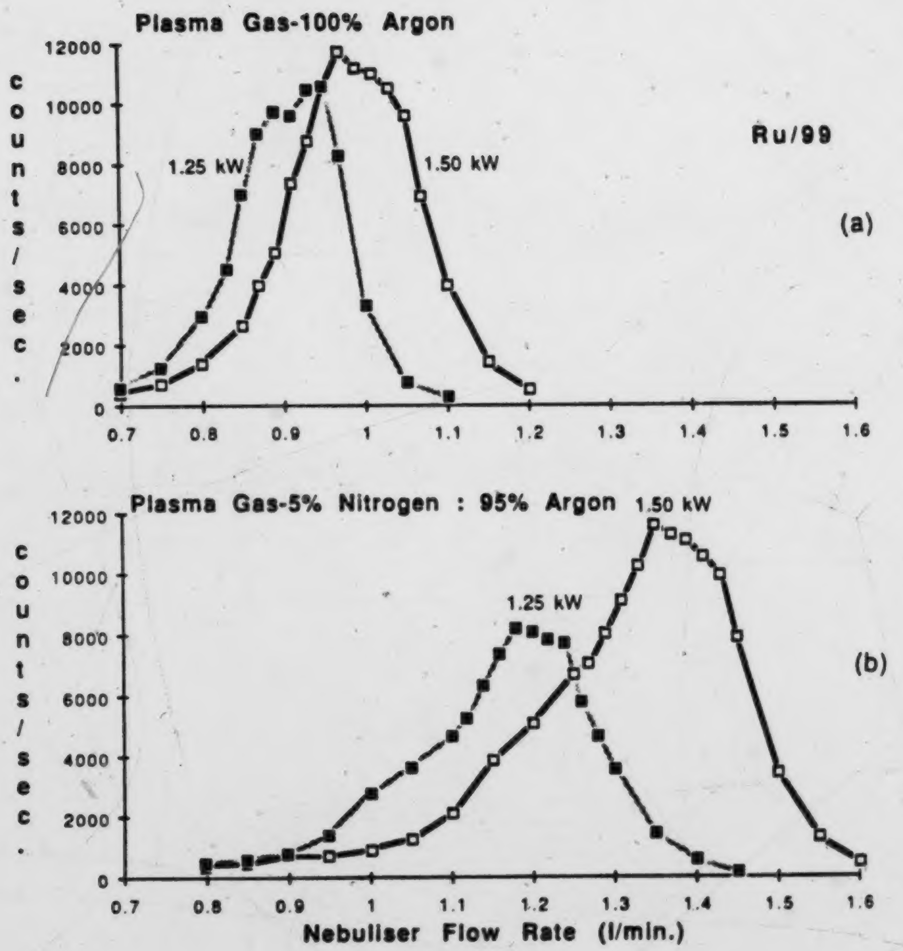

Figure 3-7. a) Dependence of Ru signal on nebuliser flow rate and plasma powers in a pure argon discharge (at 10 mm sampling depth). b) Dependence of Ru signal on nebuliser flow rate and plasma powers in a 5% nitrogen cooled discharge (at 10 mm sampling depth).

be noted that the peak signal responses are greater for most analytes in the mixed gas ICP than for the normal argon ICP. The signal enhancements, where they occur, are modest, at most a factor of 2, but they are an important consequence of the utilization of a mixed gas nitrogen plasma for ICP-MS. They will be discussed in more detail later.

In conclusion, the power-nebuliser flow rate relationship is consistent between the two types of plasma. This seems to reinforce the interpretation drawn by Vaughan and Horlick [23] earlier that the observed behaviour was in fact a spatial shift of the analyte ion zone of the plasma. With the addition of nitrogen into the outer gas, the contraction of the plasma results in a spatial shift of this zone towards the load coil. Thus, a higher nebuliser gas flow rate is necessary in order to push the ion cloud ~~closer~~ to the sampling orifice in the mixed gas plasma.

b. Effect of Sampling Depth

In the previous section, all measurements were carried out at one sampling depth, 10 mm. Because of the size changes involved in the plasma when nitrogen is added to the outer argon gas flow, it is important to map out the signal response at different sampling depths.

Signal ion response for the analyte species were observed using a 100% argon plasma as well as a 5% nitrogen cooled plasma. In both cases, the ion signals at sampling depths of 8, 9, 10 and 12 mm were measured. Plasma power was held at 1.50 kW while the nebuliser gas flow rate was changed in order to map out the nebuliser flow rate response profile at each sampling depth. The results are presented as in Figures 3-8 to 3-14 for Zn, Ge, As, Sr, Y, Zr and Ru.

For the 100% Ar plasma, there is little change in sensitivity as the sampling depth is decreased but, as would be expected, the peak signal response does shift to lower nebuliser

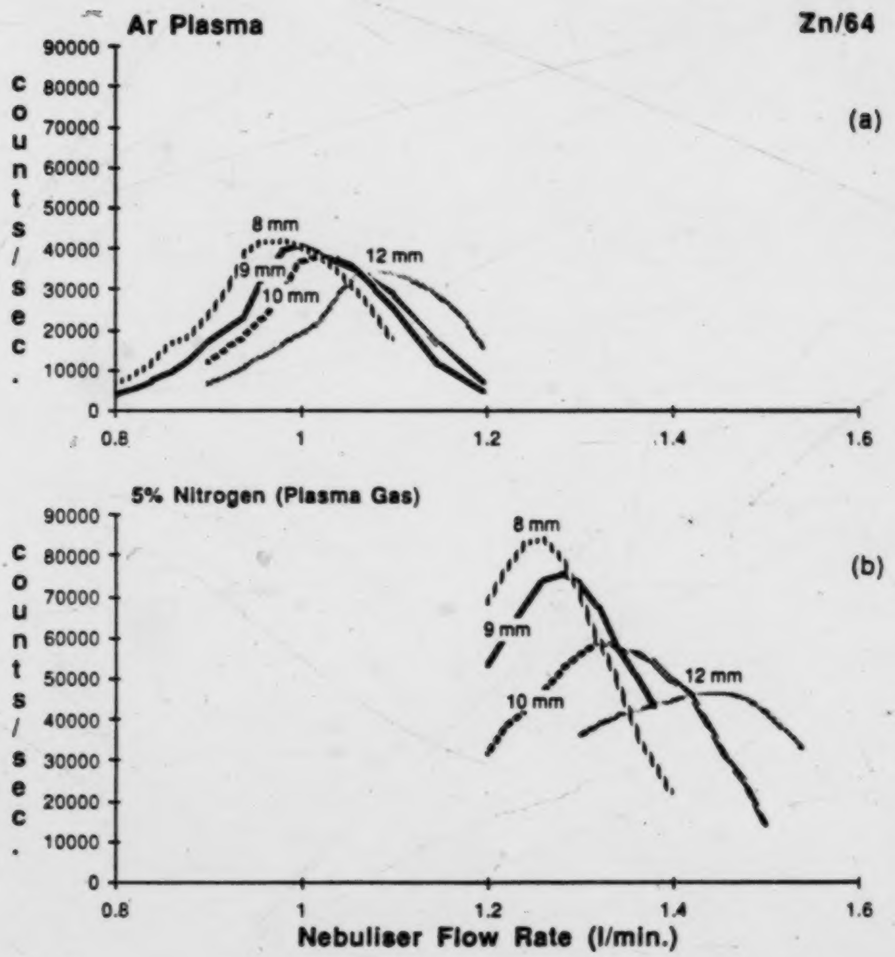

Figure 3-8. a) Dependence of Zn signal on nebuliser flow rate for a range of sampling depths in a pure argon discharge (at 1.50 kW). b) Dependence of Zn signal on nebuliser flow rate for a range of sampling depths in a 5% nitrogen cooled discharge (at 1.50 kW).

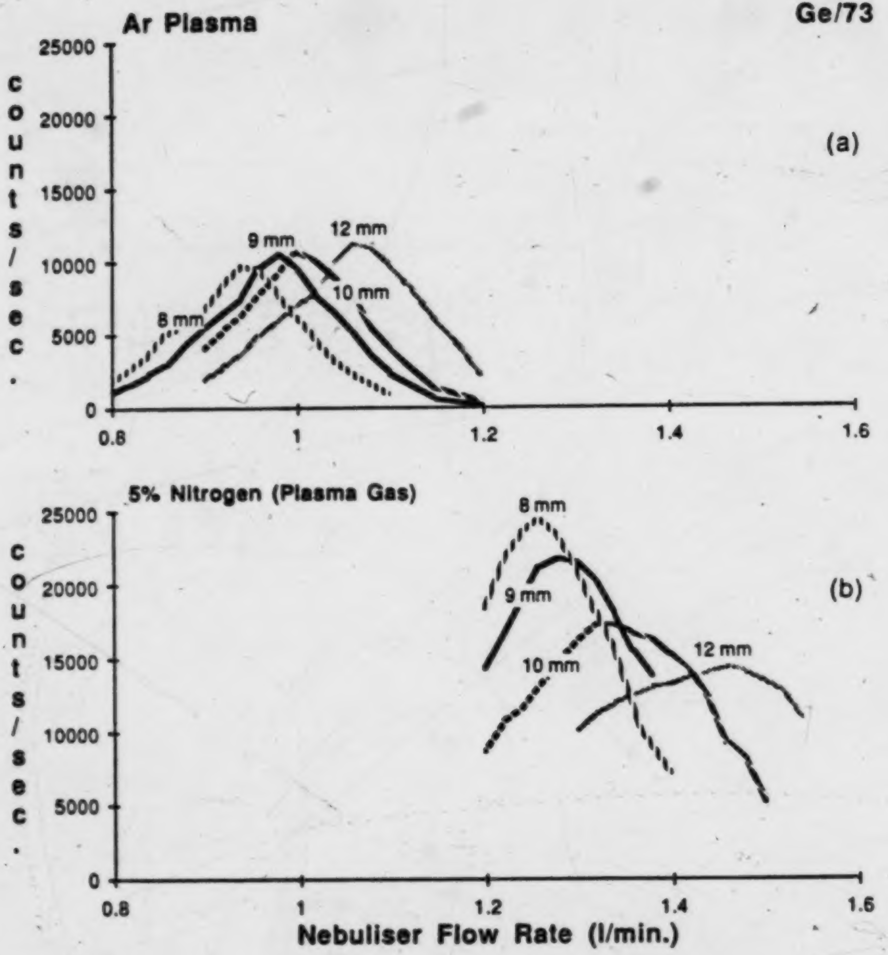

Figure 3-9. a) Dependence of Ge signal on nebuliser flow rate for a range of sampling depths in a pure argon discharge (at 1.50 kW). b) Dependence of Ge signal on nebuliser flow rate for a range of sampling depths in a 5% nitrogen cooled discharge (at 1.50 kW).

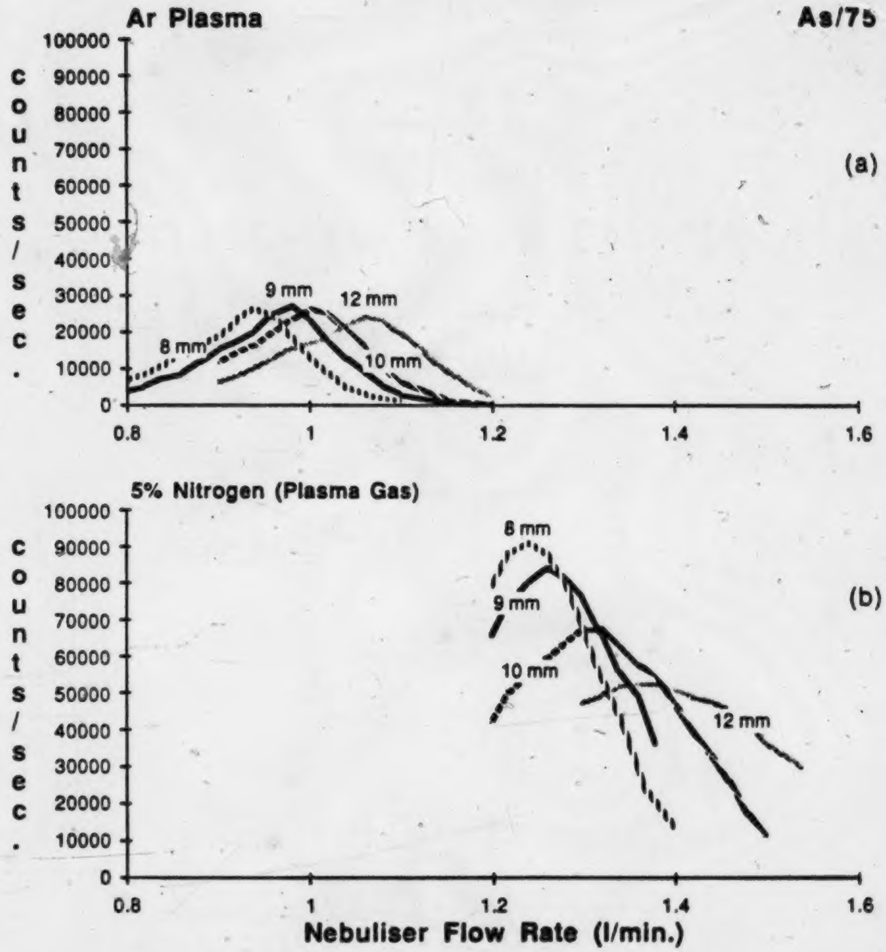

Figure 3-10. a) Dependence of As signal on nebuliser flow rate for a range of sampling depths in a pure argon discharge (at 1.50 kW). b) Dependence of As signal on nebuliser flow rate for a range of sampling depths in a 5% nitrogen cooled discharge (at 1.50 kW).

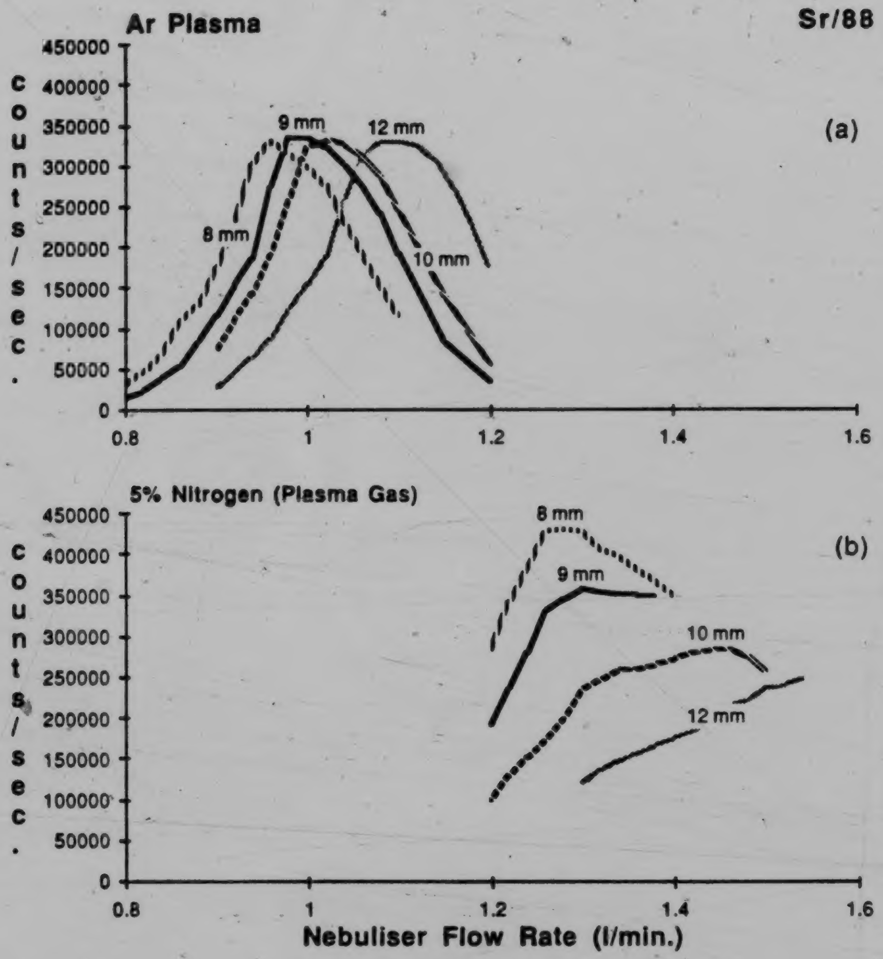

Figure 3-11. a) Dependence of Sr signal on nebuliser flow rate for a range of sampling depths in a pure argon discharge (at 1.50 kW). b) Dependence of Sr signal on nebuliser flow rate for a range of sampling depths in a 5% nitrogen cooled discharge (at 1.50 kW).

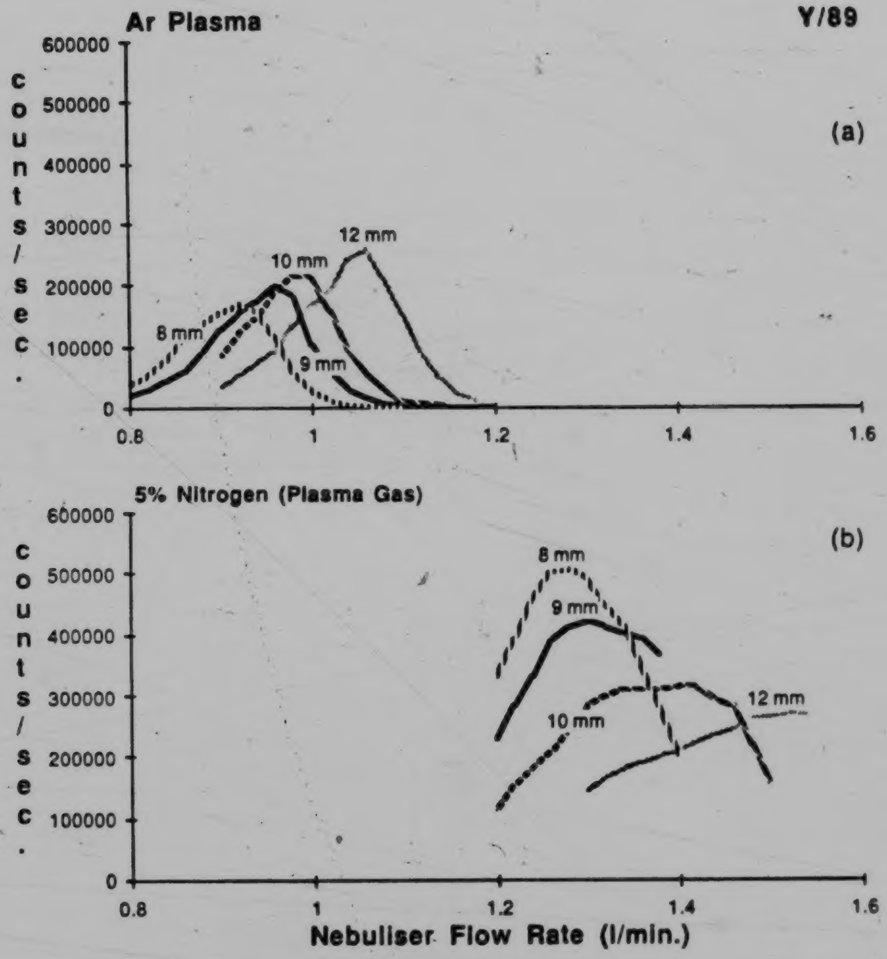

Figure 3-12. a) Dependence of Y signal on nebuliser flow rate for a range of sampling depths in a pure argon discharge (at 1.50 kW). b) Dependence of Y signal on nebuliser flow rate for a range of sampling depths in a 5% nitrogen cooled discharge (at 1.50 kW).

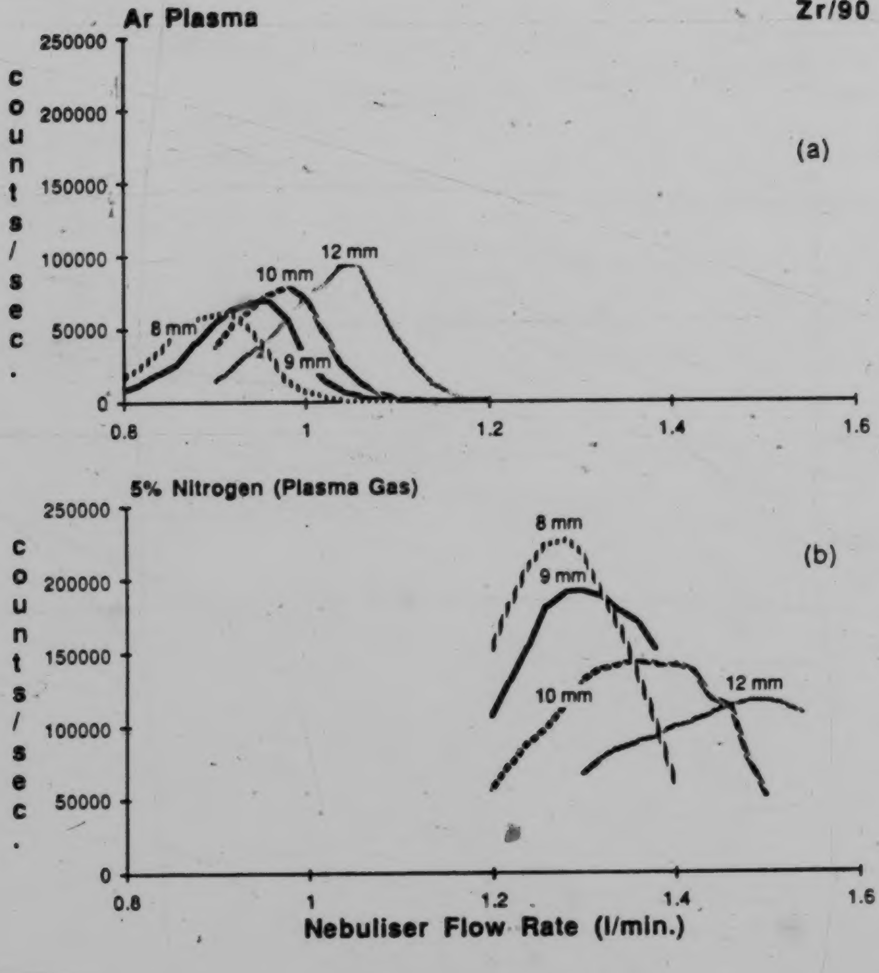

Figure 3-13. a) Dependence of Zr signal on nebuliser flow rate for a range of sampling depths in a pure argon discharge (at 1.50 kW). b) Dependence of Zr signal on nebuliser flow rate for a range of sampling depths in a 5% nitrogen cooled discharge (at 1.50 kW).

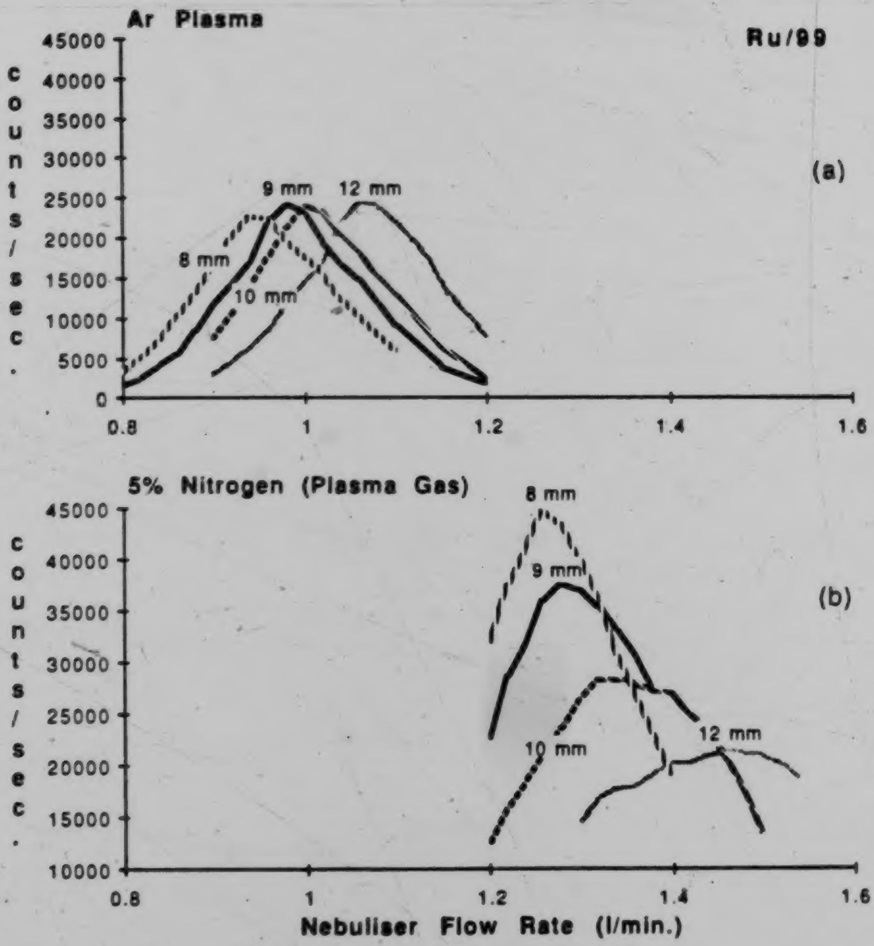

Figure 3-14. a) Dependence of Ru signal on nebuliser flow rate for a range of sampling depths in a pure argon discharge (at 1.50 kW). b) Dependence of Ru signal on nebuliser flow rate for a range of sampling depths in a 5% nitrogen cooled discharge (at 1.50 kW).

flow rates for smaller sampling depths. On the other hand, for the 5% nitrogen cooled plasma, the sensitivity increases significantly for the closer sampling positions and in particularly at the 8 mm sampling depth, it is generally superior to that of the Ar plasma by as much as a factor of 3 to 4.

Implicit in this comparison of sensitivity is the fact that the two plasmas are not being compared at the same nebuliser flow rate. It was found through out this study that meaningful comparison and correlation between these plasmas could only be made when, for all other conditions being equal, signal responses at the respective optimum nebuliser flow rates were utilized. Using this approach, the peak ion counts (with respect to nebuliser flow rate) were ratioed in order to compare the sensitivity between the two plasmas and these data are presented in Table 3-2 for all the analytes and sampling depths studied. From these results, it can be concluded that the 5% nitrogen cooled plasma has a superior sensitivity when compared to the 100% argon plasma. The sensitivity enhancement is most prominent at the closest sampling depth, and it is also dependent on the specific analyte. These enhancements will be correlated to attributes of the analytes in a later section.

c. Effect of Percent Nitrogen in the Outer Gas

Previous work with mixed gas plasmas in ICP-AES showed that the most dramatic and beneficial consequences of adding nitrogen to the outer gas came with the addition of only 5 to 10% nitrogen [10, 11, 20]. That is why the observations presented so far have been limited to a 5% nitrogen mixed gas plasma. However, it is of course necessary to determine the signal response in ICP-MS for higher nitrogen percentages. These data are shown in Figures 3-15 to 3-21 for nitrogen contents of 5%, 12% and 20% and for the analytes Zn, Ge, As, Sr, Y, Zr and Ru. The plasma power was 1.50 kW and the sampling depth was 10 mm.

Table 3-2 The signal intensity ratio for analytes obtained as a function of sampling depths using a 5% nitrogen cooled plasma to a 100% argon plasma. All comparisons were made at respective optimum nebuliser gas flow rates.

	Ion Intensity Ratio (Mixed Gas/Argon Plasma)			
Element	8 mm	9 mm	10 mm	12 mm
Sr	1.31	1.07	0.86	0.76
Y	3.02	2.12	1.46	1.04
Zr	3.75	2.77	1.81	1.25
Ru	1.98	1.56	1.17	0.88
Ge	2.53	2.08	1.61	1.27
Zn	2.01	1.86	1.59	1.36
As	3.47	3.10	2.59	2.15

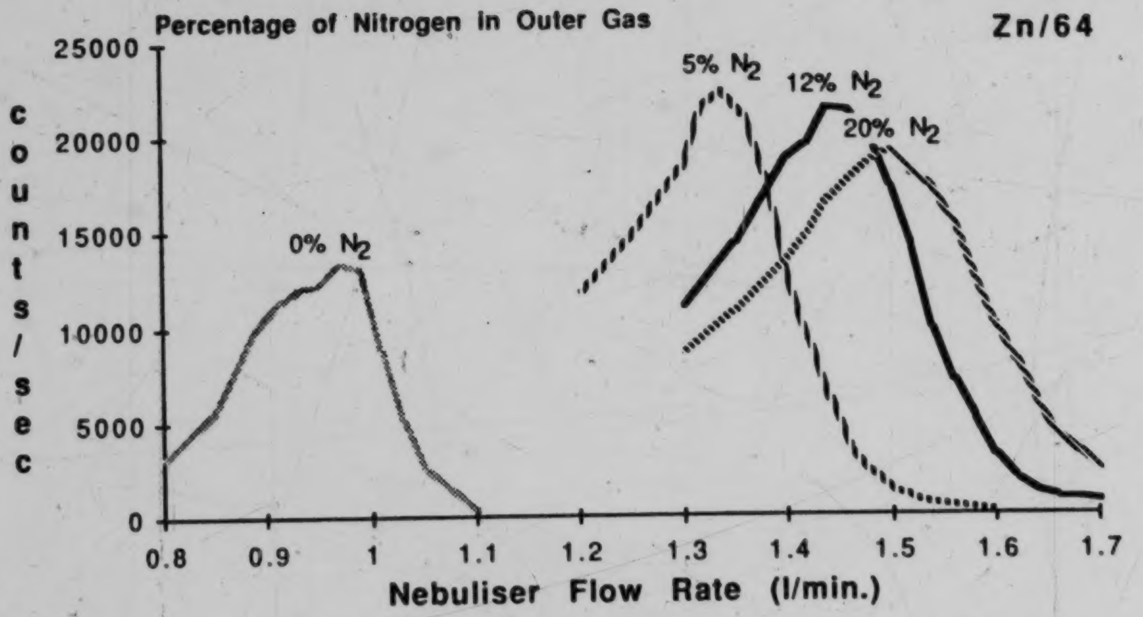

Figure 3-15. Dependence of Zn signal on nebuliser flow rate for a range of nitrogen mixed into the outer gas (at 1.50 kW and 10 mm sampling depth).

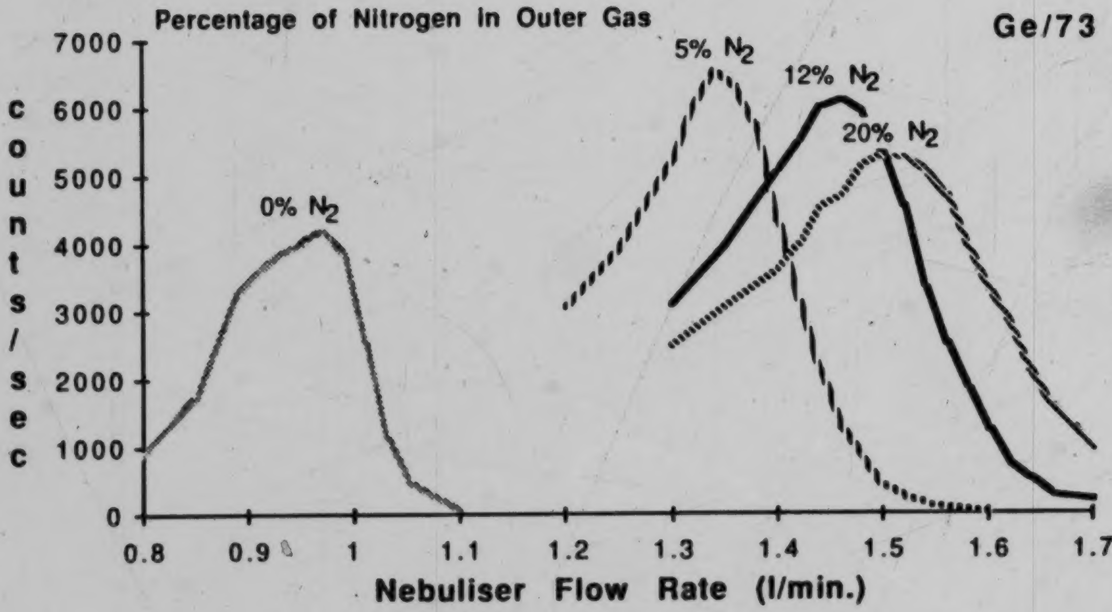

Figure 3-16. Dependence of Ge signal on nebuliser flow rate for a range of nitrogen mixed into the outer gas (at 1.50 kW and 10 mm sampling depth).

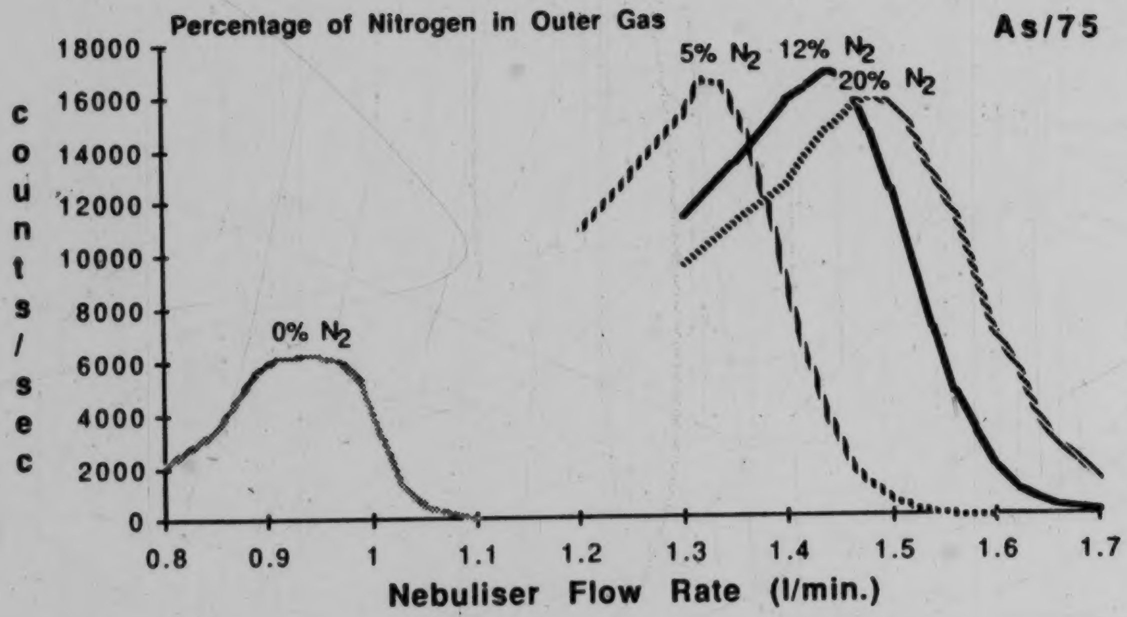

Figure 3-17. Dependence of As signal on nebuliser flow rate for a range of nitrogen mixed into the outer gas (at 1.50 kW and 10 mm sampling depth).

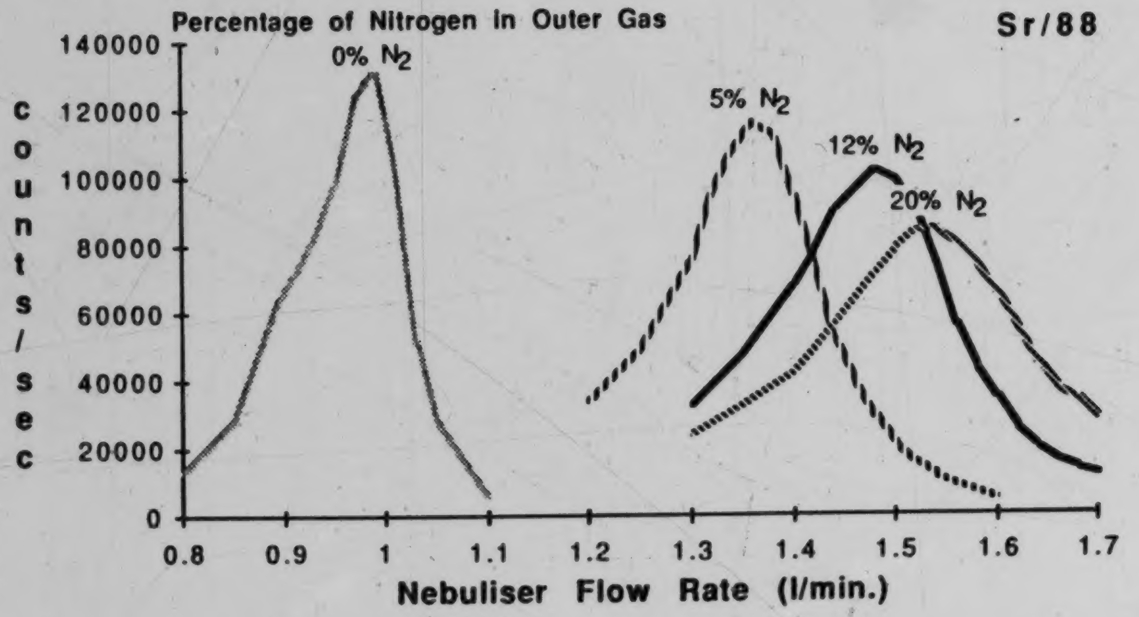

Figure 3-18. Dependence of Sr signal on nebuliser flow rate for a range of nitrogen mixed into the outer gas (at 1.50 kW and 10 mm sampling depth).

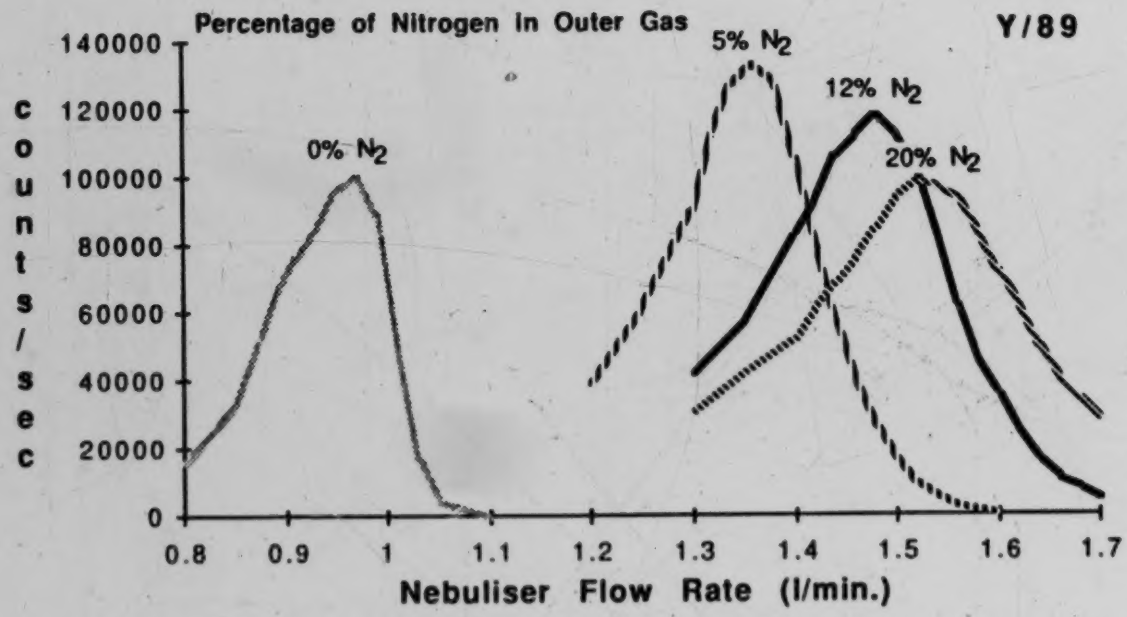

Figure 3-19. Dependence of Y signal on nebuliser flow rate for a range of nitrogen mixed into the outer gas (at 1.50 kW and 10 mm sampling depth).

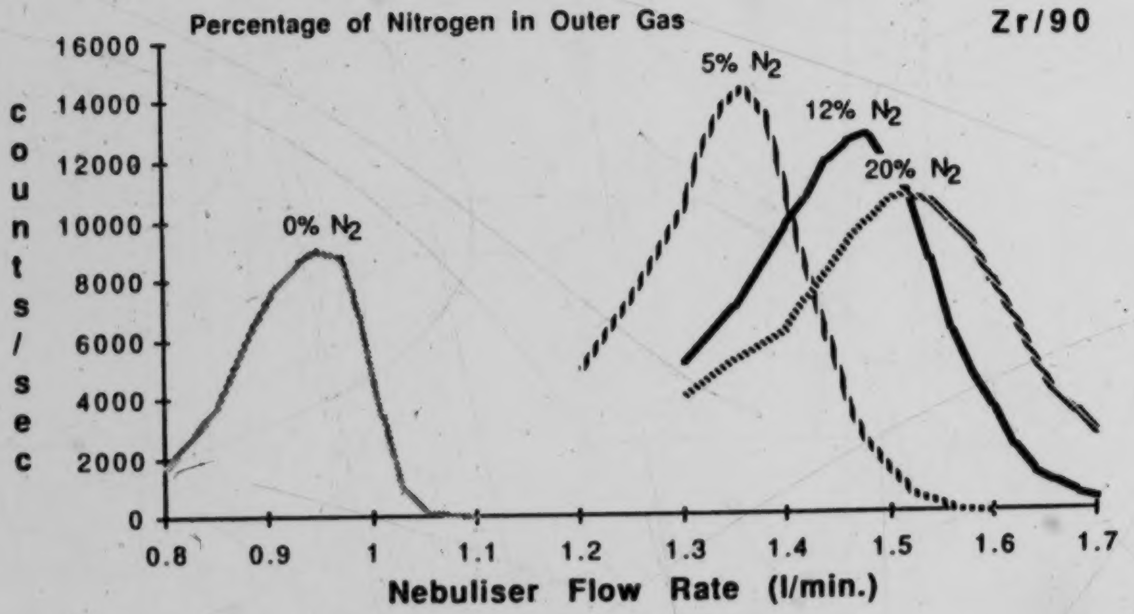

Figure 3-20. Dependence of Zr signal on nebuliser flow rate for a range of nitrogen mixed into the outer gas (at 1.50 kW and 10 mm sampling depth).

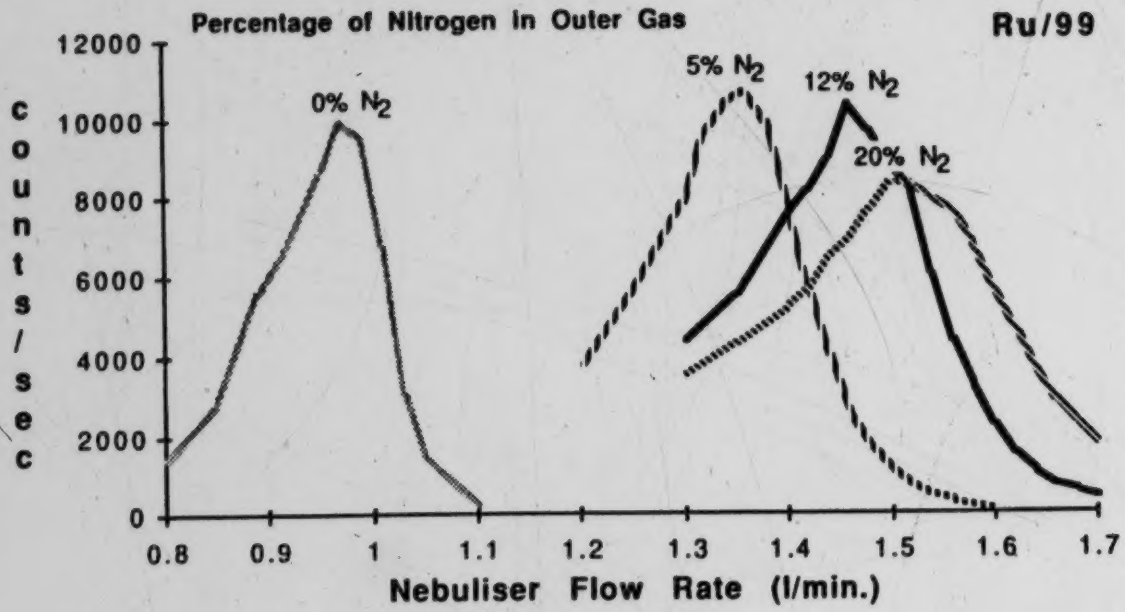

Figure 3-21. Dependence of Ru signal on nebuliser flow rate for a range of nitrogen mixed into the outer gas (at 1.50 kW and 10 mm sampling depth).

The sensitivity changes are summarized in Table 3-3 and again comparisons are made with respect to peak signal intensity obtained with the 100% argon plasma.

Overall, as the percentage of nitrogen is increased, the nebuliser flow rate must be increased in order to attain the peak response. This is consistent with the physical transformation of the plasma discharge (i.e. shrinking in size) as more nitrogen is added into the outer gas. Also, it is clear that the ion sensitivity decreases steadily as more nitrogen is added, although this effect is somewhat analyte dependent. Arsenic in particular, shows little decrease in sensitivity.

d. Effect of Percent Nitrogen in the Nebulising Gas

While the physical size of the plasma tends to shrink with the introduction of nitrogen into the outer gas, the plasma volume tends to hollow out when nitrogen is mixed into the nebulising gas. In addition, with nitrogen added into the nebulising gas, the plasma also becomes less stable and the tail plume of the discharge gives the appearance of being "blown off". With the physical dimensions of the discharge being altered to such an extent one expects the ion cloud to move further away from the load coil and thus favour a longer sampling depth. In this study, the sampling depth was set at 15 mm and the rf power at 1.50 kW. The elements chosen were Te, Cs, Ba and La. They were prepared as a multi-element solution containing 1.0 ppm concentration of each element in 2% nitric acid. Comparison of the analyte response was made between a 100% argon plasma discharge and a 20% nitrogen-argon mixed nebulising gas discharge.

The plasma parameters were the same as before with the exception that the auxiliary gas (Ar) flow rate was readjusted to 1.40 l/min.

Plots of ion signals as a function of nebuliser flow rate for the selected elements are shown in Figures 3-22 to 3-25. As can be seen from the data shown in each figure, a lower

Table 3-3 Ion signal intensity ratio for analytes obtained as a function of percent nitrogen in the outer gas to a pure argon plasma. Data were obtained at individual optimum nebuliser gas flow rates at 10 mm sampling depth.

	Ion Intensity Ratio (Mixed Gas/Argon Plasma)		
Element	5% Nitrogen	12% Nitrogen	20% Nitrogen
Sr	0.88	0.77	0.64
Y	1.32	1.17	0.98
Zr	1.59	1.42	1.19
Ru	1.06	1.02	0.81
Ge	1.51	1.39	1.18
Zn	1.68	1.61	1.43
As	2.66	2.68	2.49

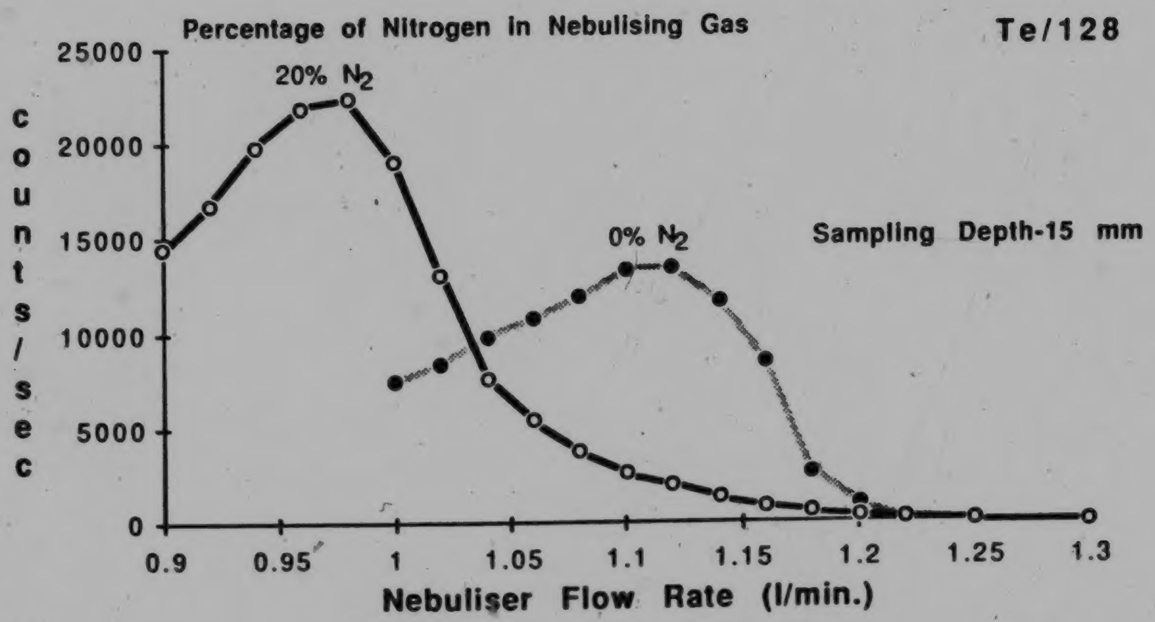

Figure 3-22. Effect of 20% nitrogen mixed nebuliser gas on Te at 15 mm sampling depth (at 1.50 kW).

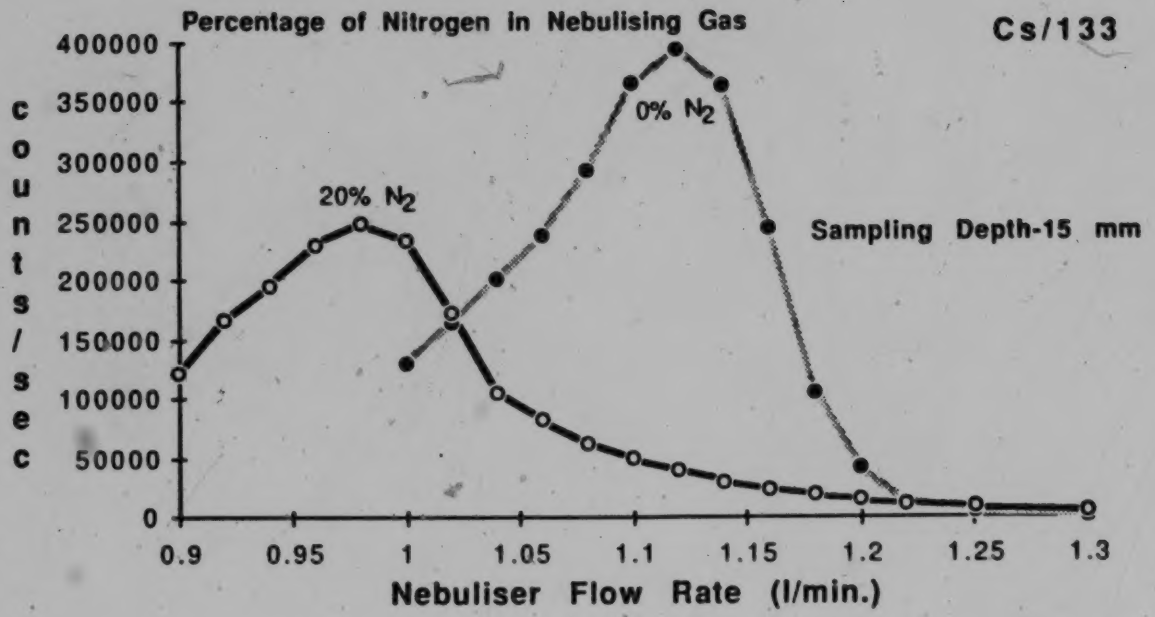

Figure 3-23. Effect of 20% nitrogen mixed nebuliser gas on Cs at 15 mm sampling depth (at 1.50 kW).

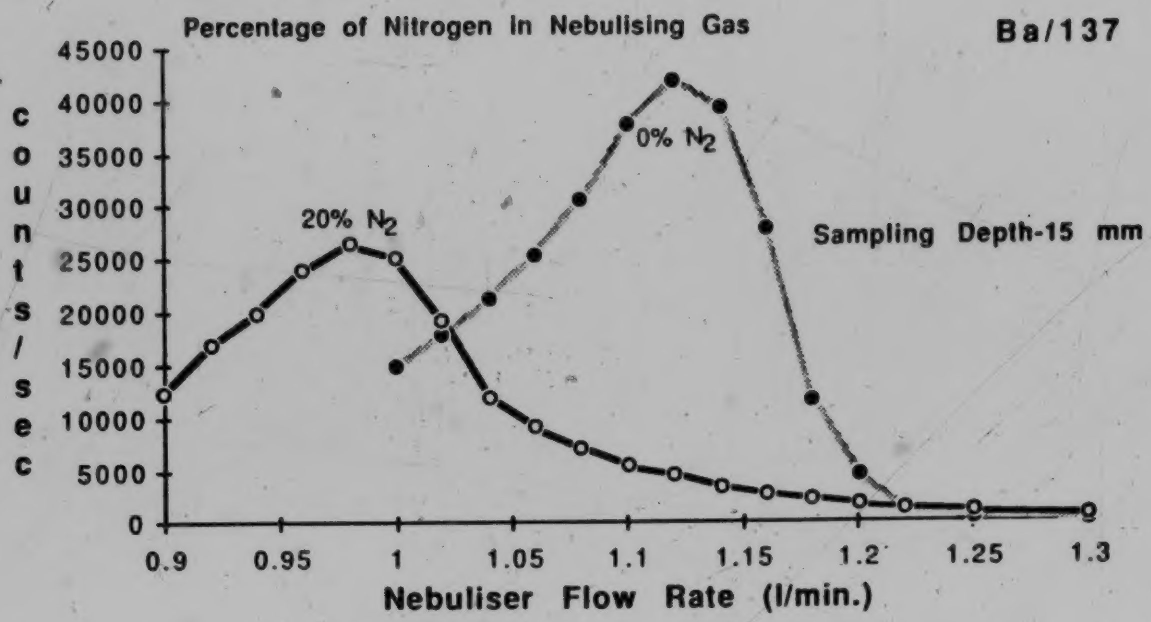

Figure 3-24. Effect of 20% nitrogen mixed nebuliser gas on Ba at 15 mm sampling depth (at 1.50 kW).

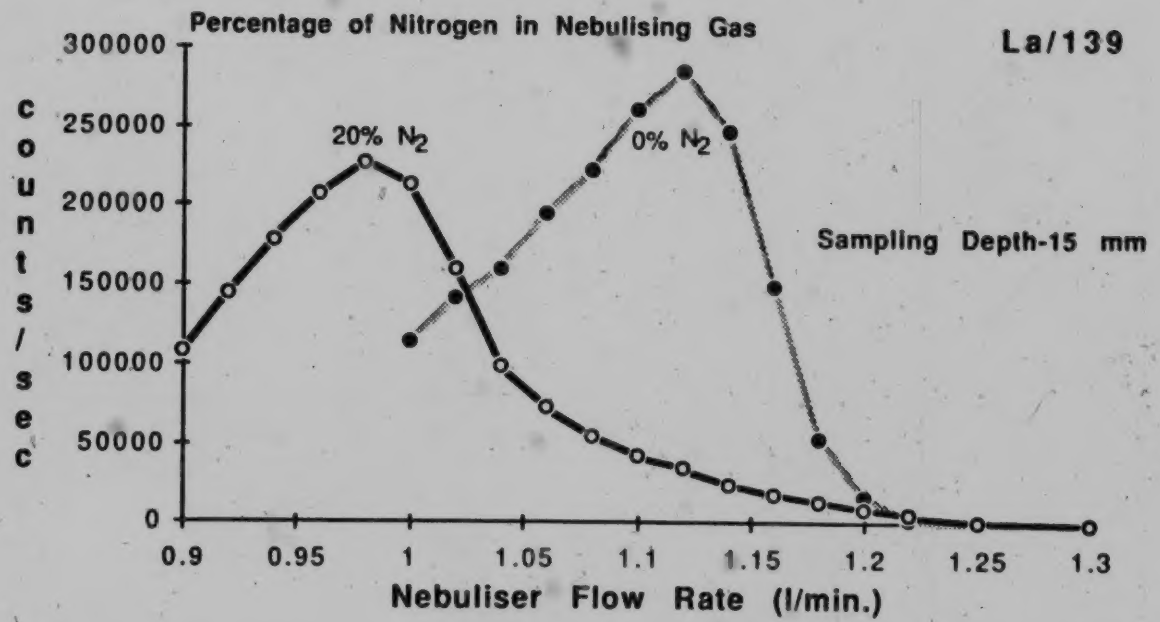

Figure 3-25. Effect of 20% nitrogen mixed nebuliser gas on La at 15 mm sampling depth (at 1.50 kW).

aerosol flow rate is necessary to attain the optimum ion signal when nitrogen is present. The two plasma types were again evaluated in terms of their analyte sensitivity by comparing the peak analyte signal intensity obtained from the two discharges and the ratioed results are presented in Table 3-4. From the rather limited data available, it is apparent that apart from the hard to ionize species (Te), the analyte sensitivity is inferior in the nitrogen mixed nebulising gas discharge compared to a 100% argon discharge.

e. Discussion

In addition to the shift of maximum signal intensity to higher nebuliser flow rates, one of the most interesting aspects of the addition of nitrogen to the plasma (outer) gas is the increase in signal intensities. So the question arises, where do these enhancements come from and why are they dependent on the analyte? A plasma with 5-10% nitrogen in the outer gas is known from atomic emission studies to be a more energetic source with a higher ionization temperature and increased emission for ionized analytes [10, 11, 20, 26]. Thus, an initial speculation could be that the observed sensitivity enhancements in ICP-MS might be due to the increase in the degree of ionization and be related to the ionization potential of the analyte. However, this is not the case. Bar graphs for the elements studied plotted as a function of ionization potential, degree of ionization and signal enhancement are shown in Figure 3-26. The data were taken from Tables 3-1 and 3-2. Clearly signal enhancement does not correlate to ionization potential. Also, based on the calculated degrees of ionization, it is impossible to obtain the observed signal enhancements by further ionizing these elements. Even for As, the most one could expect is about a factor of two increase and elements such as Y and Zr which also show significant enhancements are already calculated to be almost 100% ionized. The calculated degrees of ionization in Table 3-1 are regarded to be reliable and realistic, thus other factors must be dominant in controlling the ion population in this case.

Table 3-4 Physical properties of some chosen elements as well as the ion sensitivity ratio from a 20% nitrogen mixed nebulising gas to the argon plasma. The ion intensity ratio was acquired at the individual optimum nebuliser flow rate.

Element	Mass	IP (eV)	D° (X-O)	Signal Intensity Ratio
Cs	133	3.894	3.04	0.63
Ba	137	5.212	5.62	0.63
La	139	5.577	8.25	0.80
Te	128	9.009	4.01	1.66

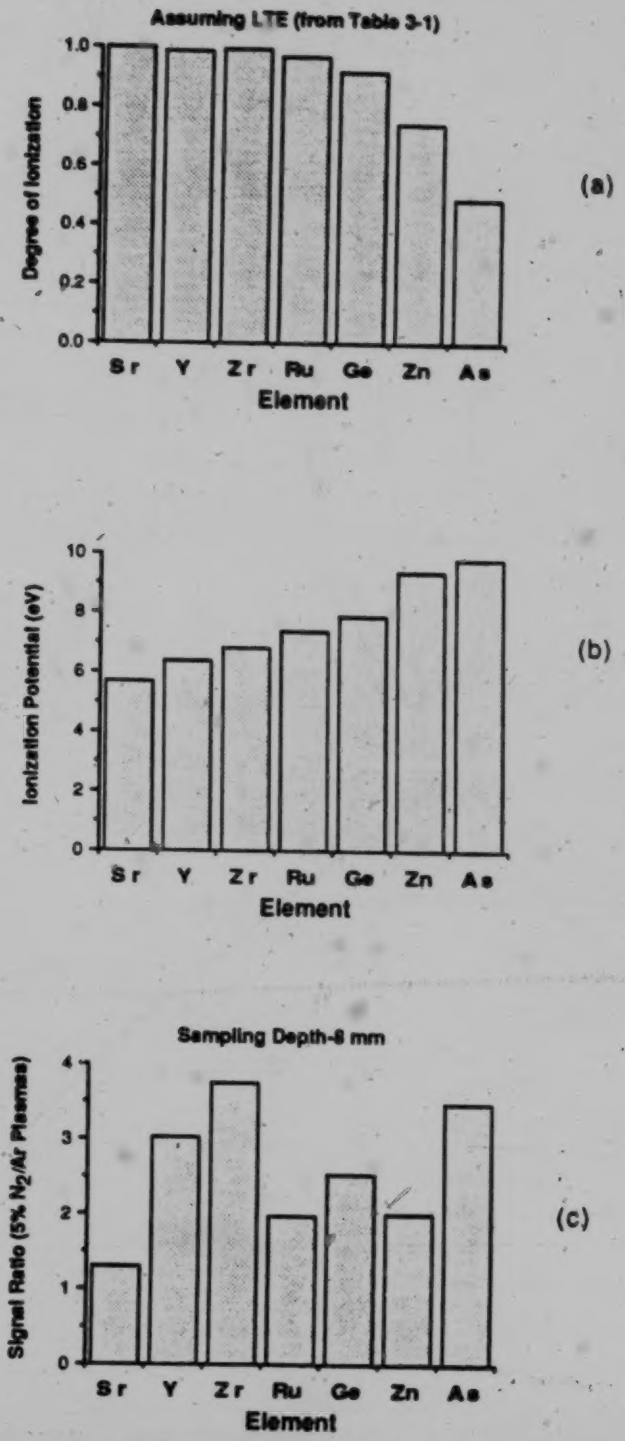

Figure 3-26. a) Figure to illustrate the degree of element ionization in ICP (from Table 3-1). b) Figure to illustrate elemental ionization energy. c) Figure to illustrate the degree of signal enhancements from a 5% nitrogen cooled plasma at the sampling depth of 8 mm.

It is possible from our data to make an estimate of the degree of ionization or what might better be called an "apparent degree of ionization". For the elements studied, Sr has the lowest ionization potential. It also has a relatively low metal-oxide bond strength and it is thus most likely to be 100% ionized and exist as the free ion. Using it as a reference and the signal levels measured in the previous section, the "apparent degree of ionization" of the other elements can be calculated relative to Sr considering, of course, concentration on a molar basis and taking into account the natural abundance of the observed isotopes. The calculations were not corrected for mass discrimination effects but the elements are not too divergent in mass, ranging only from 64 to 99.

The results of this calculation are summarized in Table 3-5 for the argon plasma and the mixed gas plasma for all the sampling depths. In addition, results for the 100% argon plasma at 12 mm and the 5% nitrogen plasma at 8 mm are plotted in Figure 3-27 along with the theoretical degree of ionization data from reference [24]. These results are really quite interesting. The "apparent degrees of ionization" in the argon plasma do not agree very well with the theoretical values. The "degree of ionization" is low in all cases and the trend is poor. On the other hand the values obtained for the nitrogen mixed gas plasma, although still low, are much closer to the theoretical values and they also follow the correct trend on an element by element comparison. In particular, Y and Zr are brought back into line. These two elements are unique from another point of view. As can be seen from the data shown in Table 3-5 for the argon plasma, they are the only elements to show an increase in this "apparent degree of ionization" as sampling depth increases. In addition, Y and Zr also have the highest metal oxide bond energies within this group of analytes (see Table 3-1). Thus, the evidence starts mounting that it is a vaporization attribute of these elements that should be correlated to the nitrogen mixed gas plasma signal enhancements. This correlation is shown in Figure 3-28 where bar graphs of the signal enhancements and the metal oxide bond energies are presented. Thus, it seems that the signal enhancements

Table 3-5 **The calculated "Apparent Degree of Ionization, α" for analytes obtained with a 100% argon plasma as well as with a 5% nitrogen cooled discharge at sampling depths from 8 to 12 mm.**

	Calculated α values with respect to Sr Signal							
	100% Argon Plasma				5% Nitrogen Plasma			
Element	8 mm	9 mm	10 mm	12 mm	8 mm	9 mm	10 mm	12 mm
Sr	~ 1	~ 1	~ 1	~ 1	~ 1	~ 1	~ 1	~ 1
Y	0.43	0.50	0.54	0.66	0.98	0.99	0.92	0.91
Zr	0.31	0.34	0.40	0.47	0.88	0.89	0.83	0.78
Ru	0.56	0.54	0.54	0.55	0.78	0.79	0.74	0.65
Ge	0.26	0.28	0.28	0.30	0.50	0.54	0.53	0.51
Zn	0.16	0.15	0.14	0.13	0.25	0.27	0.26	0.24
As	0.056	0.057	0.055	0.052	0.15	0.16	0.17	0.15

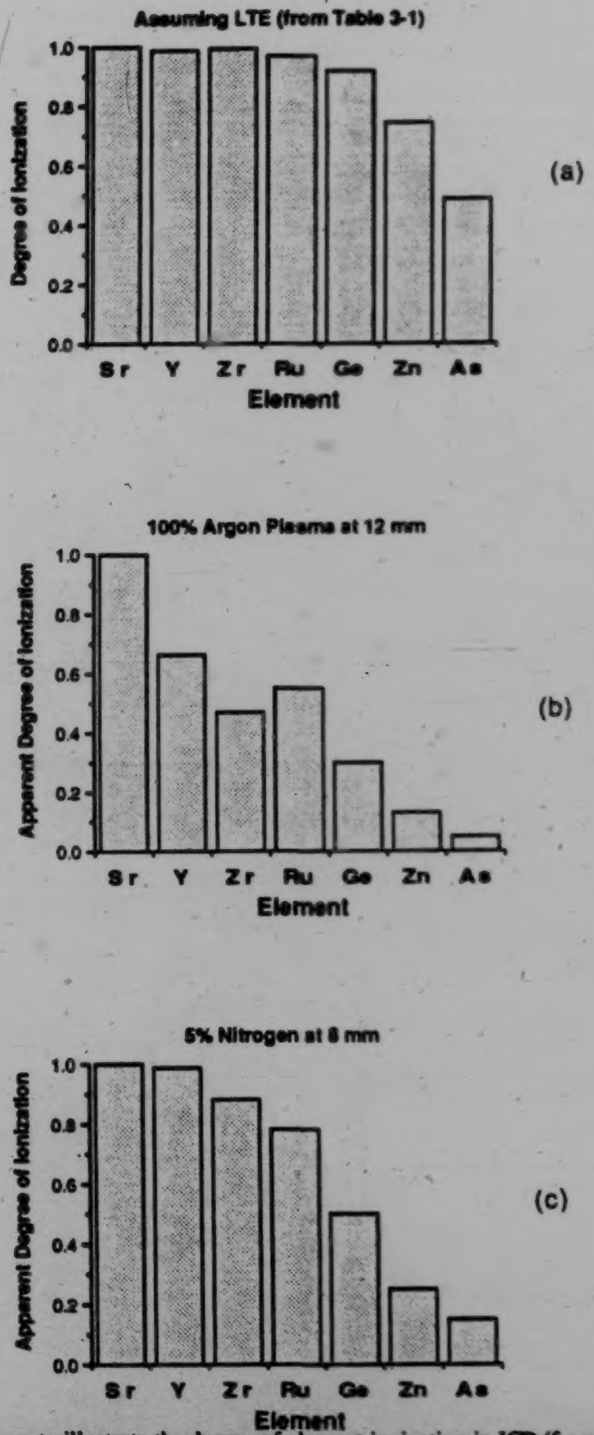

Figure 3-27. a) Figure to illustrate the degree of element ionization in ICP (from Table 3-1). b) Figure to demonstrate the "apparent degree of element ionization" obtained from an argon plasma at 12 mm sampling depth. c) Figure to demonstrate the "apparent degree of element ionization" obtained from a 5% nitrogen cooled plasma at 8 mm sampling depth.

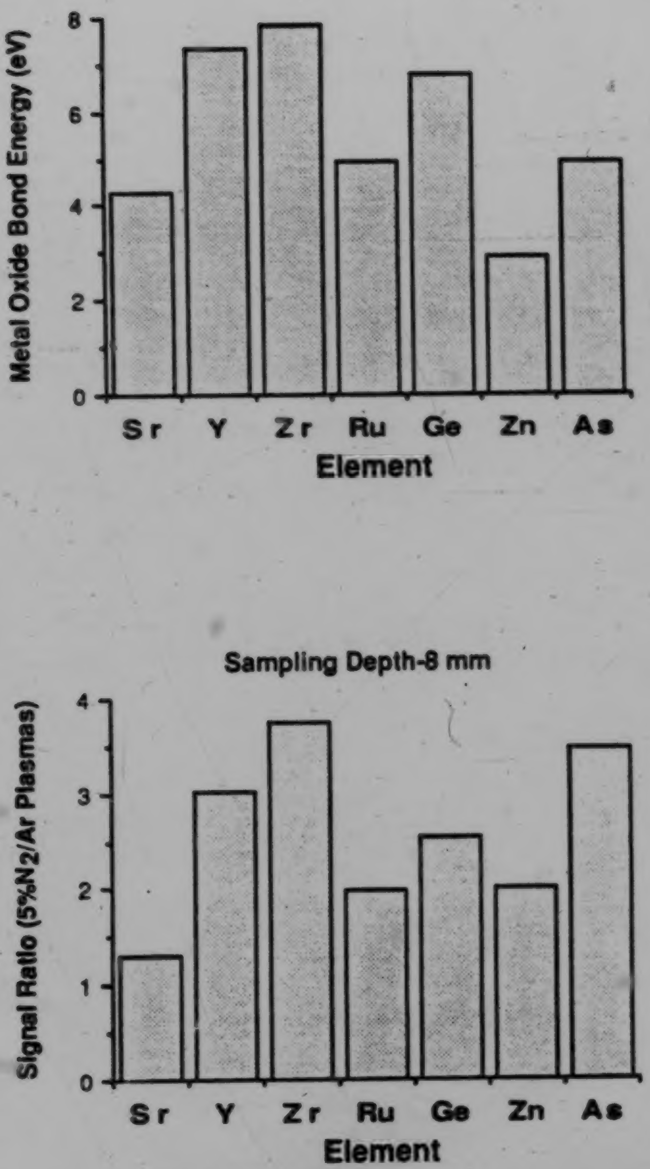

Figure 3-28. Bar graphs to correlate the metal oxide bond energy for elements to signal enhancements observed with a 5% nitrogen cooled plasma at 8 mm sampling depth (in the order of increasing ionization potentials).

observed with the addition of nitrogen to the plasma gas are directly related to the degree to which an analyte forms an analyte oxide in the argon ICP. This conclusion ties in with the observation mentioned above, that the apparent degree of ionization of Y and Zr increase with sampling depth in the argon plasma. It would appear that with the increased sampling depth more time is allowed for the vaporization of these refractory oxides and hence the observed signal increase. In the 5% nitrogen plasma, on the other hand, the oxides are dissociated "earlier" and hence there is no increase in apparent degree of ionization as a function of increased sampling depth.

This correlation is not perfect. If the data shown in Figure 3-28 are rearranged in the order of increasing metal oxide bond energy (see Figure 3-29), it can be seen that Zn and As have anomalous behaviour. They are enhanced to a greater extent than would have been expected if the consideration is only based on their oxide bond energy. Zn and As are, however, related in that they have the highest ionization potentials of this group. Thus there are two aspects to the enhancement; one related to oxide bond strength for elements with low ionization potential and the other one related solely to ionization energy of the analytes (see Figure 3-30). Hence, if an element has a degree of ionization substantially less than 1, then the nitrogen plasma can increase the signal level, in part, by increasing α. This was also shown in Figure 3-27.

Two other very interesting correlations evolve out of the correlation of nitrogen mixed gas plasma signal enhancement to analyte mono-oxide bond energy. What transpires is a model to correlate the position of peak analyte response as a function of nebuliser flow rate to an analyte attribute. When aerosol is introduced into the central channel of the plasma (100% Ar), it can be thought of as traveling along a process stream in which the aerosol is desolvated, molecular analyte species are formed (oxides among them), then are dissociated into atomic species which are finally ionized and sampled into the mass spectrometer. All this happens over 2 to 3 cm from the point of introduction into the plasma. It can certainly

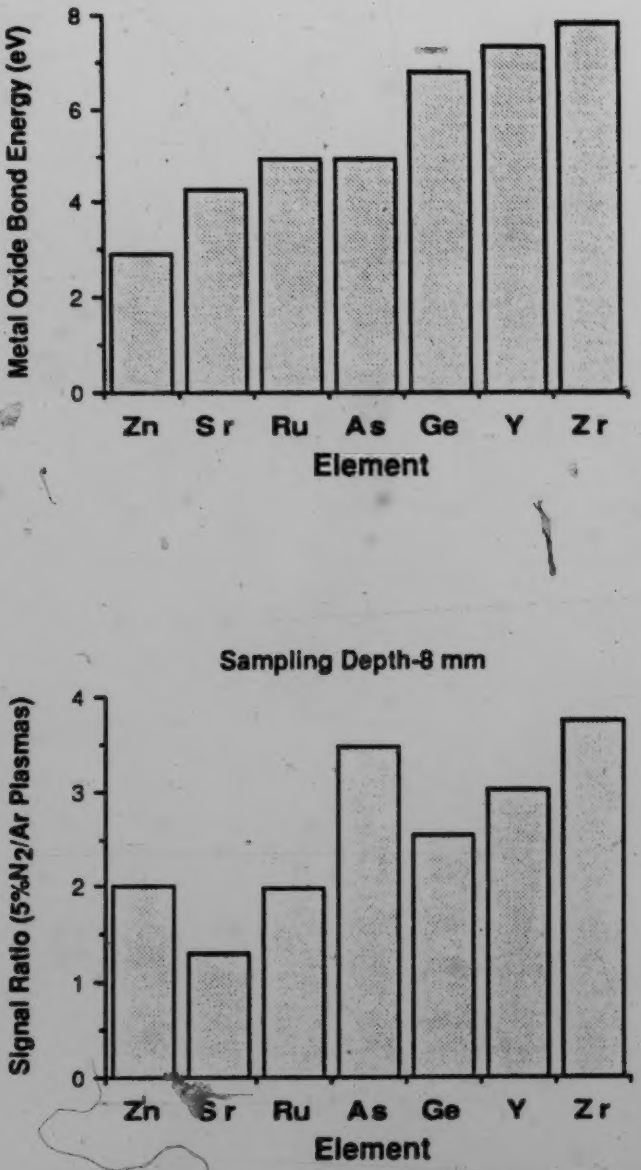

Figure 3-29. Bar graphs to correlate the metal oxide bond energy for elements to signal enhancements observed with a 5% nitrogen cooled plasma at 8 mm sampling depth (in the order of increasing metal oxide bond energies).

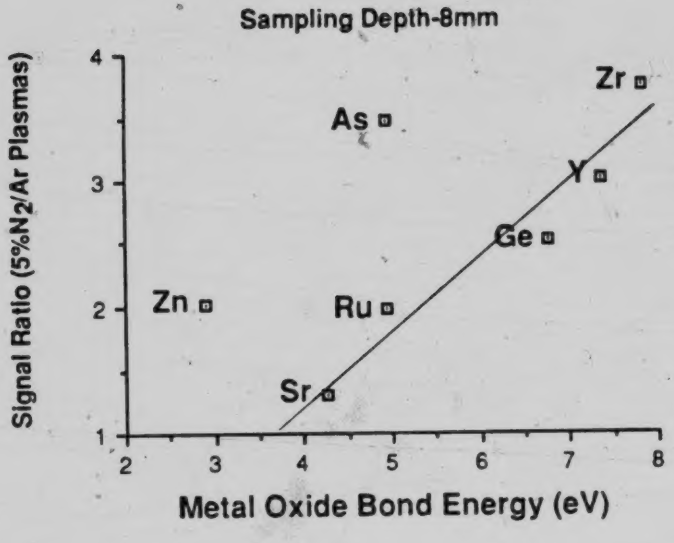

Figure 3-30. Diagram to demonstrate the relationship between signal enhancements from nitrogen mixed gas plasma to metal oxide bond energies.

be assumed that for analytes which tend to form strong oxides, the ionization process is likely to "take longer" and be "delayed". In fact, for the same sampling depth, a lower central gas flow rate would be favourable for peak intensity response of analytes in ICP-MS that have strong mono-oxide bond strengths. Thus, this simple model suggests that for the 100% argon plasma in ICP-MS, there should be some correlation between the nebuliser flow rate at which analytes have their peak signal response and analyte mono-oxide bond energy.

In their latest study of the effect of nebuliser flow rate on analyte signals in ICP-MS, Vaughan et al. [27] indicated that, in general, most analytes show a peak signal response at roughly the same nebuliser flow rate. However, in their study, no detailed quantitative assessment was carried out. What their data do indicate is that any correlation, if it does exist, occurs over a small range of nebuliser flow rates.

In order to define the position of the peak signal response as a function of nebuliser flow rate more precisely, the top five data points in the signal versus nebuliser flow rate plots measured for this study (data from Figures 3-8 to 3-14) were fitted with a parabola and the position of the peak signal response was calculated from this fit. This was carried out for the data of all analyte species at each sampling depth for both the 100% argon plasma and the 5% nitrogen plasma.

The data for the 100% argon plasma are summarized in Figure 3-31. It is clear from these data that there is a good correlation (negative) between nebuliser flow rate for optimum signal and metal oxide bond energy. For those species with larger metal oxide bond energies, lower nebuliser flow rates are required for peak signal response as predicted in the earlier discussion. This correlation holds reasonably well for all sampling depths. These data seem to validate the simple description of the spatial (time) distribution of the species in the central channel of the plasma and the sequence of events that occur as analyte

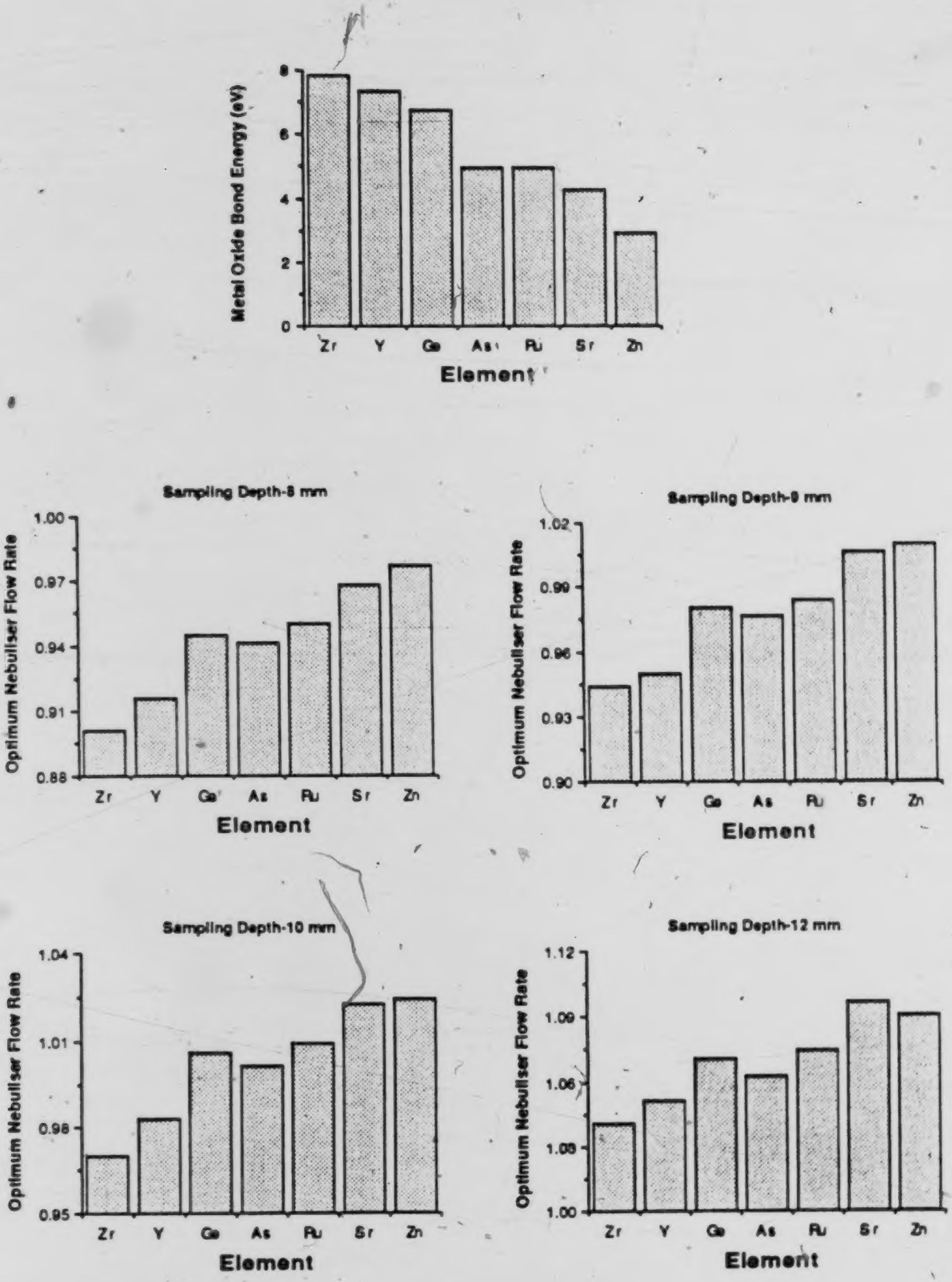

Figure 3-31. Bar graphs to illustrate the correlation between metal oxide bond energy to "optimum nebuliser flow rate" for species in an argon plasma.

and analyte oxide species pass through the plasma. While these results are focussed on ICP-MS, they are certainly pertinent to ICP-AES and indicate, perhaps, a more dominant role for vaporization phenomena in establishing the detailed spatial structure of analyte in the plasma than has hither to be appreciated.

The data for the 5% nitrogen mixed gas plasma are shown in Figure 3-32 for the 8 mm sampling depth. They do not correlate well with the metal oxide bond energy but do correlate (negatively) with analyte ionization potential. The data for all sampling depths are plotted in Figure 3-33, ordered as a function of ionization potential and the correlation is seen to hold for all sampling depths. These results make sense, based on the earlier correlation of nitrogen mixed gas plasma signal enhancement to oxide bond strength. The presence of the nitrogen has removed or minimized the vaporization character of the central channel. Now the ability of the analyte species to undergo ionization becomes dominant in determining the spatial distribution and sequence of events in the central channel. Thus species with low ionization potentials require a high nebuliser flow rate in order to be sampled optimally into the mass spectrometer. By implication, they are formed lower (sooner) in the plasma because this region of the plasma is cooler. Species with high ionization potentials have the opposite behaviour.

C. Oxygen and Air Mixed Gas Plasmas

In order to more fully appreciate analyte ion behaviour in mixed gas ICP-MS, oxygen and air mixed gas plasmas were also studied. As before, the analyte signals were measured as a function of nebuliser flow rate for various percentages of oxygen or air added to the outer argon gas. The elements studied in this section were chosen to specifically test the conclusions reached during the first part of this study. They are Te, Cs, Ba and Ce; some of their properties are summarized in Table 3-1. Te was chosen as an element with a high ionization potential but a relatively low metal oxide bond energy, i.e. in the class of As and

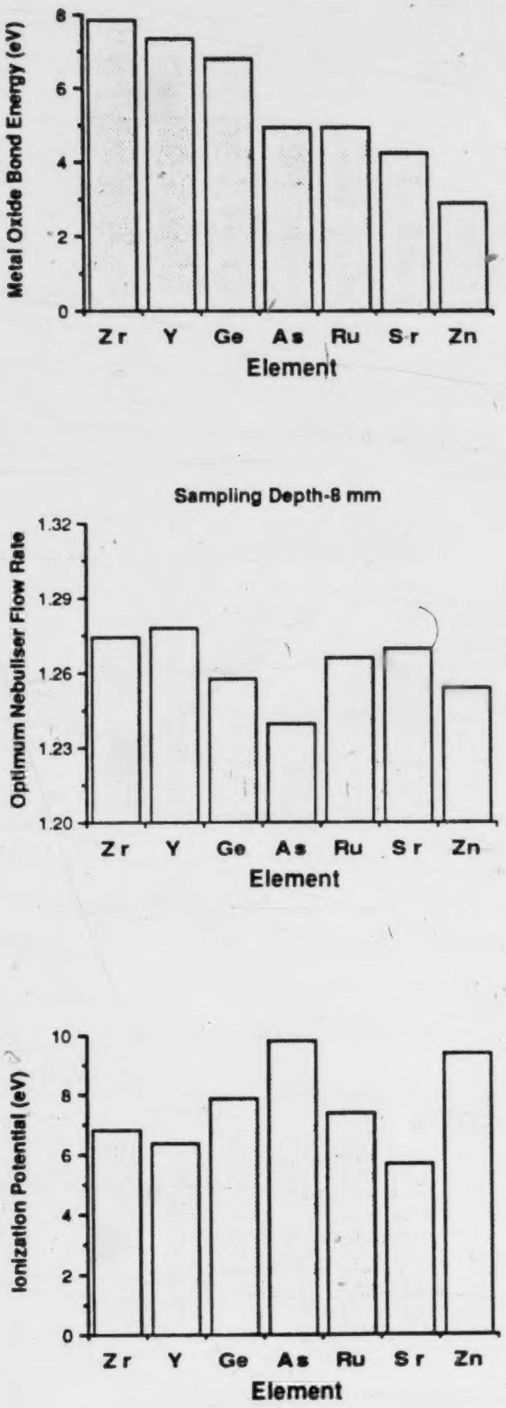

Figure 3-32. Bar graphs to demonstrate the lack of correlation between optimum nebuliser flow rate and metal oxide bond energy in a 5% nitrogen plasma.

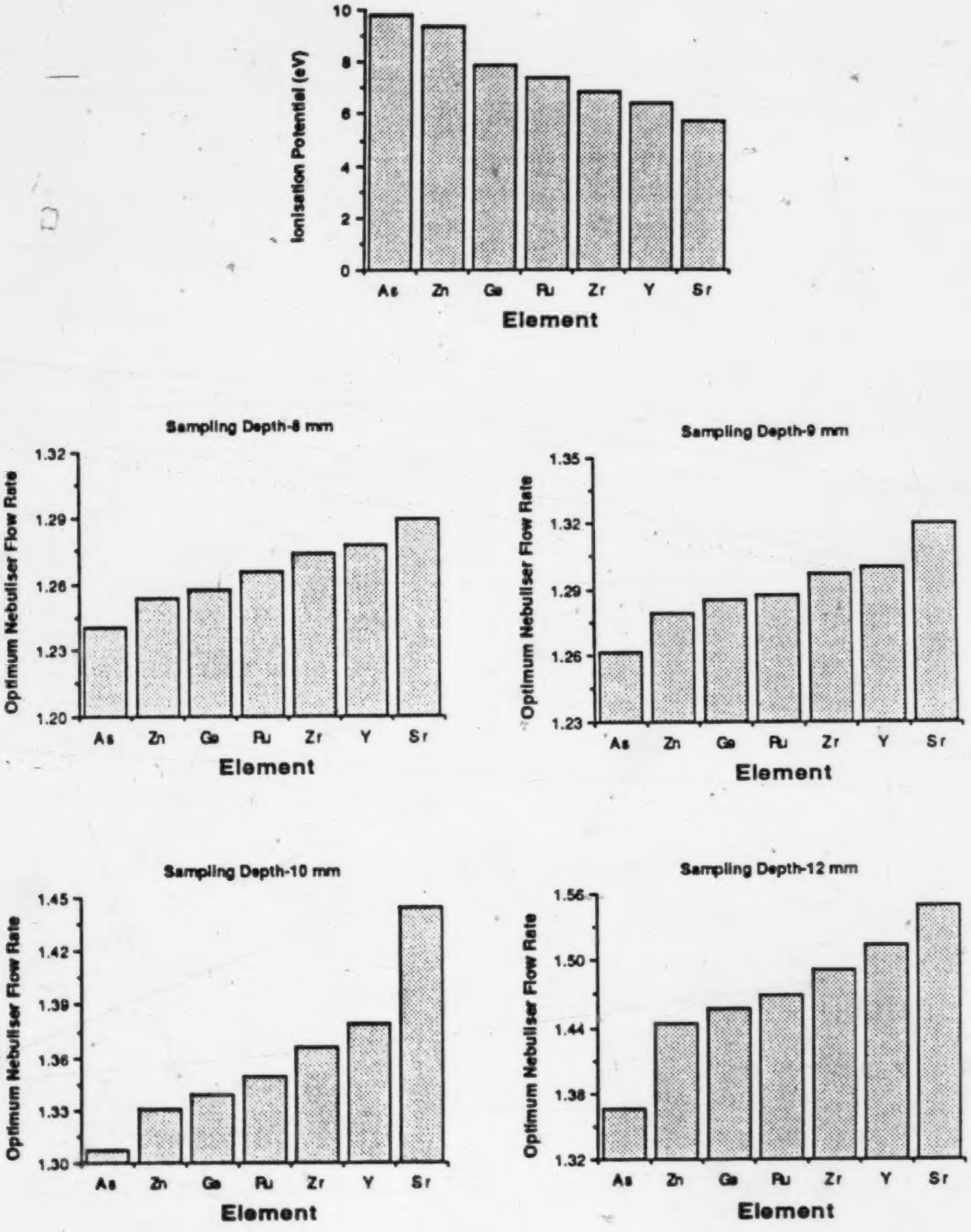

Figure 3-33. Bar graphs to demonstrate the correlation between species ionization potential to optimum nebuliser flow rate in a 5% nitrogen plasma.

Zn. Cs, Ba and Ce on the other hand have relatively low ionization potentials but have a good range of metal oxide bond energies - 3.04, 5.62 and 8.20 eV respectively.

The data were acquired from a multi-element solution containing 1 ppm concentrations of Te, Ce, Ba and Ce in 2% nitric acid. The plasma power was fixed at 1.50 kW and the sampling depth was at 10 mm throughout. The percentage of foreign gas used were 0, 2.5, 5 and 8% for the different types of discharge.

a. Effect of Percent Oxygen in the Outer Gas

The ion signal plots for oxygen-argon and nitrogen-argon mixed gas plasmas are presented in Figures 3-34 to 3-37. It is interesting to point out that while both of the plasma types require higher nebuliser gas flow rate in order to attain the optimum ion signal intensity, comparatively lower aerosol gas flow is needed with the oxygen-argon mixed gas discharge. This is consistent with the physical appearance of the plasma as nitrogen and air mixed gases have a greater effect on the physical dimension of the plasma discharge.

From the data shown in the figures, the oxygen mixed gas plasma shows very little effect on analyte sensitivity. In particularly, the properties of Te and Cs are unique. Despite their large difference in ionization energy, their oxide bond energies are similar and relatively low. In the case of Te (hard to ionize species), data from Figure 3-34 indicate that the use of an oxygen mixed gas plasma does not have much effect on its peak ion signal intensity while the corresponding nitrogen mixed gas enhances the analyte sensitivity. In contrast, while the sensitivity change for Cs remains about the same as Te, with the oxygen mixed gas, the degree of signal enhancement with the nitrogen-argon discharge is almost non-existent.

In the previous section, the advantage of using a nitrogen mixed gas is attributed to its ability to dissociate metal oxides which in turn releases the metal species and results in a net

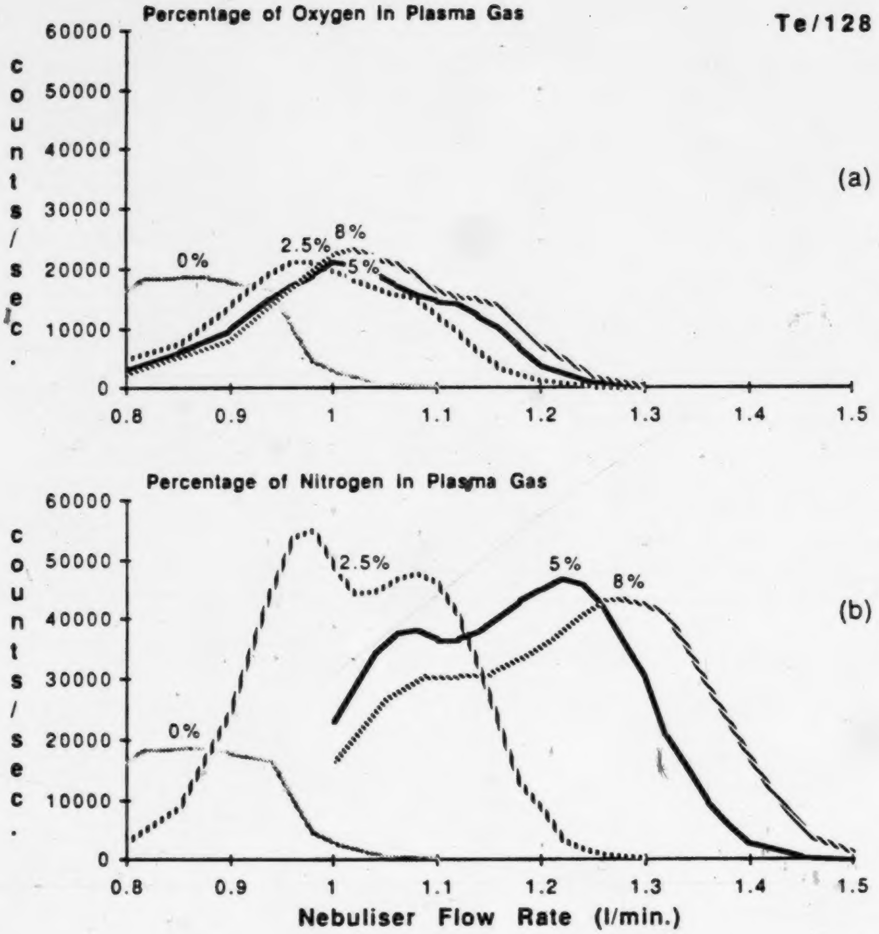

Figure 3-34. a) Dependence of Te signal on nebuliser flow rate and percentage of oxygen in the plasma gas (at 1.50 kW and 10 mm sampling depth). b) Dependence of Te signal on nebuliser flow rate and percentage of nitrogen in the plasma gas (at 1.50 kW and 10 mm sampling depth).

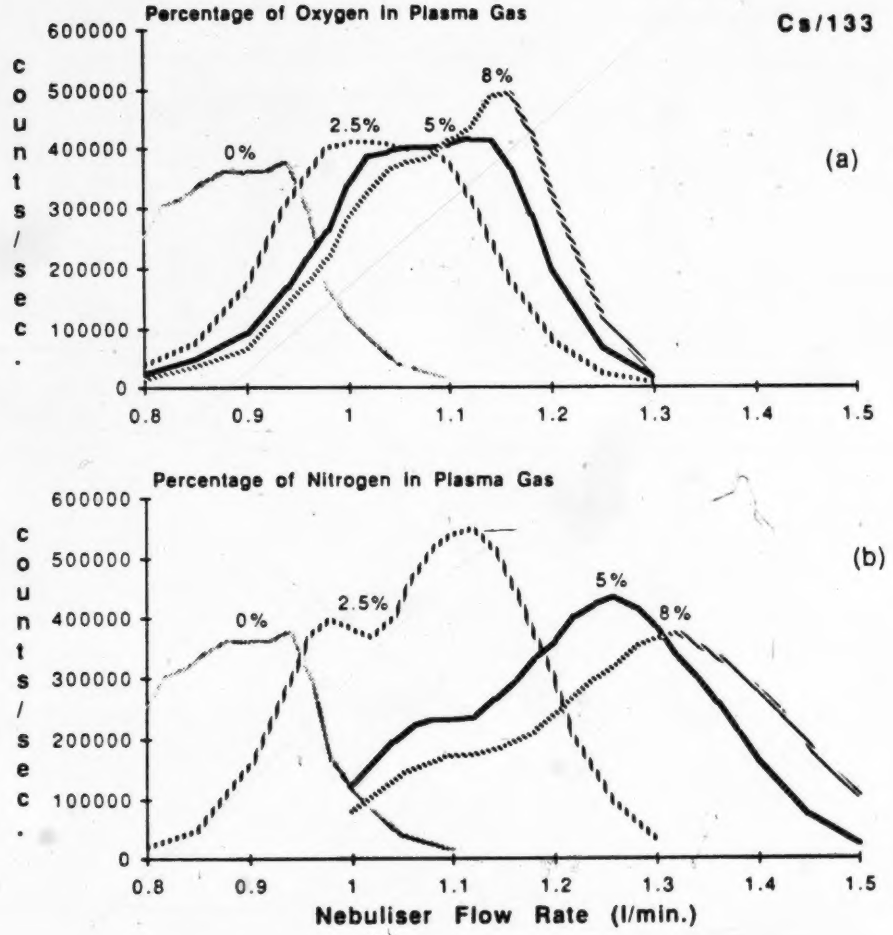

Figure 3-35. a) Dependence of Cs signal on nebuliser flow rate and percentage of oxygen in the plasma gas (at 1.50 kW and 10 mm sampling depth). b) Dependence of Cs signal on nebuliser flow rate and percentage of nitrogen in the plasma gas (at 1.50 kW and 10 mm sampling depth).

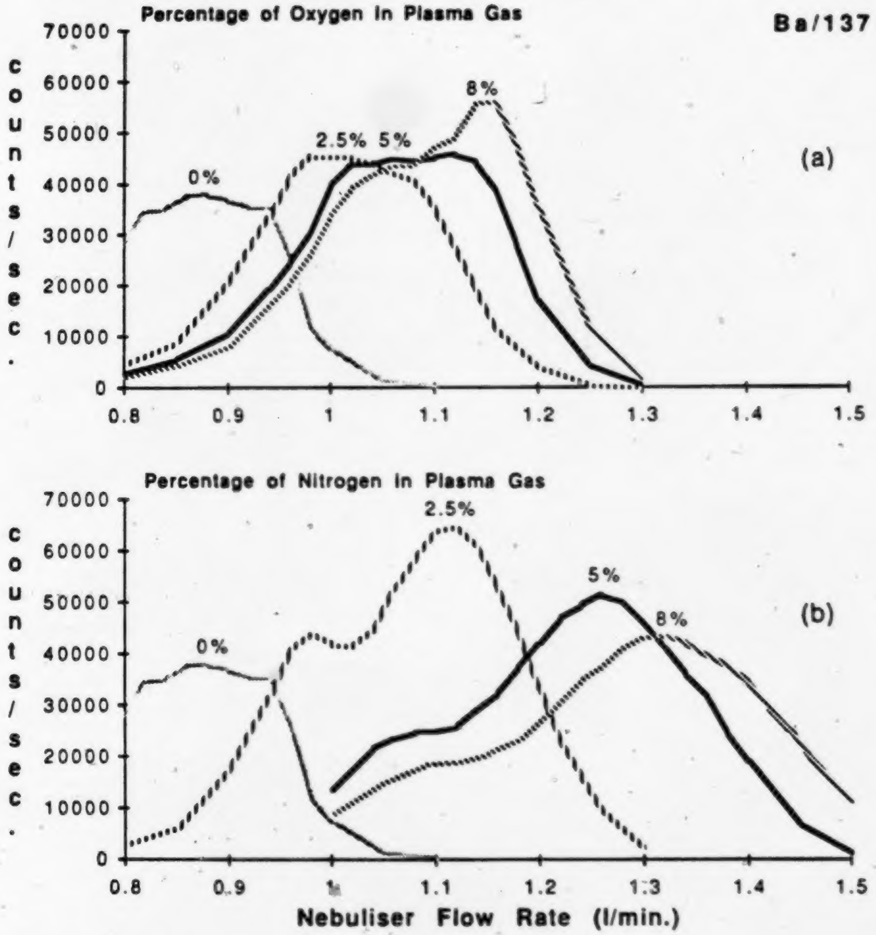

Figure 3-36. a) Dependence of Ba signal on nebuliser flow rate and percentage of oxygen in the plasma gas (at 1.50 kW and 10 mm sampling depth). b) Dependence of Ba signal on nebuliser flow rate and percentage of nitrogen in the plasma gas (at 1.50 kW and 10 mm sampling depth).

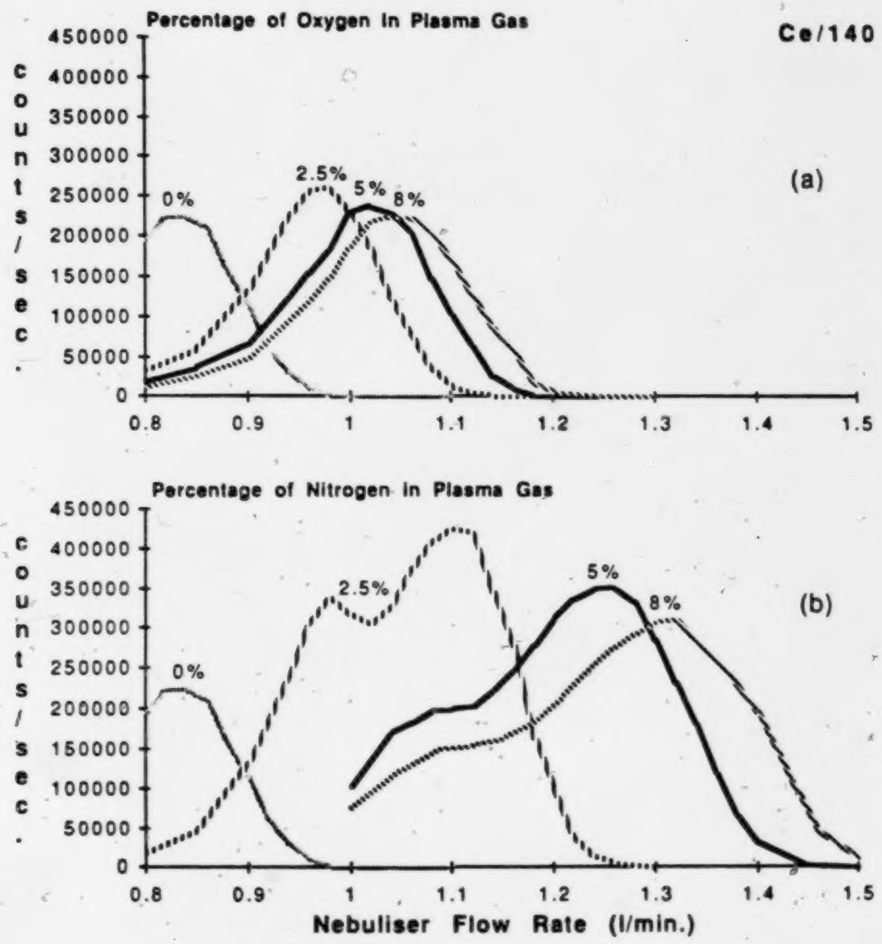

Figure 3-37. a) Dependence of Ce signal on nebuliser flow rate and percentage of oxygen in the plasma gas (at 1.50 kW and 10 mm sampling depth). b) Dependence of Ce signal on nebuliser flow rate and percentage of nitrogen in the plasma gas (at 1.50 kW and 10 mm sampling depth).

increase in the metal ion population density. Therefore, one of the expected effects of the oxygen-argon mixed gas plasma on signal intensity is perhaps a signal reduction for species which have high affinity for oxygen. Data from Figures 3-35 to 3-37 demonstrate the relative responses for weak (Cs), medium (Ba) and strong (Ce) metal oxide formation species. Rather interestingly, oxygen does not appear to have any significant effect on the weak (Cs) to medium (Ba) oxide forming species (see Figures 3-35 and 3-36), but it does decrease the metal ion signal of the strong (Ce) oxide forming species (Figure 3-37).

b. Effect of Percent Air in the Outer Gas

When a low percent air-argon mixture is used as the outer gas, the shift in signal profile with respect to the nebuliser flow rate is found to be comparable to that with the corresponding nitrogen-argon mixed gas discharge. Data from Figures 3-38 to 3-41 demonstrate the individual analyte responses to the two different plasmas. From the data, clearly the responses between different analyte types are different, yet the effects on the same analyte are more or less identical. In addition, the air-argon mixed gas discharge also appears to give a slightly better signal sensitivity. Although this slight improvement might be attributed to long term instrument sensitivity drift, since the data acquired for the nitrogen mixed gas plasmas were carried out after the air mixed gas discharges, the overall analytical performance of a low percent air mixed gas plasma is superior to the corresponding oxygen-argon mixed gas discharge.

c. Discussion

The signal enhancement results for the nitrogen, oxygen and air mixed gas plasmas are summarized in Figure 3-42 for 5% mixed gas ICP's. The data for Te, Cs, Ba and Ce clearly follow the trends established earlier for Zn, Ge, As, Sr, Y, Zr and Ru for both the nitrogen and the air plasmas. On the other hand, the oxygen mixed gas plasma has little effect on signal sensitivity.

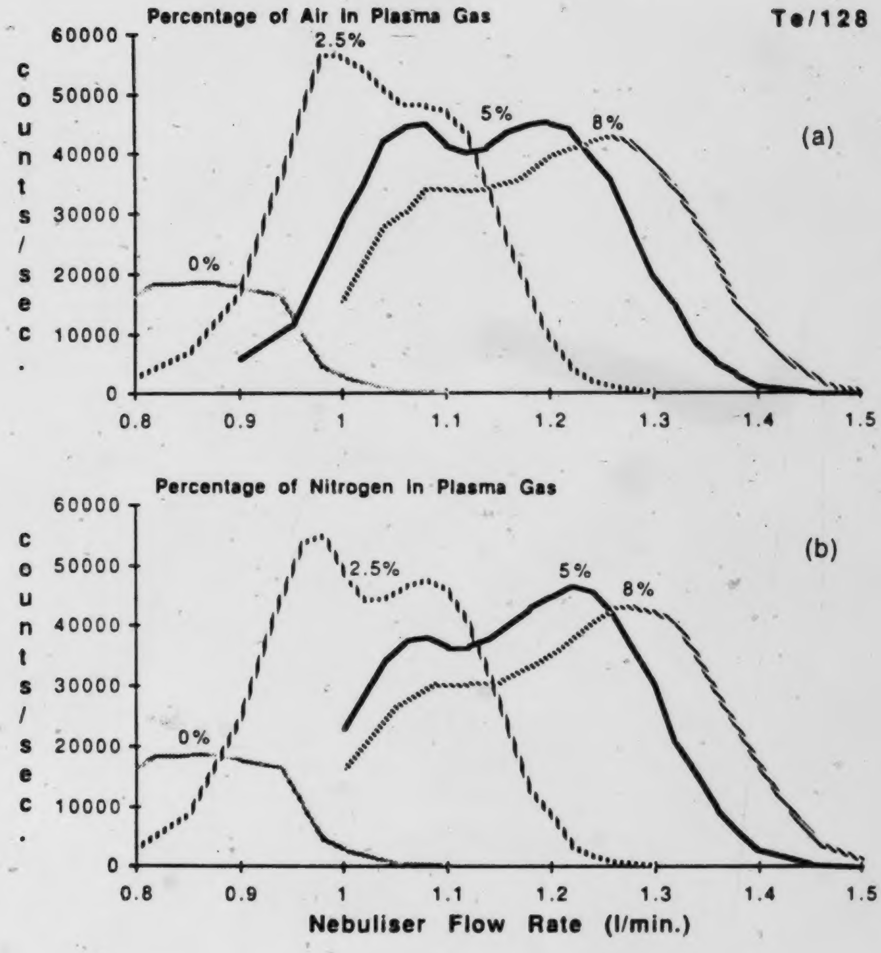

Figure 3-38. a) Dependence of Te signal on nebuliser flow rate and percentage of air in the plasma gas (at 1.50 kW and 10 mm sampling depth). b) Dependence of Te signal on nebuliser flow rate and percentage of nitrogen in the plasma gas (at 1.50 kW and 10 mm sampling depth).

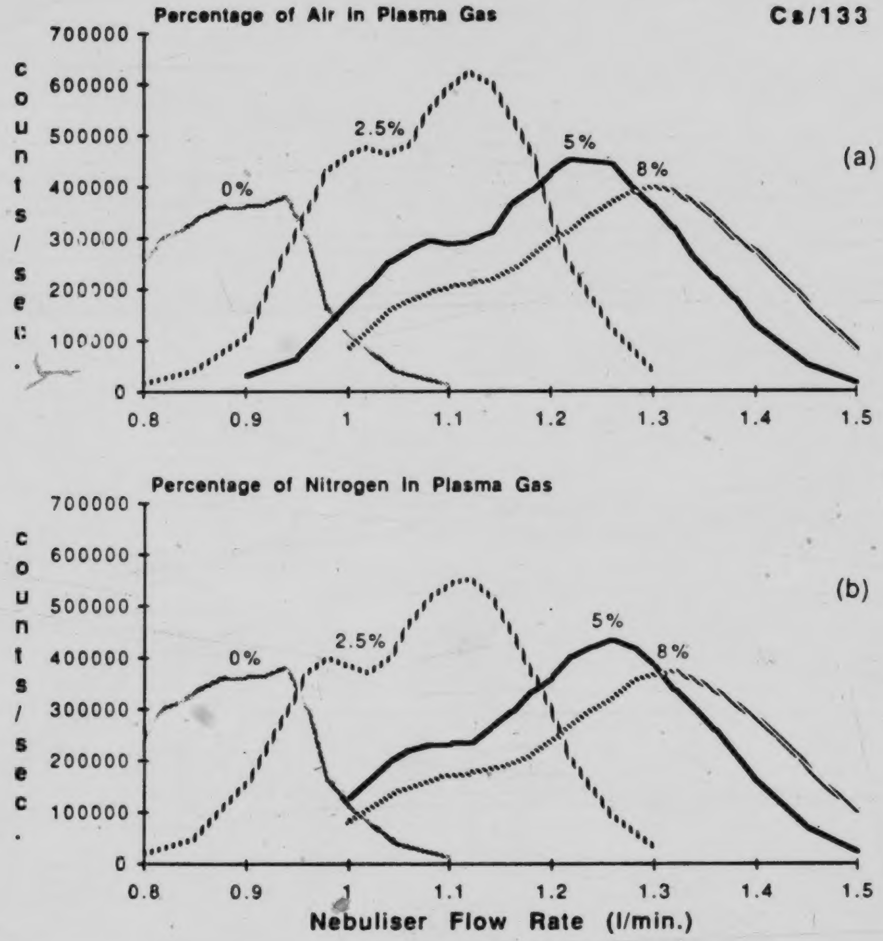

Figure 3-39. a) Dependence of Cs signal on nebuliser flow rate and percentage of air in the plasma gas (at 1.50 kW and 10 mm sampling depth). b) Dependence of Cs signal on nebuliser flow rate and percentage of nitrogen in the plasma gas (at 1.50 kW and 10 mm sampling depth).

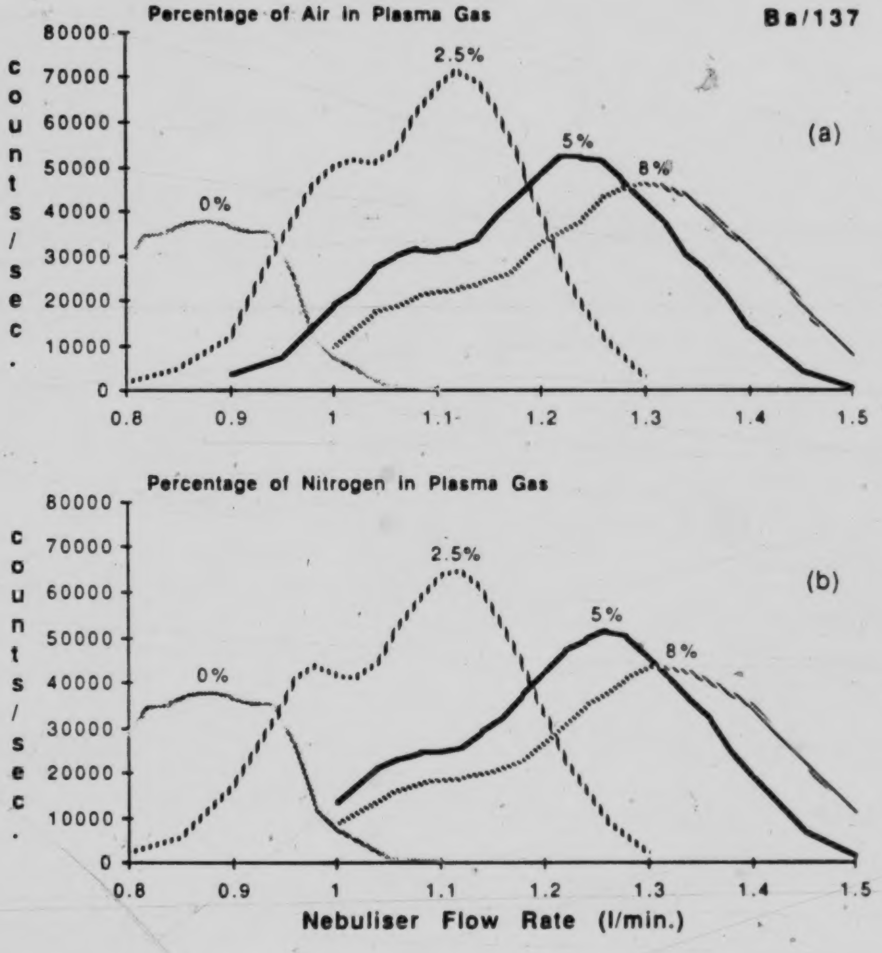

Figure 3-40. a) Dependence of Ba signal on nebuliser flow rate and percentage of air in the plasma gas (at 1.50 kW and 10 mm sampling depth). b) Dependence of Ba signal on nebuliser flow rate and percentage of nitrogen in the plasma gas (at 1.50 kW and 10 mm sampling depth).

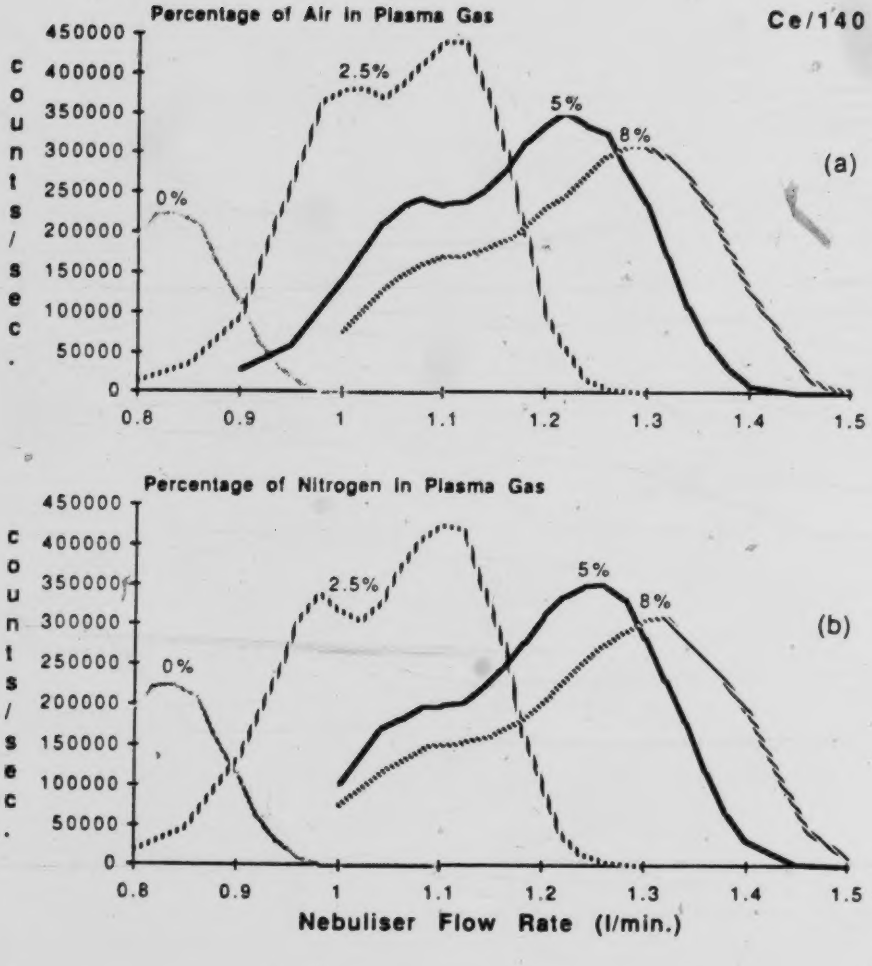

Figure 3-41. a) Dependence of Ce signal on nebuliser flow rate and percentage of air in the plasma gas (at 1.50 kW and 10 mm sampling depth). b) Dependence of Ce signal on nebuliser flow rate and percentage of nitrogen in the plasma gas (at 1.50 kW and 10 mm sampling depth).

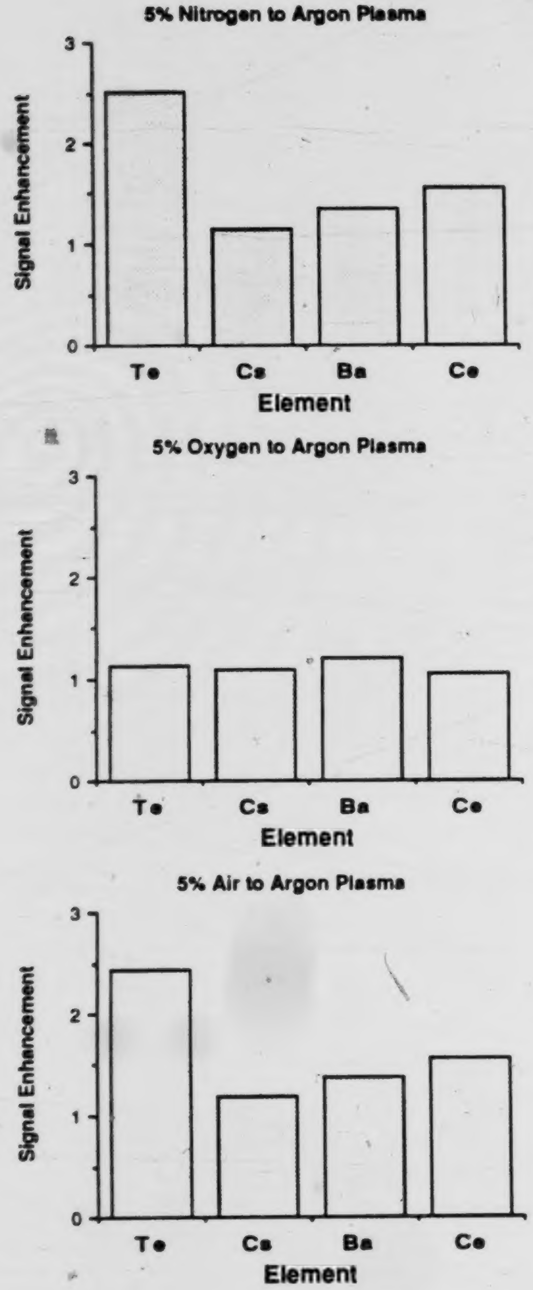

Figure 3-42. Bar graphs to demonstrate the different signal enhancement effects by 5% nitrogen, oxygen, and air mixed gas plasmas on Te, Cs, Ba and Ce at rf power of 1.50 kW and 10 mm sampling depth.

Up to now, adequate explanation has been given only for the effect of nitrogen mixed gas plasmas on analytes with relatively low ionization energies and high metal-oxide bond strengths. No specific interpretation has been provided for the rather significant signal enhancement observed for the hard to ionize species despite the fact that they possess considerably weaker oxide bond energies (see Figure 3-29). As well as summarized above, a comparable degree of sensitivity enhancement for analytes has been observed with nitrogen-argon and air-argon mixed gas plasmas, while negligible improvement is recorded with the corresponding oxygen-argon discharge. This result tends to suggest that the improvement in plasma-analyte interaction as a result of a "thermal pinch" cannot be the dominating factor, because oxygen mixed gas plasmas also reduce the physical volume of the discharge.

It has been suggested that with the addition of a molecular gas to the argon discharge, the spectroscopic environment within the discharge moves towards local thermodynamic equilibrium (LTE). Abdallah and Mermet [28] found good agreement between the rotation temperature using N_2^+ lines and the excitation temperature of analytes with a 25% nitrogen-argon mixed nebulising gas operating at 1.6 kW. However, when Houk et al. [29] measured the ionization temperature of an ICP using MS, they found that a 100% nitrogen cooled plasma had a temperature approximately 1000 K lower than what would have been obtained from an argon discharge. Unfortunately, their comparison was made at a sampling depth of 20 mm (usually not the optimum sampling location for a molecular gas plasma). Using a Reticon photo-diode array, Choot and Horlick [10] compared the line emission intensities for Cd with N_2-Ar, O_2-Ar, Air-Ar and He-Ar mixed gas plasmas. Based on their results, they were able to conclude that a 10% nitrogen-argon plasma at an observation height of 10 mm from the load coil gave the best ion/atom line emission ratio. Preliminary results from Lam [26] also indicated that the plasma ionization temperature increased for a low percent nitrogen mixed gas plasma.

Processes for the generation of analyte ions in an ICP may be summarized as the following:

i) Penning Ionization

$$Ar^m + X \rightarrow Ar + X^+ + e^- \qquad (3\text{-}1)$$

ii) Charge-Transfer Process

$$Ar^+ + X \rightarrow Ar + X^+ \qquad (3\text{-}2)$$

iii) Electron Impact Ionization

$$X + e^- \rightarrow X^+ + 2e^- \qquad (3\text{-}3)$$

where:

Ar^m = argon metastable species

X = analyte atom

X^+ = analyte ion

Choot and Horlick [12] measured the plasma electron density for oxygen and nitrogen cooled discharges. Although the measured values from a 10% oxygen mixed gas plasma were lower than those observed from a 10% nitrogen cooled discharge, they were still higher than those obtained from a 100% argon plasma. By comparing the ion signal intensities obtained from the oxygen and the pure argon discharge, process (iii) can be considered as redundant as the higher electron density values in the oxygen plasma did not correlate to analyte sensitivity enhancement (see Figure 3-34). Further, this rather uncharacteristic response was not due to the formation of metal oxide as no detectable amount of tellurium oxide ion was observed.

From the three types of mixed gas plasma studied, introduction of nitrogen and/or oxygen are common in all three cases. Therefore, a better knowledge of the properties of the two molecular gases is necessary to fully appreciate the different plasma effects on analyte sensitivity.

In considering the elevated level of electron density in mixed gas plasmas, the ionization energies for atomic and molecular nitrogen are 14.534 eV [30] and 15.5808 eV [31] respectively. Thus, it is reasonable to suggest that the electron density increase in a nitrogen mixed plasma is likely to be a result of the higher degree of ionization for nitrogen over argon (IP=15.76 eV). Hence, the nitrogen related species must have been responsible for the observed analyte sensitivity enhancement :

$$N_2^+ + X \rightarrow N_2 + X^+ \qquad (3\text{-}4)$$

$$N^+ + X \rightarrow N + X^+ \qquad (3\text{-}5)$$

$$N_2^+ + Ar + e^- \rightarrow N_2 + Ar^m \qquad (3\text{-}6)$$

$$N^+ + Ar + e^- \rightarrow N + Ar^m \qquad (3\text{-}7)$$

or rather through a 2 step process for the generation of argon ion.

If the above assumptions are valid, then the elevated analyte ion population is likely a result of the reaction rate increases in Penning ionization and/or charge-transfer processes.

By the same token, the above speculation should also be valid for an oxygen mixed gas plasma since the ionization energy for atomic and molecular species are 13.618 eV [30] and 12.071 eV [31] respectively. Since these values are much lower than the corresponding values for nitrogen species, one would expect that the degree of ionization for oxygen in the plasma is even higher. In addition, the molecular bond energy for oxygen is also weaker than nitrogen (5.115 eV for O_2 and 9.76 eV for N_2 [31]). Thus, after all things considered, the above situation should favour a higher degree of oxygen ionization and thus higher electron density values for oxygen mixed gas plasma. Yet, the experimental results obtained by Choot and Horlick [12] indicated that the electron density for a 10%

N_2-Ar cooled plasma is about twice as high as the O_2-Ar plasma along the aerosol channel. Clearly, the direct relationship between elemental ionization potential of the foreign gases to plasma electron density cannot be applicable.

From previous observations in ICP-MS using a low percentage nitrogen mixed gas plasma, nitrosonium ion (NO^+) was found to be more abundant than N_2^+ ion. This is consistent with the earlier report by Fassel and coworkers [29] in which they also suggested that the level of NO^+ was likely to be responsible for the sensitivity enhancement in a nitrogen mixed gas ICP. They proposed the following charged-transfer process for the reaction:

$$NO^+ + X \rightarrow NO + X^+ \quad \text{(IP=9.26 eV for NO)} \qquad (3\text{-}8)$$

The production of NO species requires oxygen as one of the starting materials. This can be obtained, in the case of the air-argon mixed gas plasma, from itself, or from the dissociation of water molecules bound within the aerosol droplet. In considering the bond dissociation energies for H_2O and OH groups, the reported values of 5.12 eV and 4.395 eV should be easily provided by the energetic plasma source. Also, the mechanism responsible for the generation of nitric oxide from nitrogen and oxygen at low pressure has been well documented [32, 33]. Further, NO^+ is commonly observed in the upper atmosphere and the reaction mechanism is believed to be one of the following [34, 35]:

$$N_2^+ + O \rightarrow NO^+ + N \qquad (3\text{-}9)$$

$$O^+ + N_2 \rightarrow NO^+ + N \qquad (3\text{-}10)$$

$$N^+ + O_2 \rightarrow NO^+ + O \qquad (3\text{-}11)$$

The ionization energy of 9.26 eV for NO also agrees with the electron density values observed by Choot and Horlick [12]; in this situation oxygen becomes the harder to ionize species (about 13 eV) and thus it is responsible for the observed lower electron density value. In addition, the effect of N_2-Ar and air-Ar mixed gas plasmas on analyte sensitivity (see Figures 3-38 to 3-41) also suggests that the excitation mechanisms between the two discharges are quite similar. This is especially the case for the hard to ionize species such as Te where analyte ionization by means of a charge-transfer process with nitrosonium ion is most likely.

The proposed charge-transfer mechanism is reasonable for species with ionization energy at or near 9.26 eV. However, for analytes with ionization potentials over this value, a two steps process (via an intermediate) would be required.

D. Effect of Mixed Gas Plasmas on Analyte and Analyte Oxide Signals

In the previous section, it has been observed that the use of a mixed gas plasma is particularly beneficial in terms of analyte signal sensitivity enhancement. From these results, one is able to conclude that there are two aspects to analyte signal enhancement. First, analyte with a high ionization potential, and consequently a degree of ionization in the plasma is considerably less than unity, showed significant signal enhancement. Second, element with high metal-oxygen bond strength also showed strong signal enhancement.

While circumstantial evidence indicates that the increase in the degree of ionization for the hard to ionize species is probably due to a more efficient charge-transfer process between the analyte and the nitrosonium ion generated by the nitrogen or air mixed gas discharge, the suggestion regarding the dissociation of metal-oxide in a mixed gas plasma has not been validated. In order to better appreciate the effect of mixed gases on this kind of species, analytes and the corresponding oxide ions were monitored. Again, ion signal intensities were obtained as a function of nebuliser flow rate in order to characterize fully the overall effect of mixed gases on species populations.

a. Effect of Percent Nitrogen in the Outer Gas on La and LaO

Previously, the effect of a nitrogen mixed gas plasma on metal ion signals was studied. In general, a higher nebuliser flow rate is required as increasing amounts of nitrogen are added into the discharge. Depending on the analyte, signal enhancement or reduction may result with the use of nitrogen mixed gas in ICP-MS and with all analytes, the ion signal decreases as the amount of nitrogen added into the discharge is increased.

A solution containing 1 ppm La in 2% nitric acid was used in this study. The signals from the metal and its oxide were monitored as a function of nebuliser gas flow rate with the nitrogen mixed into the outer gas at 0, 5, 12 and 20% respectively. The plasma operating parameters were the same as indicated in the Introduction and the sampling depth was at 10 mm.

Signal responses for La ion as a function of nitrogen percent are illustrated in Figure 3-43a. From the data shown in the figure, it is quite obvious that a signal enhancement for La is achieved with the use of a 5% nitrogen cooled mixed gas plasma. Also, despite the drop in sensitivity for a higher percentage nitrogen mixed gas plasma, even at 20% the peak signal intensity is still higher than that for the corresponding 100% argon plasma at its optimum flow rate. On the other hand, the behaviour of LaO ion to nitrogen is quite different (see Figure 3-43b). It is not totally unexpected that the highest population level of oxide ion is obtained when the supporting gas is 100% argon. The addition of nitrogen into the discharge decreases the oxide ion level population rather dramatically. In common with the analyte ion, the nebuliser gas flow rate for the peak signal intensity also increases with the addition of nitrogen and the resultant signal profiles shift to an even higher nebuliser flow rate offset.

The effect of nitrogen on the analyte oxide is summarized in the table below. Signal levels were taken at the peak nebuliser flow rates for each species.

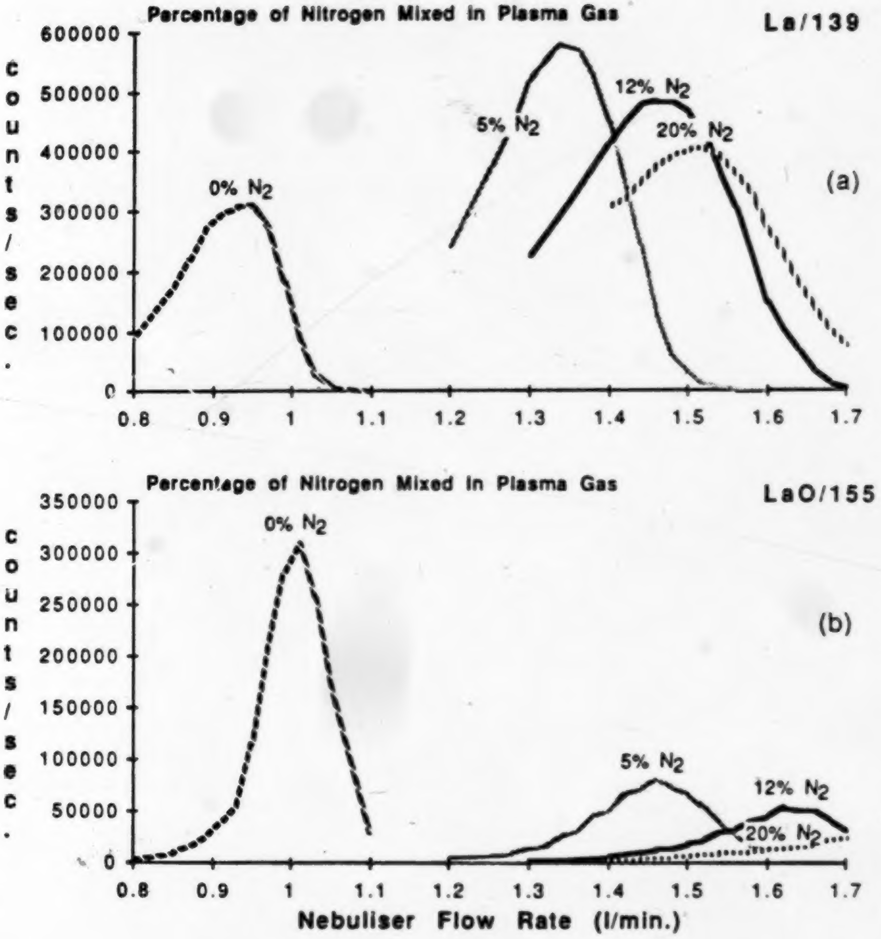

Figure 3-43. a) Dependence of La signal on nebuliser flow rate and percentage of nitrogen in the plasma gas (at 1.50 kW and 10 mm sampling depth). b) Dependence of LaO signal on nebuliser flow rate and percentage of nitrogen in the plasma gas (at 1.50 kW and 10 mm sampling depth).

Percent of Nitrogen	LaO^+/La^+
0%	37%
5%	4.4%
12%	2.5%
20%	1.9%

The above data clearly indicate that the use of a low percentage nitrogen cooled mixed gas plasma can effectively and efficiently reduce the oxide ion population. Particularly, when the outer gas consists of 20% nitrogen, the oxide level is decreased to below 2%. Although the analyte ion signal sensitivity is also reduced under this condition, it is still higher than what would have been observed using a pure argon plasma discharge.

b. Effect of Percent Oxygen and Air in the Outer Gas on Analyte and Analyte Oxide Signals

In a previous study, it was observed that an oxygen mixed gas plasma had a different effect on analyte signals compared to nitrogen and air mixed gas plasmas. Especially in the case of refractory elements, the use of a low percentage oxygen mixed gas discharge tends to decrease the analyte ion signal response. This effect is thought to be a result of refractory oxide formation inside the discharge and thus a lowering of the population level of free analyte ion available for detection. This was not observed when an air mixed gas discharge was used. This could be attributed to the reaction between nitrogen and oxygen where the bulk of the available oxygen is likely tied up by the excess amount of nitrogen also presented in air. This can be verified by comparing the signal responses for the analyte and its oxide with different percentages of oxygen or air in the outer gas with respect to the corresponding nitrogen mixed gas discharge.

In this approach, the effect of mixed gas plasmas on Ba and Ce (a medium and a strong oxide with metal-oxide bond energies of 5.62 eV and 8.20 eV) were examined. The percentages of foreign gas used were 0, 2.5, 5 and 8%. The sample analyte consisted of a 1 ppm concentration of each element in 2% nitric acid.

Figures 3-44 and 3-45 illustrate the oxide ion responses for Ba and Ce in an oxygen cooled mixed gas plasma (top frames in each figure). In addition, the ion signal responses with the nitrogen mixed gas plasma are also included (bottom frames). From the data shown in the figures, it is interesting to note that the peak signal intensity for BaO ion increases with a 2.5% oxygen plasma but it decreases with any further increase in oxygen (see Figure 3-44a). In contrast, the peak oxide signal decreases rapidly with increasing nitrogen percent (see Figure 3-44b). On the other hand, the peak CeO ion signal increases with an increase in the level of oxygen in the outer gas but decreases with the nitrogen mixed gas plasma (Figure 3-45).

Analogous data for air and nitrogen mixed gas plasmas are summarized in Figures 3-46 and 3-47. The overall trend in response between the two types of plasmas is identical. This result is consistent with analyte responses observed earlier for air and nitrogen mixed gas plasmas. Hence, the mechanism for the reduction of analyte oxide and the enhancement of analyte signal sensitivity is expected to be similar in air and nitrogen mixed gas discharges.

The effect of mixed gas plasmas on analyte oxides can be summarized by comparing the oxide to its metal ion signal obtained from the three plasma types. The results are presented in Table 3-6. From the data shown in the table, it is quite apparent that the use of an oxygen mixed gas plasma assists the formation of analyte oxide species. This is particularly so for the refractory elements (Ce). The behaviour of BaO^+ in the oxygen mixed gas plasma is rather peculiar. The population decrease at high oxygen percent can be interpreted in terms of oxide ion bond dissociation energies, $D^\circ(M\text{-}O)^+$. The D° value for

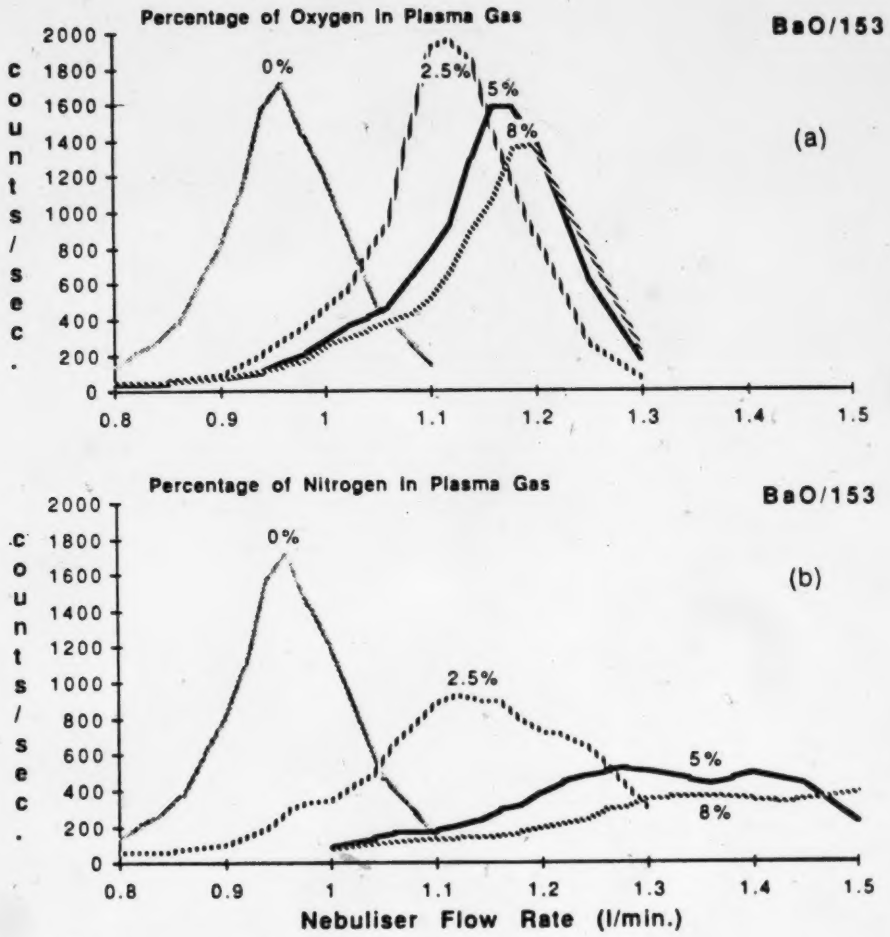

Figure 3-44. a) Dependence of BaO signal on nebuliser flow rate and percentage of oxygen in the plasma gas (at 1.50 kW and 10 mm sampling depth). b) Dependence of BaO signal on nebuliser flow rate and percentage of nitrogen in the plasma gas (at 1.50 kW and 10 mm sampling depth).

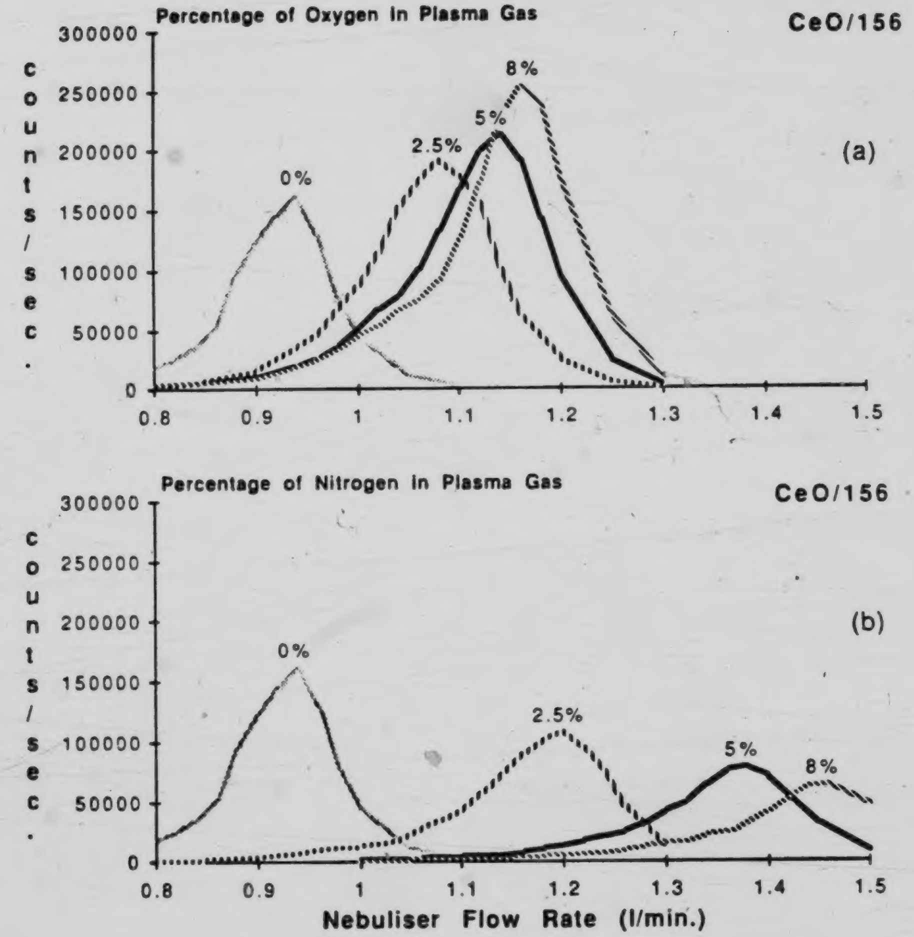

Figure 3-45. a) Dependence of CeO signal on nebuliser flow rate and percentage of oxygen in the plasma gas (at 1.50 kW and 10 mm sampling depth). b) Dependence of CeO signal on nebuliser flow rate and percentage of nitrogen in the plasma gas (at 1.50 kW and 10 mm sampling depth).

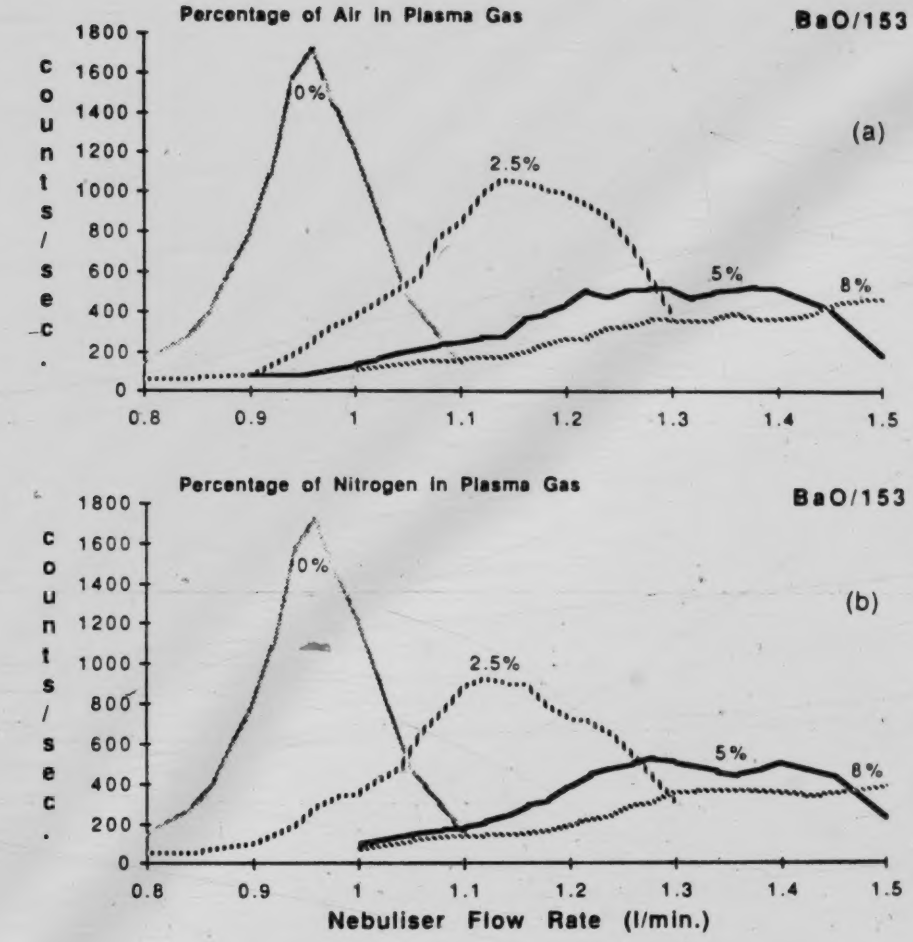

Figure 3-46. a) Dependence of BaO signal on nebuliser flow rate and percentage of air in the plasma gas (at 1.50 kW and 10 mm sampling depth). b) Dependence of BaO signal on nebuliser flow rate and percentage of nitrogen in the plasma gas (at 1.50 kW and 10 mm sampling depth).

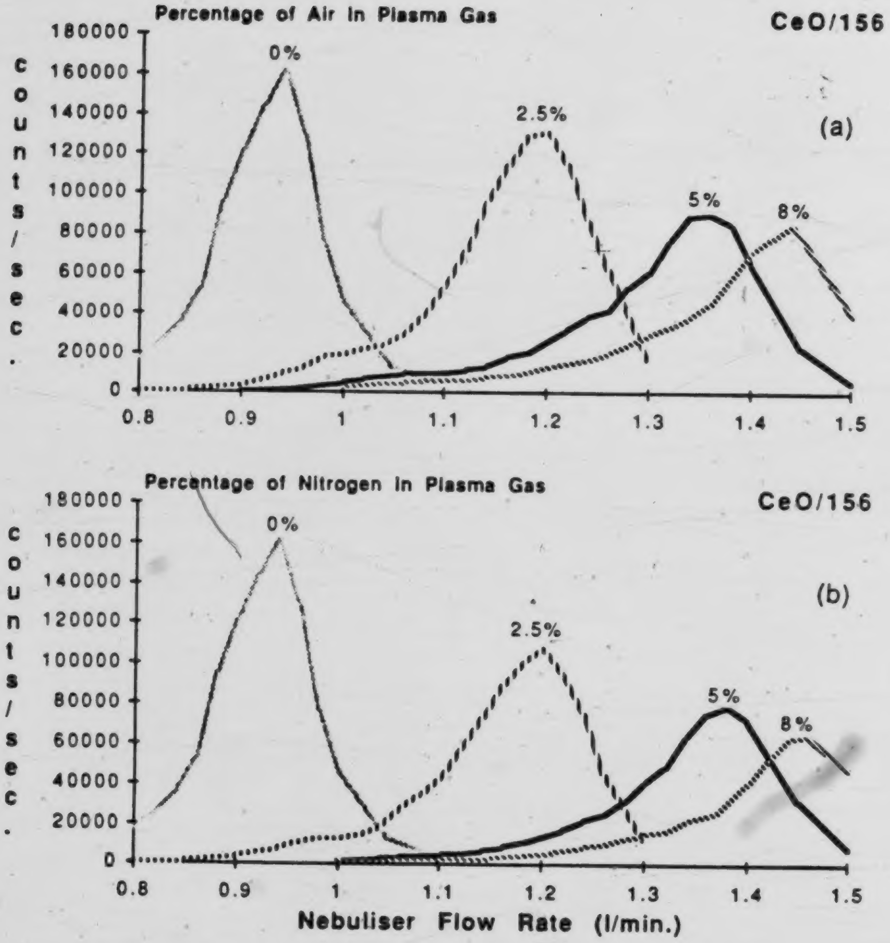

Figure 3-47. a) Dependence of CeO signal on nebuliser flow rate and percentage of air in the plasma gas (at 1.50 kW and 10 mm sampling depth). b) Dependence of CeO signal on nebuliser flow rate and percentage of nitrogen in the plasma gas (at 1.50 kW and 10 mm sampling depth).

Table 3-6 The effect of mixed gas plasmas on oxide/metal ion ratios each obtained at its respective peak metal ion sensitivity.

	BaO^+/Ba^+			CeO^+/Ce^+		
% Mixed Gas	Oxygen	Air	Nitrogen	Oxygen	Air	Nitrogen
0	1.6%	1.6%	1.6%	15%	15%	15%
2.5	0.8%	1.4%	1.4%	25%	12%	10%
5	2.0%	0.90%	0.96%	28%	8.9%	7.0%
8	1.9%	0.78%	0.82%	30%	9.2%	5.2%

BaO^+ is less than 4 eV [36]. This value is lower than the molecular bond energies of 6.663 eV and 5.115 eV for O_2^+ and O_2 respectively. Hence, an increasing percentage of oxygen in the outer gas could favour a molecular recombination process for oxygen atoms and ions and in turn enhance the dissociation of barium oxide ion. On the other hand, CeO ion has a dissociation energy of 8.8 eV [37]. This makes species dissociation extremely unlikely. Finally, the reduction of analyte oxide using the air cooled mixed gas plasma, although effective, is slightly inferior when compared to the nitrogen mixed gas discharge.

c. Effect of Percent Nitrogen in the Nebulising Gas on La and LaO

In an earlier part of this study, it was observed that when nitrogen is mixed into the nebulising gas, the analyte ion signal sensitivity decreased considerably. However, since nitrogen is felt to be a main ingredient responsible for the reduction of analyte oxide in a mixed gas ICP, the use of nitrogen as part of the nebulising gas could be quite efficient toward oxide reduction.

The sample consisted of 1 ppm La in 2% nitric acid. The plasma parameters were the same as above with exception that the sampling depth was at 15 mm and the auxiliary gas was readjusted to 1.40 l/min. The amounts of nitrogen mixed into the nebulising gas were 0 and 20%.

The ion signals for La and LaO were acquired in the usual way as a function of nebuliser flow rate. The results are illustrated in Figure 3-48. The data from the figure clearly show that the La ion signal profile is shifted to a lower nebuliser flow rate with the introduction of nitrogen and in addition, the peak analyte ion signal also decreases. This was noted earlier. However, the effect of the mixed nebulising gas on analyte oxide ion is more dramatic. The oxide ion is almost completely removed (see Figure 3-49). In summary, it is clear that nitrogen is very efficient in reducing the metal oxide signal when it

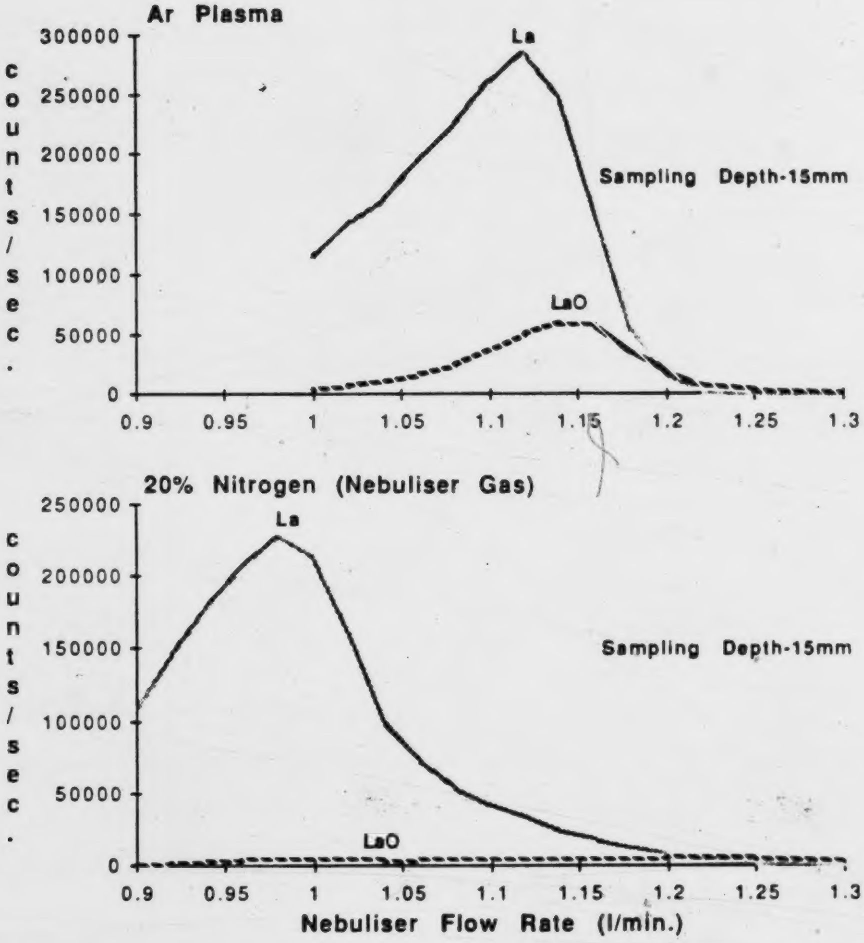

Figure 3-48. The effect of 20% nitrogen nebulising gas on La and LaO signals at sampling depth of 15 mm (rf power 1.50 kW).

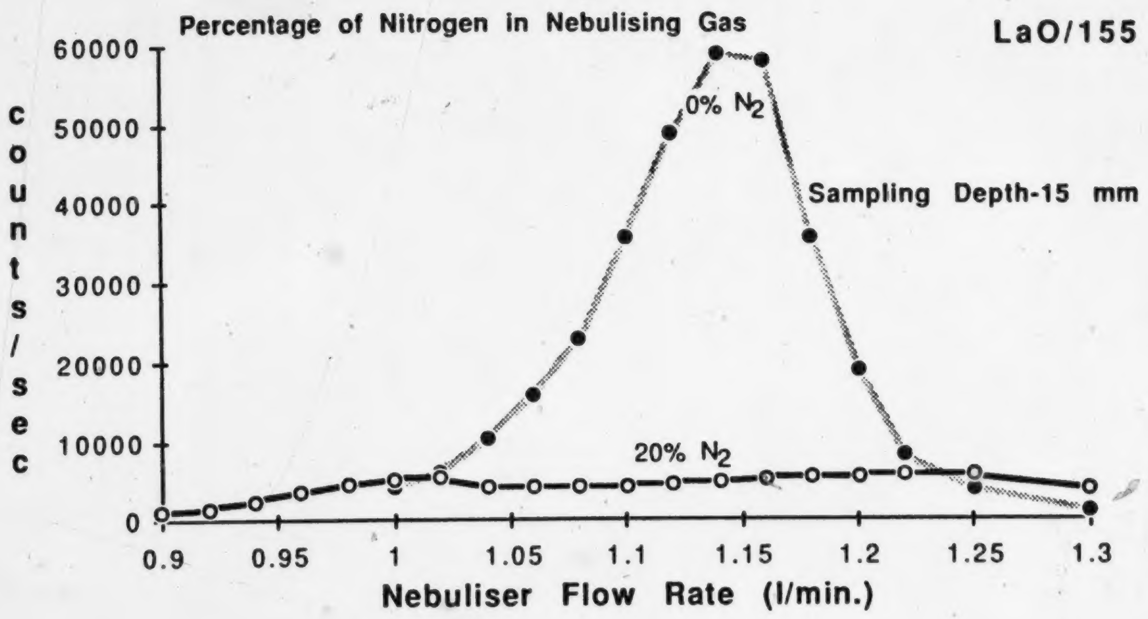

Figure 3-49. The effect of 20% nitrogen nebulising gas on LaO signal at 15 mm sampling depth.

is introduced in the form as a mixed nebulising gas. However, the trade-off is a loss of signal sensitivity as well as increased plasma instability.

E. Conclusion

The use of mixed gas plasmas in ICP-MS has been shown to be useful for basic studies. By comparing analyte performance in argon and mixed gas plasmas, one is able to correlate some aspects of the ion signal characteristics to the properties of the analyte, i.e. the stability of the analyte oxide (metal-oxide bond strength) and the ionization energy of the species. These in turn determine the optimum nebuliser gas flow rate during the analysis or, from another point of view, the spatial distribution of the species within the plasma as commonly reported in ICP-AES studies.

In addition, an enhancement effect on analyte signal sensitivity can be achieved when the mixed gas is introduced in the form of an outer gas rather than as a nebulising gas. This is consistent with the reported results obtained previously by other researchers in ICP-AES work. The addition of a low percentage of nitrogen in the outer gas also provides better signal sensitivity for elements with low ionization potentials but with large metal-oxide bond strengths and for analyte species with a degree of ionization in the plasma much lower than unity. The net effect on the first group is thought to be a result of nitrogen species interacting with the analyte oxide and eventually freeing the metal ion for detection. The second enhancement is taken to be a product of more efficient charge-transfer between the analyte and the nitrosonium ion. As demonstrated from the calculated results in Table 3-5, the application of a 5% nitrogen mixed gas in ICP-MS provides a value for the degree of ionization for all analytes much closer to the theoretical value than would otherwise be obtained using an argon discharge. However, a nitrogen mixed nebulising gas appears to be more efficient towards the removal of analyte oxide but at the expense of ion signal sensitivity. In contrast, an oxygen mixed gas plasma does not provide the same degree of signal sensitivity enhancement. In fact, for species with strong metal-oxide bond energies, the use of oxygen mixed gas has an adverse effect on the signal sensitivity.

Finally, compared to the argon discharge, a closer sampling depth and/or a higher nebuliser flow rate are necessary when the outer gas is mixed with a molecular gas. This is attributed to the dramatic change in the physical volume of the plasma discharge and more effort is required in order to push the ion cloud closer to the sampler orifice.

REFERENCES

1. E. H. Choot, Dissertation, Dept. of Chemistry, University of Alberta, Edmonton, Alberta (1982).
2. A. Montaser and R. L. Van Hoven, CRC Critical Reviews in Analytical Chemistry, 18, 45 (1987).
3. K. D. Ohls, D. W. Golightly and A. Montaser, Inductively Coupled Plasmas in Analytical Atomic Spectrometry, Ed. A. Montaser and D. W. Golightly, VCH Publishers, Inc., (1987) Chapter 15.
4. S. Greenfield, J. L. Jones and C. T. Berry, Analyst, 89, 713 (1964).
5. R. H. Wendt and V. A. Fassel, Anal. Chem., 37, 920 (1965).
6. V. A. Fassel and R. N. Kniseley, Anal. Chem., 46, 1110A (1974).
7. D. Truitt and J. W. Robinson, Anal. Chim. Acta, 49, 401 (1970).
8. D. Truitt and J. W. Robinson, Anal. Chim. Acta, 51, 61 (1970).
9. E. H. Choot and G. Horlick, Spectrochim. Acta, 41B, 889 (1986).
10. E. H. Choot and G. Horlick, Spectrochim. Acta, 41B, 907 (1986).
11. E. H. Choot and G. Horlick, Spectrochim. Acta, 41B, 925 (1986).
12. E. H. Choot and G. Horlick, Spectrochim. Acta, 41B, 935 (1986).
13. S. Greenfield and H. McD. McGeachin, Anal. Chim. Acta, 100, 101 (1978).
14. K. Ohls and D. Sommer, ICP Information Newslett., 4, 532 (1979).
15. A. Aziz, J. A. C. Brockaert and F. Leis, Spectrochim. Acta, 37B, 369 (1982).
16. R. M. Barnes and G. A. Meyer, Anal. Chem., 52, 1523 (1980).
17. G. A. Meyer and R. M. Barnes, Spectrochim. Acta, 40B, 893 (1985).
18. G. A. Meyer and M. D. Thompson, Spectrochim. Acta, 40B, 195 (1985).
19. A. Montaser and J. Mortazavi, Anal. Chem., 52, 255 (1980).
20. A. Montaser, V. A. Fassel and Zalewski, Appl. Spectrosc., 35, 292 (1981).
21. P. W. J. M. Boumans, Inductively Coupled Plasma Emission Spectroscopy,

Part 1 Methodology, Instrumentation and Performance, Chapter 4, Ed. P. W. J. M. Boumans; A Wiley-Interscience Publication, John Wiley and Sons (1987).

22. G. Horlick, S. H. Tan, M. A. Vaughan and C. A. Rose, Spectrochim. Acta, 40B, 1555 (1985).
23. M. A. Vaughan and G. Horlick, Appl. Spectrosc., 40, 434 (1986).
24. N. Furuta, Spectrochim. Acta, 41B, 1115 (1986).
25. S. R. Koirtyohann, J. S. Jones, C. P. Jester and D. A. Yates, Spectrochim. Acta, 36B, 49 (1981).
26. J. Lam, Unpublish results.
27. M. A. Vaughan, G. Horlick and S. H. Tan, J. Anal. At. Spectrom.,2, 765 (1987).
28. M. H. Abdallah and J. M. Mermet, J. Quant. Spectrosc. Rad. Transf., 19, 83 (1978).
29. R. S. Houk, A. Montaser and V. A. Fassel, Appl. Spectrosc., 37, 425 (1983).
30. CRC Handbook of Chemistry and Physics, 66th Edition, 1986. CRC Press, Inc., Florida.
31. K. P. Huber and G. Herzberg, Molecular Spectra and Molecular Structure, Vol. 4. Constants of Diatomic Molecules, Van Nostrand-Reinhold, New York (1979).
32 C. Mavroyannis and C. A. Winkler, Can. J. Chem.,39, 1601 (1961).
33. C. B. Kretschmer and H. L. Peterson, J. Chem. Phys., 39, 1772 (1963).
34. P. F. Knewstubb, Mass Spectrometry and Ion-Molecule Reaction, Cambridge University Press, London (1969) Chapter 2.
35 E. W. McDaniel, Collision Phenomena in Ionized Gases, Wiley, N. Y. (1964) Chapter 4.
36. E. Murad, J. Chem. Phys., 75, 4080 (1981).
37. E. Murad and D. L. Hildenbrand, J. Chem. Phys., 73, 4005 (1980).
38. R. S. Houk, Anal. Chem., 58, 97A (1986).

Chapter 4

The Effects of Aerosol Processing and Plasma Gas Composition on Analyte and Analyte Mono-Oxide Response in ICP-MS

A. Introduction

Most samples are introduced into the ICP as aqueous aerosols and, while it is often ignored, it is useful to keep in mind that as much as 99.9% or more of the material introduced is water. Over the years, some fundamental studies have been focussed on solvent/plasma interactions. Alder et al. [1] observed a general decrease in plasma electron density as well as a lowering of analyte excitation and ionization temperatures at various heights above the load coil after water had been removed from the aerosol stream. They attributed their observation to the difference in ionization potentials of hydrogen and oxygen as compared to argon. Blades and Caughlin [2] also studied the effect of aqueous and organic type solutions on plasma electron density (n_e) and excitation temperature (T_{ex}) at different plasma powers and viewing heights. They reported that the presence of organic aerosol not only lowered the electron density (by about 2×10^{15} cm^{-3}) but also lowered the T_{ex} by about 1500 K. They interpreted the differences to be a result of the more stable C_2 species (D° 6.5 eV) in organic matrixes as compared with the more readily dissociated OH species (D° 4.3 eV) in aqueous media. Boorn and Browner [3] correlated "limiting aspiration rates" to "evaporation factors" for some thirty common organic solvents and they concluded that plasma stability is a function of solvent vapour loading. Maessen et al. [4] have also carried out detailed studies on the effect of solvent plasma load for various solvents and analytes. Tang and Trassy [5] reported a drop in spectroscopic temperature after aerosol particles had been desolvated and they suggested the reason for the difference in temperature was due to the better thermal conductivity of hydrogen over argon. Caughlin and Blades [6] also compared the plasma electron density with and without water nebulisation at different viewing heights. They found that the greatest difference caused by the absence of water occurred deep inside the plasma discharge and yet, in the normal analytical zone (NAZ), the difference was negligible.

As with ICP-AES, solvent and the effect of solvent load can be expected to have a major effect on analyte signals in ICP-MS. In particular, reducing the solvent load in ICP-MS by cooling the spray chamber has become common place and is an advertised feature and standard procedure on commercial instrumentation. A key benefit achieved by cooling the spray chamber is a reduction in the level of oxide species observed in the spectra. This includes both analyte and matrix oxides as well as the ArO ion. In addition, the cooled spray chamber facilitates the introduction of non-aqueous solvent matrixes.

For aqueous sample introduction in ICP-MS, cooled spray chamber, solvent load and oxide reduction are all inextricably linked to the role of water in oxide formation and indeed, to the fundamentals of oxide formation in ICP-MS. A brief overview follows.

B. Oxide Behaviour in ICP-MS

In ICP-AES, metal-oxide species have been of little concern because the plasma is generally regarded as being capable of vaporizing and dissociating most, if not all, metallic oxides. This is also borne out by the fact that, for observations in the NAZ, there is little evidence in the ICP-AES literature for the existence of vaporization type interferences. However, for plasmas run at cooler conditions (i.e. low power and high nebuliser flow rates) and for observations low in the plasma analyte channel (i.e. at or below the initial radiation zone (IRZ)), vaporization interferences have been observed and molecular species can become important.

In contrast, metal oxide and hydroxide species in ICP-MS have been the subject of concern and study from the beginning. Their increased importance stem mainly from the fact the oxide species in ICP-MS constitute a serious source of spectral interferences. The problem is compounded because experimental conditions used in ICP-MS are more favourable to oxide formation than those used in ICP-AES. Because the desired analyte species detected in ICP-MS are free ground state ions rather than excited state ions (i.e. emitting ions), the ICP is normally run at lower powers and higher nebuliser flow rates than would be normal for ICP-AES. As well, the plasma is often sampled relatively close to the load coil (10 mm from the load coil), and indeed the presence of the sampling cone itself and reactions during the extraction process are all thought to contribute to increased oxide levels. Using in-house instruments, Houk et al. [7] were among the first to report the observation of metal hydroxide ions. They attributed these species to ion-atomic recombination during the extraction process. With the instrument operating in a boundary layer extraction sampling mode, Date and Gray [8] also observed oxide and hydroxide ions even when a hydride generator was used for sample introduction. However, when their instrument was adapted to operate in a continuous sampling mode (i.e. larger sampling orifice), they were able to characterize the metal oxide ion behaviour and its intensity ratio to metal ion (MO^+/M^+). Based on their results, they further suggested that the majority of oxide ions were formed at the boundary layer rather than as undissociated molecules from the ICP. Using a commercial SCIEX Elan instrument, Horlick and coworkers [10, 11] pointed out the significance of metal oxide spectral interferences and thereafter a considerable amount of work has focussed on metal oxide ion characterization [12-24].

Initially, researchers felt that the oxide species were mostly generated during the sampling extraction process, i.e. at the cool thermal boundary layer, with only a few percent of the oxide originating directly from the ICP [7, 9, 13, 17, 18, 24-26]. This explanation, as logical as it may seem, has one serious drawback. If the majority of the metal oxide species were generated during the sampling process, then the amount of oxide should not be highly dependent on plasma operating conditions. In fact, the metal oxide intensity is very dependent on nebuliser flow rate in much the same way as the analyte signal. Both show typical peak shape response, with ion signal intensity increasing with increasing nebuliser flow rate, but after reaching a maximum response, ion signal intensity then drops off rapidly with a further increase in nebuliser flow rate. In general, the oxide signal profiles are similar to the metal ion profiles but peak out at a higher nebuliser gas flow rate [11, 15, 20, 23]. Hence, the MO^+/M^+ ratio also increases with increasing nebuliser gas flow rate. Typical behaviour is shown in Figure 4-1 for La and LaO. This behaviour can be explained by a spatial shift of the initial radiation zone. As the nebuliser flow rate is increased, the lower region of the plasma, just below the IRZ, where most of the oxide species likely exist in the plasma, is pushed towards the sampling orifice [11, 26]. Alternatively, the observation of metal oxide ion at high nebuliser flow rate could also be explained in terms of increased boundary layer formation around the edge of the orifice. At high nebuliser flow rate, the aperture of the sampler is cooled to a greater extent, and as a result, oxide formation is encouraged.

The observed oxide behaviour is also dependent on the ICP-MS instrumentation utilized. In general, the instruments can be divided into SCIEX and non-SCIEX types. With the SCIEX instrument, the observed MO^+/M^+ ratio is higher for conditions optimum for metal ion intensity (i.e. the nebuliser flow rate for peak La response in Figure 4-1). However, the observed metal oxide ion signal drops rapidly at increasing sampling depth [11, 15]. In addition, any increase in plasma forward power will also result in the reduction of MO^+/M^+ ratio. In contrast, the non-SCIEX instruments exhibit a lower oxide percentage at optimum plasma conditions for the free analyte ion. Yet, the oxide ion signal shows little change when increasing the sampling depth [9] and the MO^+/M^+ ratio also increases with increasing plasma forward power [20, 23]. The only fundamental difference between the

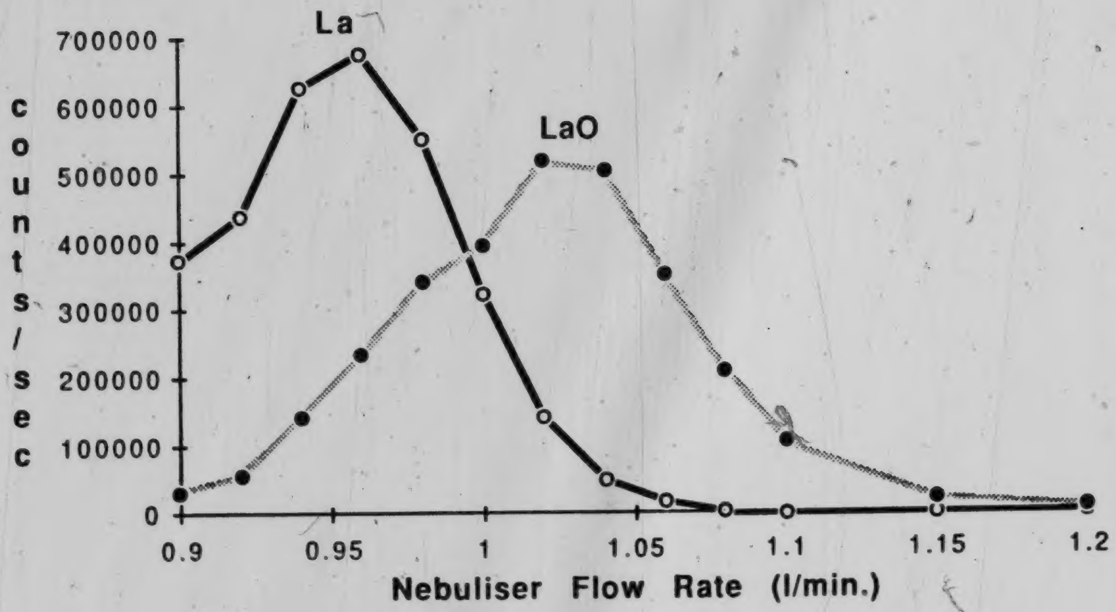

Figure 4-1. Diagram to show typical responses for La and LaO to nebuliser flow rate.

two types of instruments is the implementation of a centre-tapped grounded loaded coil at the ICP source of the SCIEX model. This idea eliminated the high rf potential between the plasma source and the sampler [17, 24], which resulted in a secondary discharge at the orifice of the instrument [24, 26-30]. Up to that time, it had been generally recognized that this pinch discharge reduces the level of metal oxide ions [26]. Thus, with non-SCIEX instruments, the percentage level of oxide ions is lower.

While the metal oxide levels observed in ICP-MS are often below 1%, their effect may become significant, especially in trace and ultra-trace metal analyses. In practice, for an element with multiple isotopes, one can shift to an interference free isotope mass if a problem exists with a metal oxide ion spectral interference. However, in most instances, this secondary mass has a lower natural abundance and thus the detection limit deteriorates. For a situation where the interfered species is mono-isotopic, the above approach will be impossible. Based on the isotopic ratio of the interferent, Doherty and Voet [31] were able to subtract the oxide interference effect during the determination of rare earth elements in geological materials. Their calculation was elaborate, taking into account considerations such as structural and non-structural background. Further, extreme precaution has to be taken with this kind of methodology because in the presence of an additional contaminant, the result may be erroneous. Alternatively, by exploiting the finite mass difference between the metal oxide ion and the interfered metal ion, the use of a high resolution mass spectrometer has also been proposed [13, 32]. This idea, although feasible, is impractical when the anticipated high cost is also taken into consideration.

The most popular method for sample delivery is the use of a pneumatic nebuliser during elemental analysis using ICP-MS. On the whole, the background spectra generated are usually complicated and matrix dependent [33]. Recently, it has been demonstrated that the use of a nebuliser arc [34, 35] can reduce the H- and O- containing species considerably. In particularly, Jiang and Houk [35] observed that the ratio of cerium oxide ion to cerium ion was reduced to less than 0.2% when the arc device was used. On the other hand, other novel sample introduction devices such as a "wire loop direct sample introduction device" [36, 37] and laser ablation of solids [38] also reduced the background H- and O- poly-atomic ions by an order of magnitude or more.

The success of these approaches in reducing oxide and poly-atomic background levels clearly indicates that reduction of the aqueous solvent load should also have a similar beneficial effect. The aim of this study is to characterize the behaviour of metal oxide ion species as a function of variables in the aerosol delivery system and in combination with mixed gas plasmas.

C. Experimental

In order to study the effects of aerosol processing, a simple "desolvation" apparatus was set-up as shown in Figure 4-2. This system consisted of a regular Meinhard nebuliser and a Scott type spray chamber connected to a heating chamber (5.5 cm dia. and 18 cm long), which is in turn connected to a coil type water-cooled condenser (4 cm dia. and 28 cm long) and finally to the ICP torch. The heating chamber was wrapped with heating ribbon and connected to Variac variable transformer. It should be emphasized that this system was not necessarily operated as a desolvation apparatus. In particular, for a number of measurements, the heating chamber was NOT heated, but left at room temperature while the condenser was operated. This form of aerosol processing was designated, "condensed aerosol". For other experiments, the chamber was heated and the system operated in a "desolvation" mode. Finally, some experiments were carried out using the system shown in Figure 4-3 which consisted ONLY of the heating chamber as the aerosol processor. Again, this chamber was not always heated, but was held at room temperature for some experiments. This form of aerosol processing was designated as "uncondensed aerosol".

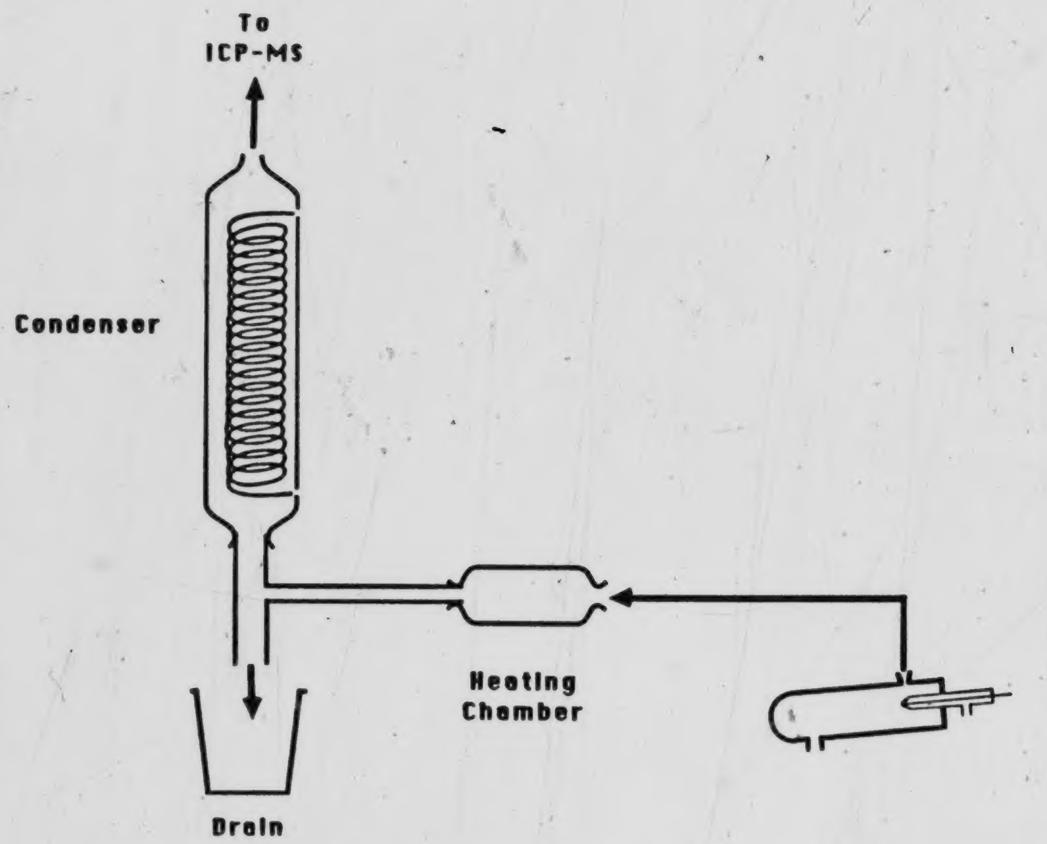

Figure 4-2. Schematic diagram of the aerosol processing set-up (for condensed and desolvated nebulisations).

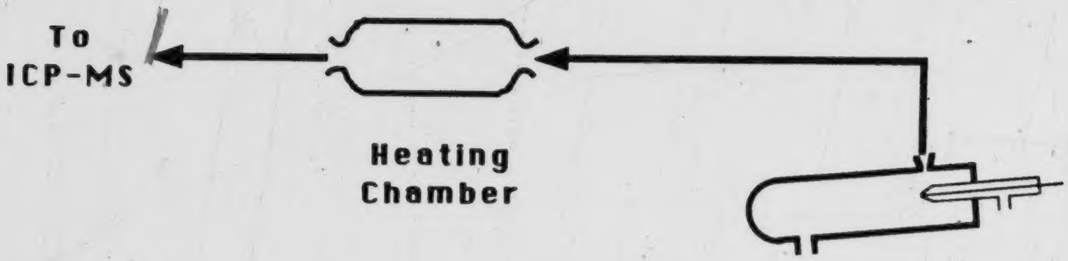

Figure 4-3. Schematic diagram of the uncondensed aerosol nebulisation.

While a study of all the above modes may seem somewhat superfluous, all of them had distinct measurable effects on the ICP-MS signal. The signals from the processed aerosol systems were compared with "direct" nebulisation, the normal SCIEX system with the nebuliser/spray chamber system connected directly to the plasma torch.

The plasma (outer) gas flow rate was 15 l/min, the auxiliary gas flow rate was 1.80 l/min, the forward power was 1.50 kW and the sampling depth was 10 mm. The nebuliser gas flow rate was varied during the experiment and unless otherwise stated, all gas flows were argon.

D. Effects of Aerosol Processing on Analyte Signals

a. Direct versus Condensed Aerosol Introduction

For this study, the aerosol processing system shown in Figure 4-2 was used. However the heating chamber was not heated, but rather, kept at room temperature (23°C) and the condenser was cooled with cold tap water. This is the condensed aerosol mode.

The sample analytes chosen for this study were Zn, Ge, As, Sr, Y, Zr and Ru. Most data were taken using a multi-element solution containing 0.2 ppm of each element in 2% nitric acid. The signal responses for each element were obtained as a function of the nebuliser gas flow rate. For brevity, only signal profiles for As, Sr, and Ru are illustrated (Figures 4-4 to 4-6). Two common features emerged from this set of results. In general, a higher nebuliser gas flow rate is necessary in order to attain the optimum ion intensity when the system is operating in the condensed aerosol mode. Also, signal sensitivity is affected by the aerosol delivery system and the changes are analyte dependent. In contrast to the signal intensity changes observed with the nitrogen mixed gas plasma, these signal intensity changes correlate best with element ionization potential rather than metal oxide

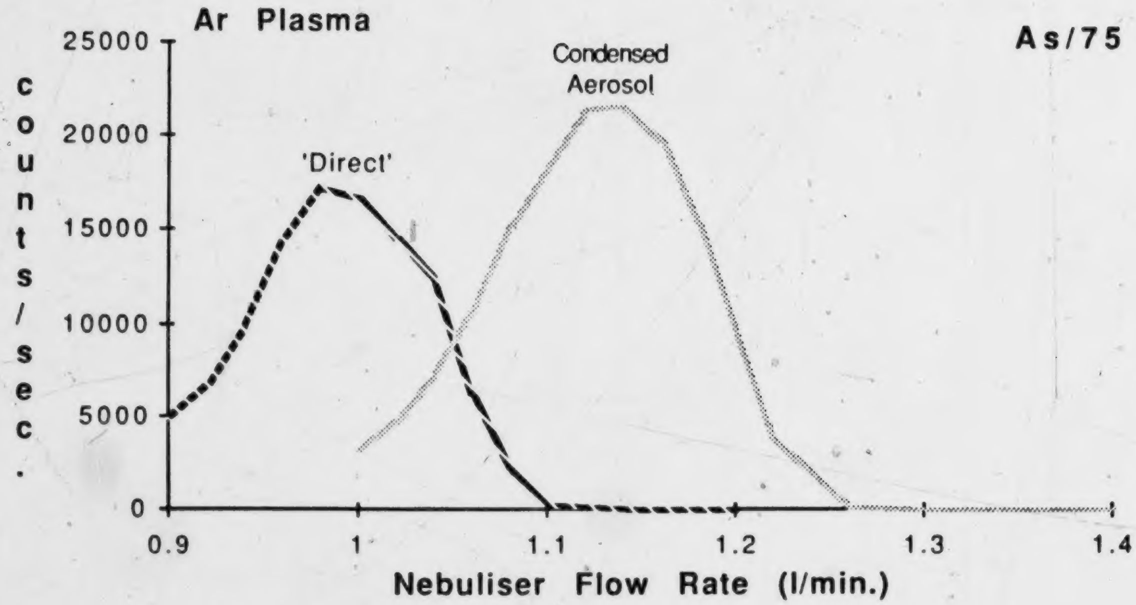

Figure 4-4. Dependence of As signal on nebuliser flow rate in "direct" and condensed aerosol nebulisations.

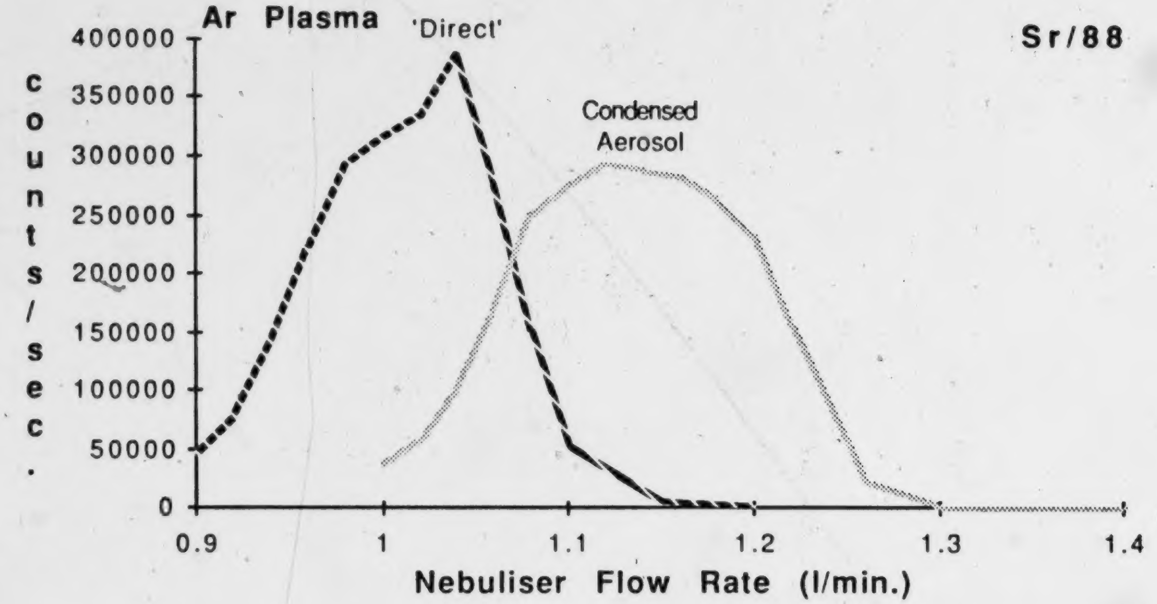

Figure 4-5. Dependence of Sr signal on nebuliser flow rate in "direct" and condensed aerosol nebulisations.

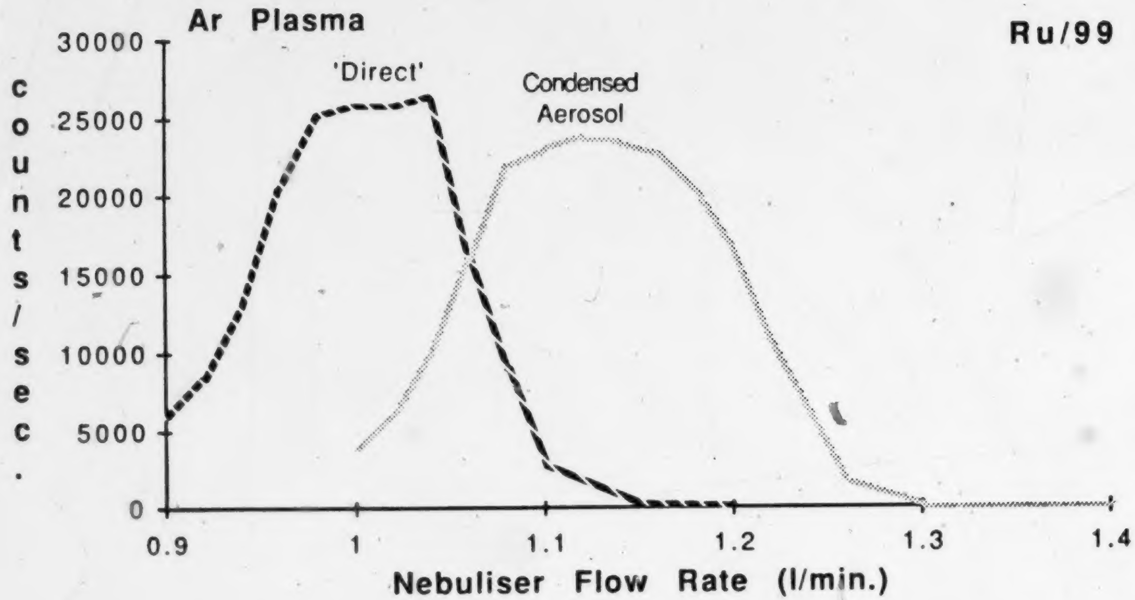

Figure 4-6. Dependence of Ru signal on nebuliser flow rate in "direct" and condensed aerosol nebulisations.

bond energy. This is shown in Figure 4-7. Although the underlying reason for this correlation is not fully understood, some inferences can still be drawn.

From the difference in signal profiles (nebuliser flow rate plots) obtained between the two modes and the relationship between spatial shift and nebuliser gas flow rate proposed in the previous chapter, one can speculate that the considerable increase in the optimum nebuliser flow rate for peak analyte signals for the condensed aerosol mode is likely a result of a spatial shift of ionic species inside the discharge. This is a consequence of either the aerosol particles desolvating earlier after they have been "processed" during the "condensation" stage or the plasma itself becomes more energetic or both. In any case, it enables the ionization process to take place "earlier", hence a higher central gas flow rate is required to attain the peak signal response.

Myers and Tracey [39] used a similar aerosol delivery system (by inserting an extra tubing connection between the spray chamber and the ICP torch) and described its function as similar to an aerosol filter. This effect can be explained by a change in physical dimension of the aerosol particle; after the droplet has left the spray chamber, it is physically altered by the additional traveling distance which allows it more time to vaporize and equilibrate with its drier surrounding. The theoretical radius of the particle can be calculated [40]:

$$r_x^3 + \frac{200\ M_s\ \sigma\ r_x^2}{\alpha\ R\ T\ a\ \rho} - r_0^3 = 0 \qquad (4\text{-}1)$$

where:

r_0 = initial radius of the aerosol droplet (μm)

r_x = radius of the droplet at equilibrium

M_s = molecular mass of the solvent

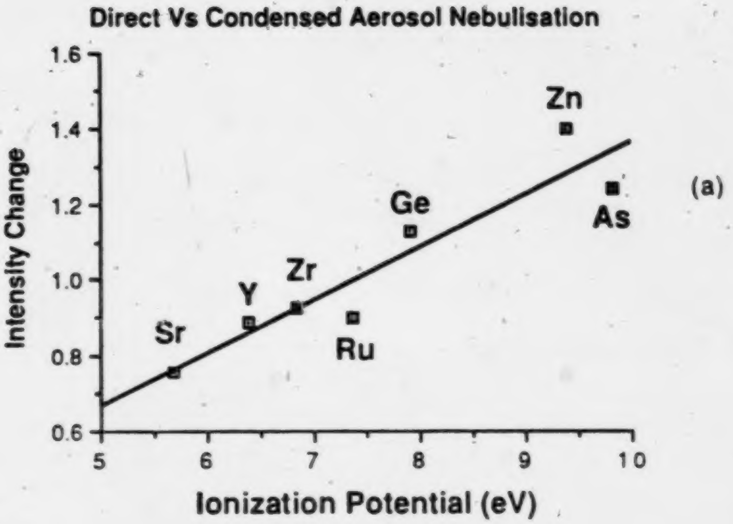

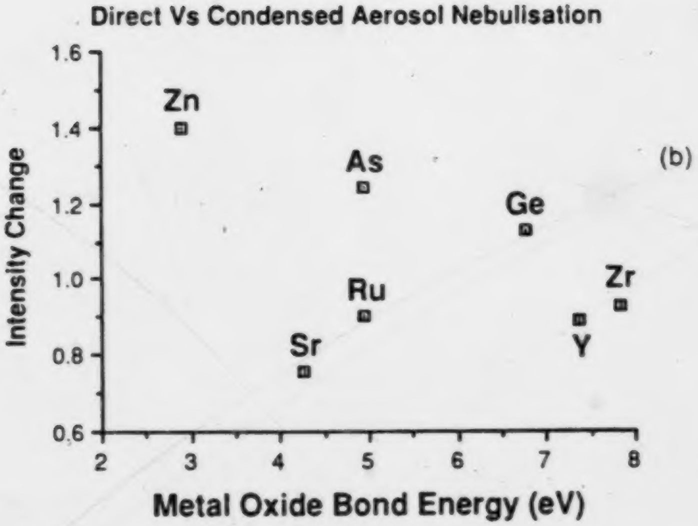

Figure 4-7. a) Bar graph to compare the relationship between signal intensity difference in direct and condensed nebulisations to analytes' ionization potential. b) The lack of correlation between signal intensity changed and metal oxide bond energy.

σ = surface tension of the solvent (dyn. cm^{-1})

ρ = gas density (g cm^{-3})

R = gas constant

T = absolute temperature (K)

a = solute concentration

α = dissociation fraction of the solute

From this equation, it can be seen that the particle radius is dependent on solute concentration and the vapour pressure of its environment, hence the aerosol droplet becomes more minute (due to solvent evaporation to the drier surrounding until a steady-state has been reached) and/or the relative size distribution of the aerosol particles becomes more uniform as larger size particles have a greater probability of elimination via wall condensation as a consequence of the extra traveling distance required. Long and Browner [41] compared the vertical and spatial analyte emission profiles in the absence and presence of water. Through their observations they speculated that with water, the analyte desolvation process within the plasma is kinetically controlled and hence, they observed spatial shifts for analyte emissions. Rybarczyk et al. [42] also observed a lowering of IRZ with respect to the load coil after nebulised aerosol had been desolvated. All of the above (established in ICP-AES work) are consistent with the general trend observed in ICP-MS (see Figures 4-4 to 4-6) for the condensed aerosol mode.

In an ICP source, the primary species are free electrons, argon atoms and argon ions. Over the years, an enormous amount of effort has been expended in the search for a better understanding of ICP excitation mechanisms, especially analyte excitation and ion formation processes. The most common measurements are those of analyte spectroscopic temperature, electron density and their dependency on plasma operating parameters. In plasma diagnostic studies using ICP-AES, lower excitation and ionization temperatures as well as lower electron density are the features commonly observed after limiting the amount of aqueous solvent entering the ICP [1, 5, 6]. Yet, strictly from the standpoint of energy conservation, the above reports do not seem to be reasonable. They appear to indicate that the energy supply from the source is less "effective" when in fact, the amount of solvent entering the plasma is actually reduced.

In considering the net effect of solvent load on ICP-MS, the excitation mechanism can be ignored since only the net effect on ground state ions is significant with this technique. The main processes are summarized as the following:

i) Penning Ionization

This is one of the earliest excitation mechanism postulations [43] in which the argon atom in metastable state excites and ionizes the analyte species with its relatively high excitation energies (11.55 eV and 11.76 eV).

$$Ar^m + X \rightarrow Ar + X^+ + e^- \qquad (4\text{-}2)$$

ii) Charge-Transfer Reaction [44,45]

The relatively larger population of Ar^+ over Ar^m favours this process. Furthermore, the ionization energy of 15.76 eV allows for a one step process observed quite commonly in emission spectroscopy.

$$Ar^+ + X \rightarrow Ar + X^+ \qquad (4\text{-}3)$$

$$Ar^+ + X \rightarrow Ar + X^{+*} \qquad (4\text{-}4)$$

However, this mechanism does not allow for the reverse process due to the much higher population level of argon neutral atoms within the discharge (degree of ionization ~ 1%)

iii) Electron Impact Ionization and Three-body recombination

$$X + e^- \rightarrow X^+ + 2e^- \qquad (4\text{-}5)$$

Using a steady-state approach, Hieftje and coworkers [46, 47] compared the spatial behaviour of analyte emission intensities to a concentration product of the reaction species. They observed good correlation between ion generation and Penning Ionization and charge-transfer processes. In addition, they also indicated that the population of excited neutral atoms is mainly generated from the three-body recombination process whereas ground state ions are excited directly by electron impact.

By extrapolating the above suggestions, it seems plausible to suggest that the dissociation and subsequent ionization of solvent components are mainly due to the Penning process and to the charge-transfer reaction mechanism. Although, the presence and subsequent ionization of solvent components would enhance the plasma electron density, the overall level of argon atoms in the metastable and ionic states would have to decrease. As a result, ionization of analyte by Penning or charge-transfer processes (hard to ionize species) would be less favourable as compared with the analyte ionization process, which depends mainly on electron impact reaction (easily ionized species).

The main difference between the direct nebulisation mode and the condensed aerosol mode is the presence of the condenser. Since no heating was applied during the study, a large scale of solvent removal was not anticipated in the condensed aerosol mode despite the presence of the condenser. On the other hand, physical conditions inside the spray chamber were different between the two modes of operations. When the system was operating in the direct nebulisation mode, the nebuliser and spray chamber set-up were placed inside the plasma cabinet. Since the cabinet temperature was significantly higher than the room temperature (heat transfer from the hot plasma source) therefore the vapour pressure inside the spray chamber and thus the carrier gas stream became higher. This in turn encouraged a larger proportion of solvent entering the plasma discharge. In contrast, the nebuliser and spray chamber set-up in the condensed aerosol mode were located outside the the Elan instrument (at room temperature environment). Hence, the carrier gas carried a lower vapour pressure gas stream and the amount of solvent introduced into the discharge was actually reduced. Now the results in Figure 4-7 begin to make sense. When the system is operating in the direct nebulisation mode, a larger amount of solvent is introduced into the plasma. This enhances the plasma electron density and favours those analyte ionization processes depending mainly on electron impact reactions (easily ionized species such as Sr). On the other hand, operating the system in the condensed aerosol mode lowers the amount of solvent entering the plasma, which in turn enriches the metastable argon and argon ion populations. This favours ionization of analyte by Penning and charge-transfer processes (hard to ionize species such as As).

The above speculation, as reasonable as it may seem, is by no means a foregone conclusion, as the population levels for argon ion and the metastable species have not been monitored independently.

b. Effect of Heating Chamber Temperature

Aerosol drying and solvent removal is achieved by reducing the vapour pressure in the aerosol stream. This encourages the evaporation of solvent from aerosol droplets until a steady-state is attained. Due to the relatively small size of the aerosol particles, a significant amount of solvent loss can take place very rapidly. The simple and common system for solvent removal is a water-cooled spray chamber [48] and it is one of the features available in commercial instrumentation. Alternatively, more elaborate methods have also been developed. They typically involve cascading heating and condensation stages. The saturated vapour pressure within a container is elevated initially by raising the temperature of the container. This encourages the evaporation of solvent from the aerosol droplets. The aerosol stream is then subjected to rapid cooling which allows the subsequent removal of vapour from the stream. In general, this step is accomplished using a water-cooled condenser. However, in a situation where "anhydrous" aerosol is preferred, a second stage of condenser is usually cascaded. This second stage of cooling generally uses solid carbon dioxide and organic solvent [49] to "freeze dry" the aerosol stream.

In this study, only a water-cooled condenser was used. The equipment set-up was as illustrated in Figure 4-2. The temperature of the heating chamber was manually adjusted to give a range from 23°C to 100°C. The plasma operating parameters and the sample analytes remained the same as in the previous section.

The summarized results are presented in Figures 4-8 to 4-10. For brevity, only data for Sr (low ionization energy and modest oxide bond strength), Y (modest ionization energy but with strong oxide bond energy) and As (high ionization potential and low oxide bond energy) are presented. In each figure, the analyte signal response as a function of nebuliser flow rate at chamber temperatures of 23°C, 37°C, 65°C and 100°C are shown.

From the results shown in each figure, the overall analyte signal profiles do not change substantially even at different chamber temperatures. However, the optimum temperature for analyte sensitivity is at 37°C and any subsequent increase in temperature results in a lost of signal intensity.

Since the above trend is similar for all of the tested analyte ions, this suggests that the limiting factor in signal sensitivity is an instrument factor rather than a factor related to the chemical properties of the analyte species. The initial increase in ion signal intensity is probably a result of solvent loading reduction (at 37°C). The subsequent lowering of signal sensitivity is likely due to a reduction of aerosol transportation efficiency. This phenomenon is probably a result of solvent recondensing back onto the surface of a particle droplet during the solvent removal stage. The sequence of events and outcome can be explained in terms of vapour density within the system. Any substantial increase in temperature gives a proportional elevation of vapour pressure inside the heating chamber. As this volume of saturated vapour reaches the cooler environment of the condenser, a

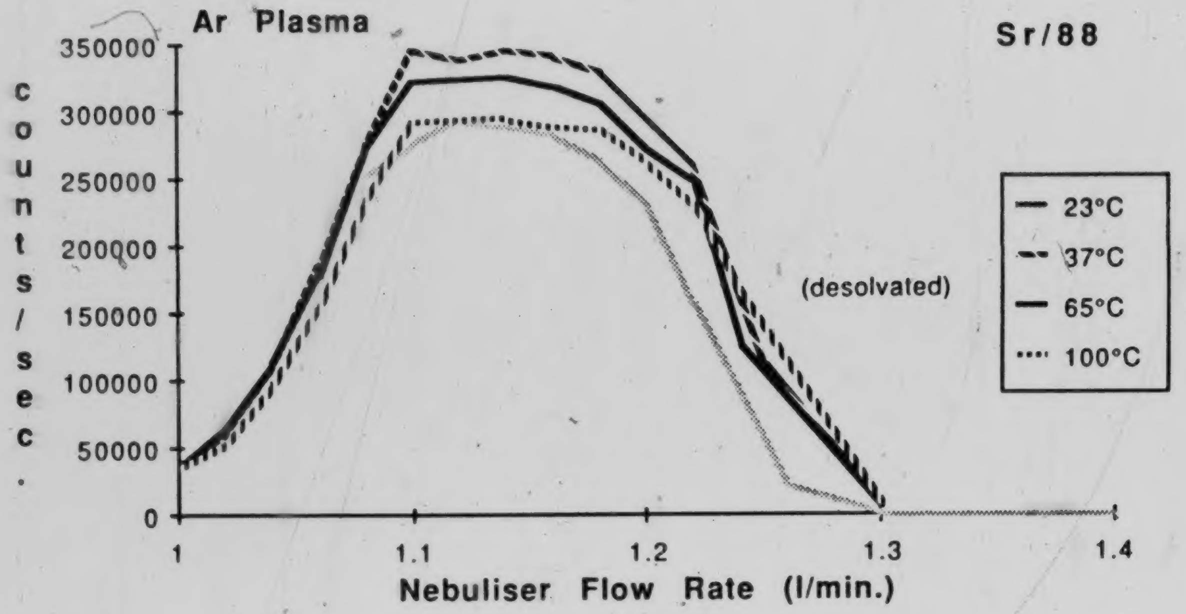

Figure 4-8. Diagram to show the effect of chamber heating temperature and nebuliser flow rate on Sr signal in an argon plasma.

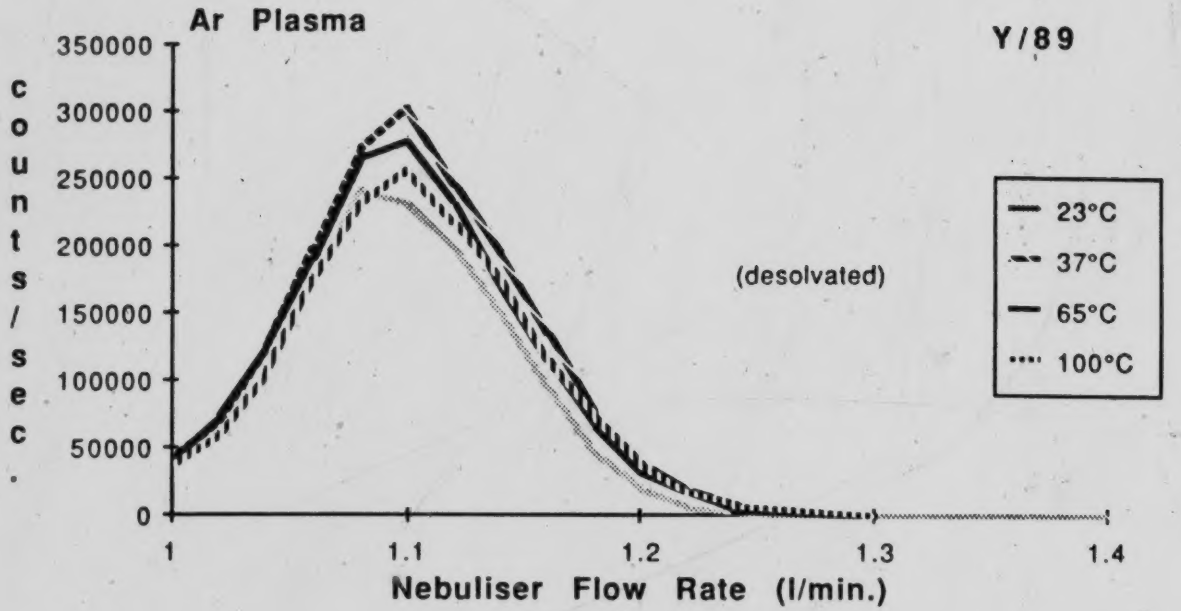

Figure 4-9. Diagram to show the effect of chamber heating temperature and nebuliser flow rate on Y signal in an argon plasma.

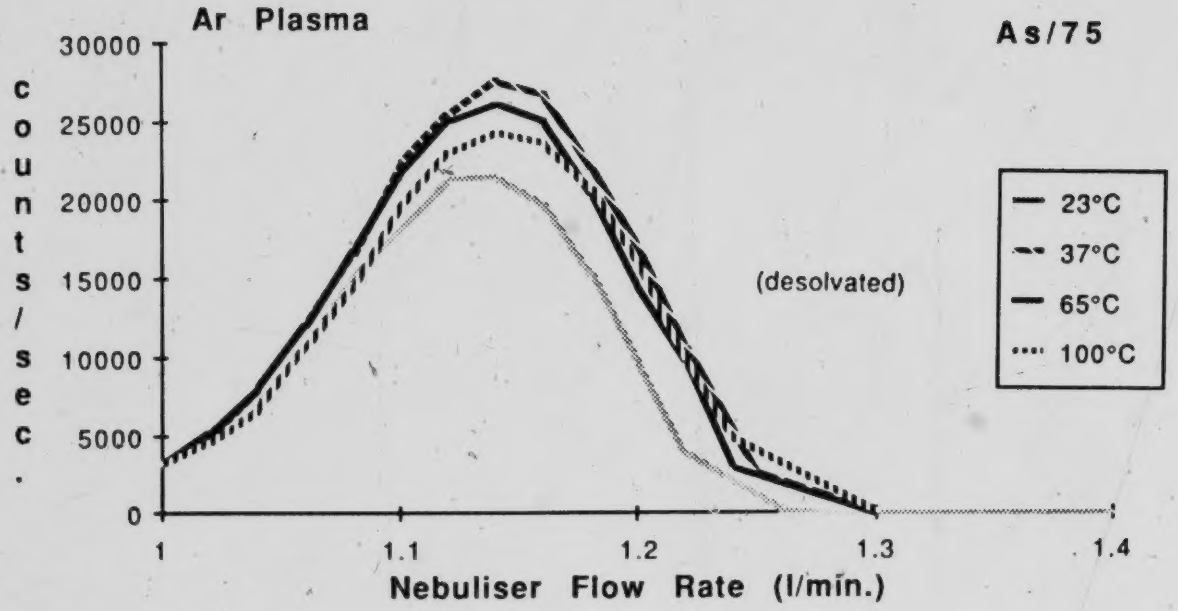

Figure 4-10. Diagram to show the effect of chamber heating temperature and nebuliser flow rate on As signal in an argon plasma.

sudden volume contraction and solvent vapour condensation take place. Theoretically, the condensed solvent, achieved by the temperature gradient developed between the main stream and the condenser wall would encourage the liquid to coalesce and recondense on the cooled surface wall (away from the stream). However, the condenser used in the study is the coiled type and this provides a more turbulent stream. As a result, the temperature gradient is poorly defined and this promotes the condensation of solvent vapour back on the surface of the "dehydrated" aerosol. As a result, the final size of the particles becomes larger and they have a higher tendency to be lost from the gas stream.

In conclusion, there is little doubt that a detailed understanding of the role of solvent in the ICP is beneficial in providing some insight into analyte ionization mechanisms in ICP-MS. In hindsight, a 'Liebig' type condenser should have been used instead as it would have allowed a better defined thermal gradient to establish and thus improves the efficiency of solvent removal.

E. Effect of Aerosol Processing on La and LaO Ions

a. Direct, Condensed and Uncondensed Aerosol Introduction

In an earlier part of this chapter, it was suggested that the amount of aqueous solvent introduced into the plasma discharge (solvent load) is particularly important for limiting the population of H- and O- related species. This concept can be examined by subjecting the nebulised aerosol stream to different aerosol processing techniques while the ion signals from the analyte and its oxide are monitored simultaneously. In this study, the aerosol processing modes were "Direct", "Condensed", and "Uncondensed" as defined earlier in the Introduction. In the case of direct nebulisation, the spray chamber was placed inside the plasma cabinet box (normal arrangement). In the other two situations, it was located outside of the cabinet. The latter two modes took the form indicated in Figures 4-2 and 4-3 respectively.

The plasma parameters were the same as in the previous section with the rf power at 1.50 kW and the sampling depth at 10 mm. An analyte solution consisting of 1 ppm lanthanum in 2% nitric acid was used. The ion responses for La and its oxide were monitored as a function of nebuliser flow rate.

The signal profiles of the two species are shown in Figures 4-11 and 4-12. The top and bottom frames in each figure illustrate the different effects on both La and its oxide ion responses to direct and indirect nebulisation respectively. Several common features evolve from the data; the individual nebuliser flow rate necessary to attain peak signal intensity is lower when using the direct nebulisation mode and the peak ion sensitivities for each species are comparable for all three types of aerosol nebulisation.

The effect of aerosol processing on analyte and its oxide ion can be evaluated by comparing the oxide percent obtained at the peak metal ion sensitivity. The calculated results are summarized as the following:

Mode of Operation	LaO^+/La^+
Direct Nebuliser	34.5%
Condensed Aerosol	15.7%
Uncondensed Aerosol	16.3%

The above results are particularly interesting. Despite the negligible difference in ion sensitivity (peak ion signal) obtained from the three aerosol nebulisation techniques, the oxide percent has been effectively reduced to half of its original value (direct nebulisation) and this is achieved simply by extending the aerosol traveling distance.

b. Effect of Heating Chamber Temperature

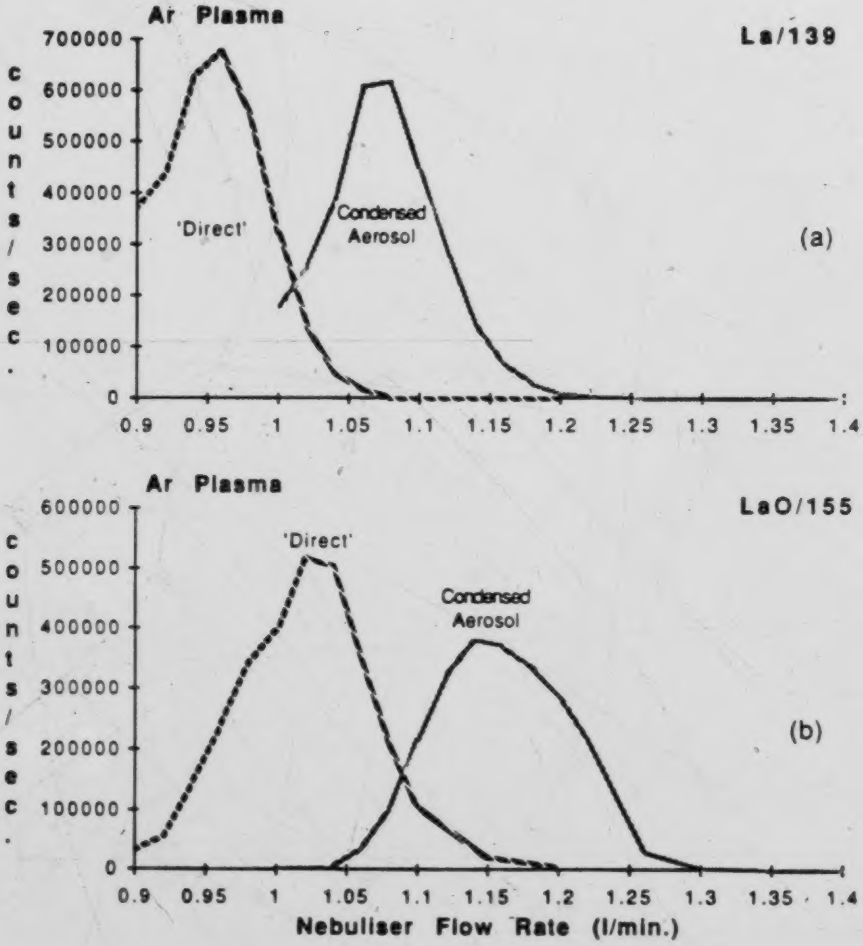

Figure 4-11. a) Diagram to show the signal responses of La in direct and condensed aerosol nebulisations. b) Diagram to show the signal responses of LaO in direct and condensed aerosol nebulisations.

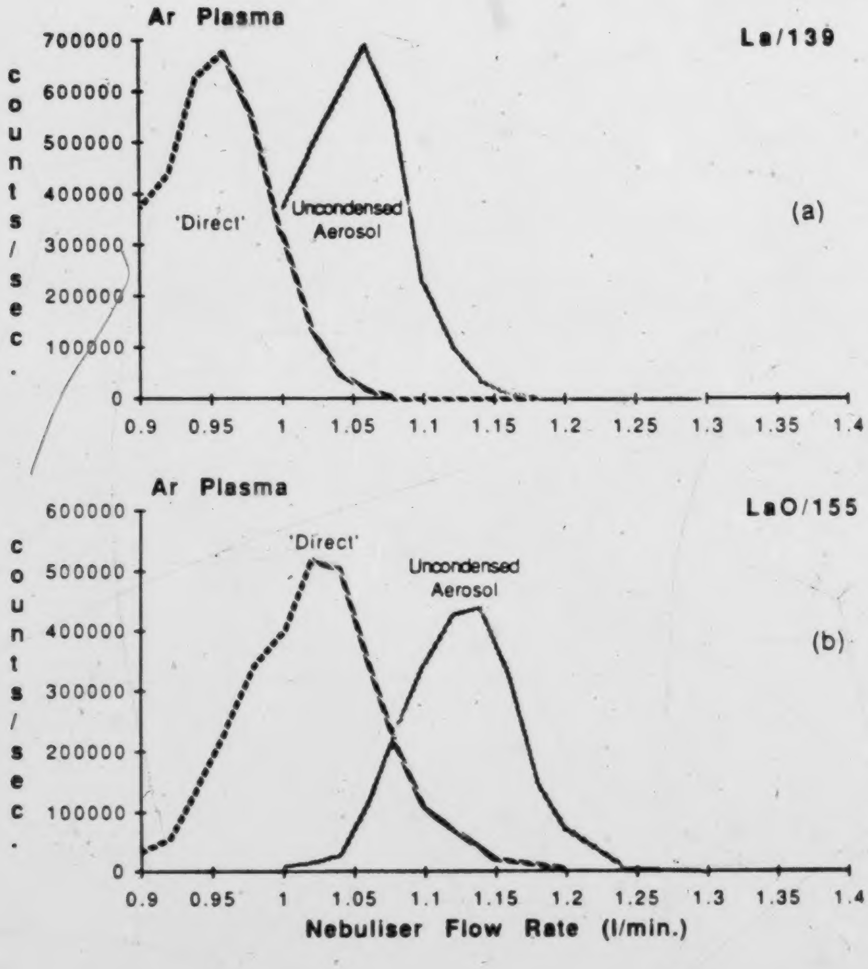

Figure 4-12. a) Diagram to show the signal responses of La in direct and uncondensed aerosol nebulisations. b) Diagram to show the signal responses of LaO in direct and uncondensed aerosol nebulisations.

It has been proposed that water is a major factor involved in the formation of oxygen-related ion species in ICP-MS. Thus, the effect of water on oxide percent was examined by progressively limiting the amount of aqueous solvent entering the discharge.

The equipment set-up was identical to the earlier study (condensed and uncondensed mode). The heating chamber temperatures were 23°C, 37°C, 65°C and 100°C. The sample analyte solution (La) and the plasma operating parameters were identical to the previous section. The signal responses for La and its oxide were monitored as a function of nebuliser flow rate at each chamber temperature for the two aerosol processing modes.

The ion intensity responses for La and LaO from desolvated and uncondensed nebulisations are illustrated in Figures 4-13 and 4-14 respectively. The overall trend shown in the two figures is consistent with the results obtained previously for aerosol heating. It is interesting to note that while the chamber temperature affects both the oxide and metal ions to the same extent, the heating effect on peak ion signal intensity is less obvious with uncondensed aerosol nebulisation (see Figure 4-14).

Finally, the effect of heating chamber temperature on oxide percent at peak metal ion intensity for the two types of aerosol processing techniques are presented in Figures 4-15 and 4-16. From the data shown in each figure, it is interesting to note that despite the larger effect of heating chamber temperature on peak signal intensity in desolvated nebulisation (see Figure 4-13), the calculated oxide percentage remains virtually unchanged. In contrast, when the system is operating in the uncondensed mode, the oxide percentage decreases with increasing chamber temperatures.

c. Discussion

By comparing the "direct" and "indirect" modes of nebulisation, it is clear that the extra pathway created between the spray chamber and the plasma torch has very little effect on

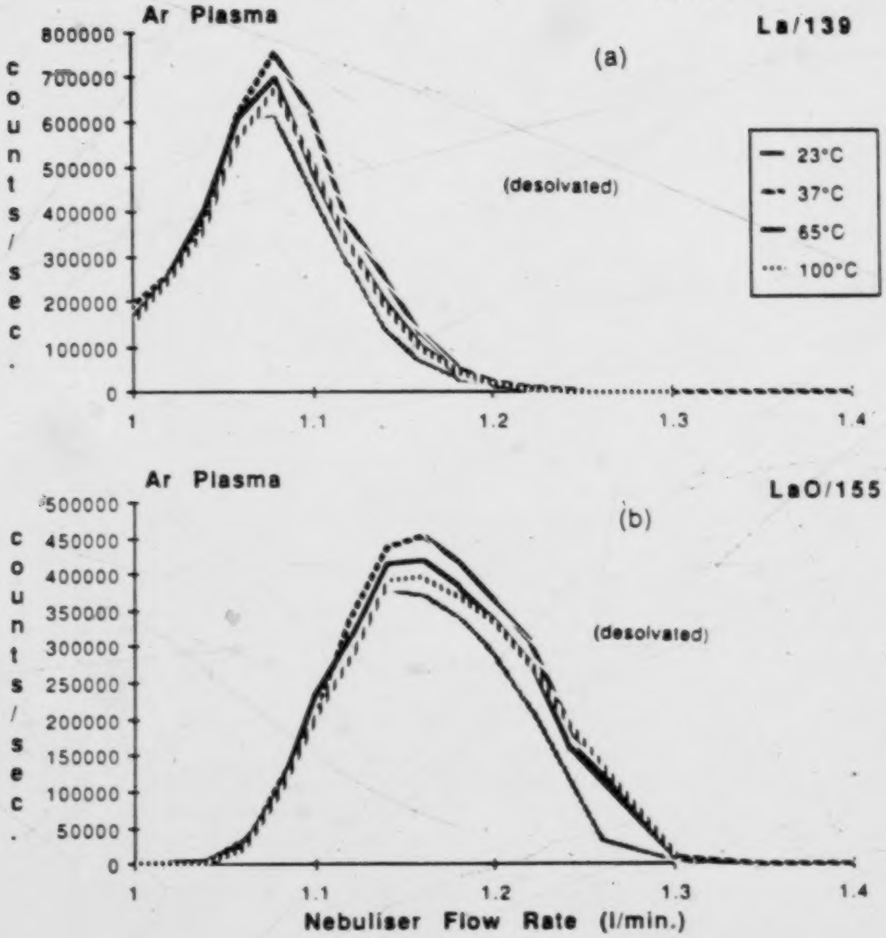

Figure 4-13. a) Diagram to show the effect of chamber heating temperature and nebuliser flow rate on La signal in desolvated nebulisation. b) Diagram to show the effect of chamber heating temperature and nebuliser flow rate on LaO signal in desolvated nebulisation.

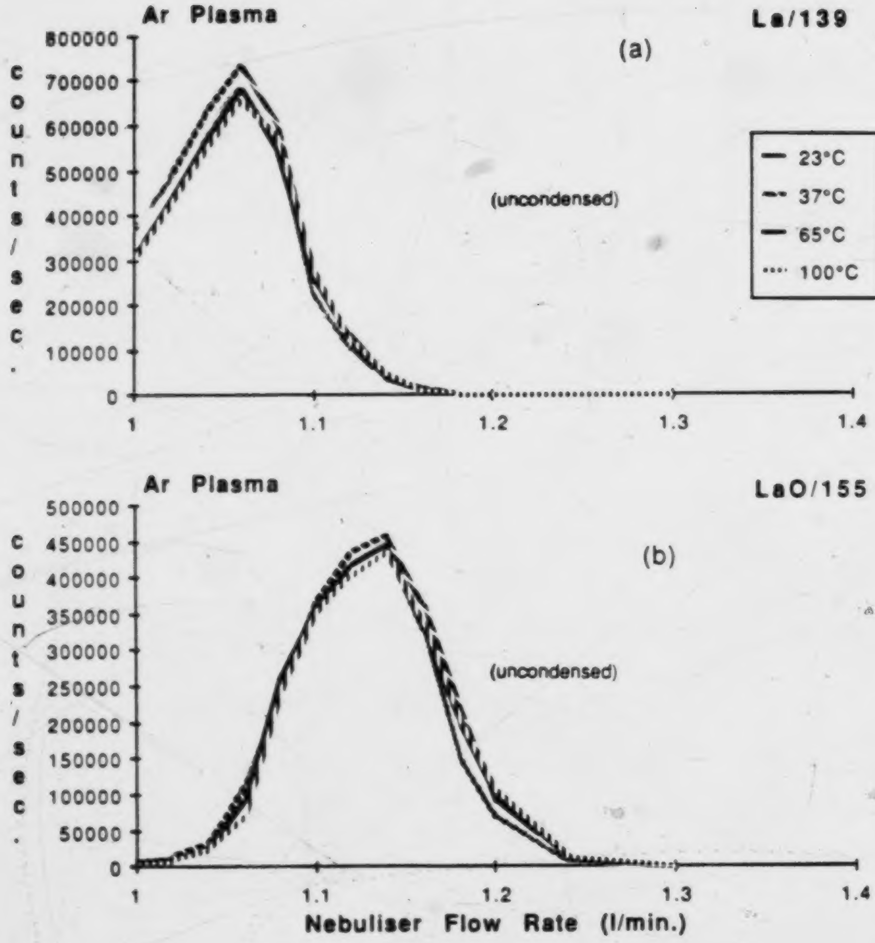

Figure 4-14. a) Diagram to show the effect of chamber heating temperature and nebuliser flow rate on La signal in uncondensed nebulisation. b) Diagram to show the effect of chamber heating temperature and nebuliser flow rate on LaO signal in uncondensed nebulisation.

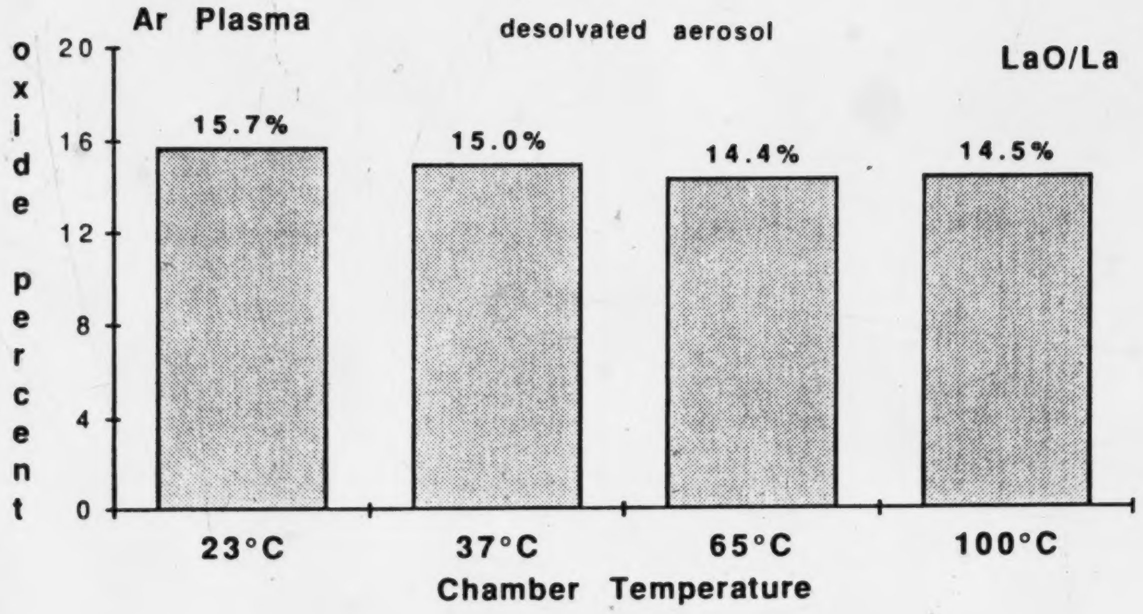

Figure 4-15. Bar graph to demonstrate the effect of chamber temperature on the percentage of LaO in desolvated nebulisation.

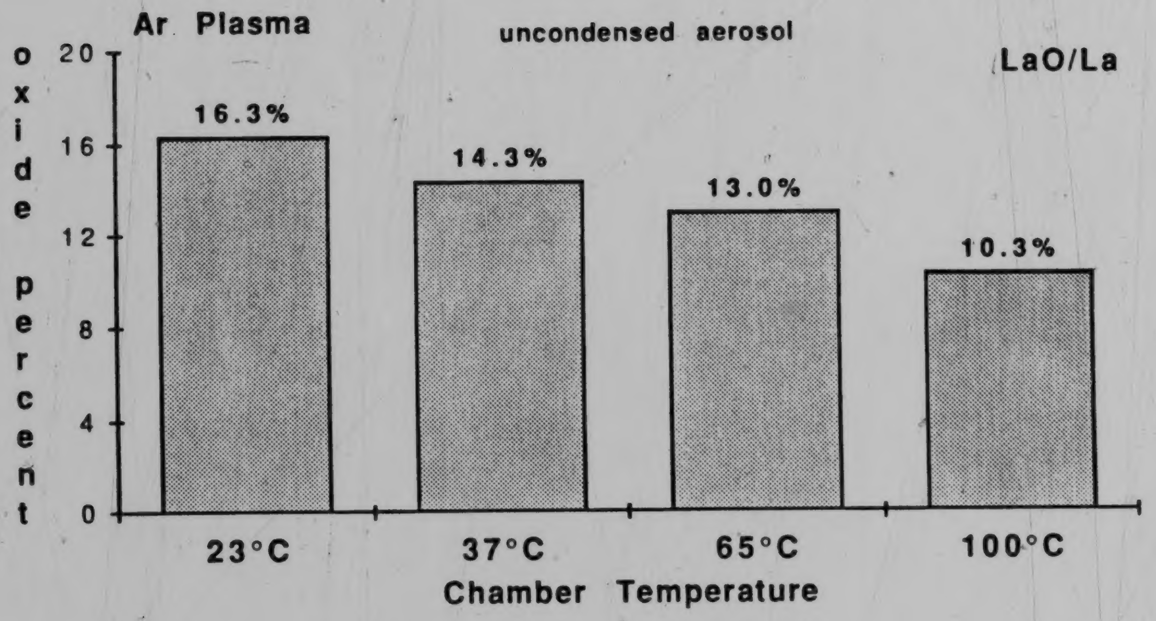

Figure 4-16. Bar graph to demonstrate the effect of chamber temperature on the percentage of LaO in uncondensed nebulisation.

the peak ion intensity, yet the percent of oxide ion at maximum metal sensitivity has been reduced. Due to the physical arrangement of the system (spray chamber inside the somewhat heated instrument enclosure), the temperature and thus vapour pressure inside the spray chamber is high in the direct nebulisation mode. Therefore, a greater amount of material (solvent vapour) is introduced into the discharge and this could be responsible for the observed higher peak oxide ion intensity.

On the other hand, the shift of the signal profile to higher nebuliser gas flow rates when it is operating in the indirect nebulisation mode suggests that there is a spatial shift of the ionic species in the central channel of the plasma (ionization process takes "shorter" time). During the direct nebulisation process, the elevated vapour pressure inside the spray chamber is likely a result of evaporation of the solvent from the condensed or coalesced droplets on the enclosed wall of the spray chamber (higher temperature) rather than evaporation from the nebulised droplets themselves. In addition, due to the close proximity of the spray chamber to the plasma torch, the aerosol particles are not expected to be altered significantly. On the other hand, it has been documented that the extra pathway created between the ICP torch and the spray chamber can allow it to function as an aerosol filter [42]. This is accomplished by increasing the probability of condensation of the larger size particles along the wall of the tubing. In contrast, for the smaller size particles, the drier environment would encourage solvent evaporation from the surface of the droplets over the prolonged traveling distance until equilibrium or steady-state can be attained. Hence, the average particle dimension is expected to decrease. This is believed to be the main cause of the spatial shift, as the aerosol desolvation process inside the discharge can be completed in a much shorter time when small aerosol particles are delivered to the plasma. This conclusion is consistent with a study on the effects of solvent vaporization and aerosol particle diameters on the positioning of the IRZ and NAZ in ICP-AES [50]. Therefore, either the IRZ has been shifted further away from the load coil during the direct nebulisation process (solvent load) or more probably, the aerosol droplets have become smaller as a result of solvent vaporization when the system is operating in the indirect nebulisation mode and the IRZ has been shifted towards the load coil.

When an aerosol particle is injected into the discharge, it is believed to undergo the following transitions :

i) Desolvation

Vaporization of solvent from the droplet to form an anhydrous salt.

ii) Vaporization

Physical transformation of the salt particle from solid to gas phase.

iii) Atomisation

Dissociation of the gas phase molecules into individual atoms.

iv) Excitation

Individual atoms undergoing spectroscopic transitions.

Spatial distribution of species in the central channel of the plasma is controlled by all of the above steps. However, steps (ii) to (iv) are specifically dependent on the chemical nature of the particle, while step (i) is determined by the characteristics of the aerosol generator. In the case where small diameter aerosol droplets are introduced into the plasma, they more readily undergo and complete the desolvation process at a lower (cooler) region of the discharge. The dehydrated salt particles are subsequently vaporized and atomized at the IRZ. In contrast the larger size aerosol droplets, generated by the direct nebulisation process, are expected to survive longer inside the plasma (extending the pre-heating zone). Thus, the atomisation process takes place further along the central channel of the plasma.

Over the years, it has been established that the plasma source is indeed non-homogeneous. Furuta and Horlick [51] measured the excitation temperature along the central-axis of the plasma and they observed a "positive" increase in spectroscopic temperature at increasing heights above the load coil until the temperature finally leveled out at the NAZ (about 20 mm from the top of the load coil). This trend is consistent with results obtained by other researchers. In the situation where large aerosol particles are injected, the desolvation process can only be completed at a zone relatively high up in the plasma. At this height, particles are likely to encounter a much higher thermal environment. Thus, ion cloud distribution along the central axis of the plasma as affected by chemical properties is not expected to be well defined. This speculation is consistent with the ICP-AES results obtained by Monnig and Koirtyohann [50] where they observed a more defined "interface" between the IRZ and NAZ after the adaptation of a tube "filter".

Previously, it has been stated that the amount of nebulised water introduced into the plasma is mainly responsible for the level of metal oxide detected in ICP-MS. However the peak oxide intensities obtained from direct, condensed and uncondensed aerosol nebulisations were similar (see Figures 4-11 and 4-12). Yet, in the condensed or uncondensed mode, the oxide percent can be reduced to less than half of its original value (direct nebulisation). These confusing observations can be explained with the illustrations shown in Figures 4-17 and 4-18 (rearranging the data in Figures 4-11 and 4-12). The data shown in both figures indicate that although the peak signal intensity for each ionic species remain comparable, they are not as well separated when the system is operating in the direct nebulisation mode (i.e. metal and oxide ions suffer from more severe overlap along the nebuliser gas flow axis). Hence, this is the main consequence for the improvement of oxide interference at the indirect nebulisation mode. As a result, better ion species separation in the central channel of the plasma can be achieved.

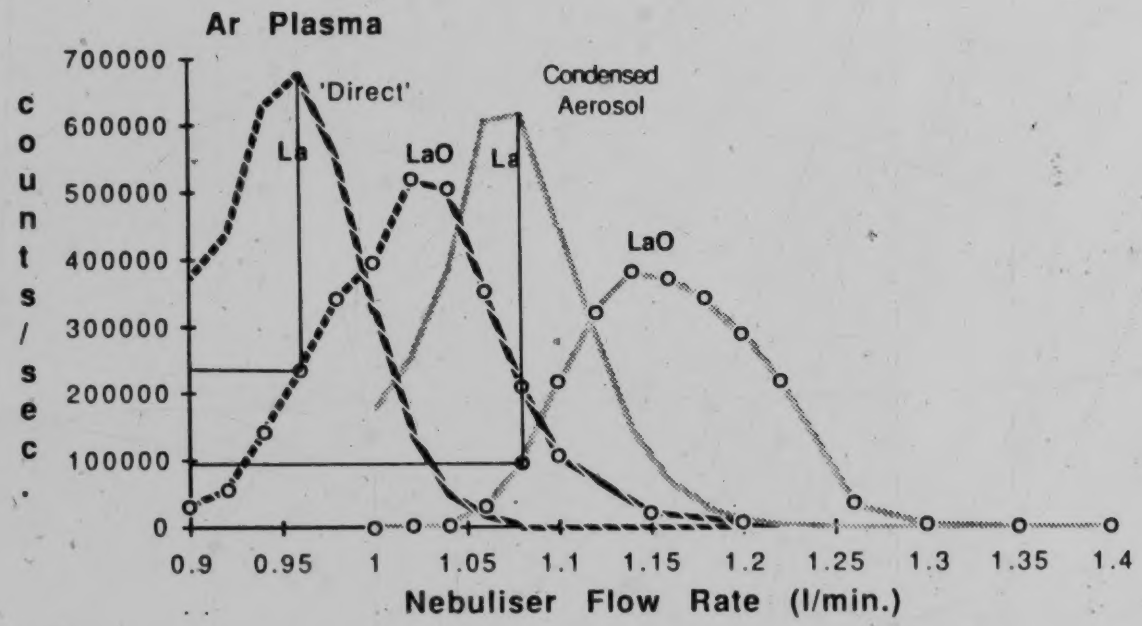

Figure 4-17. Diagram to show the different degrees of signal overlap in direct and condensed aerosol nebulisation for La and LaO.

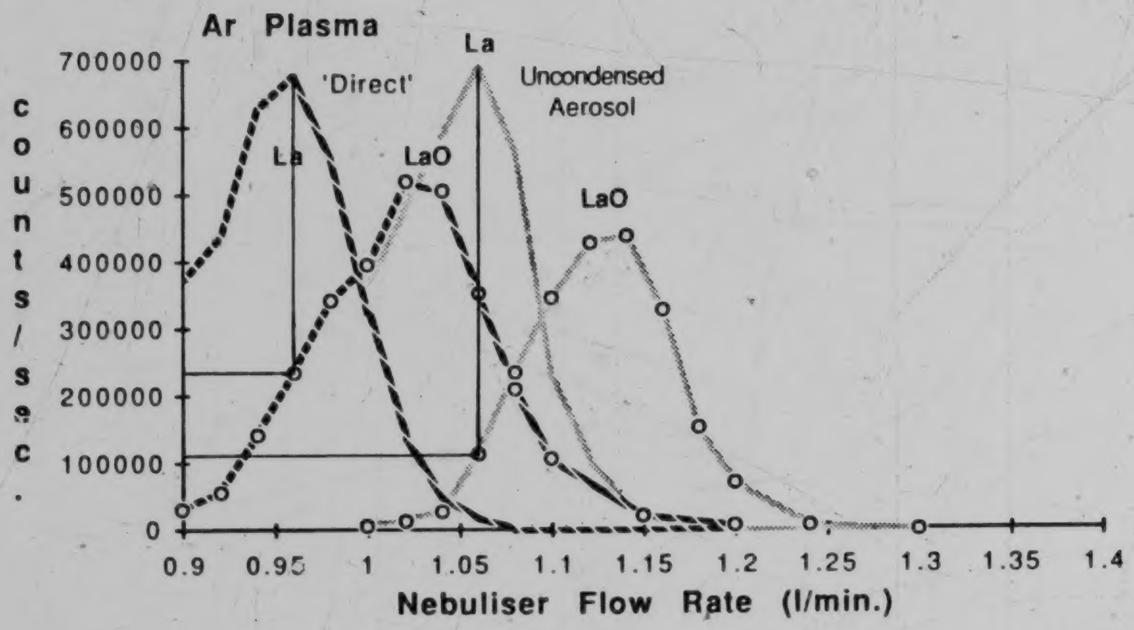

Figure 4-18. Diagram to show the different degrees of signal overlap in direct and uncondensed aerosol nebulisation for La and LaO.

As for the effect of chamber temperature on metal and metal oxide signals, clearly heating has a lesser impact on desolvated aerosol particles than on uncondensed aerosol particles (see Figures 4-13 and 4-14). This seemed rather ambiguous at first because the amount of aqueous solvent allowed into the discharge should be critical in determining the oxide level population. These observations can be more fully appreciated by examining the actual function of the water-condenser in these two instances. The heating process between the two modes was identical, the effect and hence the extent of solvent evaporation from the aerosol particles should be comparable. In the case of desolvated aerosol nebulisation, a water-cooled condenser induces a sudden drop in the temperature of the carrier stream which promotes the condensation of vapour. When this process is operated with a high efficiency condenser, dried aerosol should be obtained, with the amount of residual bounded solvent dependent on the desolvating temperature at the heating chamber. Yet the observed data suggest that the percent of oxide is independent of the chamber temperature (see Figure 4-15). In fact, the temperature of heating chamber has a similar effect on metal and the oxide ions (Figure 4-13). This result suggests that the limiting step in aerosol desolvation is at the condensation stage. In fact, the physical configuration of the condenser results in a turbulent flow of the gas stream and thus facilitates the condensation of solvent back onto the droplets until it reaches a steady-state. Hence, the higher the initial vapour pressure, the greater is the degree of condensation.

In contrast, when the system is operated in the uncondensed mode, the percent of metal-oxide decreases with increasing chamber temperature (see Figure 4-16). This phenomenon can also be interpreted in terms of solvent vapour pressure and size of the aerosol droplet. After the water-cooled condenser had been by-passed, the outlet from the heating chamber was connected directly to the plasma torch via a tygon tubing (1/4" I.D. by 4 ft.). Although this tubing was not temperature regulated (only about 1 ft. of it was exposed to the room temperature environment), the temperature inside the tubing should follow the temperature of the heating chamber rather closely. Hence, a large scale of solvent condensation (back onto the droplet) is not expected. As a result, the average particle size injected into the plasma is believed to be more closely related to the physical environment of the heating apparatus. At high temperature, the aerosol droplets inside the chamber become smaller as the vapour pressure inside the chamber is elevated. Despite the larger amount of water introduced into the plasma, it is mostly in the form of solvent vapour and it is expected to readily diffused after introduction into the discharge. On the other hand, due to the smaller size of aerosol particles introduced, the desolvation process in the plasma is expected to be completed at much earlier times (shorter pre-heating zone) and the established thermal gradient (more defined) inside the plasma can thus provide better differentiation to the chemical properties of the analyte species.

The above speculation is reinforced by the lesser degree of signal overlap between the metal and oxide ions along the nebuliser gas flow axis when it is operated in the uncondensed aerosol nebulisation mode (see Figures 4-17 and 4-18).

F. Effect of Nitrogen Mixed Gas Plasma and Aerosol Processing on La and LaO

a. Direct, Condensed and Uncondensed Aerosol Introduction

Previously, it was observed that the effects of a low percentage nitrogen mixed gas plasma on analyte signal responses are in fact species dependent. There were two aspects to sensitivity enhancement: one related to oxide bond strength for low ionization potential elements and the other related solely to ionization potential of the analytes. In the same study, it was observed that a 5% nitrogen cooled discharge had a "positive" effect on the La ion sensitivity and at the same time it decreased the metal oxide ion intensity rather dramatically. The signal enhancement of the metal ion and the reduction of oxide ion were thought to be a result of the high affinity of nitrogen for oxygen. Thus the freed metal ion is available for detection. In a different way, condensed and uncondensed aerosol nebulisations also show promising results in reducing the percentage of metal oxide in the argon plasma discharge. Thus, a combination of the two techniques seems like a reasonable approach for reducing the oxide interference.

A 5% nitrogen cooled mixed gas plasma was used. The plasma operating parameters and equipment set-up were identical to the previous section (see Figures 4-2 and 4-3). The aerosol nebulisation was carried out in three modes, direct, condensed and uncondensed. The metal and its oxide ions were again monitored as a function of nebuliser flow rate at the three aerosol introduction modes.

The signal responses obtained from this experiment are illustrated in Figures 4-19 and 4-20. The general trend is consistent with the result obtained from the argon plasma. However, the relative increase for the optimum nebuliser gas flow rate (condition for peak ion signal) during indirect nebulisations are much higher than what was required for the argon plasma. Especially in the case of the peak oxide ion signal, when the system was operating as the condensed aerosol mode, a nebuliser flow rate of close to 1.8 l/min was still insufficient to reach peak intensity. It is interesting to point out that although the aerosol processing technique had little effect on the peak metal oxide signal in the argon plasma, the oxide intensities have been reduced significantly in the mixed gas plasma.

In order to compare the performance of the aerosol processing techniques, the oxide to peak metal ion ratios were calculated in the usual way and presented as the following:

Mode of Operation	LaO^+/La^+
Direct Nebulisation	8.1%
Condensed Aerosol	0.46%
Uncondensed Aerosol	2.5%

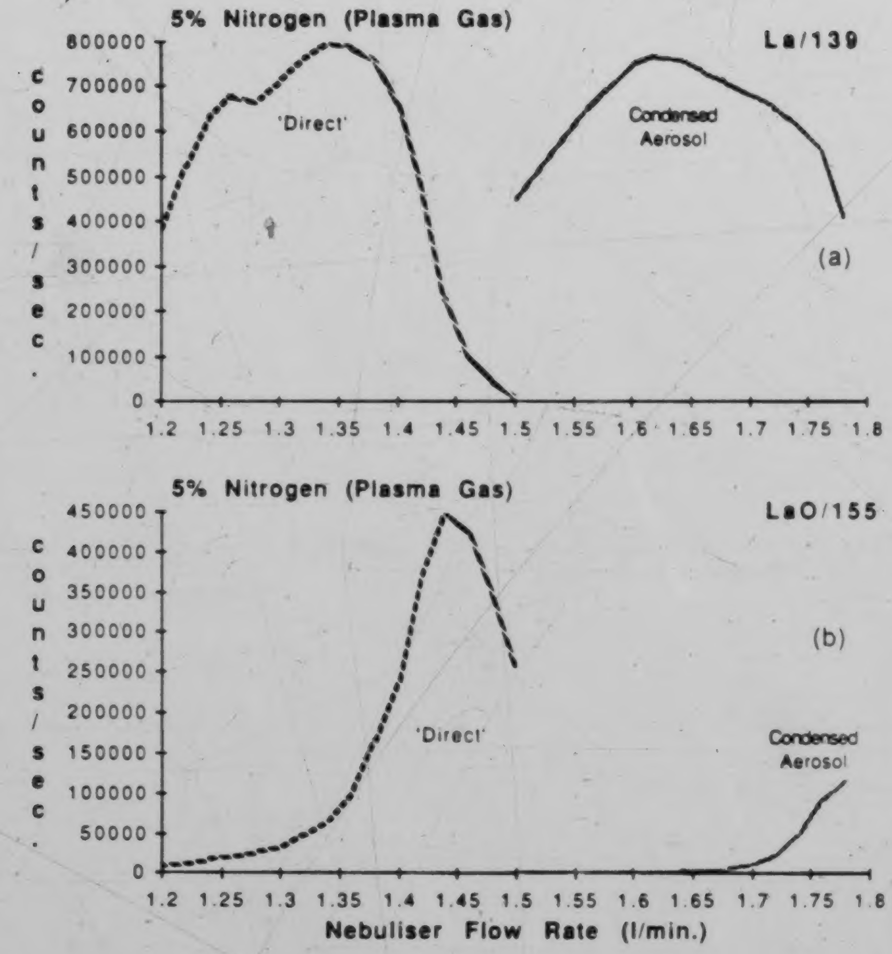

Figure 4-19. a) Diagram to show the signal responses of La in direct and condensed aerosol nebulisations. b) Diagram to show the signal responses of LaO in direct and condensed aerosol nebulisations.

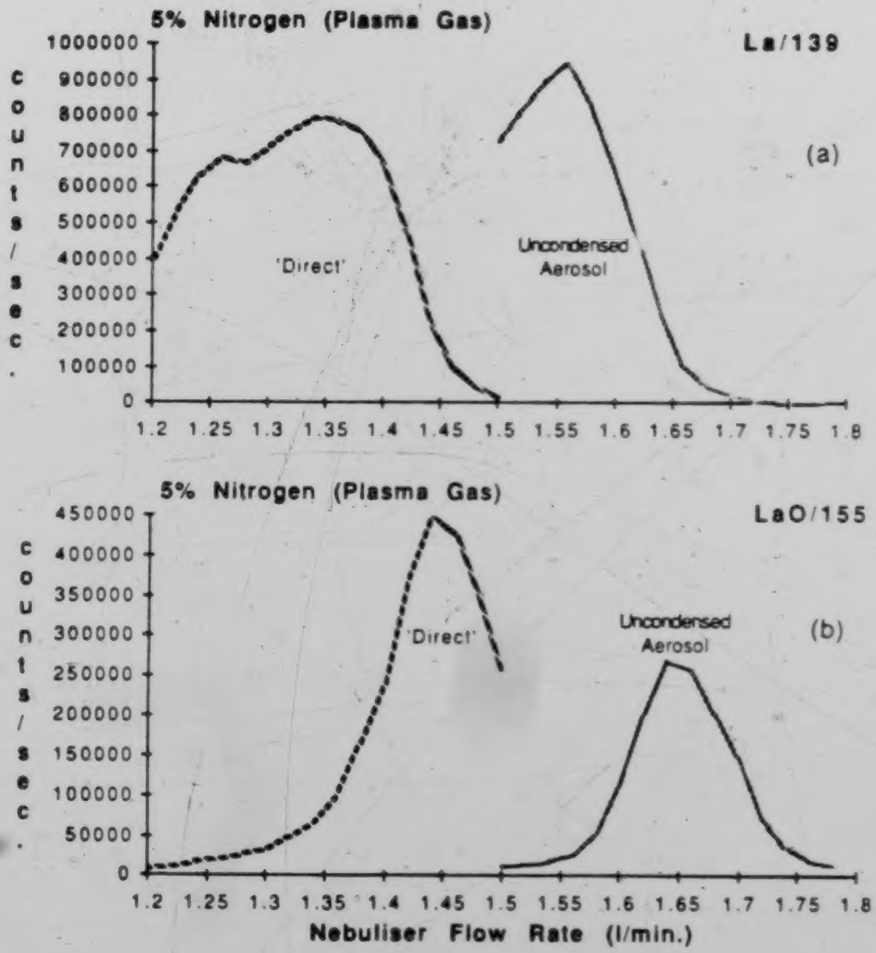

Figure 4-20. a) Diagram to show the signal responses of La in direct and uncondensed aerosol nebulisations. b) Diagram to show the signal responses of LaO in direct and uncondensed aerosol nebulisations.

These results are extremely interesting; a 5% nitrogen plasma itself reduces the oxide to about 8%, and when it is operating with the "treated aerosol", the oxide percent can be further reduced. Especially with the condensed aerosol nebulisation, the percentage of oxide was reduced to less than half of one percent. This is a major improvement from a high value of 35% when it was operating in its original form (argon plasma, direct nebulisation).

b. Effect of Heating Chamber Temperature

During the investigation of the effect of heating chamber temperature on oxide ion intensity using the argon plasma, it was found that although the oxide percent was independent of heating for desolvated aerosol nebulisation, it decreased with increasing chamber temperatures for the uncondensed mode. This difference was interpreted as due to the poor efficiency of the water- cooled condenser. In order to examine the validity of this speculation, the above study was repeated with the use of a 5% nitrogen cooled plasma discharge. The equipment set-up and plasma operating parameters were identical to the previous study with the exception that, during the uncondensed aerosol nebulisation, the set of chamber temperatures used were 23°C, 37°C and 65°C.

The signal responses were similar to the previously observed results using the argon plasma. The oxide to peak metal ion ratios at each chamber temperature are illustrated in Figures 4-21 and 4-22 (in bar graphs). In each figure, the corresponding oxide percentages obtained with the argon plasma are also included. The data shown in the two figures indicate that the oxide percent from both the uncondensed and the desolvated aerosol nebulisation processes was not significantly affected by the chamber temperature. The results for the desolvated mode are most impressive. At a chamber temperature of 100°C, the oxide percent was reduced to 0.21%. On the other hand, the uncondensed aerosol nebulisation gave a relatively higher level of oxide percent than would have been expected.

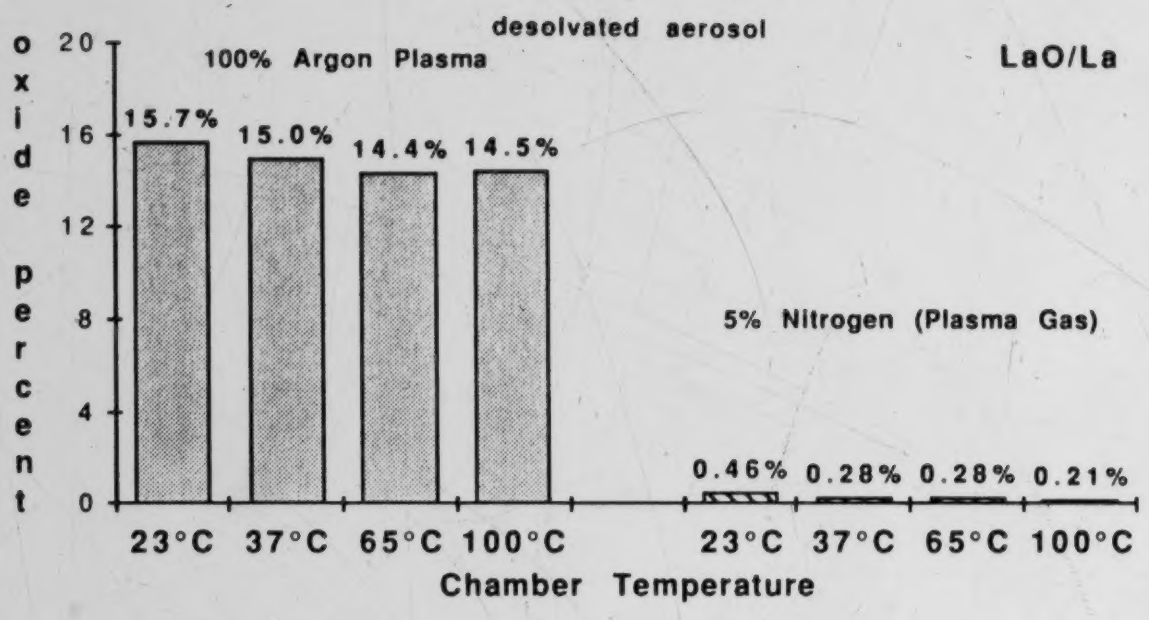

Figure 4-21. Bar graph to demonstrate the different effect of chamber temperature on the percentage of LaO in an argon and a nitrogen mixed gas plasma (desolvated aerosol nebulisation).

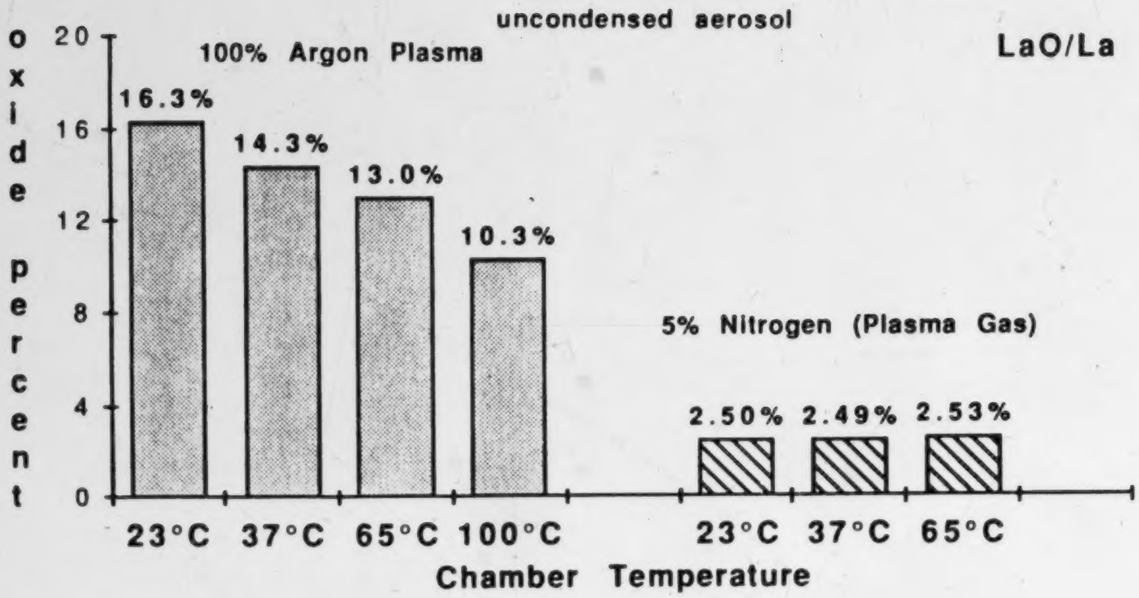

Figure 4-22. Bar graph to demonstrate the different effect of chamber temperature on the percentage of LaO in an argon and a nitrogen mixed gas plasma (uncondensed aerosol nebulisation).

c. Discussion

The results above demonstrate the synergic effect of the nitrogen mixed gas plasma and aerosol processing for the reduction of metal oxide ion. In addition, it also shows that the amount of water allowed into the discharge is important. Even with the use of a mixed gas discharge, by introducing aerosol as uncondensed nebulisation, the level of oxide was decreased to about 2.5%. However, after the removal of solvent (in the desolvated mode), the oxide was further reduced to a fraction of one percent. This is most intriguing. From the parallel data obtained with the argon plasma, the effect of heating on uncondensed aerosol and thus oxide percent was thought to be a result of particle size reduction despite a larger amount of solvent vapour being allowed into the plasma discharge.

Perhaps the above situation can be better understood by appreciating the role of nitrogen more fully. Previously, it was suggested that the function of nitrogen in the plasma was to tie up the available oxygen species, thus freeing the metal ion for detection. This proposal has certain limitations. In a situation where the metal oxide bond energy is comparable to or higher than the related nitrogen oxide bond strength (i.e. La), the reaction becomes less attractive. However, the result previously obtained also indicated that a nitrogen mixed gas plasma is indeed effective in enhancing the metal ion signal intensity and reducing the percentage of oxide ion. Closer examination of the data in Figures 4-17 to 4-20 clarified this situation. The peak LaO ion intensity measured in each case is indeed fairly strong even when the system was operating in the uncondensed aerosol mode in conjunction with a 5% nitrogen mixed gas plasma (Figure 4-20). This result certainly does not indicate a sharp decrease in oxide. However, the shift along the nebuliser flow rate axis when operating with the nitrogen mixed gas plasma suggests that the final outcome is more likely dominated by better resolution between the IRZ and NAZ as was the case with the argon plasma with indirect nebulisation. In this situation, the lowering of the pre-heating zone is more likely a result of the higher thermal energy in a nitrogen mixed gas plasma.

Data from Figure 4-23 clearly illustrate this trend. The effect of aerosol processing and nitrogen mixed gas plasma on the nebuliser flow rate for peak ion signal are similar. Both techniques result in shifting the peak ion signal to a higher value along the nebuliser gas flow rate axis. On the other hand, the amount of water introduced into the plasma is also important. In the case of desolvated aerosol nebulisation, the amount of solvent bound to the aerosol particles has been greatly reduced. Therefore, when working in conjunction with the effect of nitrogen on oxygen-containing species, this increases the efficiency of the "desolvation" process inside the plasma. In contrast, when the aerosol was nebulised in the uncondensed form, this raises the amount of solvent vapour entering the plasma and thus limits (or saturates) the effectiveness of nitrogen. As a result, the elevated level of oxide percent was observed at the peak analyte ion nebuliser flow rate setting.

G. Conclusion

The effect of solvent loading is rather important in elemental analysis using ICP-MS and its significance is not just limited to organic analysis. To a certain extent, it also affects the ionization processes for certain analytes. Furthermore, the interference cause by analyte oxide signal overlap can be minimized by aerosol processing technique. The success of this approach is thought to be a result of aerosol manipulation which reforms the droplets to smaller particles and thus provides improved resolution between the IRZ and NAZ. As a result, the oxide and its metal ion are better separated in a spectral/time sense (see Figure 4-24), and hence the observed lower oxide percentage.

The combining of aerosol desolvation and nitrogen mixed gas plasmas is particularly impressive for lowering the percentage of oxide species. This synergic approach can reduce a refractory oxide to a fraction of one percent (from a high of about 35%) and this process is accomplished by reducing both the degree of solvent load and the size of the aerosol

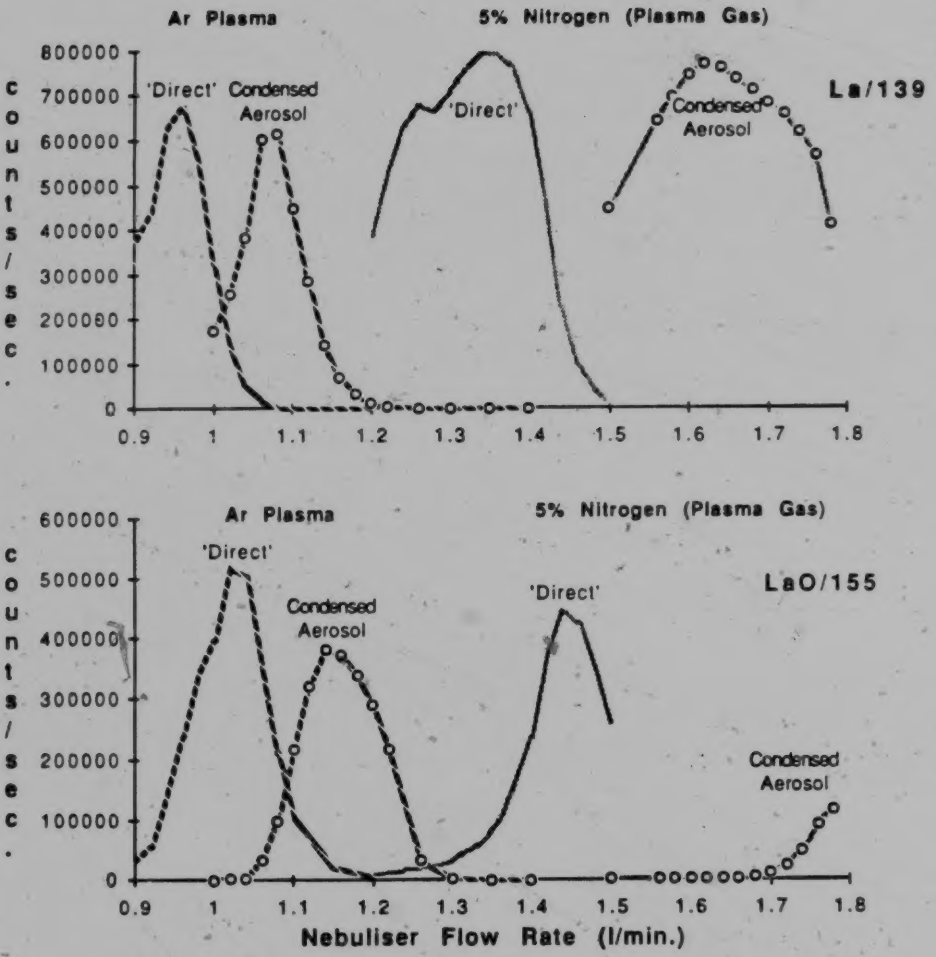

Figure 4-23. a) Diagram to illustrate the effect of aerosol processing and nitrogen mixed gas plasma on the signal profiles of La. b) Diagram to demonstrate the effect of aerosol processing and nitrogen mixed gas plasma on the signal profiles of LaO.

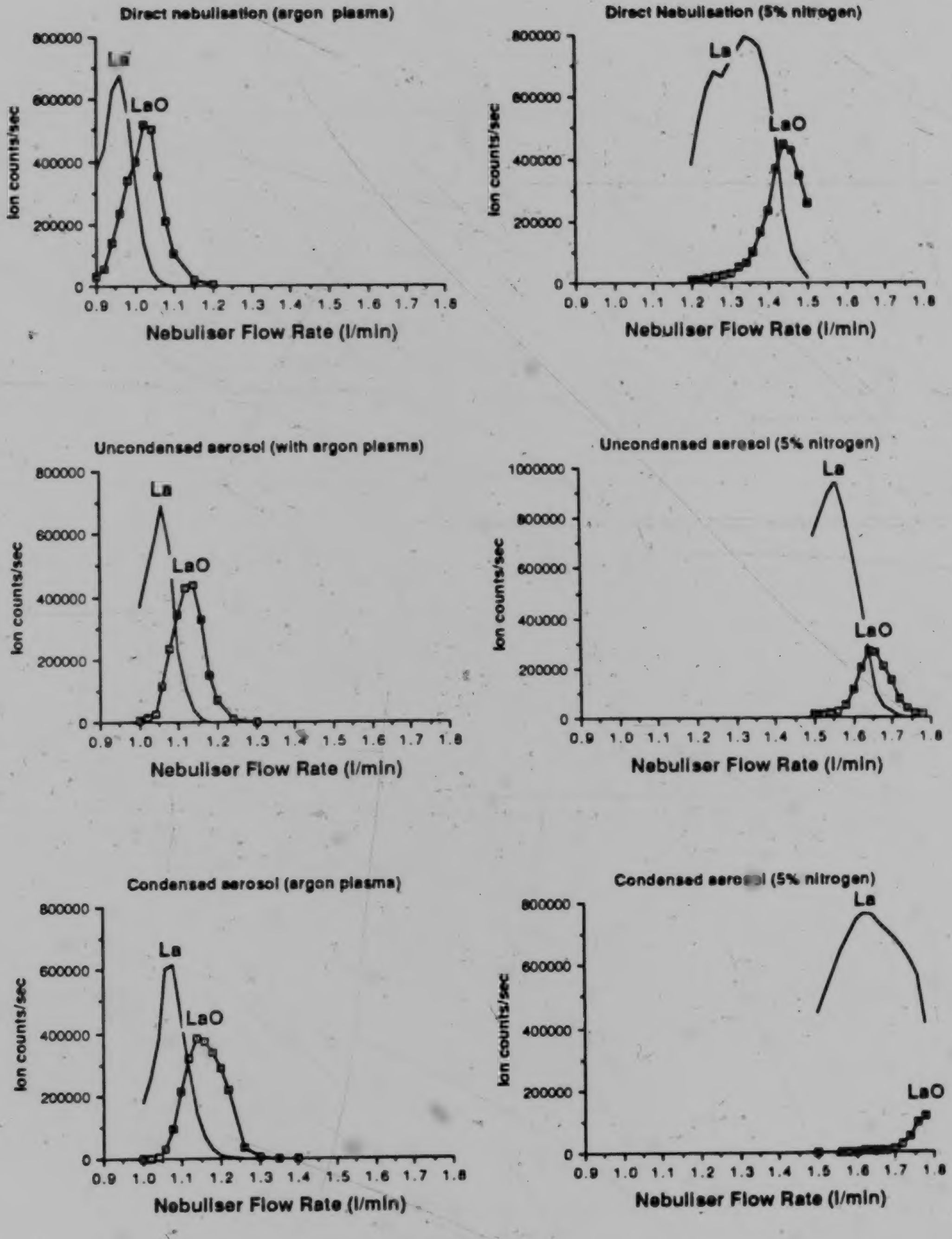

Direct nebulisation (argon plasma)

Direct Nebulisation (5% nitrogen)

Uncondensed aerosol (with argon plasma)

Uncondensed aerosol (5% nitrogen)

Condensed aerosol (argon plasma)

Condensed aerosol (5% nitrogen)

Figure 4-24. Diagram to show the different degrees of signal overlap by aerosol processing and nitrogen mixed gas plasma for La and LaO.

particles simultaneously. This thus enables the nitrogen to function efficiently inside the plasma discharge.

REFERENCE

1. J. F. Alder, R. M. Bombelka and G. F. Kirkbright, Spectrochim. Acta, 35B, 163 (1980).
2. M. W. Blades and B. L. Caughlin, Spectrochim. Acta, 40B, 579 (1985).
3. A. W. Boorn and R. F. Browner, Anal. Chem., 54, 1402 (1982).
4. F. J. M. J. Maessen, G. Kreuning and J. Balke, Spectrochim. Acta, 41B, 3 (1986).
5. Y. Q. Tang and C. Trassy, Spectrochim. Acta, 41B, 143 (1986).
6. B. L. Caughlin and M. W. Blades, Spectrochim. Acta, 42B, 353 (1987).
7. R. S. Houk, H. J. Svec and V. A. Fassel, Appl. Spectrosc., 35,380 (1981).
8. A. R. Date and A. L. Gray, Spectrochim. Acta, 38B, 29 (1983).
9. A. R. Date and A. L. Gray, Analyst, 108, 1033 (1983).
10. G. Horlick, S. H. Tan, M. A. Vaughan and C. A. Rose, Spectrochim. Acta, 40B, 1555 (1985).
11. M. A. Vaughan and G. Horlick, Appl. Spectrosc., 40, 434 (1986).
12. A. L. Gray, Spectrochim. Acta, 40B, 1525 (1985).
13. C. W. McLeod, A. R. Date and Y. Y. Cheung, Spectrochim. Acta, 41B, 169 (1986).
14. H. P. Longerich, D. F. Strong and C. J. Kantipuly, Can. J. Spectrosc., 31, 111 (1986).
15. H. P. Longerich, D. F. Strong and C. J. Kantipuly, Spectrochim. Acta, 42B, 75 (1987).
16. S. E. Long and R. M. Brown, Analyst, 111, 901 (1986).
17. A. L. Gray, R. S. Houk and J. G. Williams, J. Anal. At. Spectrom., 2, 13 (1987).
18. A. L. Gray and J. G. Williams, J. Anal. At. Spectrom., 2, 81 (1987).

19. J. W. McLaren, D. Beauchemin and S. S. Berman, J. Anal. At. Spectrom., 2, 277 (1987).

20. G. Zhu and R. F. Browner, Appl. Spectrosc., 41, 349 (1987).

21. D. A. Wilson, G. H. Vickers and G. M. Hieftje, Spectrochim. Acta, 42B, 29 (1987).

22. D. A. Wilson, G. H. Vickers and G. M. Hieftje, J. Anal. At. Spectrom., 2, 365 (1987).

23. A. L. Gray and J. G. Williams, J. Anal. At. Spectrom., 2, 599 (1987).

24. D. J. Douglas and J. B. French, Spectrochim. Acta, 41B, 197 (1986).

25. D. J. Douglas and R. S. Houk, Prog. Anal. At. Spectrosc., 8, 1 (1985).

26. José A. Olivares and R. S. Houk, Anal. Chem., 57, 2674 (1985).

27. R. S. Houk, Anal. Chem., 58, 97A (1986).

28. R. S. Houk, V. A. Fassel, G. D. Flesch, H. J. Svec, A. L. Gray and C. E. Taylor, Anal. Chem., 52, 2283 (1980).

29. R. S. Houk, V. A. Fassel and H. J. Svec, Dynamic Mass Spectrom., 6, 234 (1981).

30. A. R. Date and A. L. Gray, Analyst, 106, 1255 (1981).

31. W. Doherty and A. V. Voet, Can. J. Spectrosc., 30, 135 (1985).

32. R. S. Houk, paper presented at ICP-MS Symposium, Muskoka Sands, Canada (1987).

33. S. H. Tan and G. Horlick, Appl. Spectrosc., 40, 445 (1986).

34. S. -J. Jiang and R. S. Houk, Anal. Chem., 58, 1739 (1986).

35. S. -J. Jiang and R. S. Houk, Spectrochim. Acta, 42B, 93 (1987).

36. D. W. Boomer, M. Powell, R. L. A. Sing and E. D. Salin, Anal. Chem., 58, 975 (1986).

37. R. L. A. Sing and E. D. Salin, XXV Colloquium Spectroscopicum Internationale, Toronto, Canada, (1987). Paper no. F 5.4.

38. P. Arrowsmith, Anal. Chem., 59, 1437 (1987).

39. S. A. Myers and D. H. Tracey, 1981 Pittsburgh Conference on Analytical Chemistry and Applied Spectroscopy, (1981). Abstract no. 10.

40. J. Porstendörfer, J. Gebhart and G. Röbig, J. Aerosol Sci., 8, 371 (1977).

41. S. E. Long and R. F. Browner, Spectrochim. Acta, 41B, 639 (1986).

42. J. Rybarczyk, C. Jester, D. Yates and S. Koirtyohann, Anal. Chem., 54, 2162 (1982).

43. J. M. Mermet, C. R. Acad. Sci., ser. B, 281, 273 (1975).

44. J. A. C. Broekaert, F. Leis and K. Laqua, Spectrochim. Acta, 34B, 73 (1979).

45. D. C. Schram, I. J. M. M. Raaymakers, B. van der Sijde, H. J. W. Schenkelaars and P. W. J. M. Boumans, Spectrochim. Acta, 38B, 1545 (1983).

46. G. M. Hieftje, G. D. Rayson and J. W. Olesik, Spectrochim. Acta, 40B, 167 (1985).

47. G. D. Rayson and G. M. Hieftje, Spectrochim. Acta, 41B, 683 (1986).

48. R. C. Hutton and A. N. Eaton, J. Anal. At. Spectrom., 2, 595 (1987).

49. B. Magyar, P. Lienemann and H. Vommont, Spectrochim. Acta, 41B, 27 (1986).

50. C. A. Monnig and S. R. Koirtyohann, Anal. Chem., 57, 2533 (1985).

51. N. Furuta and G. Horlick, Spectrochim. Acta, 37B, 53 (1982).

Chapter 5

Characterization of some Major Background Species in ICP-MS

A. Introduction

In trace element analysis, a detailed knowledge of the character of the background is particularly important. In spectroscopy, background may be defined as the spectral features obtained when only the "Blank" is analysed. In practice, background is usually removed from the final result by subtracting a separately run matrix-matched "Blank Solution" during data processing.

In ICP-MS, the final decoding step of the technique is a mass filter. Ions detected are specific to the mass-to-charge ratio (m/e) for the species. As a result, the spectra obtained using the technique are usually simple and specific. Pickford and Brown [1] tabulated all naturally occurring elements in solution and found a sum total of 211 "spectral lines" in ICP-MS for the elements and their naturally occurring isotopes. Since the source of ions in ICP-MS is a high temperature plasma discharge, complex poly-atomic ion species are not expected to survive in this environment. In reality, this situation is only valid for m/e values above 80. Below this mass, the background spectrum is very complicated.

In the case of aqueous solution analysis using ICP-MS, the most dominant background species are oxygen-, argon- and hydrogen- related species and they were reported during the developing state of the technique [2-4]. At that time, they were thought to be generated during the extraction stage of the process. In fact, several studies were carried out to compare the background signal intensities obtained under the continuum mode of sampling and the boundary layer mode of ion extraction [5-7]. The first detailed report concerning the identity of background species was provided by Douglas and Houk [8] and the ion signal equivalents to analyte concentrations were estimated to be at the part per billion (ppb) range [9]. In the situation where the interfered ion concentration was high with respect to the interferent, the spectral overlap caused by the interferent can be ignored [10]. Overall, however, a detailed understanding of the behaviour of background ions with respect to analyte species as well as their relative signal intensities is particularly important.

According to its character and nature, the background observed in ICP-MS can be subdivided into "Non-structured" and "Structured".

a. Non-structured Background

The source for this type of background is thought to be generated from the photons emitted by the plasma discharge. The characteristic behaviour for this type of background is the lack of specificity and selectivity with respect to the electrostatic lenses and the mass filter. In fact, the intensity of this type of background is solely dependent on the plasma intensity. In both types of present commercial systems, the background signal resulting from photon emission is minimized by adapting a photon baffle as well as arranging the position of the ion-detector off-axis.

b. Structured Background

In general, structured background can be distinguished and characterized using the mass filter. Signal response to plasma parameters is similar to that of analyte ions. Depending on the origin of the species, this group can be further subdivided into four classes, discussed below.

i) Primary Species

Primary species are the fundamental species observed when only distilled water is introduced into the plasma discharge. Hence, they are the most basic species in ICP-MS and can only be removed by either changing the solution matrix to a non-aqueous type or by replacing the gas supply to the discharge with a different gas. Typically, they include Ar-, O- and H- related ions.

ii) Matrix Induced Molecular Species

The population level for this type of species is specifically dependent on the matrix of the sample. Thus, their occurrence is selective and they usually reflect the nature of the solution matrix. Spectral interference caused by this type of background species can usually be minimized by choosing an alternative sample dissolution method.

iii) Argon Related Matrix Induced Species

Since the bulk of the plasma consists of 99% non-ionized argon atoms, depending on the nature and type of the analyte solutions analysed, poly-atomic ions consisting of argon and matrix constituents are commonly detected in ICP-MS, i.e. ArX species.

iv) Matrix Element Itself (isobaric) and/or its Oxide

This background problem is caused by spectral overlap between natural occurring stable isotopes. This type of background interference is straight forward. Simple computations for the correction of these overlaps are provided in commercial instruments. On the other hand, the spectral overlaps caused by oxide formation from the matrix elements are more difficult to correct. As mentioned in the previous chapter, the signal intensity for the analyte oxide is dependent on plasma parameters. In order to correct for this interference, calculations using an interference free oxide species are possible [11-12]. However, in the situation where the oxide interference is caused by more than one species and/or interferences , corrections are often erroneous.

B. Behaviour of some Primary Background Species

a. 100% Argon Plasma

i) Introduction

A typical mass spectrum using ICP-MS with the aspiration of "Blank" distilled water is illustrated in Figure 5-1. The mass range covered is from 1 amu to 84 amu, the region where most of the primary background species are expected [13]. The ion intensity in this figure is presented with a logarithmic scale. For the data shown in the upper-half of the Figure 5-1 (from 1 amu to 50 amu), the power supply to the ion deflector was turned off in order to lower the transmission efficiency of ions entering the ion detector (this typically lowered the efficiency of ion detection by about two orders of magnitude). In addition, the argon signal at 40 amu was "hopped over" in order to prevent detector saturation. On the other hand, the spectrum shown in the lower-half of the figure (from 44 amu to 84 amu) was acquired with the ion deflector turned on (at 3700 Volt). Both of the spectra in Figure 5-1 look complicated. This is partly due to use of a log scale on the intensity axis; such a scale gives a rather distorted view of the relative species population.

Figures 5-2 and 5-3 are reproductions of the data shown in Figure 5-1 with the signal intensity axes on a linear scale. Within each figure, the bottom frame shows the basic features of the background while the middle and top frames are scale expanded by factors of 10 and 100 respectively. From the spectra in each figure, it is obvious that the mass range from 14 amu to 21 amu is extremely complicated (Figure 5-2). However, this is a region of little interest in ICP-MS analysis, as it covers the isotopic masses for non-metallic ions. On the other hand, the less complicated region from 27 amu to 40 amu makes analysis for aluminium, silicon, phosphorous, sulphur, potassium and calcium difficult.

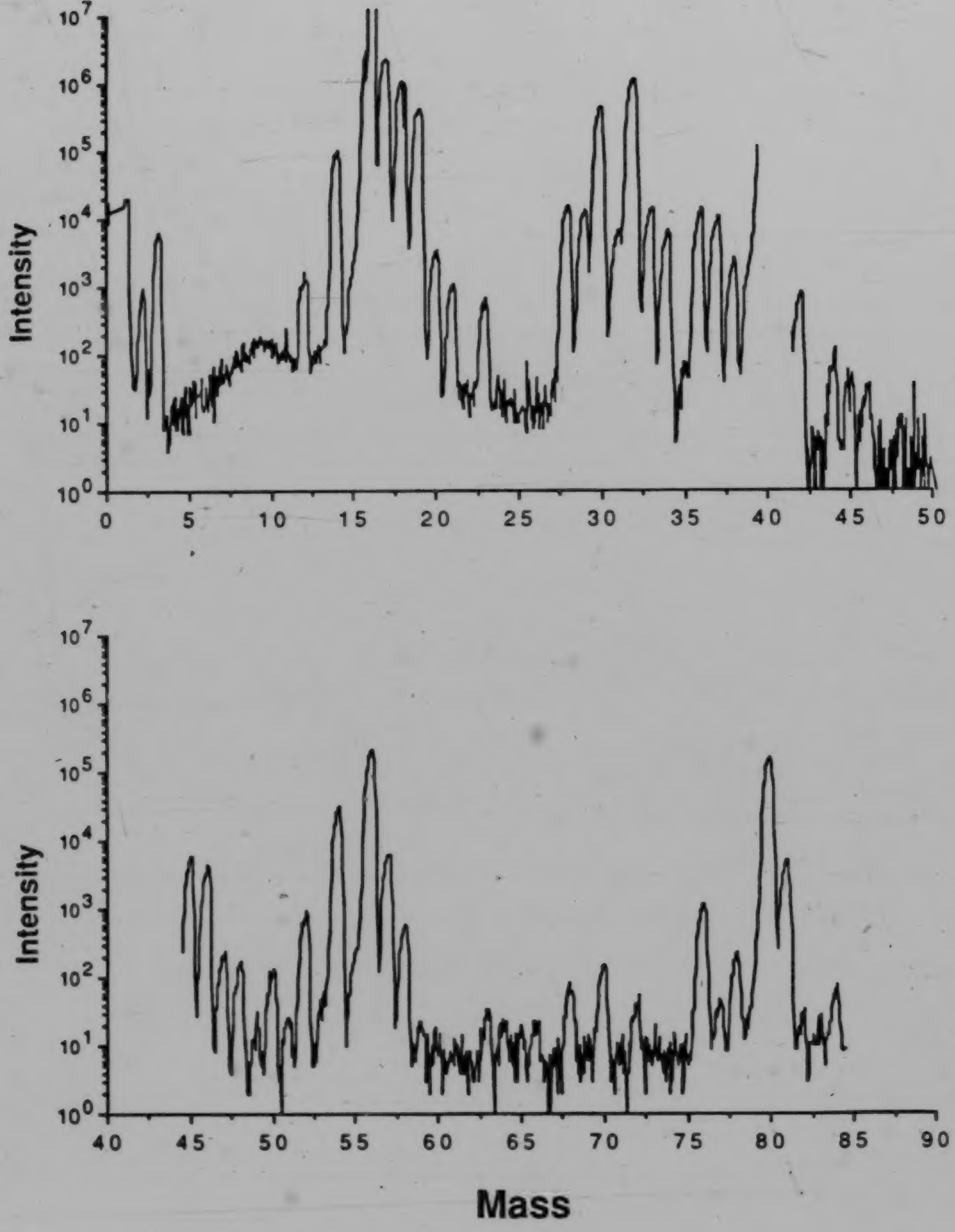

Figure 5-1. Background mass spectra for distilled water (1-84 amu).

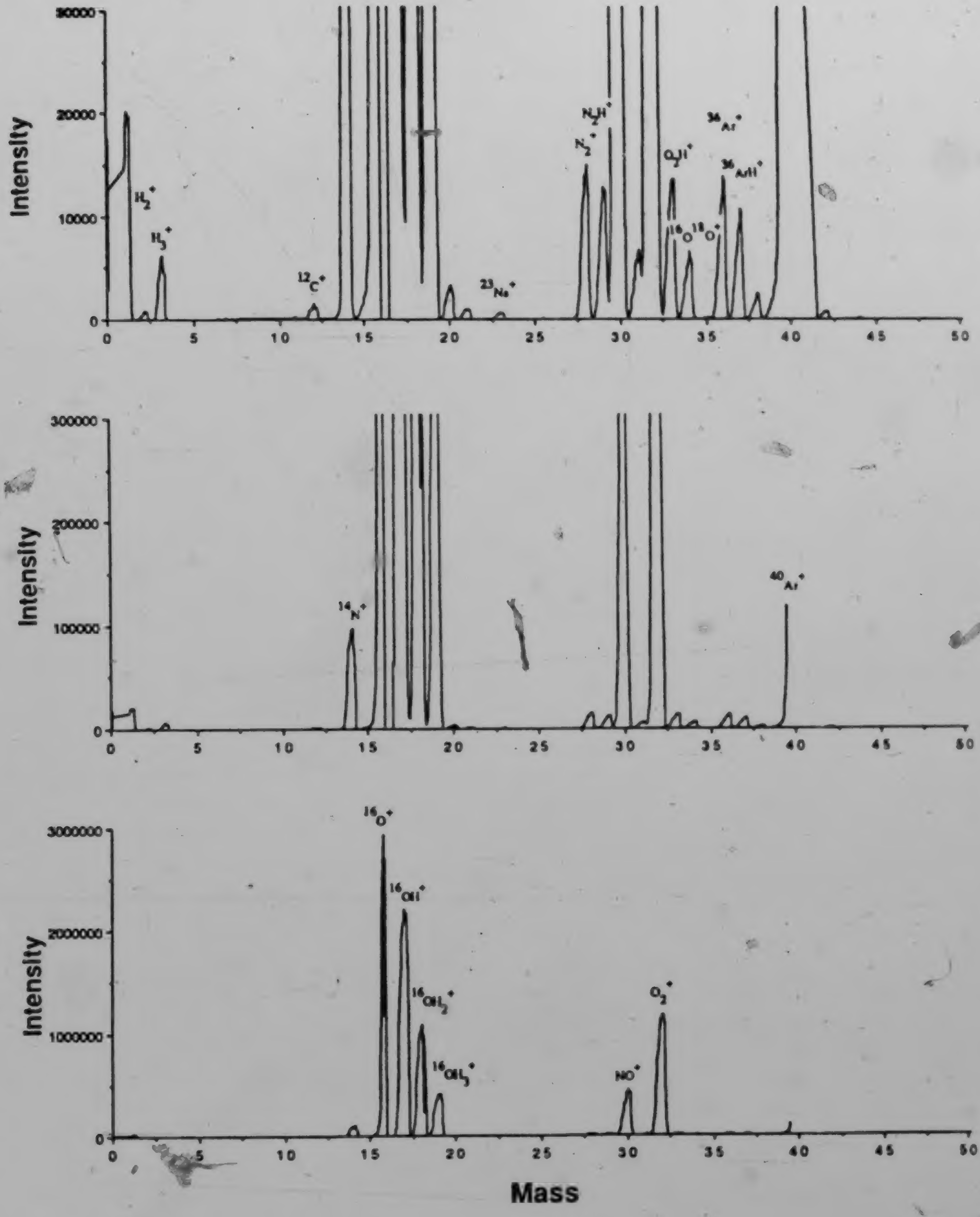

Figure 5-2. Background spectra for distilled water (1-50 amu) at amplification levels of 100 (top), 10 (middle) and 1 (bottom).

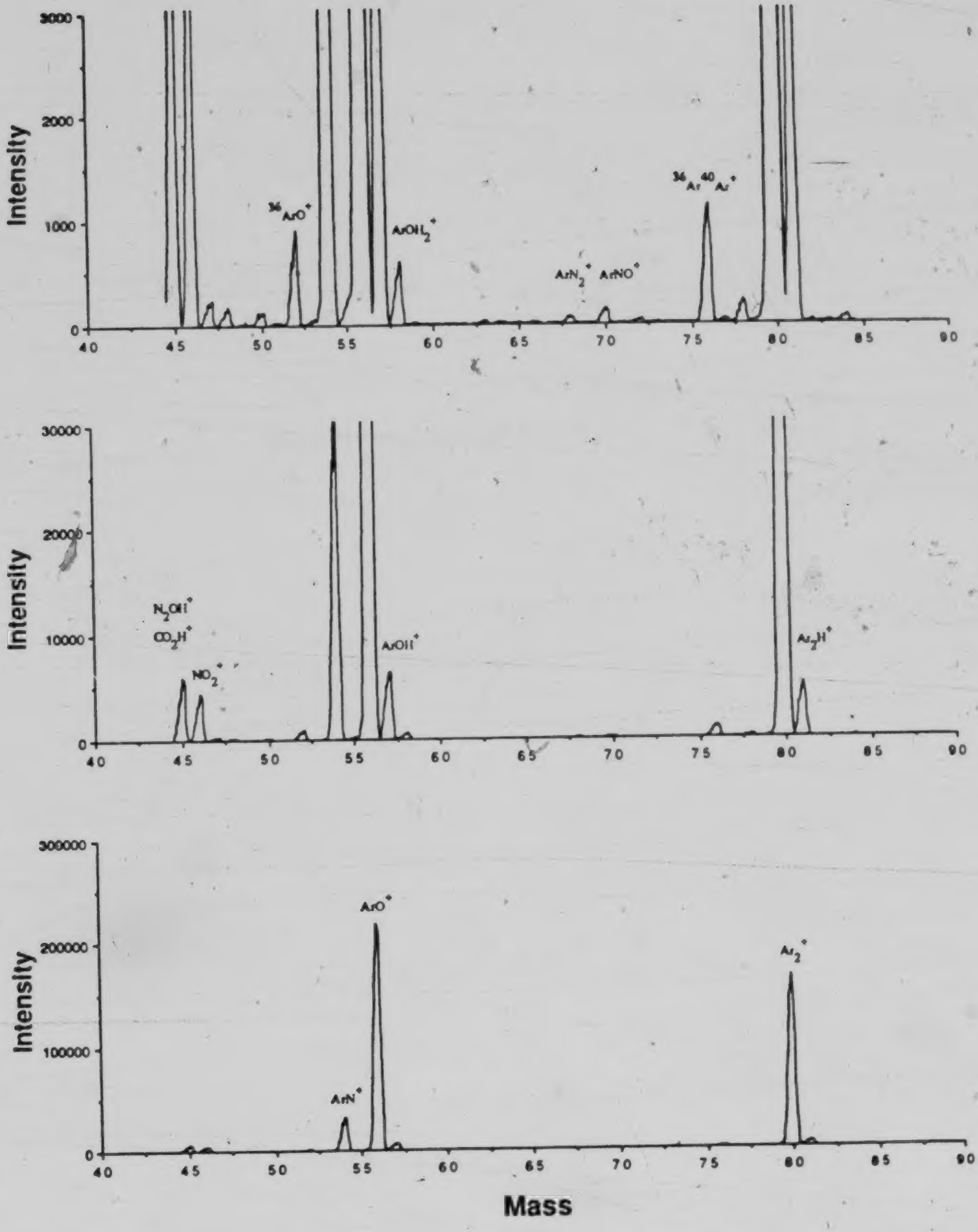

Figure 5-3. Background spectra for distilled water (44-84 amu) at amplification levels of 100 (top), 10 (middle) and 1 (bottom).

The basic features in these spectra are very similar to the tabulated species report by Tan and Horlick [13] with perhaps some minor differences. From the stand-point of species formation, the relatively high ion intensities for the H_2^+ and H_3^+ ions are rather intriguing because the probable reaction mechanism is a multi-step process involving the cleavage of OH and recombination of H groups. On the other hand, the high ion signals for the O^+ and Ar^+ groups are not unexpected because they are the main components inside the discharge. This observation is contrary to the report by Longerich et al. [14] in which NO^+ was taken to be the most common species.

In the two figures, the identity of the ion peaks was established by means of molecular weight matching. As mentioned, the labeled species are very similar to the tabulated data of Tan and Horlick [13]. However, the identity for some of the hydrogen containing species was further clarified with the use of deuterium oxide (heavy water) and these spectra are shown in Figures in 5-4 and 5-5.

For the purpose of comparison, the upper frame in Figures 5-4 and 5-5 are reproductions of the H_2O spectra obtained previously with their signal intensities on a logarithmic scale while the bottom frames are spectra obtained with the aspiration of D_2O under similar conditions. The mass range between 17 to 21 corresponds to oxygen-hydrogen species (OH_x) with values of x from 1 to 3. This is confirmed by the spectrum obtained using D_2O, where the corresponding mass ions increased by 1 amu per hydrogen atom. There was no detectable amount of di-hydroxyl molecular species observed in the spectrum. In addition, the use of D_2O also helped to establish the identity of the low molecular mass peaks between 1 amu to 3 amu. Finally, the hydride and hydroxide poly-atomic ions observed using distilled water were also confirmed using D_2O.

The overall aim of this study was not simply to re-establish the identity of these background species. Rather, the intention was to characterize the response behaviour of the

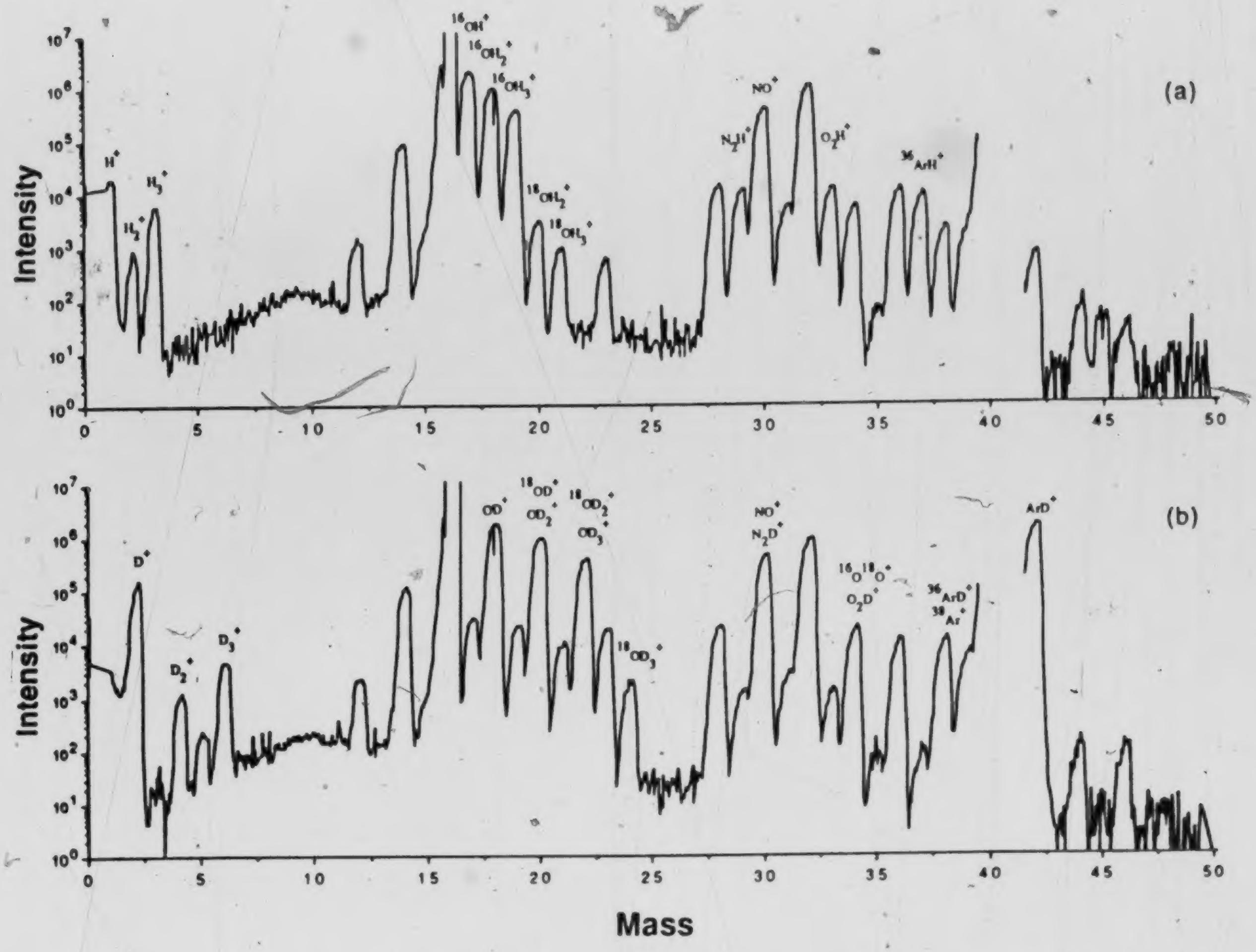

Figure 5-4. a) Background spectrum for distilled water at 1 to 50 amu. b) Background spectrum for deuterium oxide (heavy water) at 1 to 50 amu.

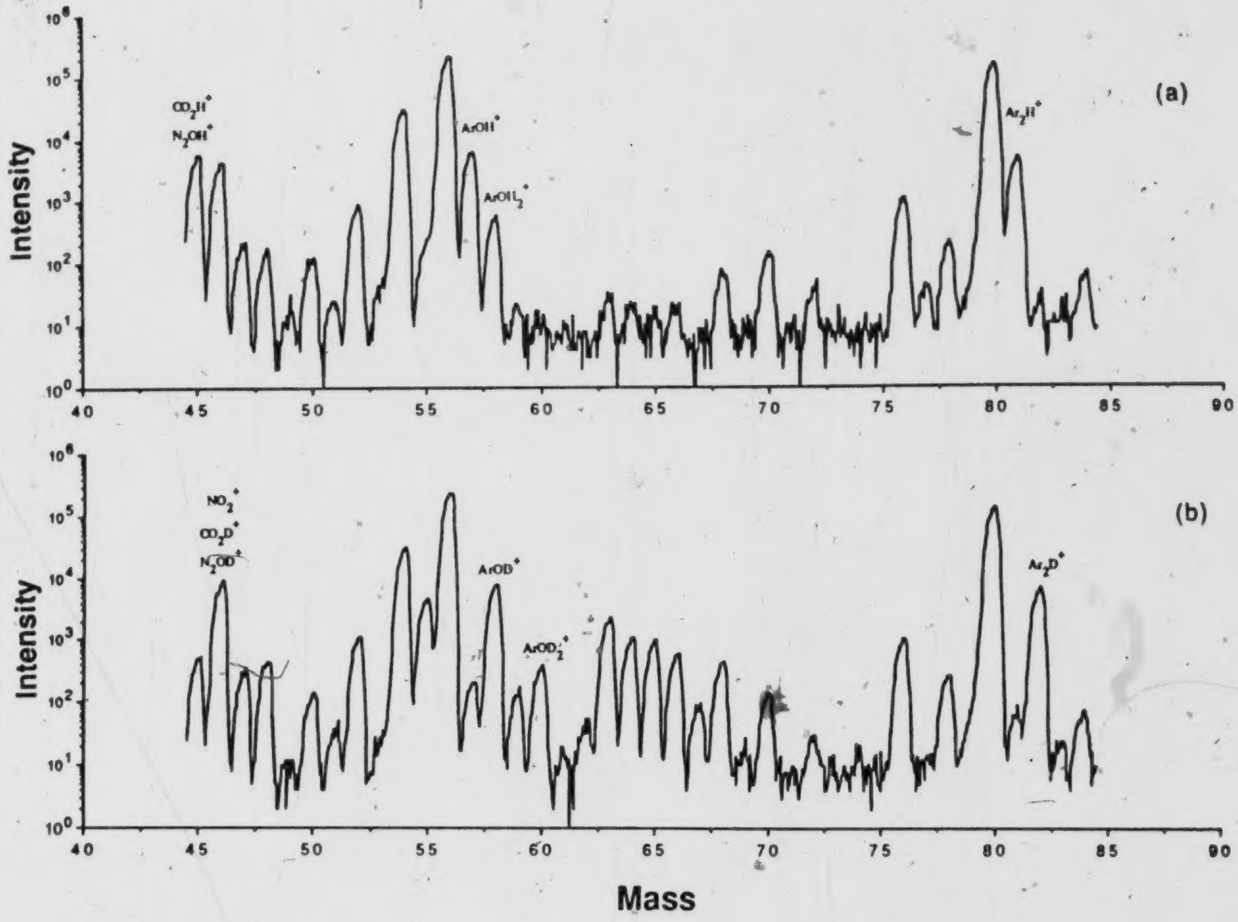

Figure 5-5. a) Background spectrum for distilled water at 44 to 84 amu. b) Background spectrum for deuterium oxide at 44 to 84 amu.

background species with respect to metal analytes, since a detailed knowledge of this response might suggest compromise analytical conditions where the interference effect would become negligible.

ii) Experimental Conditions

A solution containing a copper concentration of 1 ppm in 2% nitric acid was used. In this study, the plasma gas and auxiliary gas were 11 l/min and 1.40 l/min. The sampling depths studied were 10, 15, 20 and 25 mm with the rf forward power at 1.00, 1.25 and 1.50 kW. The ion signal intensity for each species was monitored as a function of nebuliser gas flow rate at each set of conditions.

Data observed in this part of the study were obtained with the use of the original electrostatic lenses supplied by the manufacturer. The ion signal sensitivity obtained with this set of lenses was about an order of magnitude poorer than the later production grade lenses currently in the instrument.

The background species investigated were ^{36}Ar, ^{36}ArH, ArN, ArO, ArOH, Ar$_2$ and Ar$_2$H. In addition, the ion signal for mass 63 (Cu) was also monitored and used as the analyte reference standard. The illustrations in Figures 5-6 to 5-9 show the signals for the abovementioned species under a range of plasma conditions. The overall results look rather interesting as all species show some degree of dependency on plasma parameters. From the ion signal profiles in each figure, with the exception of Ar ion, the maximum signal for each species appeared at about the same nebuliser flow rate as the analyte ion (Cu). Hence, fine adjustments on the flow rate of the nebuliser gas alone will not lower the degree of species overlap to any significant extent. In considering the signal dependency on rf power, it is interesting to note that while the optimum signal for argon dimer decreased with increasing plasma forward power, the maximum signal for argon ion remained virtually the same at all three power settings. With this knowledge, it is likely that the

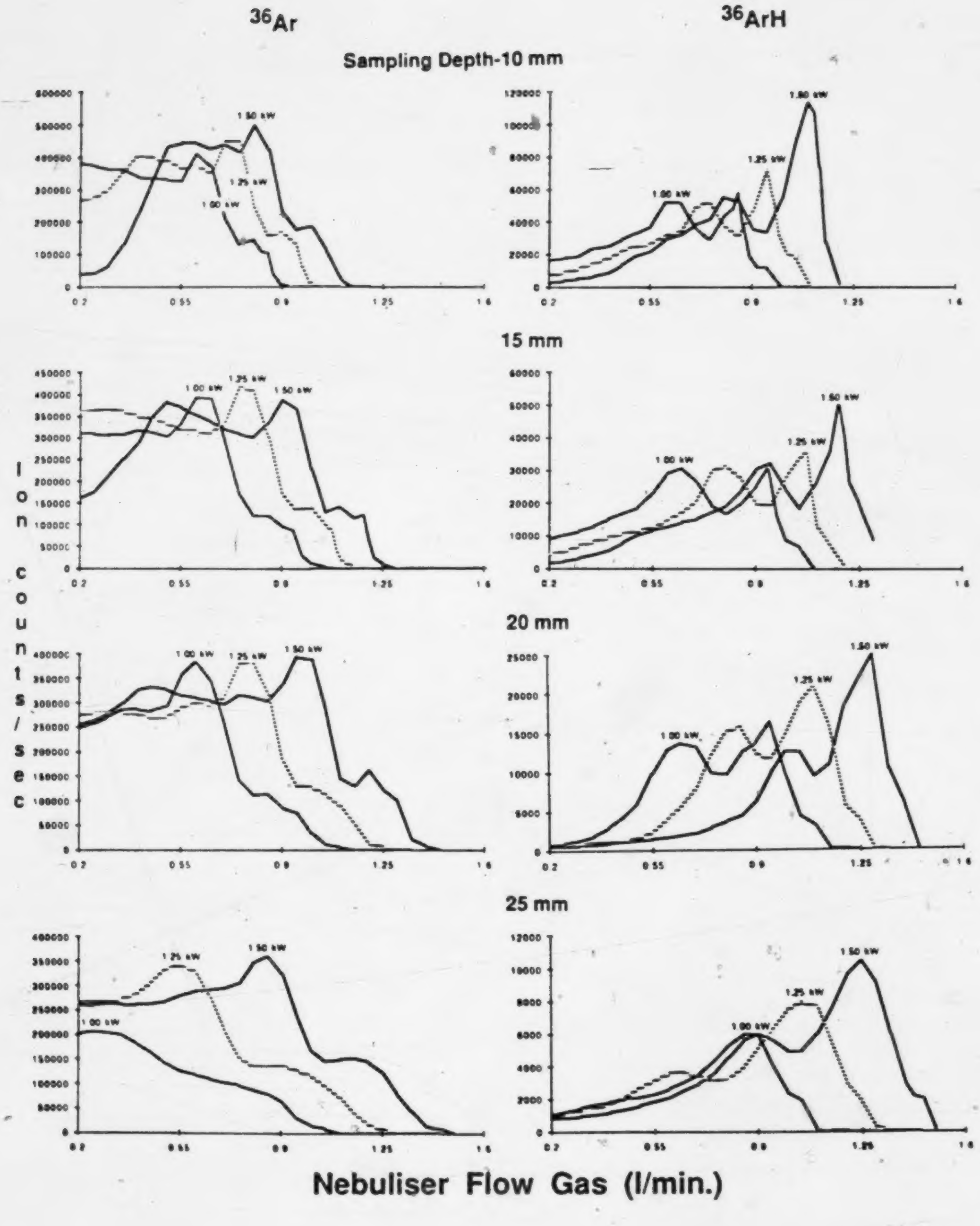

Figure 5-6. Dependence of $^{36}Ar^+$ and $^{36}ArH^+$ signals on nebuliser flow rate for a range of rf powers and sampling depths.

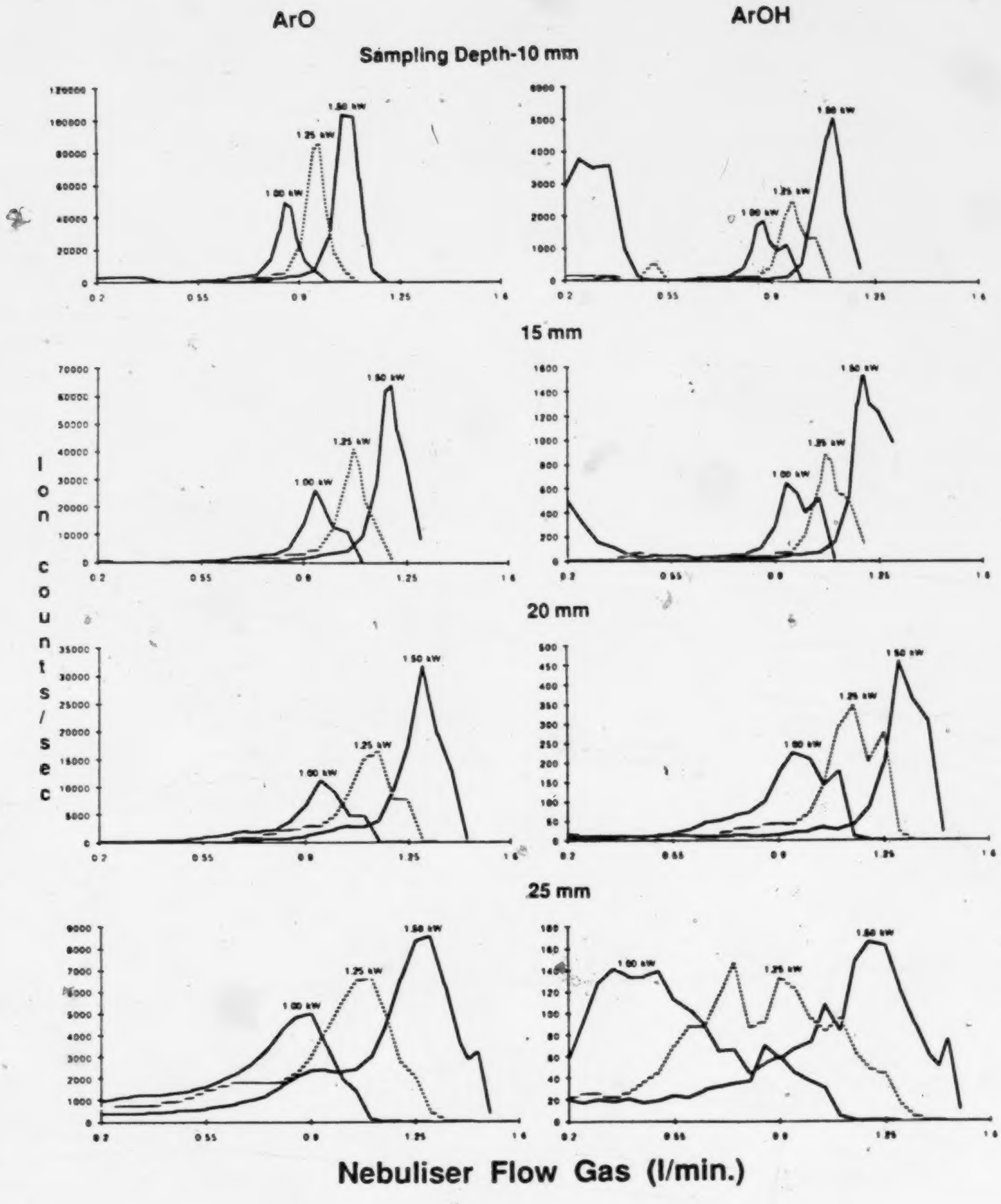

Figure 5-7. Dependence of $^{40}ArO^+$ and $^{40}ArOH^+$ signals on nebuliser flow rate for a range of rf powers and sampling depths.

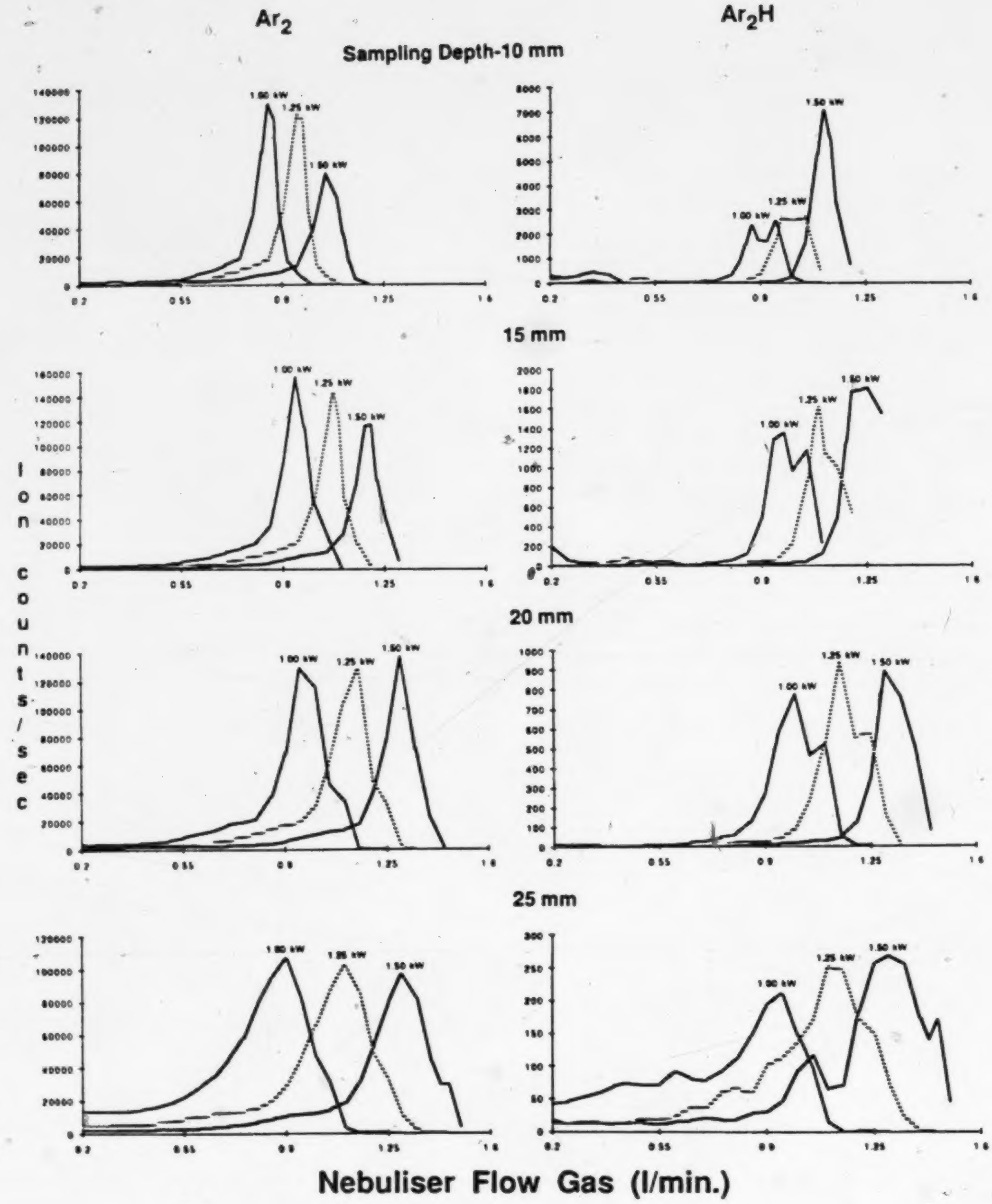

Figure 5-8. Dependence of $^{40}Ar_2^+$ and $^{40}Ar_2H^+$ signals on nebuliser flow rate for a range of rf powers and sampling depths.

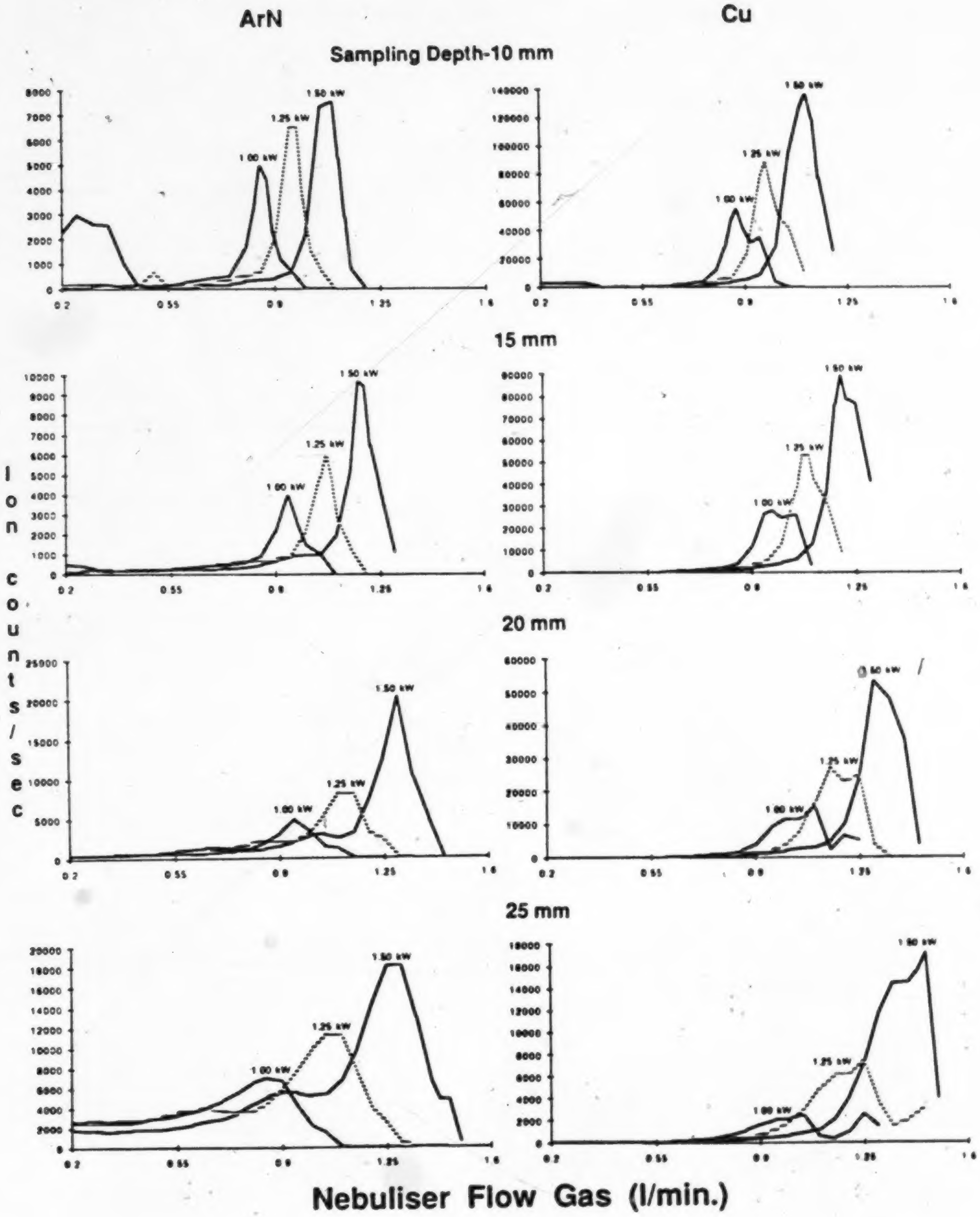

Figure 5-9. Dependence of $^{40}ArN^+$ and $^{63}Cu^+$ signals on nebuliser flow rate for a range of rf powers and sampling depths.

background interference caused by Ar can be minimized by choosing a higher nebuliser gas flow rate and a high plasma power. In contrast, the spectral overlap on Se by the argon dimer could be lowered with a high plasma power.

The effect of sampling depth on background species at 1.50 kW is illustrated in Figure 5-10. From the signal profiles shown in this figure, it is interesting to note that the argon ion population decreases gradually with increasing sampling depth. On the other hand, signals from species such as argon dimer and ArN are enhanced with increasing sampling depth up to 20 mm while the signals for the hydrogen containing species (ArH, ArOH and Ar_2H) decrease. However, the response for ArO was very similar to Cu. Hence, it is not feasible to lower this interference (on Fe) by adjustment of plasma parameters.

In conclusion, the effect of plasma parameters on background species is very complicated. There appears to be no universal set of conditions that can effectively eliminate the various species simultaneously. From the data illustrated above, it is clear that an interference caused by spectral overlap with a background ions is difficult to eliminate by manipulating the plasma operating parameters alone. In fact, only the argon ion interference (on Ca) seems likely to be minimized by setting the flow rate of the nebuliser gas to a value above the optimum condition for the analyte as well as using a high rf power plasma. Similarly, high rf power also benefits the analysis of Se at mass 80 (Ar_2). By the same token, the sampling depth used for the analysis of ^{54}Cr (by ArN) should be small because the source of nitrogen is probably from the entrainment of air. In contrast, interference caused by hydrogen-containing species (^{36}ArH, ArOH and Ar_2H) is best treated by using longer sampling depths. Therefore, a specific study must always be carried out in order to minimize problems caused by different types of ion species.

b. Nitrogen Mixed Gas Plasma

i) Introduction

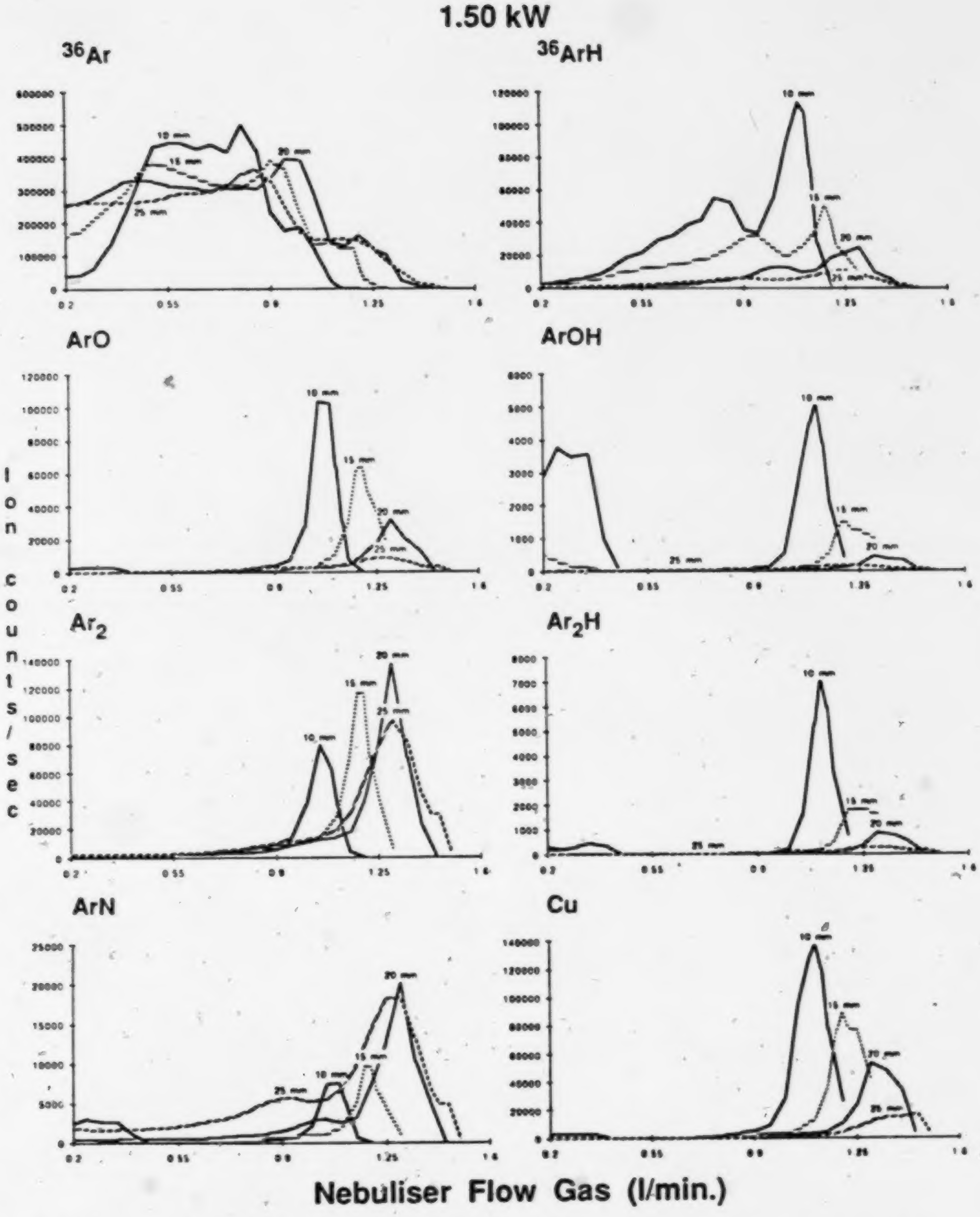

Figure 5-10. Dependence of $^{36}Ar^+$, $^{36}ArH^+$, $^{40}ArN^+$, $^{40}ArO^+$, $^{40}ArOH^+$, $^{63}Cu^+$, $^{40}Ar_2^+$ and $^{40}Ar_2H^+$ signals on nebuliser flow rate for a range of sampling depths and at 1.50 kW rf power.

Previously, it has been observed that the application of nitrogen mixed gas plasmas in ICP-MS results in a significant reduction in oxide levels as well as signal enhancement for some selected analytes. Since the majority of the background species are poly-atomic, it was thought that the introduction of nitrogen into the discharge might be beneficial towards the dissociation of those species. In particular, in the case of oxygen containing ions, the effect of a nitrogen mixed gas plasma was expected to be advantageous if their behaviour was comparable to analyte oxides.

ii) Experimental Conditions

In this study, the Background Equivalent Concentration (BEC) was estimated for some of the species in order to measure the effectiveness of a nitrogen mixed gas plasma in lowering the level of background species. A solution containing 0.2 ppm Fe and 5.0 ppm Se in 2% nitric acid was used for the estimation of BEC values for ArO, ArOH and Ar_2 (equivalent to ^{56}Fe, ^{57}Fe and ^{80}Se) respectively.

The plasma gas was mixed with 0%, 5%, 12% and 20% nitrogen. With each plasma, a "Blank" solution consisting of 2% nitric acid was aspirated at first and the signal intensities as a function of nebuliser flow rate were monitored. This was subsequently followed by the introduction of the analyte solution under identical conditions. The plasma gas and auxiliary gas were 15 l/min and 1.80 l/min respectively and the rf forward power was 1.50 kW with the sampling depth set at 10 mm throughout.

The signal profiles at the three masses are shown in Figures 5-11 to 5-13. The top frame in each figure is data for the Blank signal for the three species, while the bottom frames show the total ion signals when analyte solution is introduced.

From results shown in these figures, it is quite clear that the utilization of a nitrogen mixed gas plasma helps in the removal of ArO and ArOH. Especially in the case of ArO,

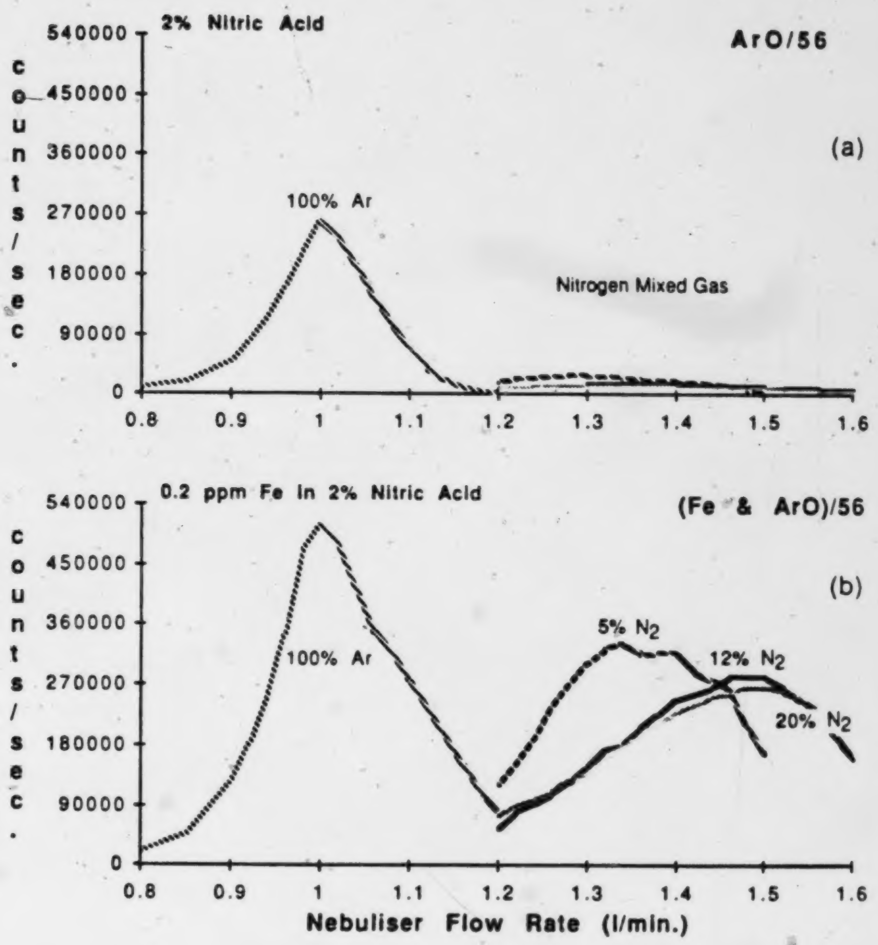

Figure 5-11. a) The effect of nebuliser flow rate and 0, 5, 12 and 20% nitrogen cooled plasmas on ArO species (2% nitric acid "Blank" solution). b) The effect of nebuliser flow rate and 0, 5, 12 and 20% nitrogen cooled plasmas on mass 56 (Fe and ArO) from a solution containing 0.2 ppm Fe in 2% nitric acid.

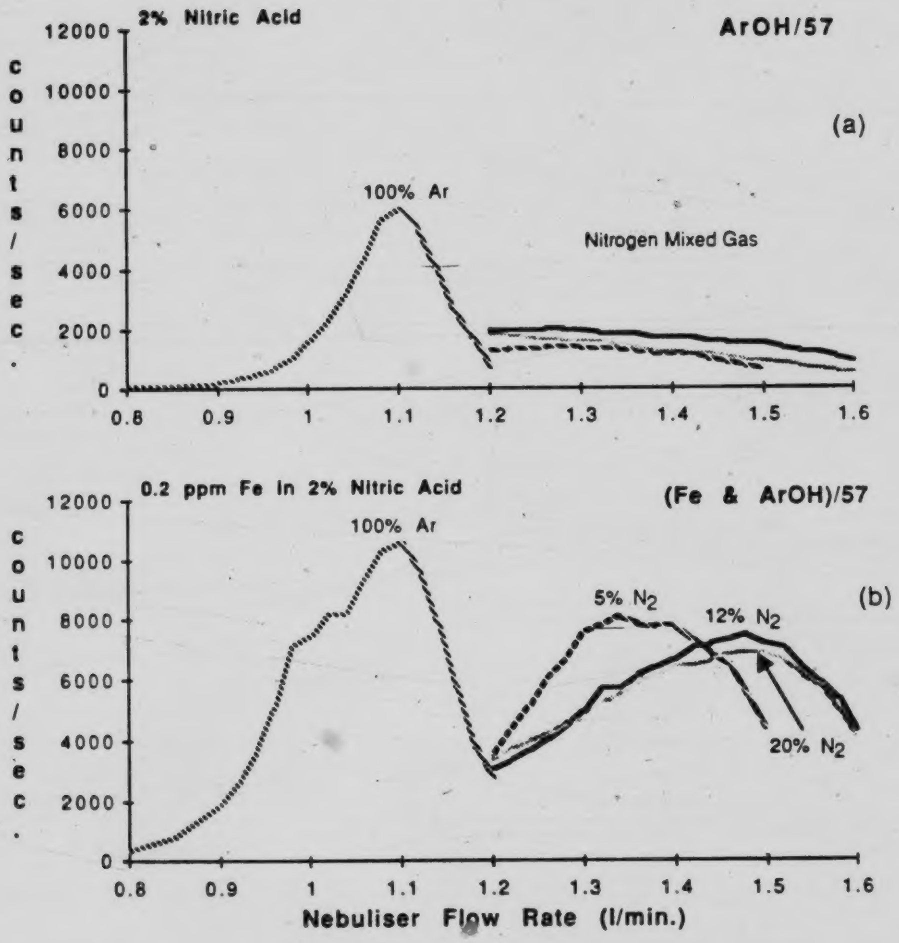

Figure 5-12. a) The effect of nebuliser flow rate and 0, 5, 12 and 20% nitrogen cooled plasmas on ArOH species (2% nitric acid "Blank" solution). b) The effect of nebuliser flow rate and 0, 5, 12 and 20% nitrogen cooled plasmas on mass 57 (Fe and ArOH) from a solution containing 0.2 ppm Fe in 2% nitric acid.

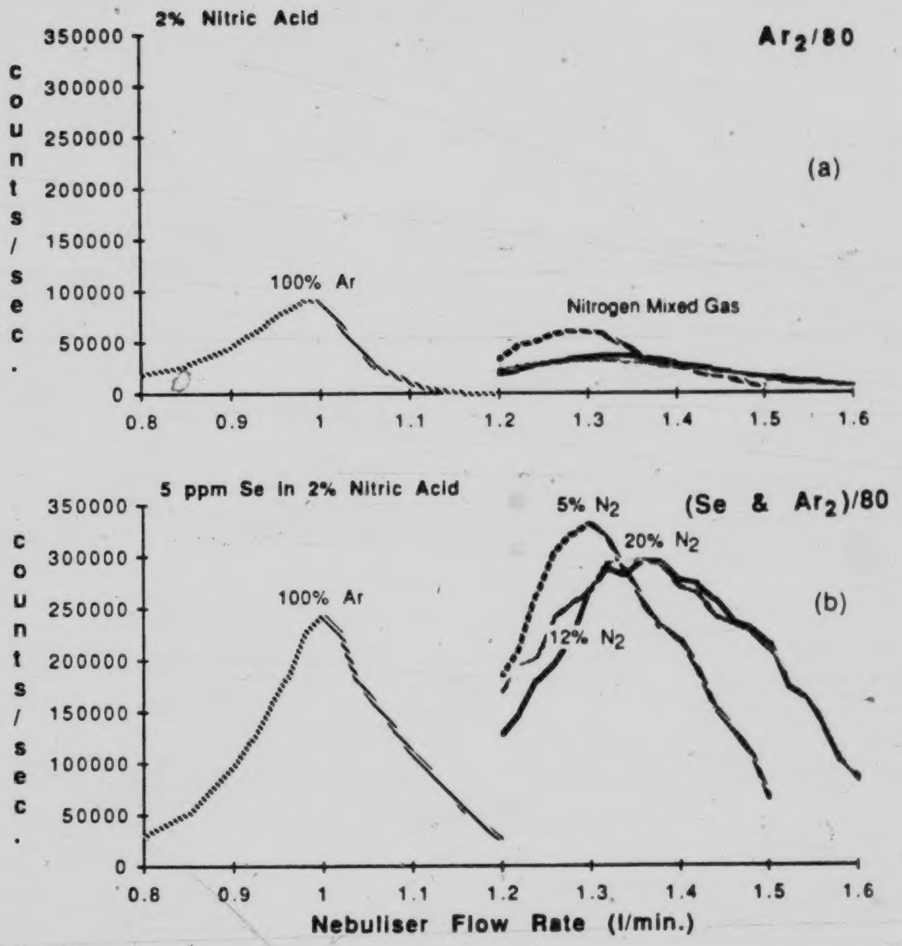

Figure 5-13. a) The effect of nebuliser flow rate and 0, 5, 12 and 20% nitrogen cooled plasmas on argon dimer (2% nitric acid "Blank" solution). b) The effect of nebuliser flow rate and 0, 5, 12 and 20% nitrogen cooled plasmas on mass 80 (Se and Ar$_2$) from a solution containing 5 ppm Se in 2% nitric acid.

the use of a 5% nitrogen cooled mixed gas plasma resulted in the reduction of the background signal by more than an order of magnitude (see Figure 5-11). However, it also appeared that the introduction of nitrogen into the plasma resulted in the lowering of analyte sensitivity (see Figures 5-11 and 5-12). This misleading information can be clarified by stripping the "Blank" signals from the analyte intensities (ion signals in the top frame subtracted from the bottom frame point by point in each figure). The net signal is illustrated in the top frames of Figures 5-14 to 5-16. From the results in each figure, it is obvious that the use of nitrogen mixed gas plasmas actually resulted in better analyte sensitivities. However, this advantage diminishes at higher nitrogen percentages. Moreover, the optimum nebuliser flow rates for mass 56 and 57 are different than the values observed after "Blank" subtraction. In the case of mass 57, the optimum value was found to be 1.10 l/min before background subtraction. Yet, the actual optimum flow rate for ^{57}Fe was at 0.98 /min using a pure argon plasma. The bottom frames of Figures 5-14 to 5-16 illustrate the calculated BEC values for each of the background species obtained at the optimum condition for each species using the different nitrogen mixed gas plasmas. It should also be pointed out that the enhanced intensity of "Unstructured Background" (photon noise) from the nitrogen mixed gas plasma makes calculation of BEC for the species erroneous (particularly for species with low intensity). Therefore, the photon background signals were manually subtracted in these calculations. From the results, it is interesting to note that the use of a 20% nitrogen cooled mixed gas plasma lowered the BEC values by more than a decade in some instances. In the case of ArO, the BEC value decreased from 160 ppb equivalent (with pure argon plasma) to 7 ppb using a 20% nitrogen discharge. The degree of improvement for ArOH was not as impressive as for ArO. This is probably due to the difference in nature of the species. In fact, at the nebuliser flow rate of 1.10 l/min (optimum signal for ArOH), a calculated BEC value of 150 ppb was obtained. Also, it is worth pointing out that despite the relatively low natural abundance of ^{57}Fe compared to ^{56}Fe (2.14% to 91.7%), the lower BEC value at mass 57 makes it more attractive for trace

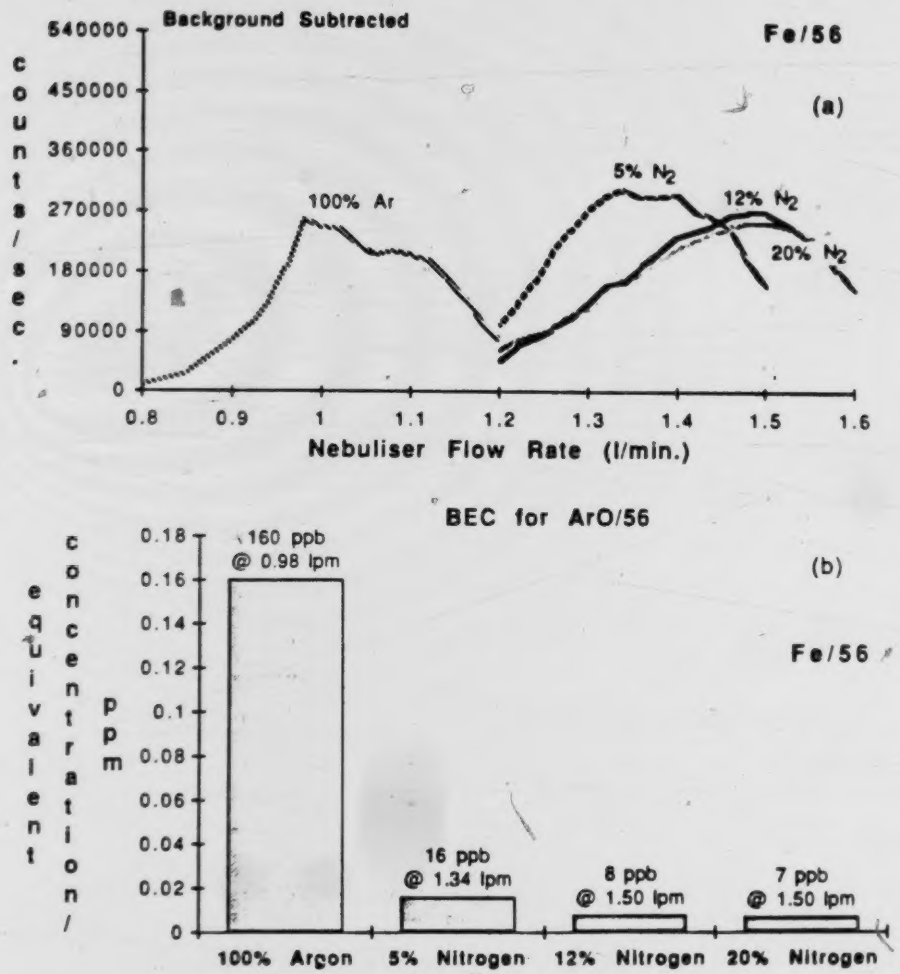

Figure 5-14. a) The net signal responses for ^{56}Fe (after blank subtracted) in 0, 5, 12 and 20% nitrogen cooled plasmas. b) The BEC values for ArO to Fe signals (each at peak Fe intensity).

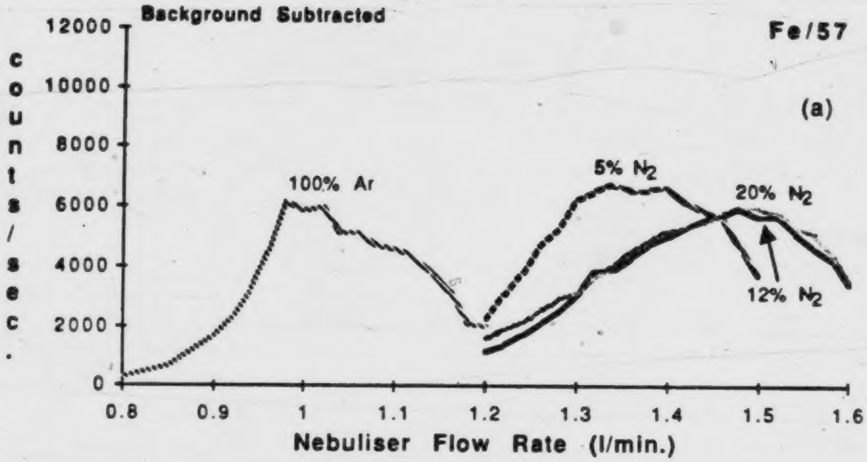

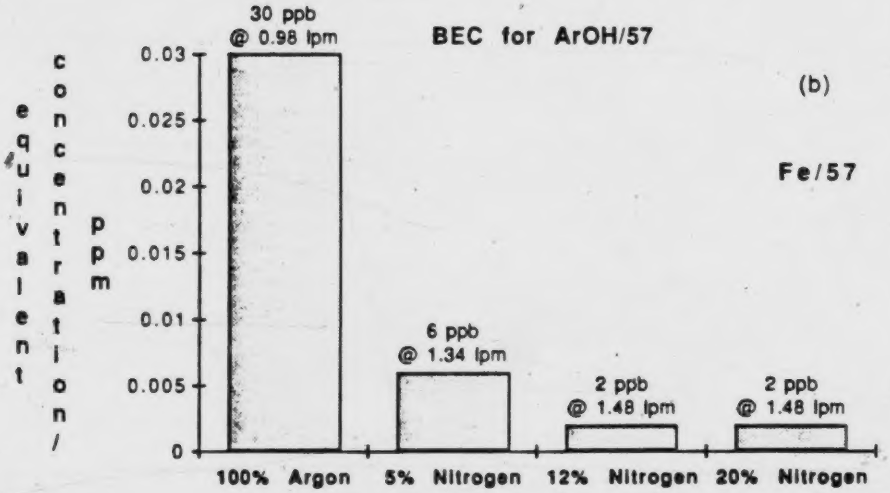

Figure 5-15. a) The net signal responses for ^{57}Fe (after blank subtracted) in 0, 5, 12 and 20% nitrogen cooled plasmas. b) The BEC values for ArOH to Fe signals (each at peak Fe intensity).

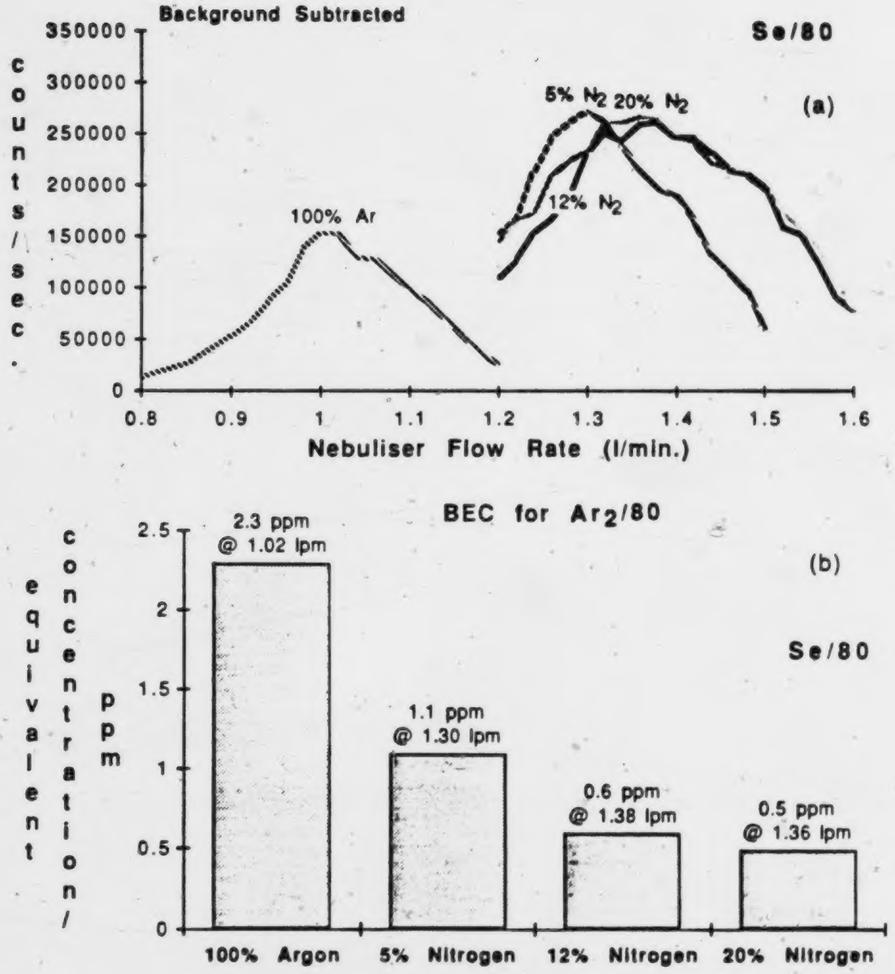

Figure 5-16. a) The net signal responses for ^{80}Se (after blank subtracted) in 0, 5, 12 and 20% nitrogen cooled plasmas. b) The BEC values for Ar_2 to Se signals (each at peak Se intensity).

element analysis (see Figure 5-14 and Figure 5-15). Finally, the use of nitrogen for the dissociation of argon dimer (Se analysis) did not give the same degree of success. In fact, the BEC value was decreased only to 0.5 ppm (about 5 fold) from a high value of 2.3 ppm (see Figure 5-16).

c. Effect of Desolvation on Background Species

i) Introduction

It was reported in Chapter 4 that some types of "aerosol processing" involving condensation and/or a heating chamber could have significant effects on the population of analyte and its oxide. The effects were most profound for the refractory elements. Since the majority of the primary background species contain oxygen, the application of such "aerosol processing" techniques could be promising towards the lowering of their populations.

ii) Experimental Conditions

A solution containing 0.1 ppm copper in 2% nitric acid was used in this study. The background ions ArN, ArO, ArOH, Ar_2 and Ar_2H were monitored (with ^{63}Cu ion also observed as a reference) as a function of nebuliser gas flow rate. The aerosol processing techniques were similar to the previous set-up (Chapter 4, Figure 4-2) with the aerosol stream subjected to either heating (at 150°C inside the heating camber) or kept at room temperature. The treated or untreated aerosol stream was introduced to a pure argon plasma or a 5% nitrogen cooled mixed gas discharge. The flow rates for plasma gas and auxiliary gas were 15 l/min and 1.80 l/min respectively, the rf power was 1.50 kW and the sampling depth at 10 mm throughout.

iii) Results and Discussion

The data for the species were recorded and are summarized in Figure 5-17. The ion responses for Cu showed that there was a drop in signal sensitivity after the aerosol stream was "desolvated". This trend was consistent in both types of plasma discharges and was likely due to a lower aerosol transportation efficiency. The lack of sensitivity change using a 5% nitrogen cooled plasma as compared to the 100% argon plasma is not unexpected because Cu has a rather modest first ionization energy (7.726 eV) and also a relatively low affinity for oxygen ($D^{\circ}$for C-O is less than 3 eV) [15]. These two characteristics correlate with little if any signal enhancement when using a nitrogen mixed gas discharge (see Chapter 3).

From data presented in Figure 5-17, the effect of solvent removal on the background species was somewhat different than that for Cu. Instead of lowering the signal level, it either had no effect or there was an increase in the ion intensity. Hence, background interference may become worse after desolvation of the aerosol stream. This observation was in contrast to that of Gray [7] where a reduction in the level of ArO was observed after desolvation. Yet, the above behaviour was consistent and reproducible. On the other hand, the use of a 5% nitrogen plasma resulted in a general reduction in intensity for some of the primary background species with the exception of ArN, which was increased due to the extra amount of nitrogen in the plasma.

In an attempt to clarify the process of aerosol "desolvation", the low mass oxygen related species as well as argon and argon hydride ions (OH, OH_2, OH_3, O_2, ^{36}Ar and ^{36}ArH corresponding to masses of 17, 18, 19, 32, 36 and 37 respectively) were monitored. Due to the high ion signal intensities for most of the species, the power supply to the ion deflector was turned off. For this part, the experimental set-up and conditions were identical to the above section with the exception that the undesolvated measurements were not carried out when the 5% nitrogen mixed gas plasma was used

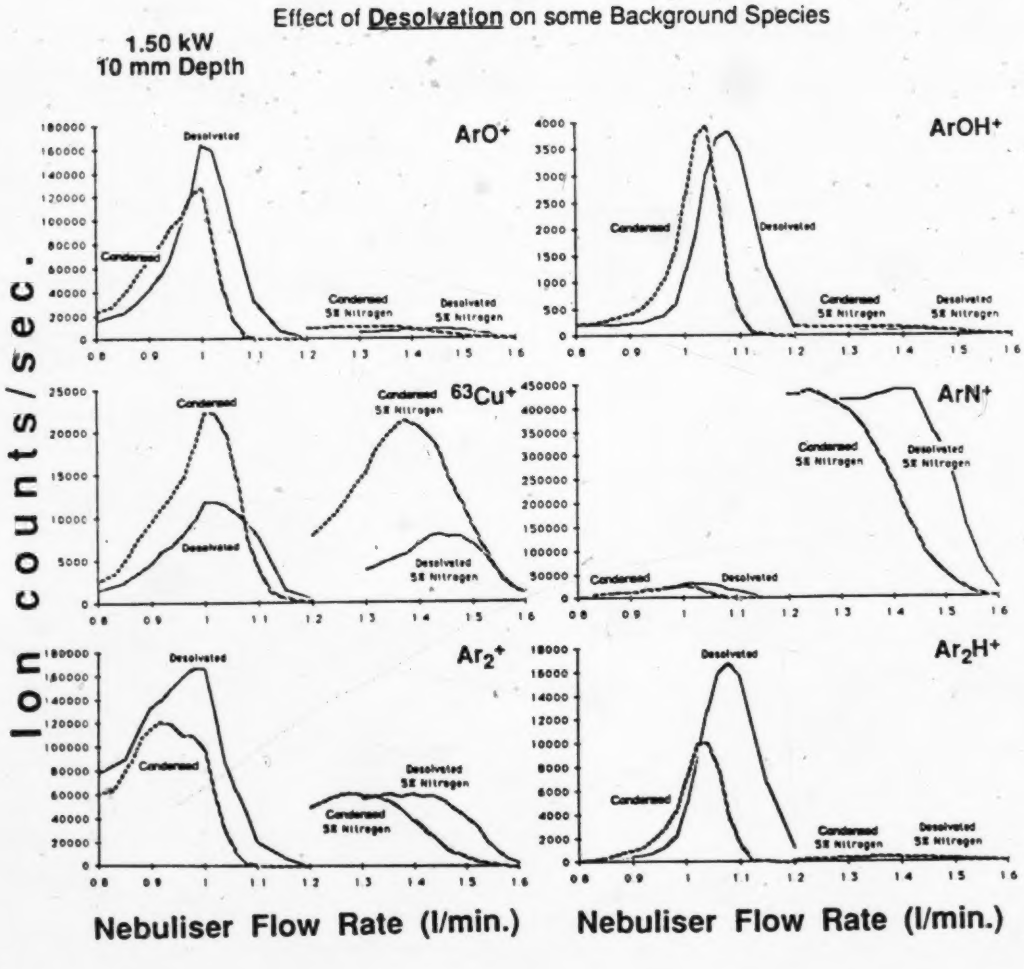

Figure 5-17. The effects of desolvated nebulisation on ArO, ArOH, Cu, ArN, Ar_2 and Ar_2H ion species in a 100% argon plasma and a 5% nitrogen cooled discharge.

The signal responses for the oxygen related species (OH, OH_2, OH_3 and O_2) are illustrated in Figures 5-18 to 5-21 for the three different experimental conditions. It is interesting to note that the ion counts for the hydroxyl species were affected to a larger degree by the desolvation process (see Figures 5-18 to 5-20) than was the molecular oxygen ion (Figure 5-21) when a pure argon plasma was used. However, when they were subjected to the 5% nitrogen plasma, with the exception of the response for mass 18 (OH_2), their optimum ion counts were reduced to about 10% of their original values. The different response to the nitrogen plasma for the OH_2 species seemed unusual (see Figure 5-19). In an earlier report by Houk et al. [16] they compared the data observed using a 0% to 100% nitrogen cooled mixed gas discharge and they also recorded an initial increase in ion signal at mass 18 when the nitrogen percent was low in the plasma. They attributed the signal increase to the formation of NH_4^+ ion in the nitrogen mixed gas discharge. However, the identity of this species cannot be easily verified even with the use of D_2O because the ammonium ion will give a mass of 22 which itself overlaps with the OD_3 species.

The behaviour of the hydroxyl and molecular ions was as would be anticipated with desolvation, i.e. the level of the ion signal decreased after the solvent removal process had taken place. However, this is opposite to the results observed earlier regarding the other oxygen related species (ArO, ArOH in Figure 5-17). Figure 5-22 illustrates the signal intensities for Ar and ArH ions. As can be seen from the data, the argon ion signal increased when the aerosol stream was desolvated for both the argon plasma and the 5% nitrogen plasma while an opposite trend was observed for ArH. This observation is in agreement with the results by Houk et al. [16] in which the argon ion intensity was increased in a low percentage nitrogen mixed gas plasma.

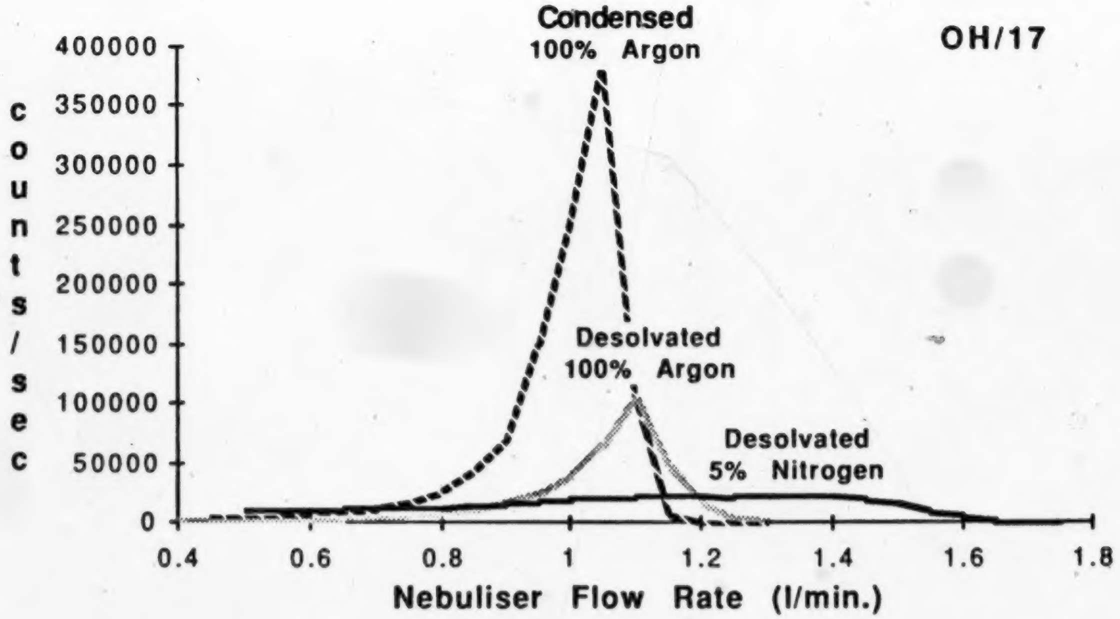

Figure 5-18. The effects of aerosol processing on mass 17 (OH) in a 100% argon plasma and in a 5% nitrogen cooled discharge.

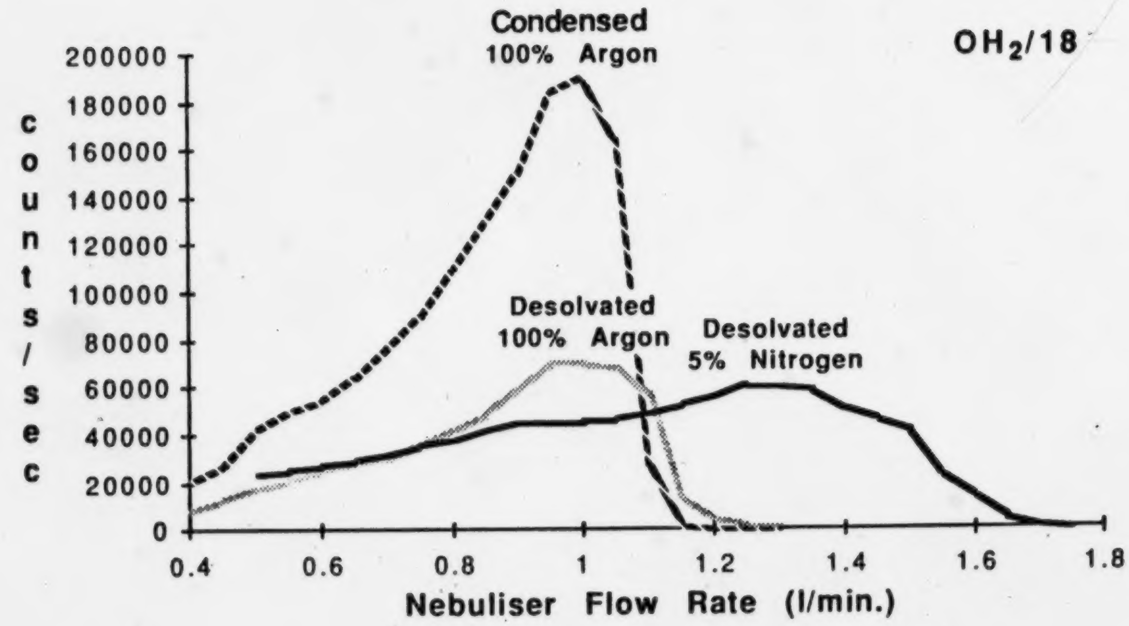

Figure 5-19. The effects of aerosol processing on mass 18 (OH_2) in a 100% argon plasma and in a 5% nitrogen cooled discharge.

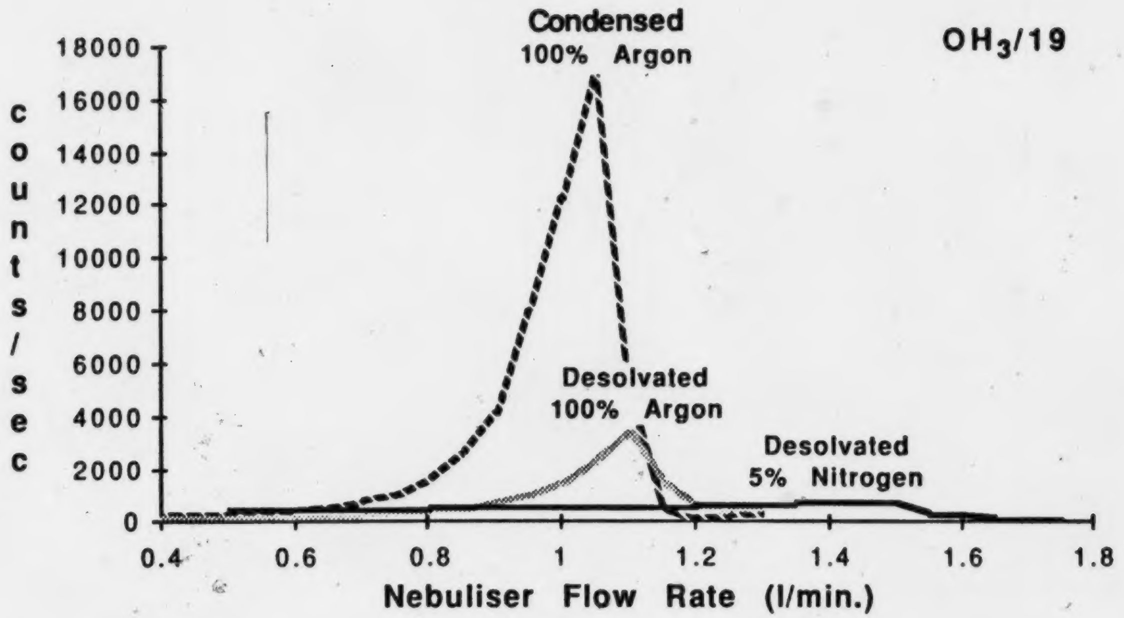

Figure 5-20. The effects of aerosol processing on mass 19 (OH_3) in a 100% argon plasma and in a 5% nitrogen cooled discharge.

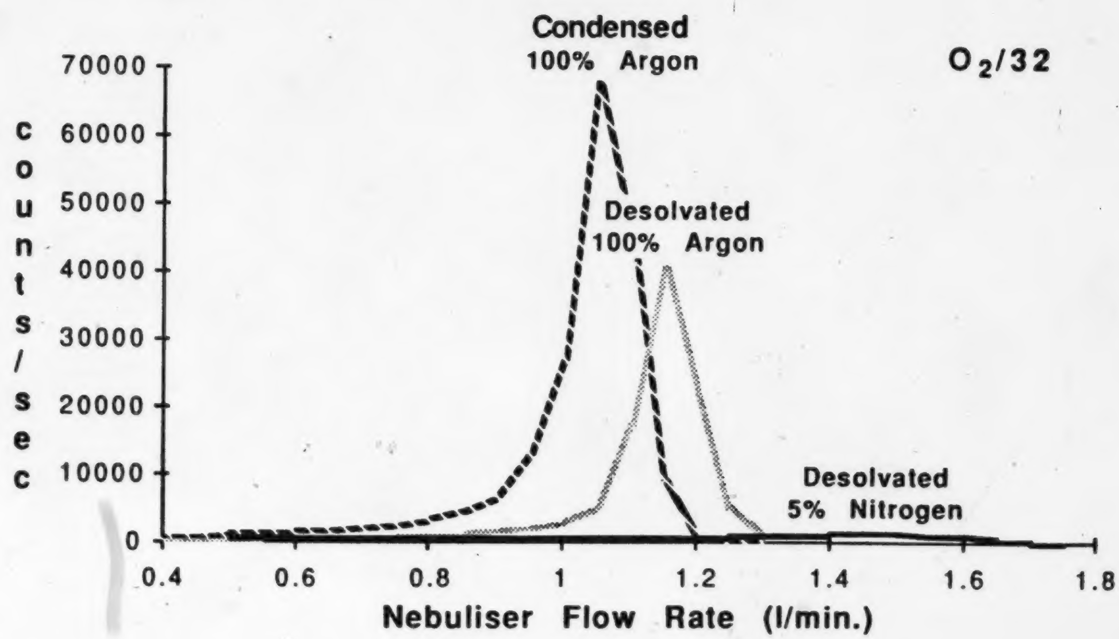

Figure 5-21. The effects of aerosol processing on mass 32 (O_2) in a 100% argon plasma and in a 5% nitrogen cooled discharge.

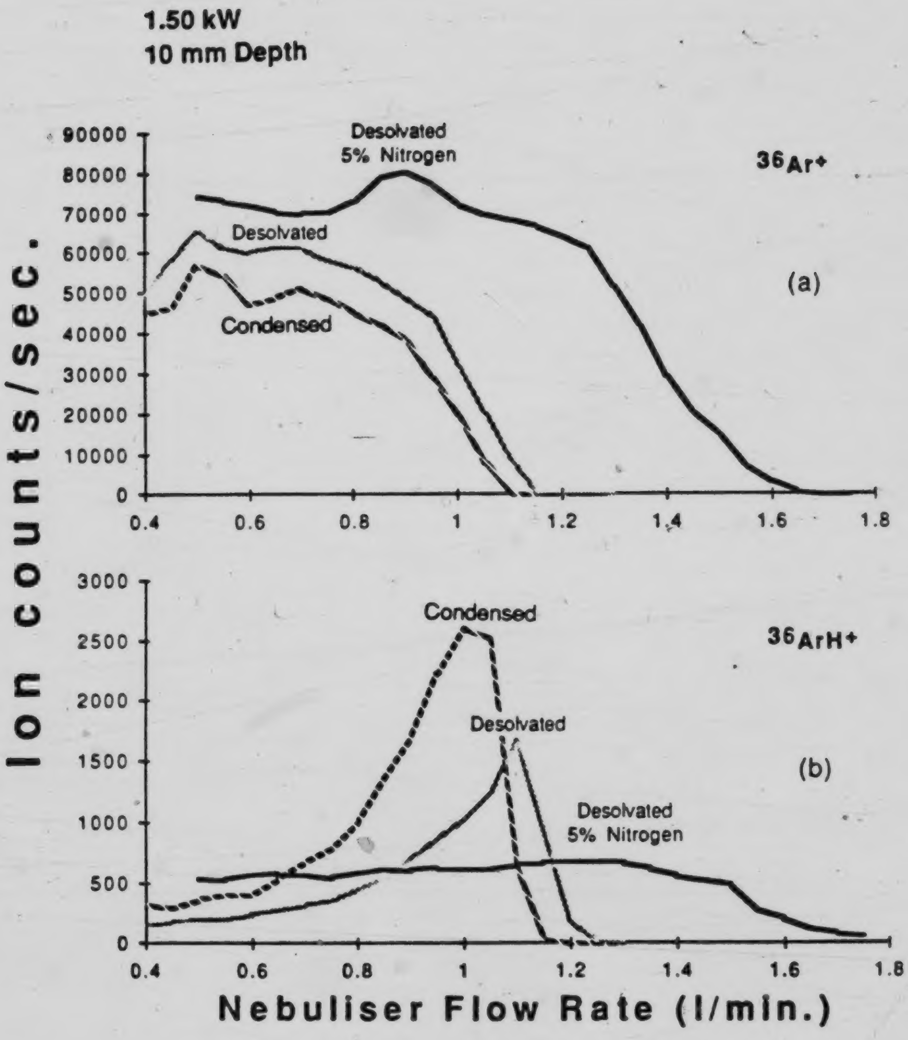

Figure 5-22. a) The effects of aerosol processing on mass 36 (^{36}Ar) in a 100% argon plasma and in a 5% nitrogen cooled discharge. b) The effects of aerosol processing on mass 37 (^{36}ArH) in a 100% argon plasma and in a 5% nitrogen cooled discharge.

The above observations can be rationalized in terms of the relative population densities for O^+ and Ar^+ ions. Assuming a Saha relationship, Gray [7] estimated their ion densities to be $3 \times 10^{14}/cm^3$ and $1.2 \times 10^{15}/cm^3$ respectively. Assuming this estimation to be applicable, then the population density for Ar ion is less than an order of magnitude higher than the oxygen ion. Since the degree of ionization for oxygen is calculated to be about 0.04% [17], then the oxygen atom density can be estimated to be about $7 \times 10^{17}/cm^3$. This is more than two decades higher than the estimated argon ion density. In a simple bimolecular reaction involving only a single step, the reactant with the lower concentration is expected to be the limiting species controlling the extent of the reaction. Hence, it is likely that the limiting reagent during the formation of argon-oxygen poly-atomic background is argon ion, since the desolvation process did not lower the water supply in the plasma by a sufficiently large amount. The process of desolvation only increased the population level of argon ion (see Figure 5-22) as the concentration of oxygen was still in excess. Hence, ion intensities for the oxygen-argon background ions such as ArO, are increased.

However, the same rationale cannot be applied to the results obtained with the nitrogen mixed gas plasma. In this situation, although the ion population density for argon also increases, the level of oxygen is thought to be greatly diminished due to the reactive nature of nitrogen (forming NO). Hence, the concentration of oxygen might then become the limiting reagent during reaction in this plasma.

d. Conclusion

The use of a nitrogen mixed gas plasma with and without aerosol desolvation seems promising for lowering O- and H- related background species. In fact, the signal intensities for most species were found to be reduced by more than an order of magnitude. However, a big drawback to this approach is the formation of more nitrogen related species, although analyte-nitrogen (X-N) have not appeared to surface. The most seriously affected masses as a result of using a nitrogen mixed gas are mass 54 for ArN (see Figure 5-17) and the nitrogen ions at 14, 28 and 30 corresponding to N, N_2 and NO ions. Problems caused by these nitrogen ions at low masses are of no real consequence as this region is already heavily populated with background species, even with argon plasma. The increased level of ArN has no real effect on the analysis of either Fe or Cr (minor isotopes for both species at mass 54) and to its advantage the mixed gas plasma also reduces the interferences caused by ArO and ^{36}ArO on the major ions for ^{56}Fe and ^{52}Cr respectively.

The addition of nitrogen into the plasma did result in a more condensed and brighter discharge. Hence, the non-structured background caused by photons is worse. However, this type of interference is non-specific, therefore, it can easily be removed by subtracting the ion counts at any mass unit so long as it is species free.

The advantage of using a nitrogen mixed gas plasma in ICP-MS is best demonstrated in Figure 5-23. This figure illustrates the background signal obtained between mass 43 amu and 90 amu when a 5% nitrogen cooled mixed gas plasma is used. The solution aspirated was "Blank" distilled water and the flow rate for the nebuliser gas was adjusted to give optimum signal sensitivity for Cu. From the spectrum shown in this figure, there are fewer background species compared to a pure argon plasma (see bottom frame in Figure 5-1). In fact, there are only 14 identifiable mass peaks in the figure as compared to more than 20 species observed using the argon plasma. However, the background continuum signal was higher when the mixed gas plasma was used.

Since the majority of the argon related background species are thought to be generated by the argon ions inside the axial channel of the plasma [16], the use of nitrogen as the nebuliser gas seems reasonable in order to lower this type of interference. Unfortunately, this part of the study was not carried out.

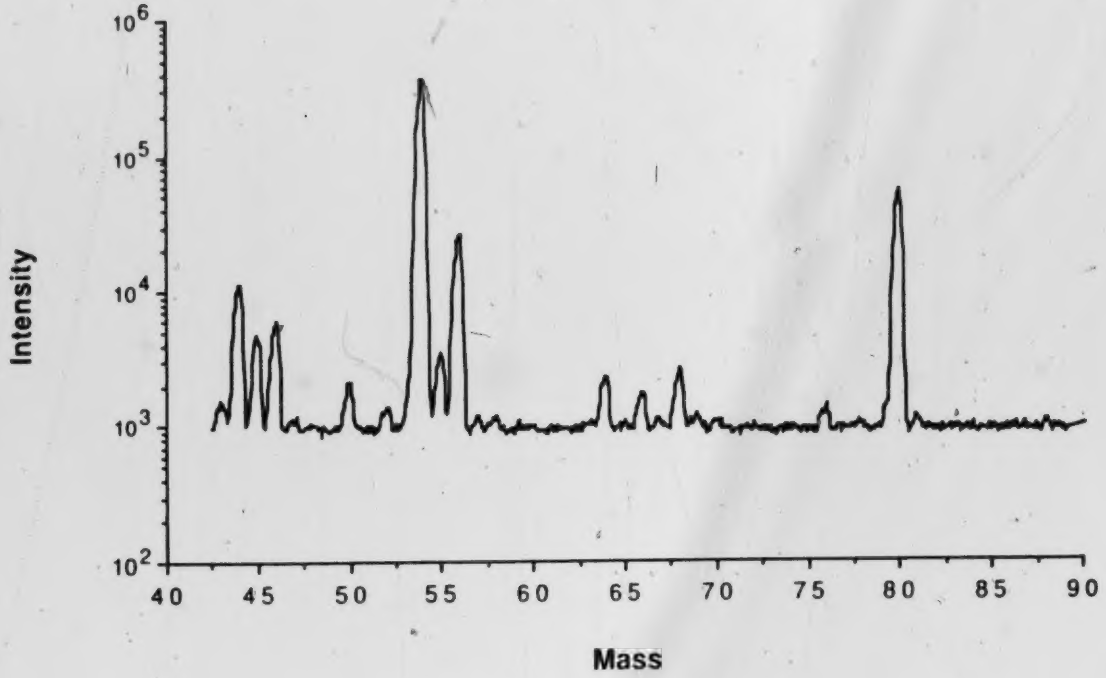

Figure 5-23. Background mass spectrum for distilled water (43 to 90 amu) obtained using a 5% nitrogen cooled plasma.

C. Behaviour of some Matrix Induced Molecular Species

a. Introduction

In solution analysis using ICP-MS, potentially the most challenging step is the sample dissolution medium. Tan and Horlick [13] presented a detailed tabulation of poly-atomic ions caused by the aspiration of the three most common mineral acids while Hieftje and coworkers [18] also illustrated some typical background spectra observed using different types of acid matrixes with a non-commercial ICP-MS instrument. HCl and H_2SO_4 are particularly troublesome. From the stand-point of an application scientist, this situation is unfavorable if one were using the instrument routinely for the analysis of a wide range of matrix elements. Hence, the procedure for sample dissolution and the resulting matrix becomes important. In general, one usually dissolves the sample with the minimum amount of applicable mineral acid. This is followed by solvent evaporation and finally dilution to the right concentration with 2-5% nitric acid. Nitric acid is the acid of choice as it gives rise to the least number of undesirable poly-atomic spectral ion interferences [13, 18]. This procedure is tedious and time consuming. Moreover, the extra steps involved in the sample dissolution process also increases the likelihood of sample contamination during the preparation stage. However, despite the enormous problem of interference cause by spectral overlap from HCl and H_2SO_4 species, very little effort has been devoted towards the elimination of the offending species [7, 18, 20].

Figure 5-24 and 5-25 show the background spectra obtained when solutions of 2% hydrochloric acid and sulphuric acid were introduced into the plasma discharge. The mass range of interest illustrated is from 43 amu to 85 amu. In each figure, the top frame consists of acid solution from stock and diluted to the appropriate concentration using distilled water. The spectra presented in the bottom frame were obtained from the same stock solution but diluted with a 50% v/v D_2O. The intensity axis in each spectrum is on a

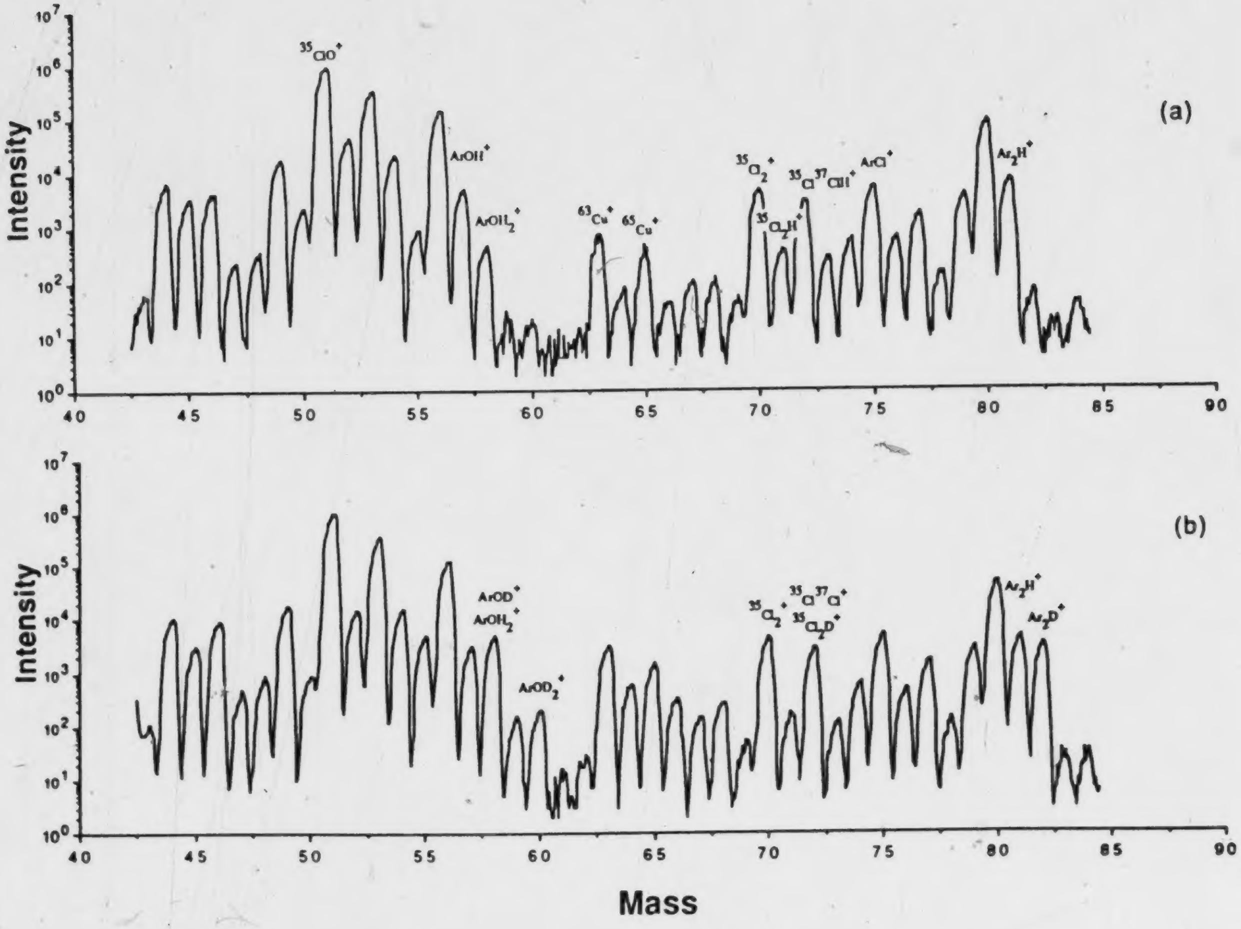

Figure 5-24. a) Background mass spectrum for 2% hydrochloric acid (43 to 90 amu). b) Background mass spectrum for 2% hydrochloric acid in a 50% v/v deuterium oxide solution.

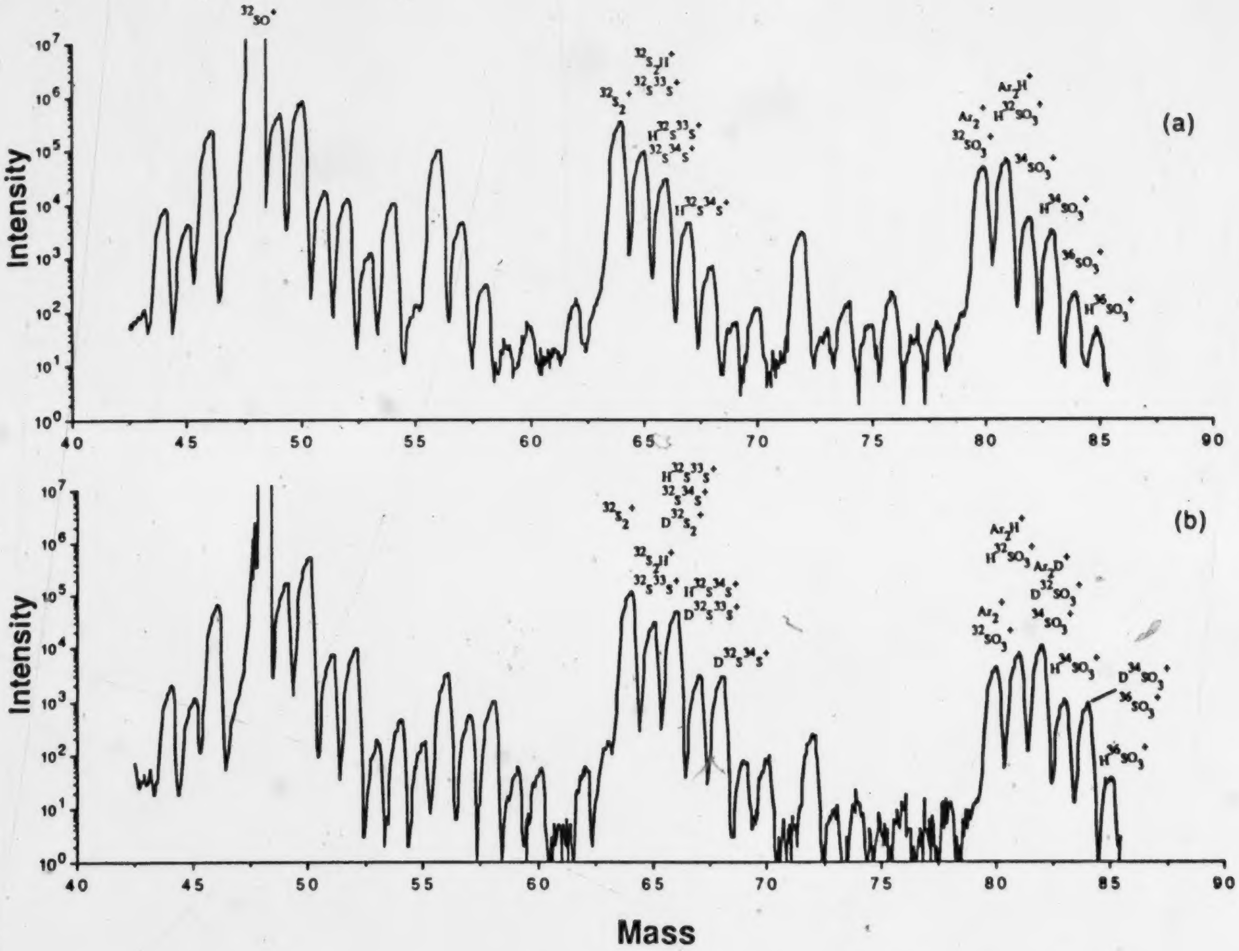

Figure 5-25. a) Background mass spectrum for 2% sulphuric acid (43 to 90 amu). b) Background mass spectrum for 2% sulphuric acid in a 50% v/v deuterium oxide solution.

logarithmic scale. From the ion signals in each figure, it is rather interesting that both ClO and SO ions were the dominating species in this mass range when the respective acid solution was aspirated. In addition, apart from the Cl_2H ion, no other chlorine hydride ions were observed. For H_2SO_4, due to the large number of the stable isotopes for sulphur, the spectrum became rather complicated. Between the prescribed mass range, hydride ion species such as S_2H and HSO_3 can be identified.

Despite the seemingly complicated spectra shown in the two figures, most of the interference effects can be minimized by monitoring alternative isotope elements. The problem of spectral overlap only becomes serious when the element itself is either mono-isotopic or the natural abundance of the minor isotope is very low. From the summary table presented by Tan and Horlick [13], the most problematic elements are Sc, Ti, V, Cr, Mn, Fe and As. For Cr and Fe, it has been previously demonstrated that the interference caused by the spectral overlap of ArO (^{36}Ar and ^{40}Ar) can be minimized with the use of a nitrogen mixed gas discharge. On the contrary, spectral overlap by species with masses at 45, 48 and 55 on Sc, Ti and Mn are difficult to eliminate. In the case of Sc, the identity of the interferent is difficult to establish. From the data presented in Figure 5-5, there is little doubt that the background ion is a hydrogen related species. Tan and Horlick [13] tentatively identified this species as CO_2H. The bond energy for O=CO is about 1 eV lower than N-O [15], yet, the use of a nitrogen mixed gas plasma did not have any significant effect on these species (compare Figure 5-1 to 5-23 at m/e 44 and 45). On the other hand, ^{48}Ti (the major isotope) has an interference from SO while Mn (mono-isotopic) is affected in the use of a nitrogen mixed gas plasma as Ar^{15}N species becomes significant. In addition, the interference effect on V and As by ClO and ArCl are also important as their natural abundance are 99.7 and 100 respectively.

The aim of this study was to evaluate the performance of a nitrogen mixed gas plasma for the removal of background spectral overlap on V and As caused by hydrochloric acid.

b. Experimental Conditions

A solution containing a mixture of 0.5 ppm V and 2 ppm As in 2% hydrochloric acid was used in this study. The experimental conditions were the same as before with the plasma gas and auxiliary gas at 15 l/min and 1.80 l/min respectively. The rf power was set at 1.50 kW and the sampling depth at 10 mm. The amount of nitrogen mixed into the plasma gas was 0%, 5%, 12% and 20%. In each situation, the "Blank" was 2% hydrochloric acid and was run prior to the aspiration of the analyte solution in each instance. This was necessary in order to monitor the background species of interest. The ion signals were observed as a function of nebuliser gas flow rate and the results are illustrated in Figures 5-26 and 5-27. For the interference effect of ClO, the use of a nitrogen mixed gas reduced this ion species considerably (see upper frame in Figure 5-28). The net analyte signals (background subtracted) in each plasma discharge are illustrated in Figure 5-28 with the calculated BEC values (at optimum analyte response) shown in the bottom frame of the figure. The interference effect caused by ClO was changed from an analyte equivalent concentration of more than 0.5 ppm (Ar plasma) to less than 80 ppb when a 20% nitrogen cooled plasma discharge was used. Although the result is not as impressive as in the situation for ArO, at least it is a step in the right direction. Figure 5-27 shows the ion signal for ArCl at mass 75. As demonstrated by the data shown in the figure, the introduction of 5% to 12% nitrogen into the plasma gas reduced the interferent signal.

c. Conclusion

The use of a 5% to 12% nitrogen cooled mixed gas plasma was found to be effective for the removal of ArCl interferent in 2% hydrochloric acid. The potential benefit is enormous as ArCl interferes with the analysis of As ion (mono-isotopic). In addition, the application of a nitrogen mixed gas plasma was also found to be satisfactory in the situation caused by spectral overlap between ClO and ^{51}V. Although the degree of removal was not

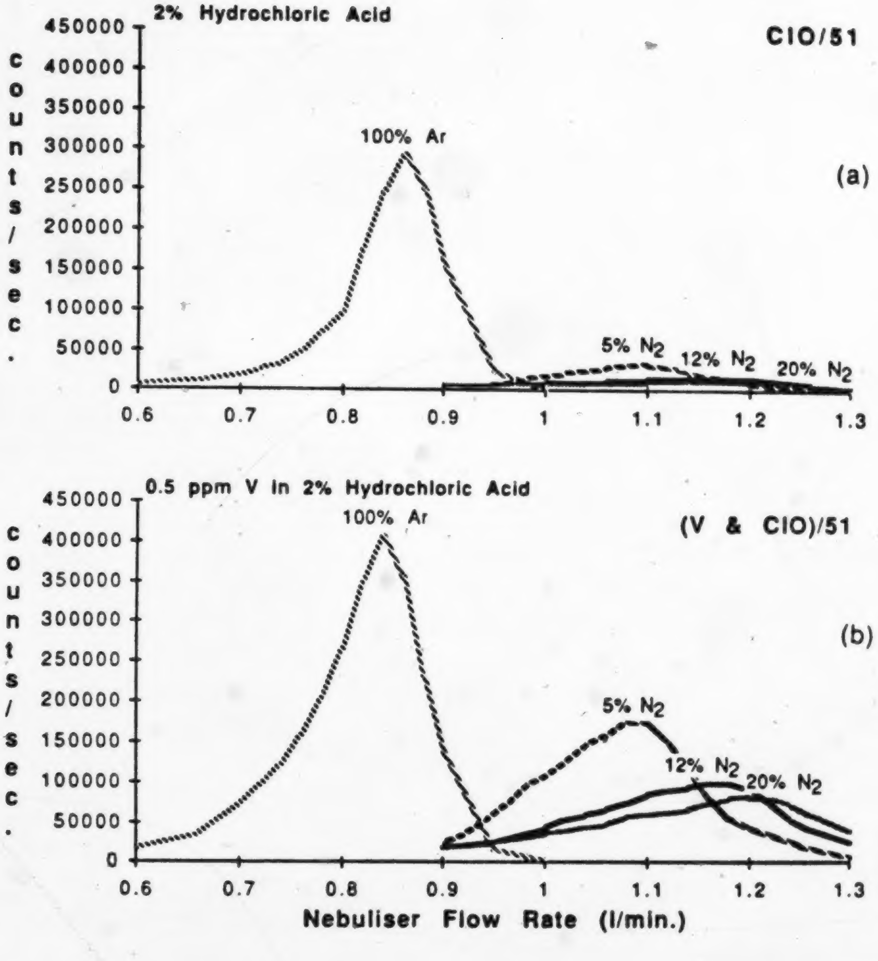

Figure 5-26. a) The effect of nebuliser flow rate and 0, 5, 12 and 20% nitrogen cooled plasmas on ClO species (2% hydrochloric acid "Blank" solution). b) The effect of nebuliser flow rate and 0, 5, 12 and 20% nitrogen cooled plasmas on mass 51 (V and ClO) from a solution containing 0.5 ppm V in 2% HCl.

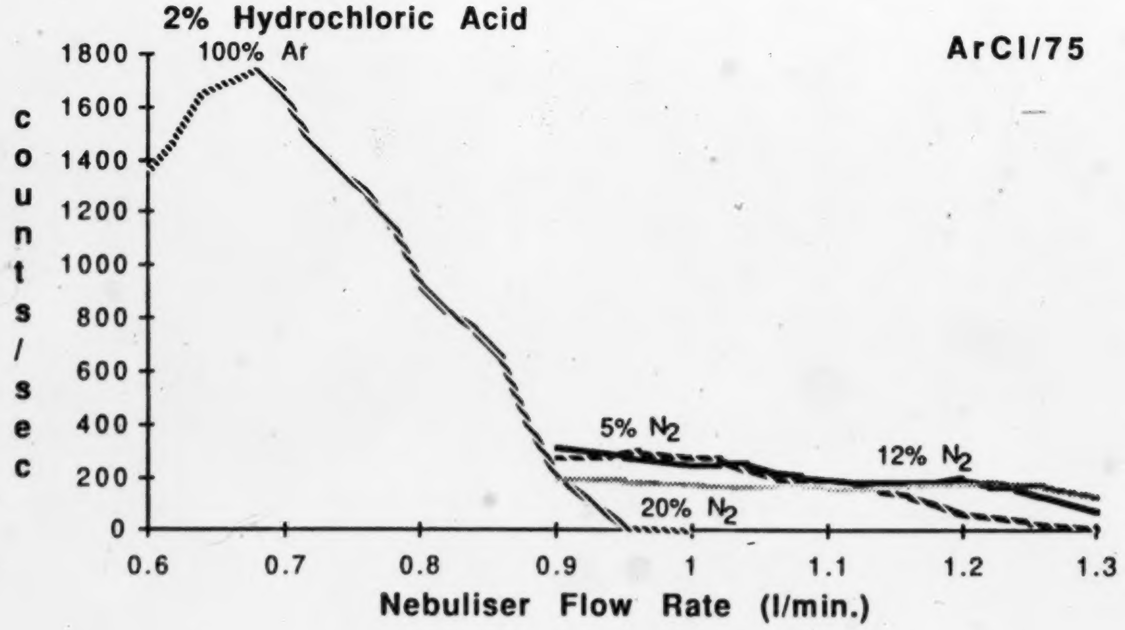

Figure 5-27. The effect of nebuliser flow rate and 0, 5, 12 and 20% nitrogen cooled plasmas on ArCl species (2% hydrochloric acid "Blank" solution).

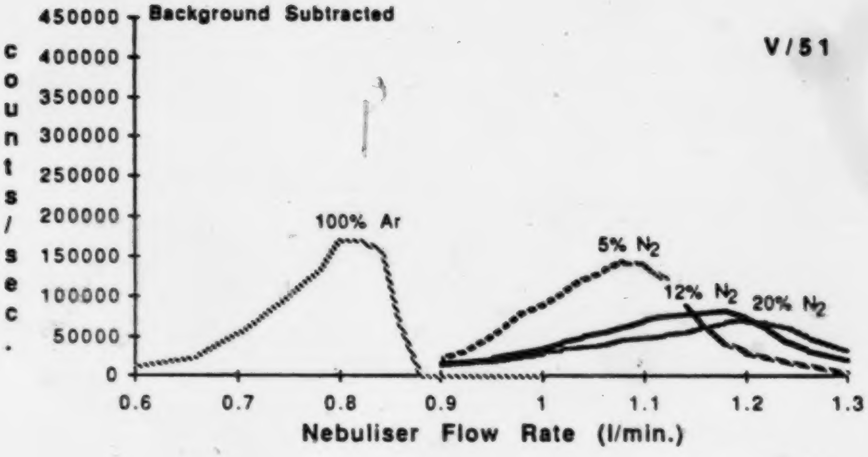

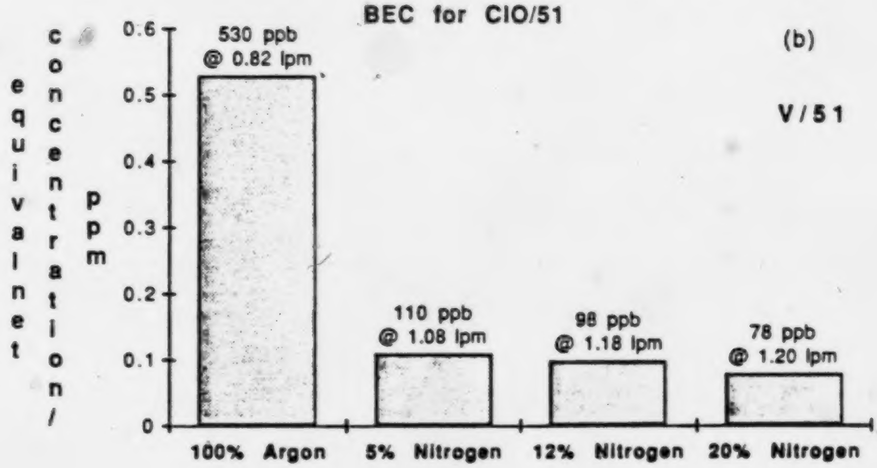

Figure 5-28. a) The net signal responses for ^{51}V (after blank subtracted) in 0, 5, 12 and 20% nitrogen cooled plasmas. b) The BEC values for ClO to V signals (each at peak V intensity).

as impressive as with some of the other background species, this initial result is still very encouraging.

D. Behaviour of some Argon Related Matrix Induced Species

a. Introduction

According to the title of this section, this class of background species should theoretically include all of the poly-atomic ions in which argon is present as part of the constituent. Therefore, species such as ArO, ArN, ArCl, ArS should also be included. However, only argon-analyte related ions are dealt with in this section. Also by definition, this group cannot be classified as background because their existence is also dependent on the presence of analyte species. A prior running of a "Blank" would be inadequate for their removal. They are species from analytes in the sample.

Tan [21] recognized the potential problem caused by this type of species. In her early study of the matrix effect caused by sodium on analyte ion signals, she observed signal enhancement for ^{63}Cu instead of suppression when 1000 ppm Na was aspirated. This "enhancement" was subsequently explained as due to the formation of Ar-Na ion species. Up to now, no detailed research has been done in the characterization of this type of background species except that they are less common with the non-SCIEX type instruments. In systems without a centre tap grounded coil [22], it is believed that a discharge helps in the dissociation of some of the poly-atomic ions. Thus, a lot of controversy exists regarding to the usefulness of having the centre tap grounded load coil. However, recent results from non-SCIEX instruments seem to indicate that ArX species are in fact common to both instruments.

In order to minimize the effect of an interferent in elemental analysis, a better understanding of the background species is necessary. A detailed study concerning the behaviour of these argon species to changes in plasma operating parameters, sampling depth and response to mixed gas plasmas is important. Also, a positive correlation between the physical properties of the matrix analyte to the population density of the analyte-argon background may also be beneficial.

b. Experimental Conditions and Results

i) Effect of Plasma Operating Parameters on Ar-Na Species

In this study, the ion signal responses for Ar-Na ions with respect to operating parameters such as plasma power, sampling depth, and nebuliser gas flow rates as well as a nitrogen mixed gas plasma were examined. The test solution was prepared from the sodium nitrate salt (analytical grade) and dissolved into 2% nitric acid in order to give a Na concentration of 1000 ppm.

The plasma gas and auxiliary gas were 15 l/min and 1.80 l/min respectively. Rf powers of 1.25 kW and 1.50 kW were used while the sampling depth settings were 10 and 15 mm. The ion signals were monitored as a function of nebuliser gas flow rate at the above prescribed plasma conditions.

The signal responses for the above conditions are summarized and presented in Figure 5-29. The top frame in the figure presents data observed at a sampling depth of 10 mm while the bottom frame presents data obtained at 15 mm. Also included in the figure was the acquired signal profile for Ar-Na using a 5% nitrogen cooled discharge at a 10 mm sampling depth with the rf power at 1.50 kW. From the data in the figure, the Ar-Na ion appeared to responded similarly to an analyte species. Especially at the sampling depth of 10 mm, the ion signal profiles shifted to higher nebuliser gas flow rates at increased plasma power. Also, the peak ion signal was also increased. However, the increase of the sampling depth from 10 to 15 mm resulted in a rapid decrease of the peak ion sensitivity by

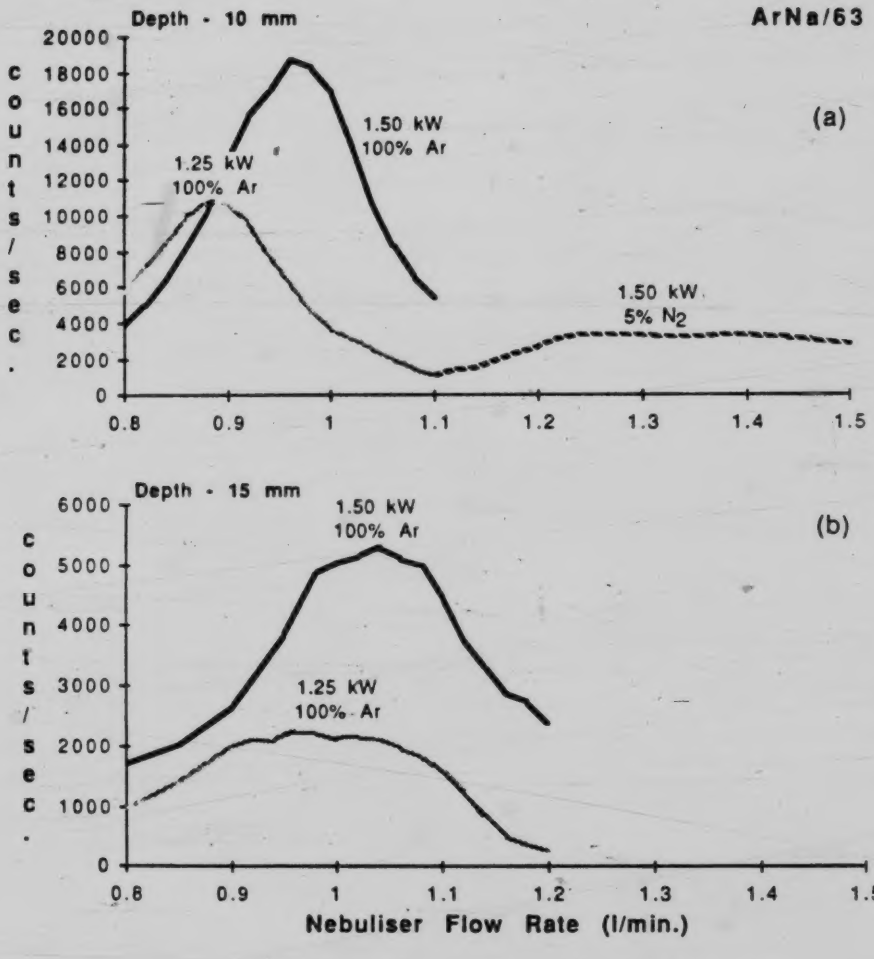

Figure 5-29. a) Dependence of ArNa signals on rf powers and nebuliser flow rate in an argon plasma and in a 5% nitrogen cooled plasma at 10 mm sampling depth. b) Dependence of ArNa signals on nebuliser flow rate and rf powers at 15 mm sampling depth.

more than two-thirds and the signal profiles also became less distinct. On the other hand, the use of a 5% nitrogen cooled mixed gas plasma at 10 mm reduced the ion signal by about an order of magnitude, in marked contrast to the effect of such a plasma on most analytes.

In conclusion, it appears that for the Ar-Na ion, use of a 5% nitrogen mixed gas discharge, or simply increasing the sampling depth from 10 to 15 mm, lowers the background interference adequately. However, an increase of sampling depth also lowers the analyte sensitivity (see Figure 5-9).

ii) Effect of Nitrogen Mixed Gas Plasma on Ar-Cr and Ar-Cu Species

Since the use of a nitrogen mixed gas plasma was found to be satisfactory in the reduction of the Ar-Na background ion, further study was deemed necessary in order to examine the applicability of this method to other argon-matrix ions.

A solution, 2% nitric acid containing Cr and Cu at 100 ppm each was prepared. The gas flow rates for plasma gas and auxiliary gas were 15 l/min and 1.80 l/min respectively. The plasma forward power was 1.50 kW with the sampling depth at 10 mm for this part. The percentage of nitrogen mixed into the plasma gas was 0%, 2.5%, 5%, 8%, 12% and 20%.

The ion signals for ArCr and ArCu (at m/e of 92 and 103) were monitored as a function of nebuliser flow rate and with different nitrogen percent plasmas. The data obtained are summarized and presented in Figures 5-30 and 5-31. From the data in the two figures, it is quite obvious that the use of a nitrogen mixed gas discharge for the reduction of argon-analyte background was not as impressive in these cases. Despite its seeming effectiveness for the ArNa species, the population level of ArCr ion remained virtually unchanged even with a 20% nitrogen cooled discharge (see Figure 5-30).

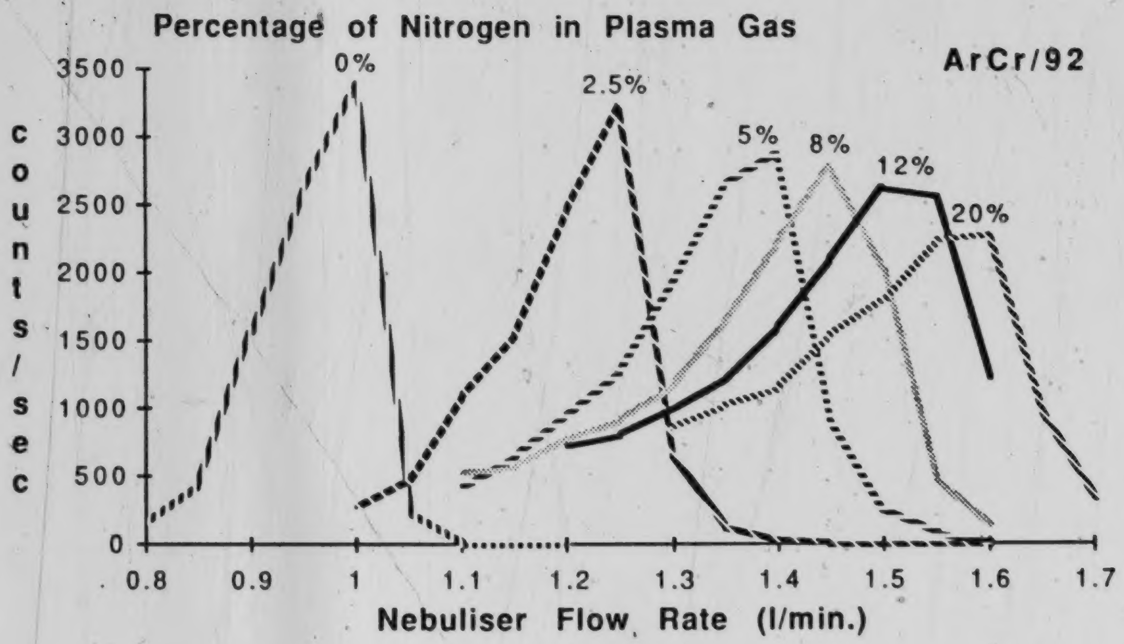

Figure 5-30. Dependence of ArCr signals on nebuliser flow rate and different percentage of nitrogen mixed gas plasmas.

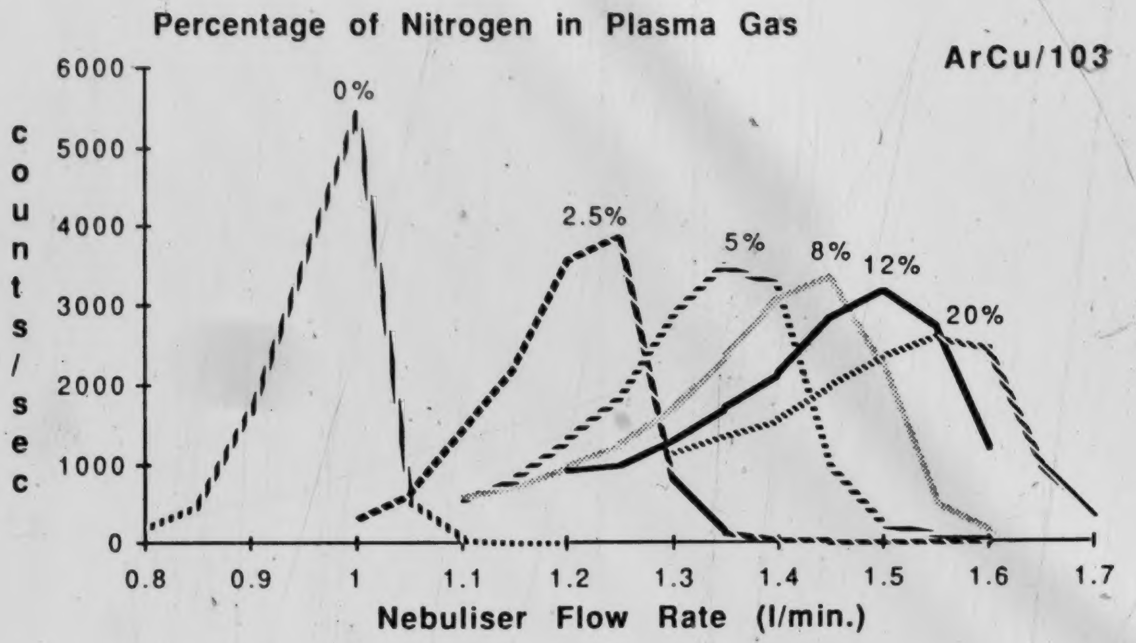

Figure 5-31. Dependence of ArCu signals on nebuliser flow rate and different percentage of nitrogen mixed gas plasmas.

From the above data, it appears that the stability of this type of matrix-induced species is governed by the character of the constituent species.

In the study of metal oxide behaviour described in the previous chapter, it was observed that the addition of a small amount of nitrogen into the nebulising gas resulted in a drastic reduction of the metal oxide signal. This reduction was thought to be a result of better and more efficient interaction between the oxide and nitrogen species. Perhaps this might also be applied to the situation with the argon-matrix ions.

The test solution and thus the background species were the same as above. The plasma parameters were modified with the plasma gas flow rate at 11 l/min and the auxiliary gas at 1.40 l/min. The rf power was 1.50 kW and the effects of sampling depth at 10 mm and 15 mm were examined. Typically, nitrogen was mixed into the nebuliser gas in the usual way with the mixture at the 25% to 20% level at sampling depths of 10 mm and 15 mm during the study. The data were acquired in the usual way (as a function of nebuliser gas flow rate) and they are presented as in Figures 5-32 and 5-33 for ArCr and ArCu. From the data in both figures, the effect of sampling depth on ion signal levels was not as critical as it was in the case of ArNa when a 100% argon discharge was used (see Figure 5-29). However, the use of a nitrogen mixed gas (nebuliser gas) also resulted in a significant reduction of the two species. The effect of the mixed nebuliser gas on analyte signal was not monitored at the same time. Hence, it is difficult to evaluate the true performance for this type of nitrogen mixed gas plasma. Alternatively, the preliminary studies obtained in Chapter 3 also indicated that the use of nitrogen mixed nebuliser gas in ICP-MS resulted in a decrease of analyte signal sensitivity. By extrapolating that information to the present situation, the signal to background ratio is only expected to improve slightly when compared with the situation where nitrogen was introduced as the plasma gas and this is only achieved at the expense of signal sensitivity.

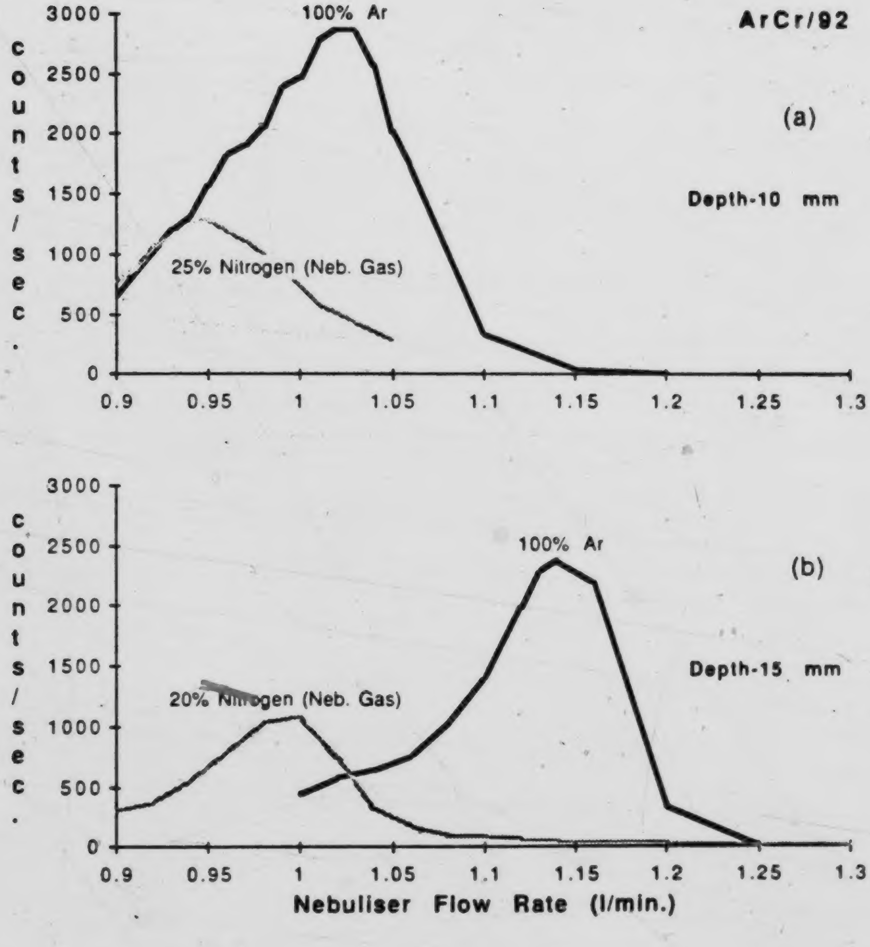

Figure 5-32. a) Effect of 20% nitrogen mixed nebuliser gas on ArCr at 10 mm sampling depth. b) Effect of 20% nitrogen mixed nebuliser gas on ArCr at 15 mm sampling depth.

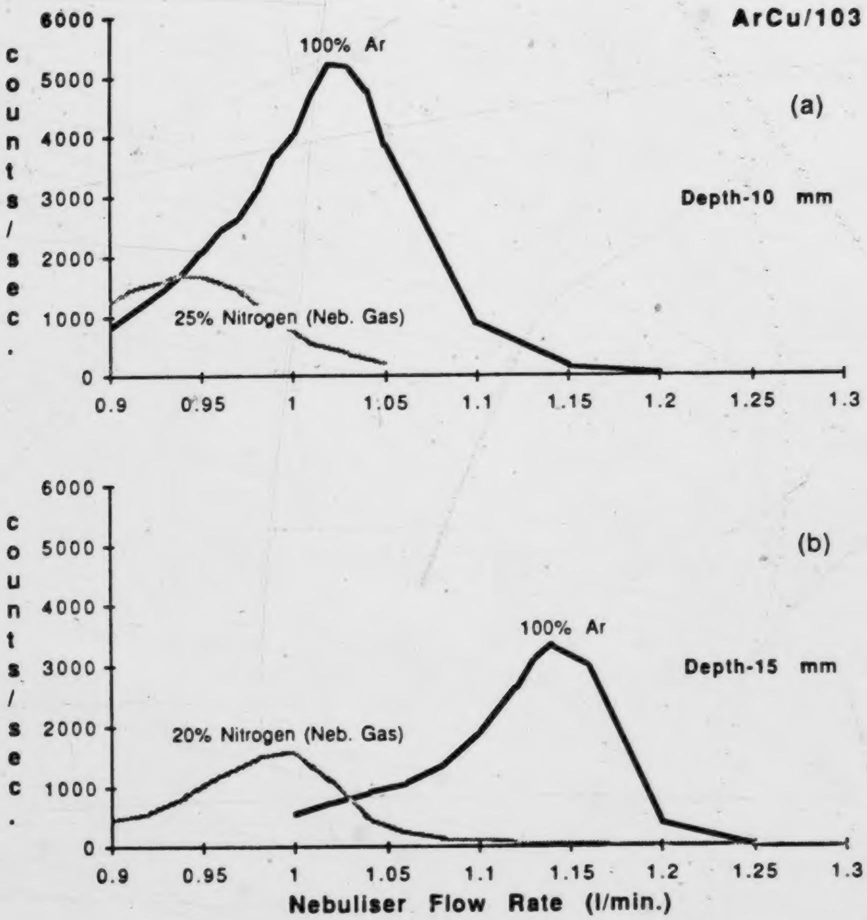

Figure 5-33. a) Effect of 20% nitrogen mixed nebuliser gas on ArCu at 10 mm sampling depth. b) Effect of 20% nitrogen mixed nebuliser gas on ArCu at 15 mm sampling depth.

iii) Effect of Analyte Species on ArX levels

In an attempt to better understand the nature of an analyte ion and the population of an argon-analyte species a large number of analytes were examined in order to establish a possible correlation between the analyte and the population density of the background species. The analytes used were pre-determined in order to give a large range of ionic radii and ionization potentials. The concentration for each of the species was 1000 ppm. In this situation, a pure argon discharge was used with the flow rate of the plasma gas at 11 l/min, auxiliary gas at 1.40 l/min. In addition, the nebuliser gas flow rate was fixed to be at 1.02 l/min. The sampling depth was 10 mm and the rf power was set at 1.50 kW throughout.

In this part, the set of electrostatic lenses were frequently adjusted to give optimum signal responses for the individual ion species [23].

Since the observed ion signals are dependent on the natural abundance of the stable isotope as well as the atomic mass of the analyte, the ion counts from the background species were calculated to give values of Ion counts/mMol. In addition, due the difference in the degree of ionization (α) for the species, the theoretical values of α as calculated by Furuta [17] were also taken into consideration. These normalized values in counts/mMol are summarized and presented in Table 5-1 with the calculated ion counts shown for each "element-argide". For those with no observable argon-metal ion, a value of zero was given. A bracketed yes means that while that argon background species has been observed, it has not been quantified.

From the data in the table, it is very difficult to establish any meaningful trend through the observations. Perhaps, ArX species have a higher tendency to form with the Group IA Elements as well as with the first row of transition elements. In addition, the data also indicate that the relative population for these type of species decreases at increasing atomic number for the same group in the Periodic Table. Initially, the formation of argon related

Table 5-1 Normalized ion populations for some argon related matrix induced species, expressed in ion counts/mMol.

ArLi 580								ArB 1050	ArC (yes)*1	ArN (yes)	ArO (yes)	
ArNa 460	ArMg 570										ArS (yes)	ArCl (yes)
ArK 90	ArCa none*2		ArCr 650	ArFe (yes)	ArNi (yes)	ArCu 1830	ArZn 220	ArGa 70	ArGe none	ArAs none	ArSe none	
ArRb 15	ArSr none	ArZr none	ArMo 260	ArRu none			ArCd 60				ArTe none	
ArCs 7	ArBa none											
		ArLa none	ArCe none									

Also observed in significant quantities were ArOB and ArOK

---

*1 Argon background species has been observed but has not been quantified.

*2 No observable amount of argon background species.

matrix background was thought to be related to the instability of an analyte ion in the interface region. This is analogous to the electron affinity for a positively charged ion and the charge density can be diluted by associating with the argon atom. Hence, the smaller the ionic radii, the higher the charge density and thus more likelihood for formation of argon related species. The normalized ArX signals and the ionic radii of the metal species [15] are compared in Figure 5-34. From the data in the figure, no identifiable trend is observed. This observation may be explained by the following:

1) The initial speculation is not applicable, and the mechanism for the formation of the argon related species is different from that proposed.

2) The proposed mechanism is valid; however, the observed ion counts do not necessary represent the true population of the species because the sensitivity response of the mass spectrometer is not constant throughout the entire mass range. Since the sensitivity of the instrument has not been calibrated, the comparison may be meaningless.

3) The true degree of ionization for the analytes may be different from the theoretical values. In Chapter 3, it was established that the estimated level of species ionization in ICP-MS is very much lower than the values provided in the literature [17].

4) Ion signal suppression (matrix effects) must be considered; Tan and Horlick [24] have reported that signal sensitivity suppression in ICP-MS by a matrix element is complicated. The degree of suppression was found to be highly dependent on the concentration of the matrix element as well as its mass. In this study, the molar concentration of the analyte solutions and the mass of the analyte were very different because they were all run at a concentration of 1000 ppm. In addition, the chosen species covered a wide range of the atomic mass spectrum; hence the ion signal responses from the species might have been suppressed to a different extent by their own matrixes.

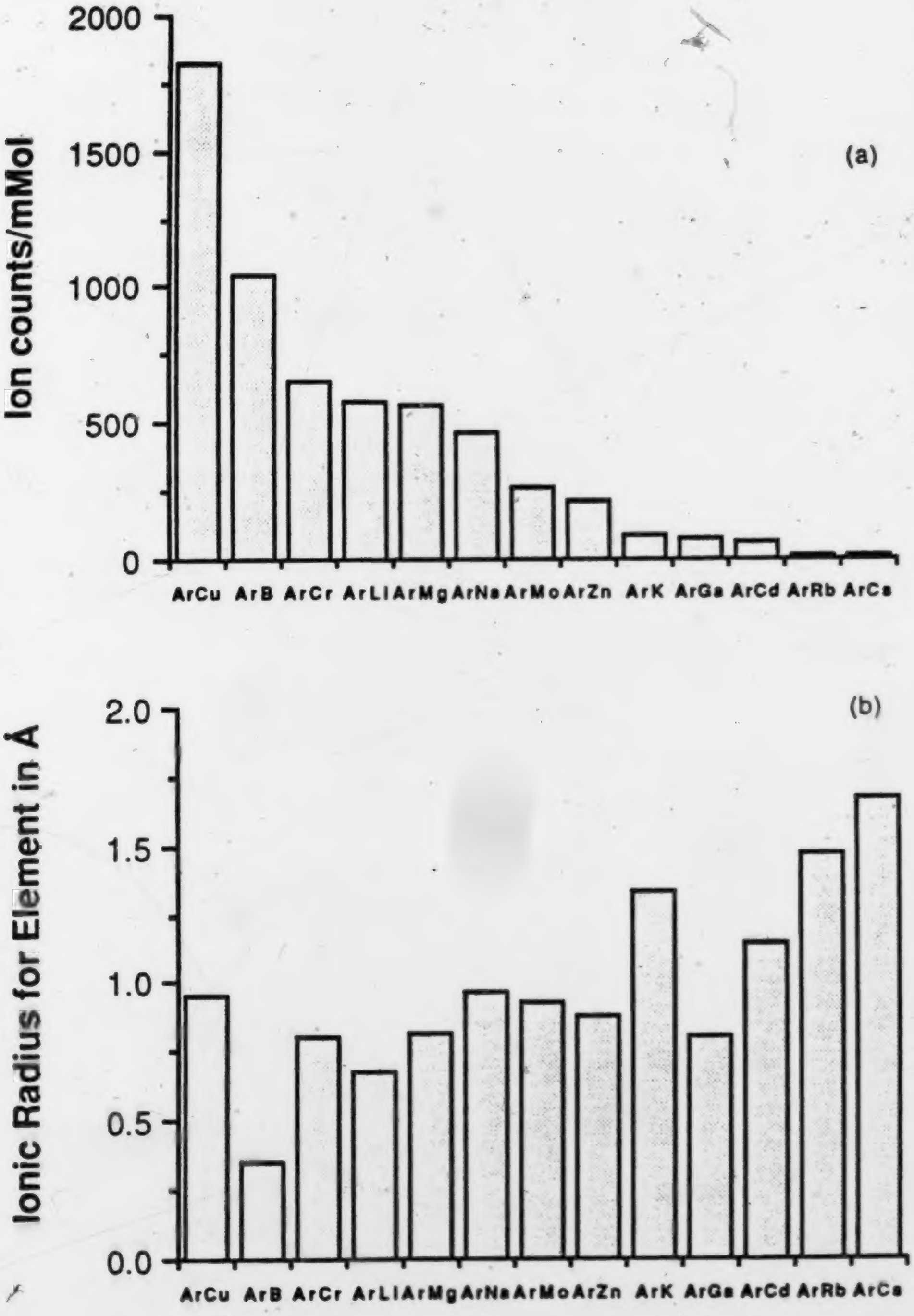

Figure 5-34. a) Bar graph to show the normalized ArX ion signal for elements detected in an argon ICP. b) Ionic radii of element species as provided in reference [15].

A combination of all or part of above might be responsible for the irregular correlation observed in Table 5-1. However, with the limited data available, it is difficult to clarify the situation.

c. Conclusion

Signal responses for argon related matrix induced species are dependent on plasma operating parameters. These dependencies are related to characteristics of the matrix ion. In fact, ArNa has the most intense signal at low sampling depth and it drops off rapidly at increasing distance from the load coil. However, this situation does not apply to species such as ArCr and ArCu because the sampling depth effect is less critical with those two species. In addition, the utilization of a 5% nitrogen mixed gas plasma reduces the peak sodium argide signal by about an order of magnitude (see Figure 5-29) but is less effective in reducing the signal level of the other two species (see Figure 5-30 and 5-31). The use of a nitrogen mixed nebuliser gas plasma is effective in reducing both ArCr and ArCu signals but at the expense of analyte sensitivity.

Although there was no identifiable trend observed between ArX population and ionic radius of the element (Figure 5-34), there appears to be some correlation between species population within the same group in the Periodic Table (see Group IA in Table 5-1). The reason for this is not clear. It might be a factor related to the actual degree of ionization of species in ICP-MS, which differs from the theoretical value (as observed in Chapter 3) and could make calculation of the normalized ion counts for the species erroneous. Alternatively, it might be related to ion signal suppression (matrix effect) originating from the instrument; that is, the ion signal responses from the species might have been suppressed to a different extent by their own matrixes.

Therefore a more thorough understanding of the characteristics of the ICP-MS is necessary in order to have better insight into the argide species behaviour.

REFERENCES

1. C. J. Pickford and R. M. Brown, Spectrochim. Acta, 41B, 183 (1986).
2. R. S. Houk, V. A. Fassel, G. D, Flesch, H. J. Svec, A. L. Gray and C. E. Taylor, Anal. Chem., 52, 2283 (1980).
3. A. R. Date and A. L. Gray, Analyst, 106, 1255 (1981).
4. D. Douglas, Canadian Research, 16, 55 (1983).
5. A. R. Date and A. L. Gray, Spectrochim. Acta, 38B, 29 (1983).
6. A. L. Gray and A. R. Date, Analyst, 108, 1033 (1983).
7. A. L. Gray, Spectrochim. Acta, 41B, 151 (1986).
8. D. J. Douglas and R. S. Houk, Prog. Anal. At. Spectrosc., 8, 1 (1985).
9. A. L. Gray, Spectrochim. Acta, 40B, 1525 (1985).
10. B. T. G. Ting and M. Janghorbani, Anal. Chem., 58, 1334 (1986).
11. F. E. Lichte, A. L. Meier and J. G. Crock, Anal. Chem., 59, 1150 (1987).
12. W. Doherty and A. Vander Voet, Can. J. Spectrosc., 30, 135 (1985).
13. S. H. Tan and G. Horlick, Appl. Spectrosc., 40, 445 (1986).
14. H. P. Longerich, B. J. Fryer, D. F. Strong and C. J. Kantipuly, Spectrochim. Acta, 42B, 75 (1987).
15. CRC Handbook of Chemistry and Physics, 66th Edition, 1986. CRC Press, Inc., Florida.
16. R. S. Houk, A. Montaser and V. A. Fassel, Appl. Spectrosc., 37, 425 (1983).
17. N. Furuta, Spectrochim. Acta, 41B, 1115 (1986).
18. D. A. Wilson, G. H. Vickers and G. M. Hieftje, J. Anal. At. Spectrom., 2, 365 (1987).
19. J. W. McLaren, D. Beauchemin and S. S. Berman, J. Anal. At. Spectrom., 2, 277 (1987).

20. J. W. McLaren, A. P. Mykytiuk, S. N. Willie and S. S. Berman, Anal. Chem. 57, 2907 (1985).

21. S. H. Tan, Dissertation, Dept. of Chem., Univ. of Alberta, Edm. AB., (1987).

22. D. J. Douglas and J. B. French, Spectrochim. Acta, 41B, 197 (1986).

23. M. A. Vaughan, G. Horlick and S. H. Tan, J. Anal. At. Spectrom., 2, 765 (1987).

24. S. H. Tan and G. Horlick, J. Anal. At. Spectrom., 2, 745 (1987).

Chapter 6

An Evaluation of Mixed Gas ICP's for the Running of Organic Matrixes in ICP-MS

A. Introduction

Use of the ICP as an excitation source for samples in organic solvents has met with some degree of success. However, due to vastly different properties between different solvents, optimum experimental conditions for a specific analysis are difficult to attain. Nevertheless, progress has been made in alleviating this problem. Two different approaches have been utilized. One approach is to limit the amount of organic solvent entering the plasma. Alternatively, reactive components are introduced into the discharge that are capable of destroying the solvent. Also, a water-cooled spray chamber has been used to lower the amount of solvent entering the plasma discharge. Ng and coworkers [1] demonstrated the use of a low consumption, 100% argon ICP in the handling of organic solvents at low rf powers (0.75 to 1.25 kW). More traditionally, high rf power and mixed gas plasmas were thought to be necessary to generate and stabilize ICP's when organic solvents were introduced. Using a nitrogen-argon plasma at a rf power of 5.5 kW, Greenfield and Smith were the first to apply the ICP technique in the analysis of organic samples [2]. Further, Broekaert et al. [3] demonstrated the use of a 4 kW nitrogen-argon plasma for the multi-element analysis of organic matrix solutions. Lau [4] showed that a lower power plasma (2.0 kW) with 20% oxygen-argon mixed gas was capable of improving analyte signal sensitivity for organic sample analysis. Recently, Magyar et al. [5] demonstrated the synergic effect of aerosol drying and an oxygen-argon mixed nebuliser gas to enhance the analyte signal in the analysis of organic solutions using

ICP-AES. Finally, Meyer [6] has described the application of a 100% air plasma for the determination of trace elements in xylene.

The introduction of organic matrixes poses an additional difficulty in elemental analysis using ICP-MS. In the optical emission technique, there is no direct physical interaction and/or connection between the plasma source and the spectrometer. Apart from the potential problem of plasma instability, the most important physical concern is the build up of carbon and uncombusted organics on the wall of the injector tube and the outer tube of the ICP torch. This problem can be alleviated with the use of high rf power and higher auxiliary gas flow. However, with ICP-MS, because the sampler interface is situated well within the tail plume of the plasma, uncombusted organic constituents condense onto the cooler surface of the sampler. In particular, the orifice of the sampler in a matter of minutes can be clogged up with soot. More seriously, any amount of uncombusted organics, once they have passed into the mass spectrometer, can condense on the surface of the electrostatic lenses as well as on the quadrupole rods, resulting in a dramatic loss in signal sensitivity and a major clean-up problem.

With all the above difficulties, organic sample analysis using ICP-MS has not been widely carried out. In a Technical Information paper provided by VG Instruments [7], a VG PlasmaQuad Organic System is described which incorporates a water-cooled spray chamber with the use of 5% oxygen mixed at the spray chamber in order to destroy the organic components. Also, the system requires a solution uptake rate of no more than 0.5 ml/min. Hutton [8] used the VG PlasmaQuad instrument for the determination of trace metals in organics, but again, a micro-volume sample size was necessary. With a modified VG PlasmaQuad instrument, Hausler [9] used an additional amount of a 2% oxygen-argon mixture which was introduced tangentially through a glass tubing connector between the spray chamber and the ICP torch for the destruction of organic components.

From another point of view, Houk et al. [10] observed protonated molecular ions of organic species in aqueous solution using a "cooled" plasma source. In a recent paper, Chong and Houk [11] used a GC-ICP-MS instrument to analyse the elemental composition of some organic compounds. Also, Tepperman and Elder [12] demonstrated the use of a SCIEX "Organic kit" with 5% oxygen mixed into the nebuliser gas in order to reduce the building-up of soot. This system was applied to the analysis of gold drug metabolites.

The aim of this study is to examine the performance of ICP-MS in the handling of organic matrixes using aerosol processing and mixed gas plasmas.

B. Preparation of Organo-metallic Standard Solutions

Cadmium cyclohexanebutyrate from the U. S. Department of Commerce, National Bureau of Standards, SRM 1053a was used in this study. Treatment of the standard was carried out as directed except where 2-ethylhexylamine was required, 1-methylhexylamine (Eastman Organic Chemical) was substituted. The other chemicals necessary for dissolution of the standard were xylene (Terochem Laboratories Ltd., Edmonton, Canada) and 2-ethylhexanoic acid (Eastman Kodak Company, Rochester, N. Y. 14650).

The dissolved standard was made into a solution giving a cadmium concentration of 500 ppm using light white paraffin oil (American Chemical Ltd., Montreal, Quebec). For this study, about 0.4 g of the above solution was weighed accurately into a 100-ml volumetric flask and subsequently diluted to volume using xylene. This provided a final solution with a cadmium concentration of about 2 μg/ml.

C. Performance of a Nitrogen-argon Mixed Gas Plasma

It is generally believed that despite the high spectroscopic temperature of the plasma discharge, the organic component still cannot be efficiently decomposed due to the inert properties of the argon species.

In previous chapters, the overall superior analytical performance of a low percent nitrogen-argon mixed gas plasma was demonstrated. Among other things, it has a higher spectroscopic temperature, making species ionize more readily. Further, the introduction of nitrogen also enhances the chemical activity of the plasma discharge and formation of stable species like CN should promote the destruction of organic solvents.

Several attempts were made to nebulise organics directly through a spray chamber into the plasma discharge. The introduction of nitrogen (~ 20%) into the nebuliser gas helped to minimize the formation of soot on the sampling cone orifice and was superior to nebulisation with 100% argon. However, the discharge became unstable if a higher percentage of nitrogen was added to the nebuliser flow.

In order to reduce the amount of solvent entering the plasma, the desolvating apparatus shown in Figure 6-1 was used. The component set-up was similar to that used for the aerosol processing studies in Chapter 4. The heating chamber temperature was fixed at 100°C. The condenser was modified with the addition of an external water-cooled jacket. This home-made device was designed to improve the condensation efficiency of the condenser by utilization of an internal spiral coil tube as well as external wall cooling. In addition, a second condenser was also utilized. This condenser took the form of a cold finger (4 cm dia. × 25 cm) with an inner glass tubing of 1.5 cm in diameter. In order to improve the efficiency of the cold finger, about twenty pieces of glass tubing (0.5 cm × 1 cm) were used to half fill-up the void volume of this container. The cold finger was immersed in a saturated sodium chloride ice-bath kept at -15°C. In conjunction with the nitrogen mixed gas plasma, this system was found to be satisfactory from the stand-point of avoiding carbon build-up at the sampler orifice.

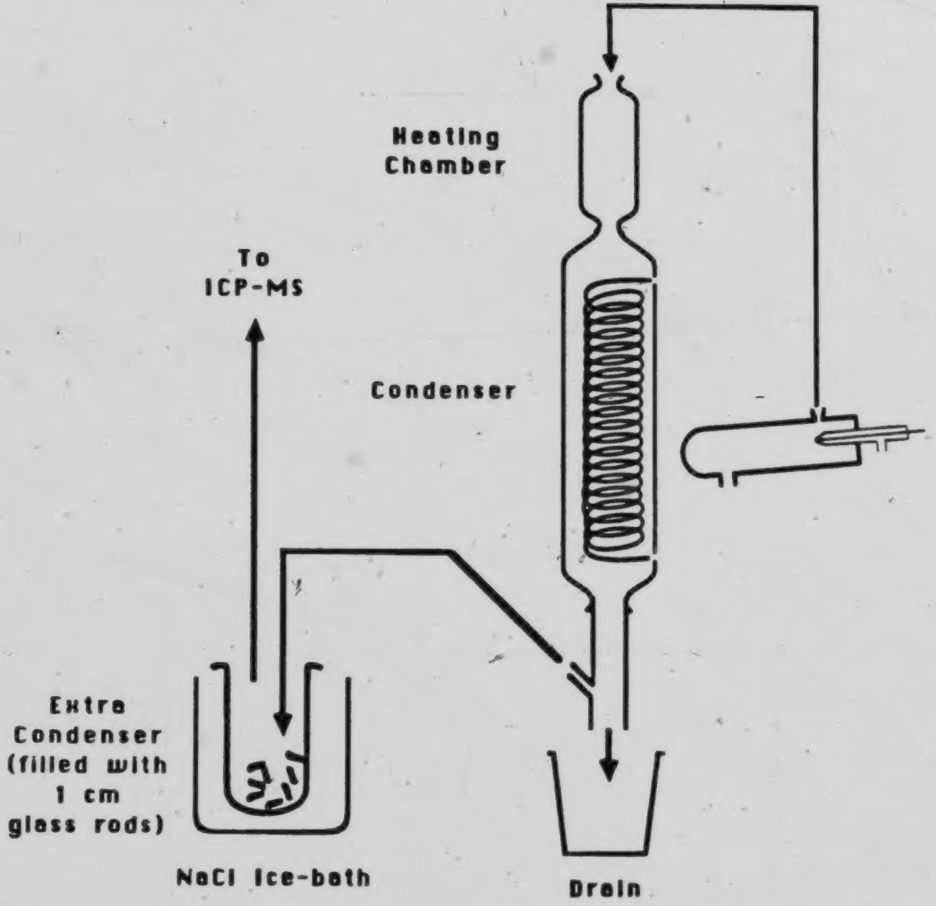

Figure 6-1. Diagram to illustrate the solvent condensation system.

The plasma conditions for this study are as follows:-

Plasma Gas	-	15 l/min
Auxiliary Gas	-	1.40 l/min
Rf Power	-	1.50 kW
Sampling Depth	-	15 mm

Initially, a mixture of 20% nitrogen-argon was used as the nebuliser gas. The ion signal intensity for cadmium as a function of nebuliser gas flow rate is illustrated in Figure 6-2a. The optimum signal occurs at a nebuliser flow rate of 0.90 l/min. When 2% nitrogen was mixed into the plasma gas (Figure 6-2b), there was no significant change in the analyte signal sensitivity, but the optimum nebuliser gas flow rate shifted to 1.25 l/min.

The sensitivity for cadmium was found to be about 4000 counts ml/μg using this technique. This rather poor response might be a result of poor aerosol transport efficiency due to the aerosol condensation stages.

D. Performance of an Oxygen-argon Mixed Gas Plasma

In general, oxygen is the most desirable foreign gas for the handling of organic solvent matrixes in ICP-MS [7-9]. It is commonly believed that the addition of oxygen into the nebuliser channel enhances "combustion" of hydrocarbons in the plasma discharge.

In this study, the solvent removal set-up was the same as shown in Figure 6-1 except that the cold finger system was removed. The plasma parameters were the same as before, except the sampling depth was 16 mm. The ion signal response for cadmium with a 20% oxygen-argon mixed nebuliser gas is shown in Figure 6-3a as a function of nebuliser gas flow rate. The optimum nebuliser flow rate was 1.0 l/min and the optimum ion counts were about five times more intense than those obtained with the nitrogen mixed gas plasma. This

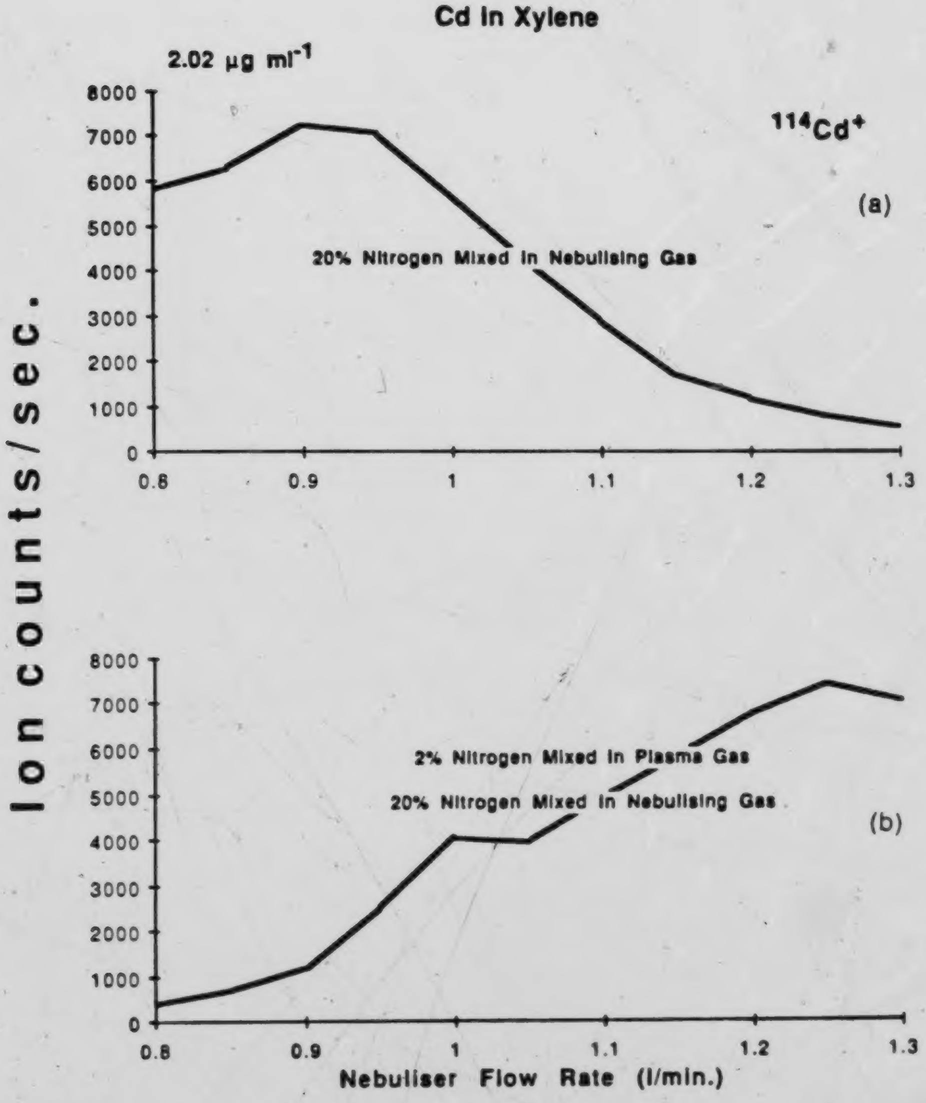

Figure 6-2. a) Dependence of Cd signal in xylene on nebuliser flow rate in a 20% nitrogen mixed nebulising gas plasma. b) Dependence of Cd signal in xylene on nebuliser flow rate in a 20% nitrogen mixed nebulising gas and a 2% nitrogen cooled plasma.

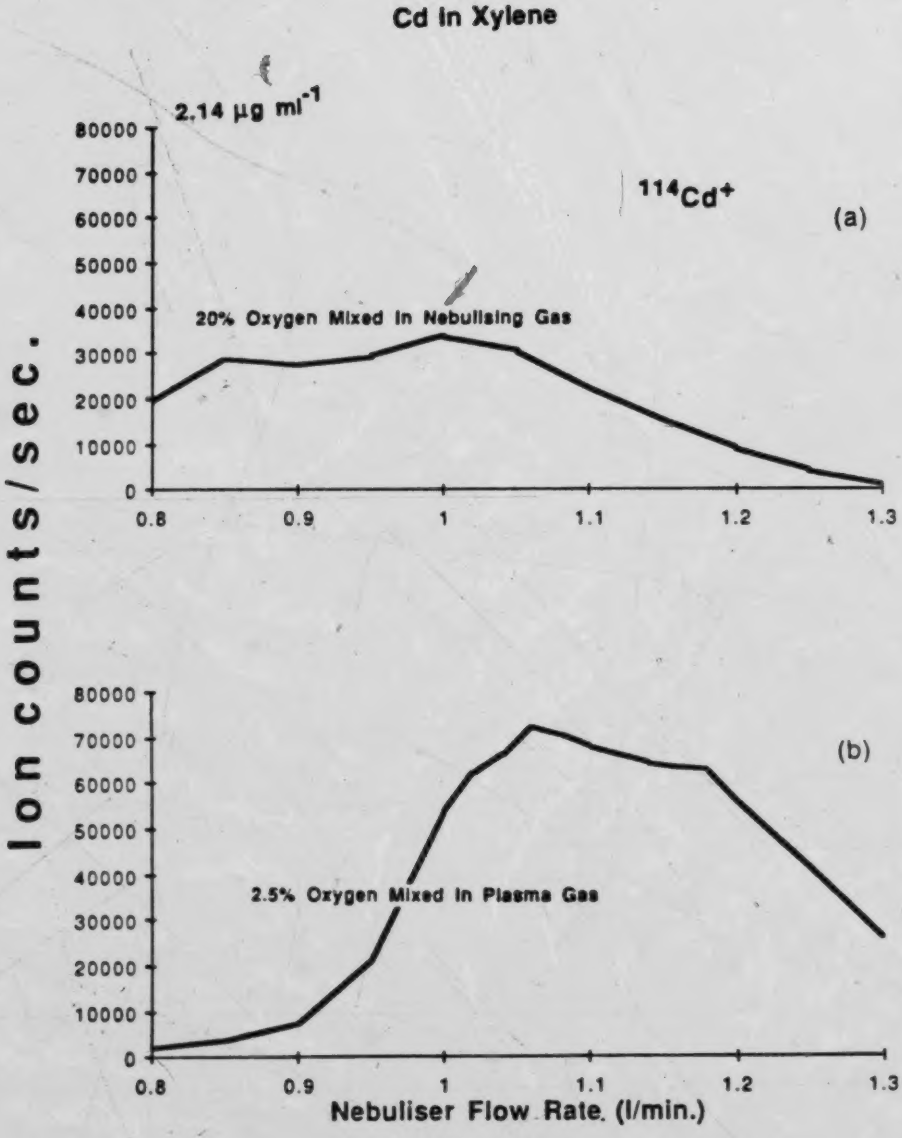

Figure 6-3. a) Dependence of Cd signal in xylene on nebuliser flow rate in a 20% oxygen mixed nebulising gas plasma. b) Dependence of Cd signal in xylene on nebuliser flow rate in a 2.5% oxygen mixed gas plasma.

was likely a result of the improvement in the aerosol transportation efficiency due to removal of the cold finger sub-system.

If "combustion" of the organic constituents in the plasma discharge is the main reason why oxygen is successful in the destruction of hydrocarbon species, then it should not make any difference if oxygen is introduced into the discharge via the nebuliser gas flow or the plasma gas flow [13]. In Chapter 3, it was noted that the introduction of nitrogen or oxygen into the nebuliser channel resulted in inferior signal performance. In contrast, when nitrogen or oxygen was introduced as part of the plasma gas, the thermal pinch effect on the discharge gave rise to better plasma and analyte interaction and consequently generally improved signal performance.

In this part of the investigation, oxygen was introduced into the plasma gas. The equipment set-up was the same as above, but the plasma parameters have been modified. The auxiliary gas flow rate was increased to 1.80 l/min and the sampling depth was changed to 10 mm. Keeping the nebuliser gas as 100% argon, a 2.5% of oxygen-argon mixture was introduced as the plasma gas. The signal intensity as a function of nebuliser gas flow rate is illustrated in Figure 6-3b. Now the optimum nebuliser flow rate is shifted to about 1.05 l/min and the analyte sensitivity is improved to about twice that when an oxygen-argon mixed gas was used as the nebuliser gas.

In conclusion, it appears that mixing a low percentage of oxygen into the plasma gas is superior to using a similar approach with the nebuliser gas. Not only does it allow better signal sensitivity, it also provides a more stable plasma when running organic solvent matrixes.

E. Performance of an Air-argon Mixed Gas Plasma

Although an oxygen mixed gas plasma works well in assisting the analysis of samples in organic solvents, it is a bit tricky to use. In particular the exact amount to use is difficult to set. Introduction of excess oxygen leads to corrosion of the copper sampler, and too little leads to sooting problems. Further, as demonstrated in Chapter 3, an excess amount of oxygen will also give rise to an overall increase in the level of metal oxide. This not only lowers the metal ion population and thus the signal sensitivity, but also the metal oxide ion may be a potential spectral interference to the detection of other analyte species.

The use of air as the "combusting" gas should be a good choice based on the simple wisdom that air contains about 20% oxygen and 80% nitrogen. Thus, this amount of available oxygen can be utilized towards the oxidation of the hydrocarbons while the excess amount will be mopped up by the surrounding nitrogen in air in the formation of nitrogen-oxygen molecular species. Therefore, air should be an effective foreign gas to use in ICP-MS when running organic matrixes.

In this study, the equipment set-up was the same as in the previous section. The plasma parameters were identical as for the 20% oxygen-argon mixed gas study except that the sampling depth was set at 15 mm. Initially, a 20% air-argon mixture was used as the nebuliser gas. The cadmium signal intensity as a function of nebuliser gas flow rate was measured and shown in Figure 6-4a. The data indicate that air as a mixed gas in the plasma discharge was capable of dissociating the organic matrix with comparable sensitivity and response to that observed using the 20% oxygen-argon mixed gas plasma (Figure 6-3a).

In addition, use of an air-argon mixture as the plasma gas was also investigated. A 5% air-argon cooled mixed gas plasma was used in this part of the study. The set-up of the apparatus remained the same as above, but the plasma parameters were changed to those used in the 2.5% oxygen-argon plasma gas section of this study. The results are shown in Figure 6-4b. From the data presented in the above figures, it is obvious that the use of an

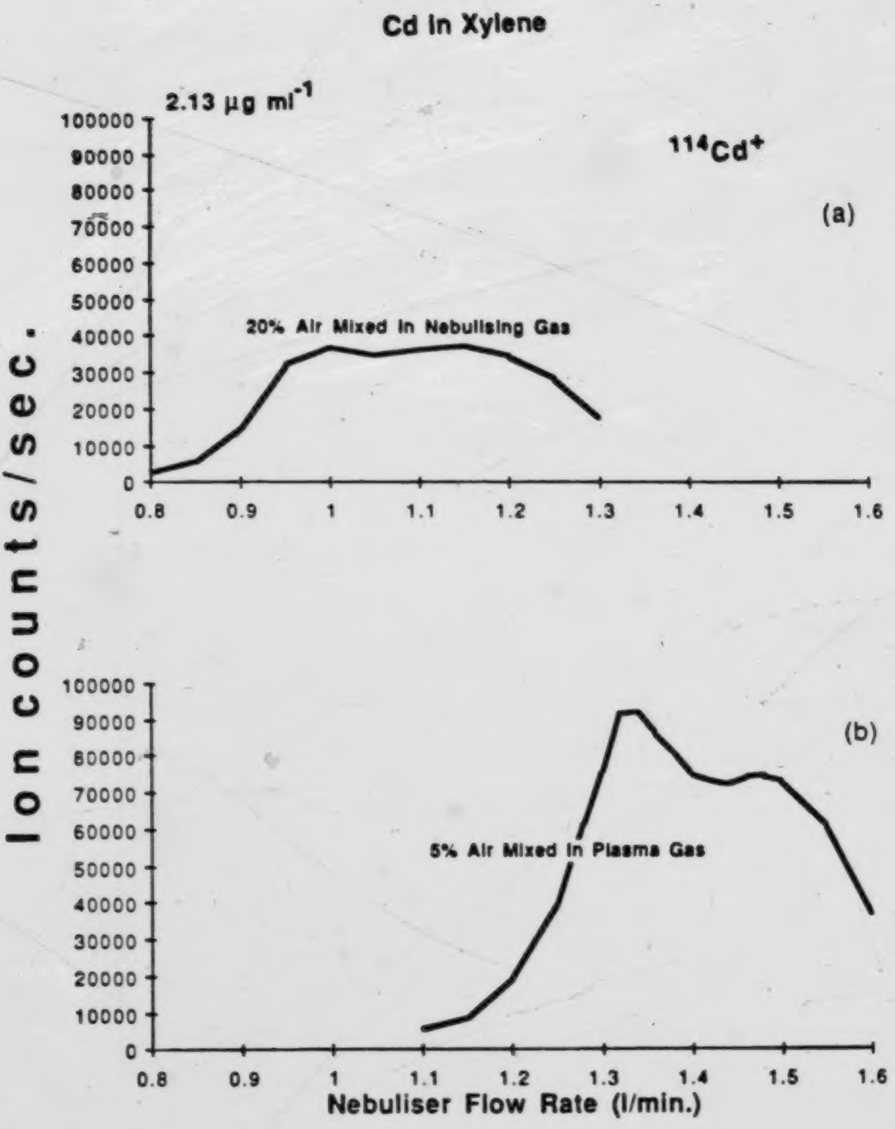

Figure 6-4. a) Dependence of Cd signal in xylene on nebuliser flow rate in a 20% air mixed nebulising gas plasma. b) Dependence of Cd signal in xylene on nebuliser flow rate in a 5% air mixed gas plasma.

air-argon gas mixture as the plasma gas is superior to when it is used as the nebuliser gas for the determination of Cd in xylene.

F. Discussion

In the handling of organic matrixes using ICP-MS, addition of oxidizing gases provide the necessary capability for the destruction of organic components. Nitrogen mixed gas ICP's were found to be effective only after extensive removal of the organic vapour had been carried out. As a consequence, the aerosol transportation efficiency was lowered significantly and resulted in low signal levels. Oxygen mixed gas ICP's seemed to manage the organics rather handily (probably due to the stronger carbon bonding for oxygen than nitrogen: (D°C-O = 11.2 eV) as compared with a value of (D°C-N = 7.98 eV [14])). However, sufficient care must be taken to minimize corrosion of the copper orifice as well as the formation of metal oxide species.

Air mixed gas plasmas were found to be a rather good compromise. They not only possess the ability to combust organic materials but the excess oxygen can be tied up by the readily available nitrogen species.

Finally, in all cases, superior performance was found when the mixed gas was applied to the outer (plasma) gas flow rather than to the nebuliser gas.

REFERENCES

1. R. C. Ng, H. Kaiser and B. Meddings, Spectrochim. Acta, 40B, 63 (1985).
2. S. Greenfield and P. B. Smith, Anal. Chim. Acta, 59, 341 (1972).
3. J. A. C. Broekaert, F. Leis and K. Laqua, Talanta, 28, 745 (1981).
4. M. P. Lau, Dissertation,Dept. of Chem., Univ. of Alberta, Edm. AB. (1981).
5. B. Magyar, P. Lienemann and H. Vonmont, Spectrochim. Acta, 41B, 27 (1986).
6. G. A. Meyer, Spectrochim. Acta, 42B, 201 (1987).
7. Technical Information PQ012, VG Instruments, Ion Path Road Three, Winsford, Cheshire, England.
8. R. C. Hutton, J. Anal. At. Spectrom., 1, 259 (1986).
9. D. Hausler, Spectrochim. Acta, 42B, 63 (1987).
10. R. S. Houk, V. A.Fassel and H. J. Svec, Organic Mass Spectrom., 17, 240 (1982).
11. N. S. Chong and R. S. Houk, Appl. Spectrosc., 41, 66 (1987).
12. K. G. Tepperman and R. C. Elder, poster presented at ICP-MS Symposium, Muskoka Sands, Canada. (1987).
13. R. S. Houk, A. Montaser and V. A. Fassel, Appl. Spectrosc., 37, 425 (1983).
14. CRC Handbook of Chemistry and Physics, 66th Edition, 1986. CRC Press, Inc., Florida.

Chapter 7

A Preliminary Study on the Effect of Sampler-Skimmer Separation in ICP-MS

A. Introduction

During the development of ICP-MS as an analytical tool, the most challenging step was the physical marriage of a high temperature, high gas flow atmospheric pressure plasma source to a high vacuum mass spectrometer. To overcome this difficulty, a water-cooled metal interface with the shape of a cone (to facilitate stream-line sampling) and a small aperture (typically on the order of 0.05 mm in diameter) was first developed [1]. However, when the plasma plume reached the cold surface of the sampler, a boundary layer of cool gas developed over the orifice of the structure. As a result, the plasma was incapable of penetrating this barrier and this mode of extraction was termed "boundary layer sampling". The ions extracted with this system were modified significantly as a result of the drastic change in the physical environment and extensive ion-molecule reactions. In order to overcome this difficulty, Douglas and French [2] adopted the idea of a supersonic molecular beam sampler-skimmer arrangement and applied that to a microwave plasma. In their approach, the orifice of the sampler was much larger (typically 0.5 mm diameter or more). With this increase in the size of the orifice, the boundary layer formed previously in front of the orifice was eliminated and the plasma was able to be sampled directly. However, their design also resulted in the extraction of a large amount of material through the sampler. To overcome this difficulty, they attached a secondary skimmer to sample the centre flow of the molecular beam before it was allowed into the high vacuum of the mass spectrometer. With this configuration, the base pressure between the sampler and skimmer (interface region) was typically held at about 1 torr. This expansion of gas is termed a supersonic beam jet and their idea was subsequently adopted into all the commercial ICP-MS systems.

It is obvious that the physical environment inside the interface is important as it may result in the modification of the molecular beam. If the pressure is lower than about 10^{-3} torr, the expanding jet originating from the orifice of the sampler encounters negligible scattering with the background gas and this is termed free-jet expansion [3]. The expansion of gas into the low pressure region also results in decreasing gas densities with increasing distance from the point source of the orifice. It is finally converted to free molecular flow as the collision rate between species decreases.

The rate of molecular gas expansion in a supersonic jet can be expressed in terms of Mach number (M). By definition, it is expressed as the ratio of the bulk flow speed to the local speed of sound and can be calculated as [4] :

$$M = A\ \{(X - X_0) / D_0\}^{\gamma-1} - \{(\gamma+1)/(\gamma-1)\}/\{2 \times A\ [(X - X_0) / D_0]\}^{\gamma-1} \qquad (7\text{-}1)$$

where:

A = coefficient constant

X = axial distance from nozzle exit plane

X_0 = projection of streamlines to the central axis

D_0 = diameter for the sampler orifice

γ = specific heat capacity, C_p/C_v for the bulk gas.

If the bulk of the gas is argon, under the condition where $X/D > 4$, the coefficient for some of the variables can be simplified to [4-5] :

$A = 3.26$

$X_0 / D = 0.075$

and $\gamma = 1.67$

Thus, the final format of the equation becomes :

$$M = \{3.26\,(X / D_0)^{2/3}\} - \{(2 / 3.26) \times (X / D_0)^{-2/3}\} \qquad (7\text{-}2)$$

In ICP-MS, the typical running pressure in the interface region is about 1 torr. Under this condition, a shock wave pattern develops (Figure 7-1a) and encloses the molecular beam axis with a 'Mach disc' situated perpendicularly to the beam axis. The interior of the shock barrel is unaffected by the background pressure and the most uniform portion of the beam occurs just in front of the Mach disc.

The location of the Mach disc can be calculated as [4] :

$$X_M = 0.67\,D_0\,(P_0 / P_1)^{1/2} \qquad (7\text{-}3)$$

where:

X_M = distance between the sampling orifice and the Mach disc

P_0 = pressure from the source

P_1 = background pressure at the interface

Therefore, any decrease in P_1 results in expansion of the shock barrel and migration of the Mach disc further away from the sampling orifice. As a result, the distance separating the two cones and hence the position of the skimmer relative to the Mach disc all depend on the background pressure. Under these circumstances three basic scenarios may arise, resulting in formation of the Mach disc either at the skimmer (Figure 7-1a), in front of the skimmer (Figure 7-1b) or well within the skimmer cone (Figure 7-1c).

In the situation where the Mach disc is located in front of the skimmer, the sampled molecular beam is badly scattered by the background shock wave. In contrast, when the Mach disc is formed well behind (within) the skimmer, the shock wave developed either inside the skimmer or at the electrostatic lenses makes ion focussing extremely difficult [6]. In addition, the particle density along the centre line is proportional to the inverse square

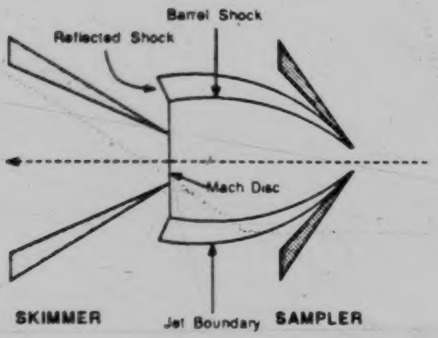

Figure 7-1a. Skimmer cone sampling at Mach disc.

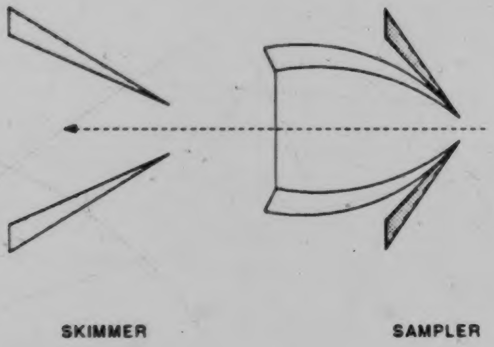

Figure 7-1b. Skimmer cone sampling after Mach disc.

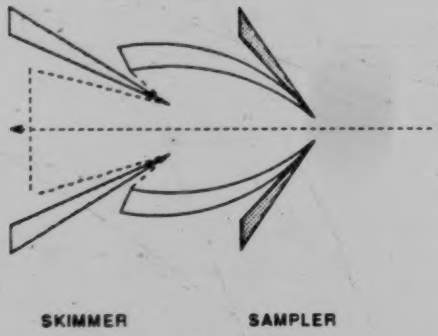

Figure 7-1c. Skimmer cone sampling before Mach disc.

distance from the source [4]. Thus, the beam density is less intense at increasing distances from the point source. As this beam of particles travels through the opening of the skimmer, those striking the external surface of the skimmer are reflected back into the jet. When the density of the beam is low, the collision rate between the reflected particles and the approaching jet is negligible. However, as the jet intensity is increased, the degree of collision becomes more severe and this is called a skimmer interference [7]. In the worse case scenario, this may even overload the pumping capability of the instrument as more particles are extracted into the system. Hence, it is best to sample when the Mach disc is located at the aperture of the skimmer cone [3] as minimal perturbation of the beam is anticipated.

The supersonic expansion of the molecular beam in the interface region can be classified as either adiabatic or isentropic. In the case for isentropic expansion, there is no formation of shock fronts between the two cones. However, in the situation for ICP-MS, adiabatic expansion is the norm as the random thermal motions of the particles are eventually converted into an orderly unidirectional jet stream. At large distances from the point source, the particle trajectories along the flow axis are nearly parallel. At this point, the particles achieve a terminal velocity underwhich they become collisionless. The axial distribution of the beam is effectively 'frozen' while its radial distribution approaches zero.

Typically, the particles reach their terminal speed (v) at M > 5. The terminal speed can be calculated:

$$v \quad = \quad (5\, k\, T_0 / m)^{1/2} \qquad (7\text{-}4)$$

where:

k = Boltzmann constant

T_0 = temperature of the source

m = unit mass of the bulk material in Kg

For argon gas at a source temperature of 6000 K, ν can be calculated to be at about 3×10^5 cm/sec. Hence, for a typical distance between the sampler and the skimmer of 1 cm or less, the time span for a particle to travel through the region is on the order of a micro-second. During that time period, particle interactions due to collisions can take place. Therefore, it is easy to envision that the interface region of the ICP-MS is extremely complicated. During the early development stage of this technique, a wide range of ion molecular species were observed. They were duly assumed to be a result of reactive collisions in the interface region.

This study is an attempt to investigate the effect of the interface on some of the molecular ion species in ICP-MS. A more detailed understanding of this region may help to clarify some aspects of the technique.

B. The Physical Arrangement of the Interface

The distance between the sampler and skimmer was fixed by the manufacturer. According to a presentation by Douglas and French [8], when the unit is operating and set-up normally, the background pressure in the interface should be 5 torr with the distance separating the two cones equal to 0.61 cm. However, when the diameter of the sampler orifice (D_0 = 0.114 cm) is substituted into the equation for the location of the Mach disc a value of X_M equal to 0.94 cm is calculated. As a result, the position of the skimmer in a SCIEX Elan instrument is about one-third of the distance up-stream from the Mach disc (Figure 7-1c). This, according to Pertel [3], is not an ideal location for sampling an ion beam in a supersonic jet. On the other hand, the exact location of the Mach disc is also a function of the background pressure in the interface as well as the exact diameter of the sampler orifice. For our instrument a copper sampler with an orifice diameter of 0.094 cm is normally used. This is slightly smaller than the specification given by the manufacturer and the background pressure in the interface region is expected to be lower. Also, it is well known that the aperture of the sampler deteriorates with time; hence the actual location of the Mach disc varies according to the life-time of the sampler and the plasma conditions.

In order to obtain some appreciation of the effects that the interface zone has on ion molecular species, the separation distance between the sampler and the skimmer was modified by inserting copper spacers with different thickness between the sampler and the water-cooled copper interface-face-plate (Figure 7-2). With different spacers, this changed the physical separation between the two cones without modifying the background pressure and thus, the physical nature of the shock barrel. In this study, spacers with thickness of 0.23 cm and 0.57 cm were used which gave separations of 0.84 cm and 1.18 cm along with the normal 0.61 cm separation.

C. Effect of Sampler-Skimmer Separation on Analytes and their corresponding Oxides

a. Introduction

In their study of the sampling interface performance, Olivares and Houk [6] compared a calculated signal intensity to the observed ion signal for various sampler-skimmer separation distances. They observed the largest negative deviations from the theoretical results at large and small separations. They interpreted the above results as due to the scattering of ions by the shock wave. As a result, this lowered the extraction efficiency of the instrument for ion detection. Since the position of the skimmer aperture in the Elan Model 250 is about one-third of the distance from the Mach disc [8], the ion beam has been scattered to a certain extent (see Figure 7-1c) if the situation is similar to that observed by Olivares and Houk. Therefore, the signal sensitivity is expected to improve as the sampler-skimmer separation is increased (0.23 cm spacer). However, if the interface region is rich with reactive collisions, then any subsequent increase in the ion-path in the interface region should result in the formation of a higher ion oxide ratio. Douglas and French [8] estimated that the number of collisions per test particle with oxygen is about 1 for a trace of one

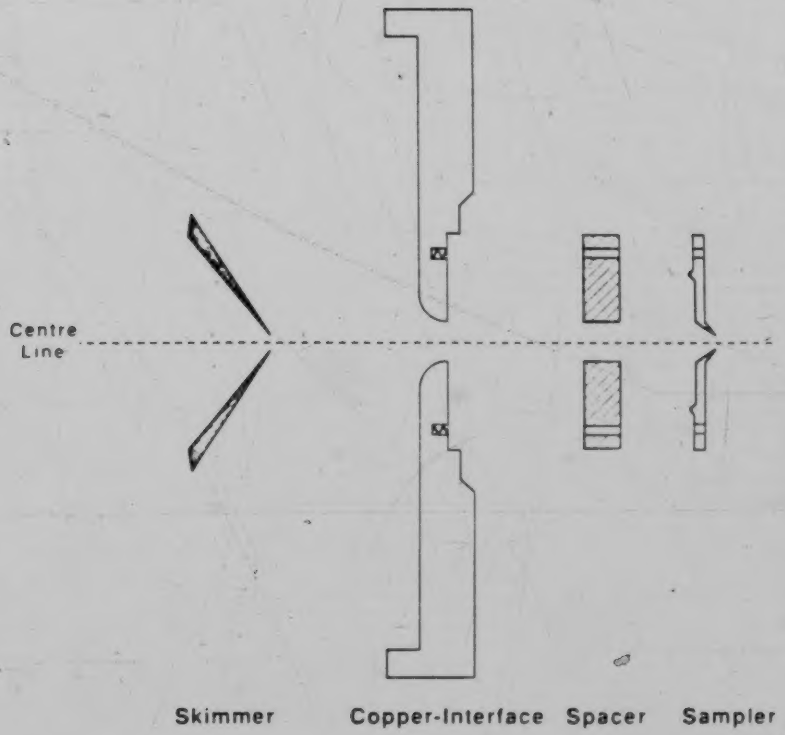

Figure 7-2. Schematic layout of the sampler-skimmer interface with the spacer insert.

percent oxygen concentration. They further concluded that the interface "is not a region rich in ion-molecule chemistry as the average probability of a reactive collision is 0.1". Although their estimated number is small, the figure in fact translates to a reactive product of about ten percent. This could be troublesome if the reactive product is oxide. Lichte et al. [9] studied the effect of sampler-skimmer separation on ion signals by halving, equaling or doubling of the distance of the original design. Rather surprisingly, they did not observe any noticeable change in ion signal sensitivity and the level of oxide population remained quite similar under the three situations.

b. Experimental Conditions

The behaviour of Te, Cs, Ba, La and Ce were observed in this study. During the investigation, a 0.23 cm copper spacer was used and the analytes were introduced as a solution with individual concentrations of 1 ppm. Data acquisition was carried out in the usual way with the ion signal intensities acquired as a function of nebuliser gas flow rate. However, the plasma had to be shut down in order to allow for the insertion of the spacer. Hence, there is no real certainty regarding the alignment of the plasma to the interface as well as the operation conditions of the mass spectrometer although all effort was made to insure reproducible results. Therefore, it is important to realize that the object of the study is to establish the trend of species response rather than the absolute magnitude of analyte ion counts/sec at each condition. Also, the analyte responses for a 5% nitrogen cooled mixed gas plasma and a 100% argon plasma were compared in this study.

The gas flow rates for the plasma gas and the auxiliary gas were 15 l/min and 1.80 l/min respectively. The rf power of the discharge was kept at 1.50 kW and the sampling depth was 10 mm through out and as always was defined as the distance from the load coil to the sampling cone tip.

c. Results and Discussion

The signal intensities for the analytes and their oxides were measured as a function of nebuliser gas flow rate. An illustration of the signal responses for Ce and its oxide in the absence and presence of the 0.23 cm spacer using a 100% argon discharge is shown in Figure 7-3. From the data, it is obvious that the addition of the spacer results in a decrease in signal intensities for the analyte as well as its oxide. Also, it is worthwhile pointing out that even though the general shape of the signal profiles remained similar, the addition of the spacer resulted in a slight decrease of the optimum nebuliser flow rate. The reason for this change is not clear at this time. It is apparent that the analyte signal profiles are not only a function of plasma parameters, but they are also dependent on the interface. Therefore, it is more meaningful to compare the effect of the interface on ion species at individual optimum signal conditions rather than at a fixed nebuliser gas flow rate.

The signal intensities (at their respective optimum nebuliser flow rate) for each of the ion species with and without the 0.23 cm spacer were ratioed and are summarized in Table 7-1. From the results, it appears that the effect of the spacer in ICP-MS is species dependent. For analyte ions, signal sensitivity was found to decrease by about forty percent with the attachment of the spacer. However, for the oxygen containing species, the signal sensitivity decreased by about sixty percent.

The gas flow rate extracted through the sampler U_0 and skimmer U_S can be quantified theoretically [6]:

$$U_0 = \pi f(\gamma) N_A D_0^2 P_0 / [4(m R T_0)^{1/2}] \qquad (7\text{-}5)$$

where:

U_0 = gas flow rate through the sampler in molecule/sec

N_A = Avogadro's number

m = mean molecular weight of the gas in g/mol

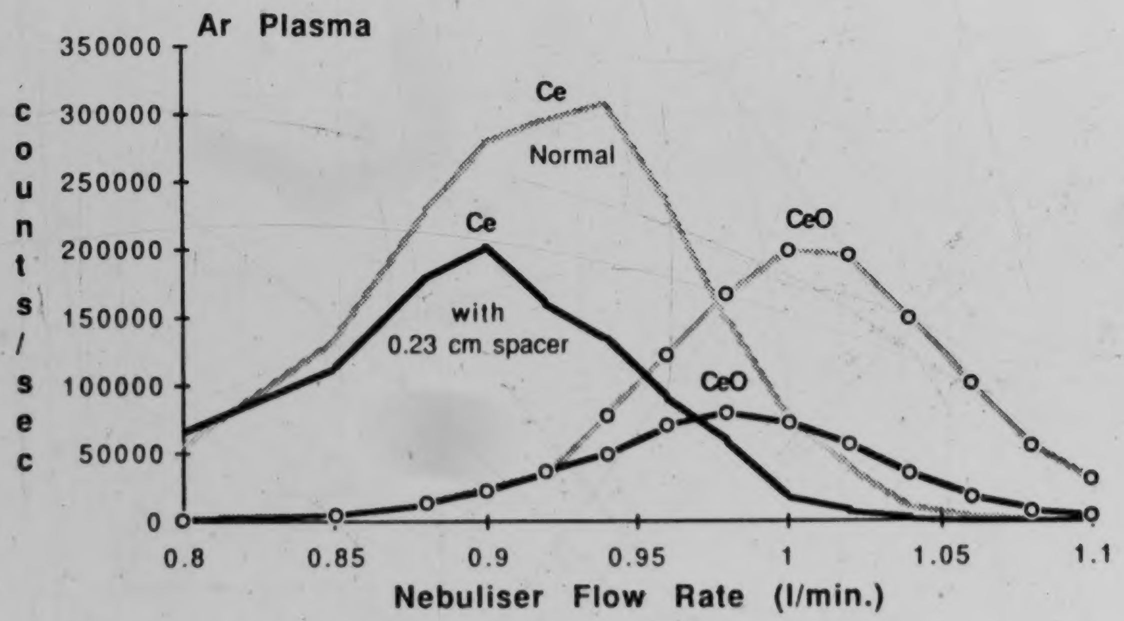

Figure 7-3. Effect of a 0.23 cm spacer insert on Ce and CeO signals in a 100% argon plasma.

Table 7-1. The sensitivity ratio for ion species with and without the 0.23 cm spacer, each at its optimum nebuliser flow rate.

Ionic Species	Intensity Ratio (spacer/no spacer)
Te	0.60
Cs	0.52
Ba	0.56
La	0.67
Ce	0.66
LaO	0.41
CeO	0.40

$f(\gamma)$ = coefficient constant

$= \gamma^{1/2} [2 / (\gamma+1)]^{(\gamma+1)/2(\gamma-1)}$

and

$$U_S = U_0 f(\gamma) \times (D_S / X)^2 \qquad (7\text{-}6)$$

= gas flow rate through the skimmer

D_S = skimmer diameter

From the equations, it can be shown that the effect of the spacer (sampler-skimmer separation) to the mass flow rate of gas molecules extracted through to the mass spectrometer is inversely proportional to the square of the separation distance if the value for U_0 is constant. With the attachment of a 0.23 cm spacer, the calculated amount of gas flow through the skimmer was only 53% of the original value. This agrees well with the observations for metal analytes but it is slightly higher than the experimental results obtained for metal oxides (Table 7-1). From this, it appears that the additional ion-path at the interface region has a larger effect on the population of analyte oxides than it does on the analyte.

Finally, the percentage of metal oxides with respect to their ions obtained at the optimum nebuliser gas flow rates were calculated for La and Ce and presented as the following:

	CeO^+/Ce^+	LaO^+/La^+
without spacer	26%	30%
with spacer	12%	12%

From the above summary, it is quite obvious that the insertion of a 0.23 cm spacer had a more adverse effect on the oxide species.

The insertion of a spacer also seems to have the same kind of effect on the ionic species when a 5% nitrogen-argon mixed plasma discharge is used. The response profiles for all analytes were comparable and the results for Ce are illustrated in Figure 7-4. From the data presented in the figure, it is clear that the attachment of the spacer had a smaller effect in the modification of the Ce^+ ion signals when compared to the argon plasma, despite a similar drop in the optimum nebuliser gas flow rate necessary in both cases. In contrast, the signal intensity for the CeO^+ ion was decreased by a larger degree. The effects of the spacer on ion species using a 5% nitrogen mixed gas plasma are summarized and presented in Table 7-2.

From the tabulated data, the metal ions on average decreased to about 70% of the original signal (with the exception of Te) while the oxide ions were lowered to less than 30%. This suggests that the use of a spacer in conjunction with a 5% nitrogen plasma affects the analysis in a more "positive way" as the level of the rather undesirable oxide species is reduced without great modification to the system.

Again, the percentage of metal oxide ions to metal ions at their respective optimum nebuliser gas flow rates were calculated for La and Ce and are as the follows:

	CeO^+/Ce^+	LaO^+/La^+
without spacer	6.9%	5.0%
with spacer	2.9%	2.6%

Although the magnitude in the reduction of oxide percent using a spacer was not as dramatic as before, the degree of improvement in terms of the oxide ion population was rather substantial. The results observed above are contrary to earlier speculation that the oxide ion species are by-products of reactive collisions generated in the interface region. If this speculation was correct, then any increase in the ion-path should have lead to an eventual elevation of the oxide level providing that the jet stream of the molecular beam was not completely "frozen". Alternatively, the level of oxide ion would remain unchanged if they were generated primarily as undissociated species from the discharge. On the other

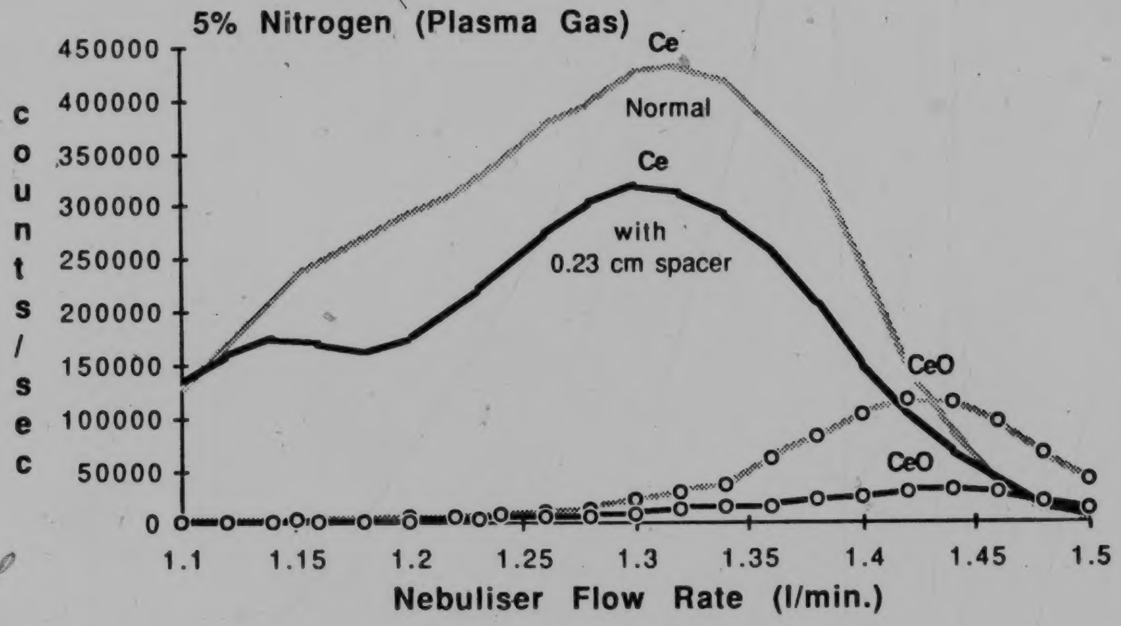

Figure 7-4. Effect of a 0.23 cm spacer insert on Ce and CeO signals in a 5% nitrogen cooled plasma.

Table 7-2. The sensitivity ratio for ion species with and without the 0.23 cm spacer, each at its optimum nebuliser flow rate.

Ionic Species	Intensity Ratio (spacer/no spacer)
Te	0.81
Cs	0.68
Ba	0.68
La	0.72
Ce	0.73
LaO	0.27
CeO	0.28

hand, the effect of Mach-number focussing [10] caused by the "seeding effect" of lighter particles to the heavier ones and effectively concentrating the heavier species along the centre line of the beam would result in an increase in the level of oxide species with respect to analyte. Since the relative level and percentage of oxide ion were decreased after the insertion of the spacer, none of the above explanations or speculations are completely valid.

Up to now, no detailed attention has been given to the boundary layer at the edge of the sampling orifice. Using a solution containing 1000 ppm of Y, Gray [11] observed emission from YO in the cooler region of this layer. In the same paper, he concluded that the ratio between the aperture diameter to the thickness of the sampling aperture should be important as this is the region where ion-molecule reactions would likely take place during ion extraction. In a situation where the ratio was unity, the proportion of particles allowed to travel through the aperture undisturbed was estimated to be only 17% [12] while the remaining 83% would strike against the wall and interact at the boundary layer. Finally, after several collisions the modified products would either be back scattered or be extracted through and entrained into the supersonic jet [13]. Since these ions are allowed back into the jet stream by means of diffusion, they are not expected to be as densely populated along the centre line of the expanding beam compared to the edges. Thus, a large proportion of this product was believed to be at the boundary of the flow stream. As a consequence, the sampling of an expanding jet by a skimmer would often result in a higher proportion of the centre materials as the sampler-skimmer distance is increased. Therefore, the decrease observed in the ratio of the oxide signal to the analyte signal at increasing sampler-skimmer separation might be attributed to sampling a larger proportion of the central part of the molecular beam. In a situation where the beam was uniform, there would not have been any change in the observed ratio. On the other hand, if a larger proportion of the oxide is distributed along the outer edges of the expanding beam, then an increase in the skimmer sampling distance leads to a lower level of oxide ions being detected.

This idea of oxide generation at the boundary layer can be further supported by an earlier observation presented in Chapters 3 and 4. During the study of the oxide behaviour of La, it was observed that the diameter of the skimmer aperture affected the level of analyte oxide detected. In a situation where a large skimmer orifice was used (~ 1.2 mm dia.), LaO^+/La^+ was found to be close to 40% but it was reduced to about 20% when a skimmer with aperture of ~ 1 mm dia. was used. This situation is analogous to the effect of sampler-skimmer separation distance because a larger diameter orifice also allowed the sampling of a wider solid angle of the supersonic beam. As a result, a larger proportion of the boundary jet was extracted and consequently, the detection of a higher amount of metal oxide ions resulted.

D. Effect of Sampler-Skimmer Separation on some Background Species

a. Introduction

In the previous section, it was reported that the separation distance between the sampler and skimmer was a factor in determining the level of analyte oxides with respect to analyte ion. Theoretically, it has been estimated [8] that argon is the dominant species inside the collision regime of the interface region and its concentration ratio with respect to oxygen species is estimated to be 100 to 1. Hence, a study of argon related background species as function of sampler skimmer spacing could provide some elucidation of their origin. For this part of the study, two copper spacers with thickness 0.23 cm and 0.57 cm were used.

b. Behaviour of some Primary Background Species

For this part of the investigation, a solution containing 0.4 ppm of Cu in 2% nitric acid was used. The behaviour of the background species (ArN, ArO, ArOH, Ar_2 and Ar_2H) were monitored as well as the signal from Cu ion which was used as the "reference standard" to provide behaviour typical of an analyte. The plasma parameters were identical to above with the rf power at 1.50 kW and the sampling depth at 10 mm.

Ion signals for the individual species, observed as a function of nebuliser flow rate in a 100% argon discharge, are presented in Figure 7-5. From the data presented in the figure, the responses for ArOH and ArN were distinctly different from the rest of the ion species. In the case of ArN, the copper spacer did not appear to have a significant effect on the ion intensity. In fact, its peak intensity increased at larger sampler-skimmer separation. The signal level for ArOH decreased using a 0.23 cm spacer but increased with a 0.57 cm spacer. On the other hand, a species such as Ar_2H seemed to be very dependent on the relative location of the skimmer. At the largest sampler-skimmer separation (0.57 cm), its ion signal dropped to a negligible level. The trends in signal changes are certainly confusing and complex. They were summarized by comparing the optimum signal counts for each species at each of the sampler-skimmer locations and illustrated graphically in Figure 7-6. These results were further normalized with respect to maximum ion signal obtained without the spacer and tabulated in Table 7-3. From the data, it is interesting to note that ArO and Ar_2 behave very much like Cu ion (an analyte). This suggests that these species are likely generated within the plasma discharge. Species such as ArOH and Ar_2H behaved similarly when the 0.23 cm spacer was used, but at the largest sampler-skimmer separation (1.18 cm), the signal intensity for Ar_2H became insignificant while the relative population level for ArOH increased. The above results can be rationalized by the following: at low separation, the mechanism for the formation of ArOH and Ar_2H could be similar to analyte oxide generation in ICP-MS with some portion of the molecular ions produced at the boundary layer surrounding the edge of the orifice and then diffusing into the main stream; at a larger sampler-skimmer separation, the situation is confusing for these species. For Ar_2H, the population decrease was probably due to dissociation of the species. The increase in the level of ArOH might be due to an increase in reactive collisions

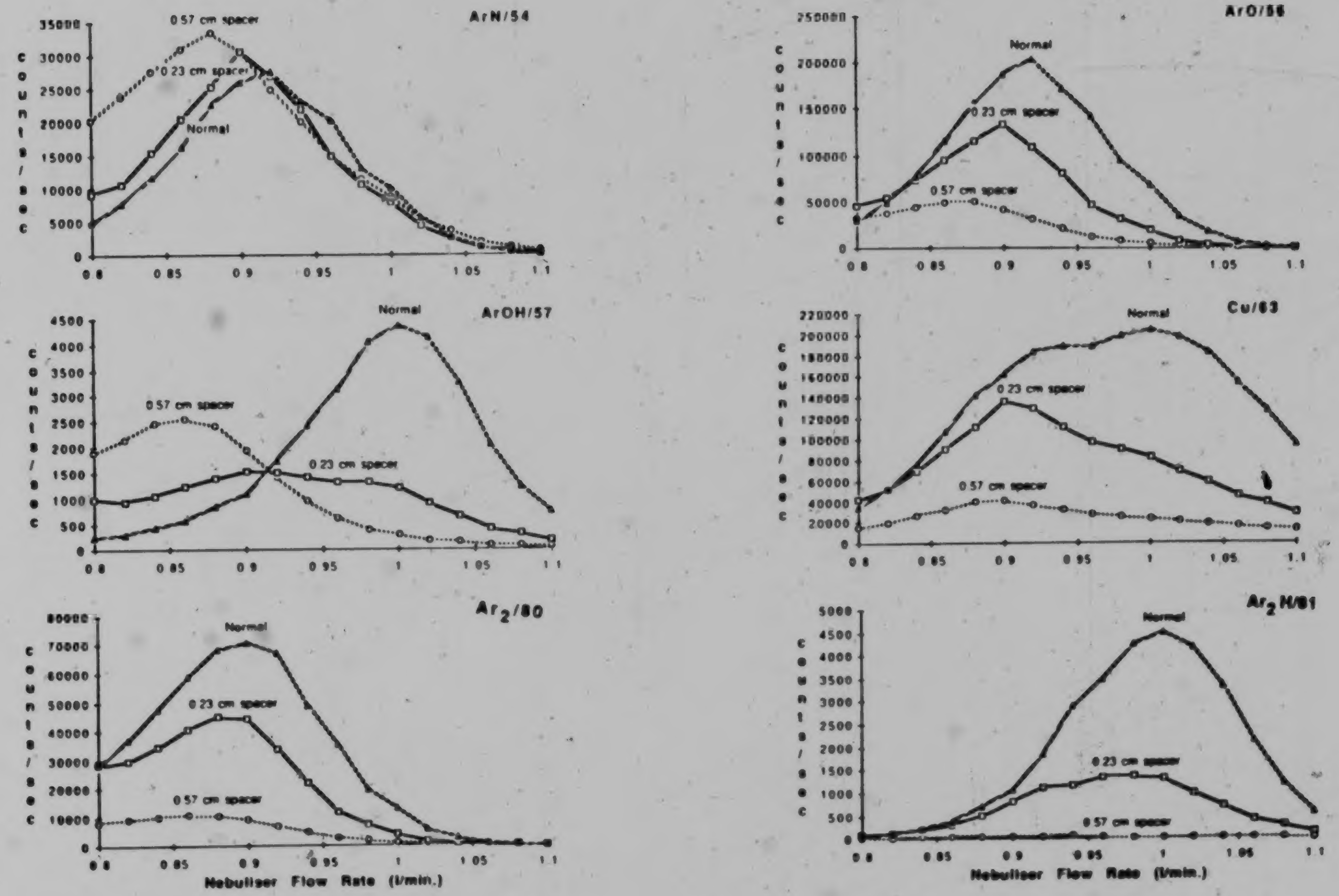

Figure 7-5. Effect of sampler-skimmer separation distances on some background ion species in a pure argon plasma.

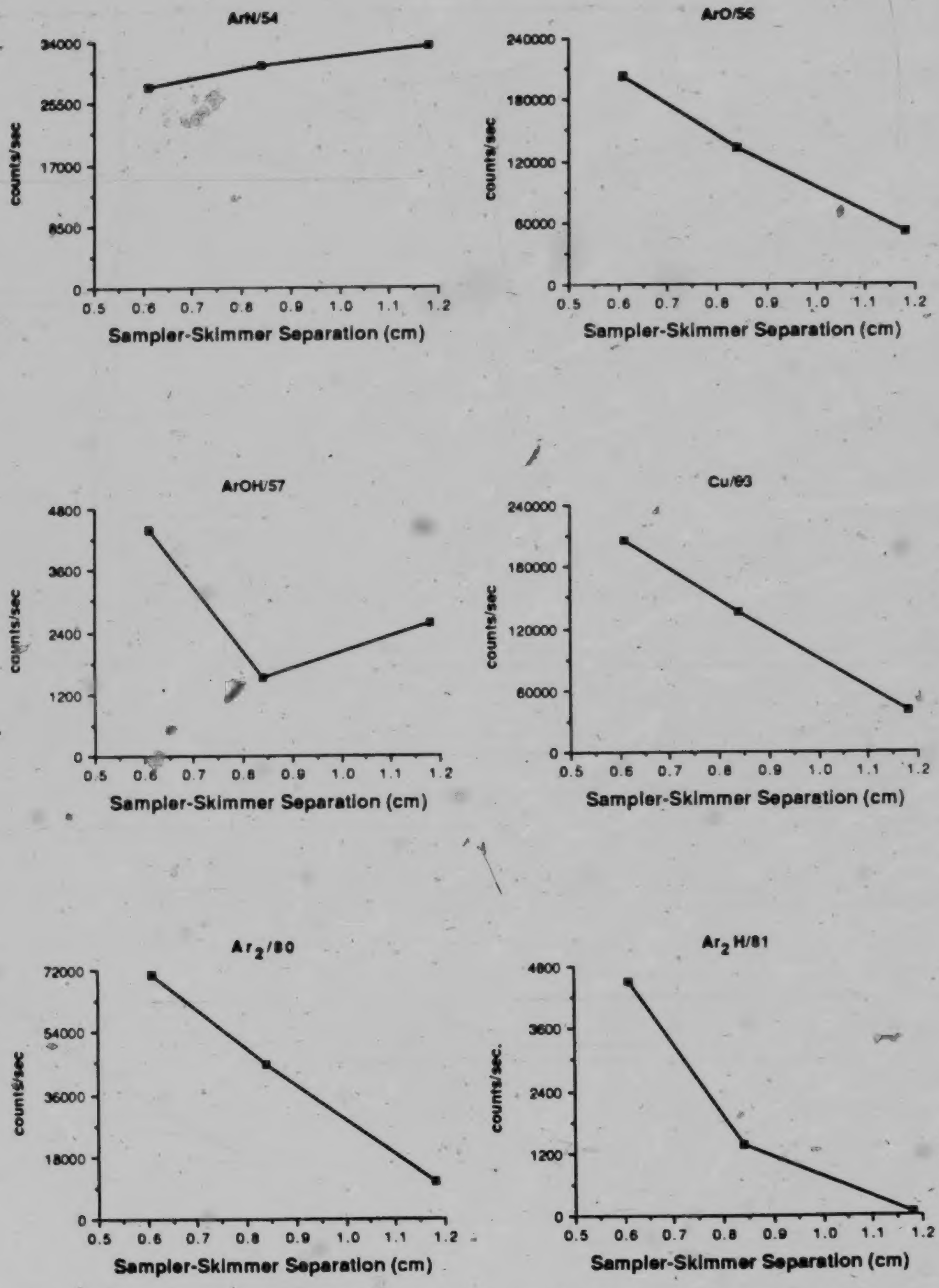

Figure 7-6. Effect of sampler-skimmer separations on peak background ion signals in a 100% argon plasma.

Table 7-3. The normalized signal ratio for ion species at sampler-skimmer separations using 0.23 cm and 0.57 cm spacers. The signals were acquired each at its optimum nebuliser flow rate.

Ionic Species	Normalized Signal (spacer/no spacer)	
	0.23 cm spacer	0.57 cm spacer
ArN	1.1	1.2
ArO	0.65	0.25
ArOH	0.35	0.58
Ar_2	0.63	0.15
Ar_2H	0.30	—
Cu	0.66	0.20

occurring in the 1 torr region. In ICP-MS, it has been observed that the level of hydroxyl ions is high when aqueous solutions are used during analysis. Argon is also expected to be a major species inside the interface region. Thus, this creates a favourable condition for generating collisional products in this region if the beam is not completely "frozen". Therefore, the overall signal response for ArOH might be understood as the contribution of three competing and interacting processes. Assume that normally hydroxyl ions are simply mainly generated in the ICP source while a small fraction are produced at the boundary layer surrounding the orifice. With the insertion of the 0.23 cm spacer, the hydroxyl species generated at the boundary layer are preferentially eliminated from the sampling beam and the secondary product generated from within the extended interface (through reactive collision) is responsible for the signal increase using the 0.57 cm spacer. In contrast, ArN was least affected by the change in spacer arrangement. The exact mechanism for this is not clear at this time. However, there is little doubt that the majority of this species is not generated deep in the ICP. Rather, they are the product of reaction with nitrogen due to air entrainment in the plasma and are thus generated on the outer edges of the plasma discharge.

From the data presented in Chapter 5, it was observed that the use of a 5% nitrogen cooled mixed gas plasma resulted in a significant reduction for some of the background species. For the oxygen and hydrogen containing ions, the application of a nitrogen mixed gas was particularly successful because those species were lowered by an order of magnitude or more. The function of nitrogen in the discharge was thought to be equivalent to a scavenger competing for the available oxygen/hydrogen species. Therefore, the effect of sampler-skimmer separations on background species using the nitrogen mixed gas plasma is expected to be different than that with the argon discharge.

The plasma parameters used in this study were identical to those described above. The signal profiles for the species are illustrated in Figure 7-7*. From the data, the most distinct difference between this set of results and those obtained using a 100% argon plasma (Figure 7-5) was that the insertion of the 0.23 cm spacer gave increased signal levels. This trend was unexpected. The above results suggested that with the introduction of nitrogen into the plasma, the normal sampler-skimmer distance becomes sub-optimal.

The situation could be thought of as due to shock wave scattering downstream from the skimmer. With the introduction of nitrogen into the discharge, the plasma volume contracts rather significantly. As a result, the mass flow rate of materials introduced through the interface is expected to decrease. Therefore, the background pressure in the sampler-skimmer region is lowered. This might cause the formation of a shock wave inside the skimmer. The insertion of a 0.23 cm spacer moves the sampling position of the skimmer further away, thus minimizing shock formation inside the mass spectrometer. However, this effect was not observed with the argon plasma because of higher particle through-put into the interface. This gives rise to a higher background pressure and subsequently a smaller size shock barrel.

Due to the lack of experimental data, the above speculation cannot be assessed independently. In any case, the observed trend was reproducible. However, if one accepts the validity of the above argument, then the observed result (using a 0.23 cm spacer) could only indicate the outcome of skimmer interference or shock formation inside the mass spectrometer, rather than the intended formation mechanism study of the background species.

---

* Because of their low signal intensities, ion counts for ArO and Ar_2H were photon background subtracted.

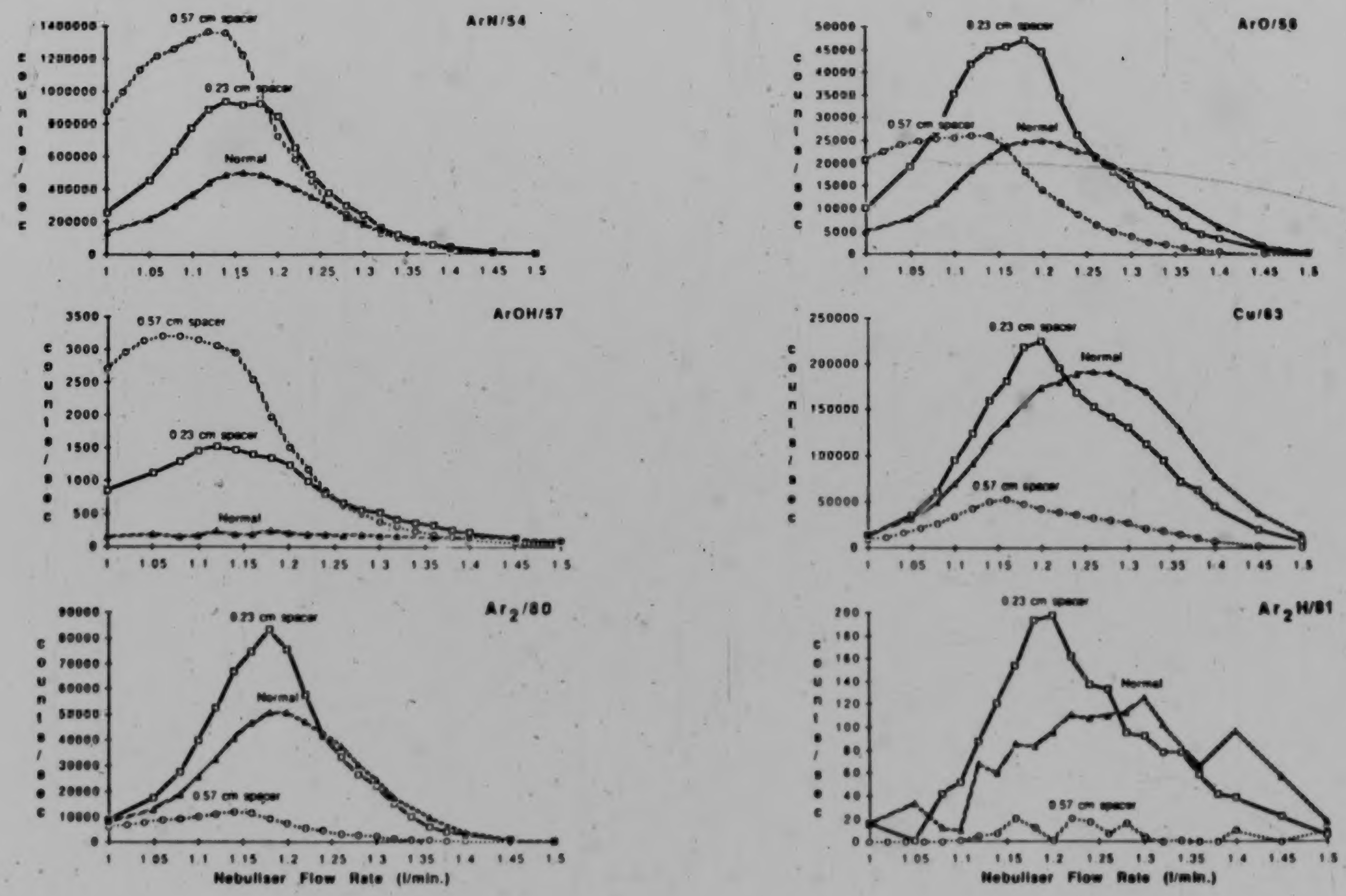

Figure 7-7. The effect of sampler-skimmer separations on $^{40}ArN^+$, $^{40}ArO^+$, $^{40}ArOH^+$, $^{63}Cu^+$, $^{40}Ar_2^+$ and $^{40}Ar_2H^+$ species in a 5% nitrogen cooled plasma.

The effect of spacers on background species in a 5% nitrogen mixed gas plasma is demonstrated by illustrating the optimum signal counts for each species at each of the sampler-skimmer location, the results are presented in Figure 7-8. These sets of data were further normalized with the ion signal obtained without the spacer and tabulated in Table 7-4. As expected, this group of data is very different from that obtained with the pure argon discharge.

Since the trend obtained between normal and the 0.23 cm spacer is predominated by the effect of shock formation inside the mass spectrometer, information regarding species formation mechanisms in ICP-MS is more relevant from data obtained using the 0.57 cm spacer. From the data shown in Figure 7-8, it is interesting to note that ArO, Ar_2 and Ar_2H behave very much like Cu ion (an analyte) while the spacer effect on ArOH and ArN remained different from the rest of the ion species. In fact, the relative degree of interaction of ArOH and ArN to sampler-skimmer separation is similar. For ArN ions, they are generated either at the outer edge of the plasma discharge or inside the interface region (reactive collision). Since ArOH is generated deep in the ICP (with pure argon), then the different trend observed using a 5% nitrogen plasma is a result of ArOH species generated from different sources. In a mixed gas plasma ArOH species, generated inside the discharge, are destroyed by nitrogen. Thus, the additional amount must have been produced at the outer edge of the plasma (by mixing with air) or by reactive collisions occurring inside the interface region. The effect of sampler-skimmer separations on ArO is quite similar to analyte. Yet, the developed trend is rather unique. It is because the ArO ions generated deep in the plasma, despite that they are largely destroyed by the nitrogen mixed gas, are still present in a significant numbers. Thus, the net contribution from other sources (outer edge of the plasma and inside the interface), although more significant (compared to pure argon plasma), is still less prominent than the original amount.

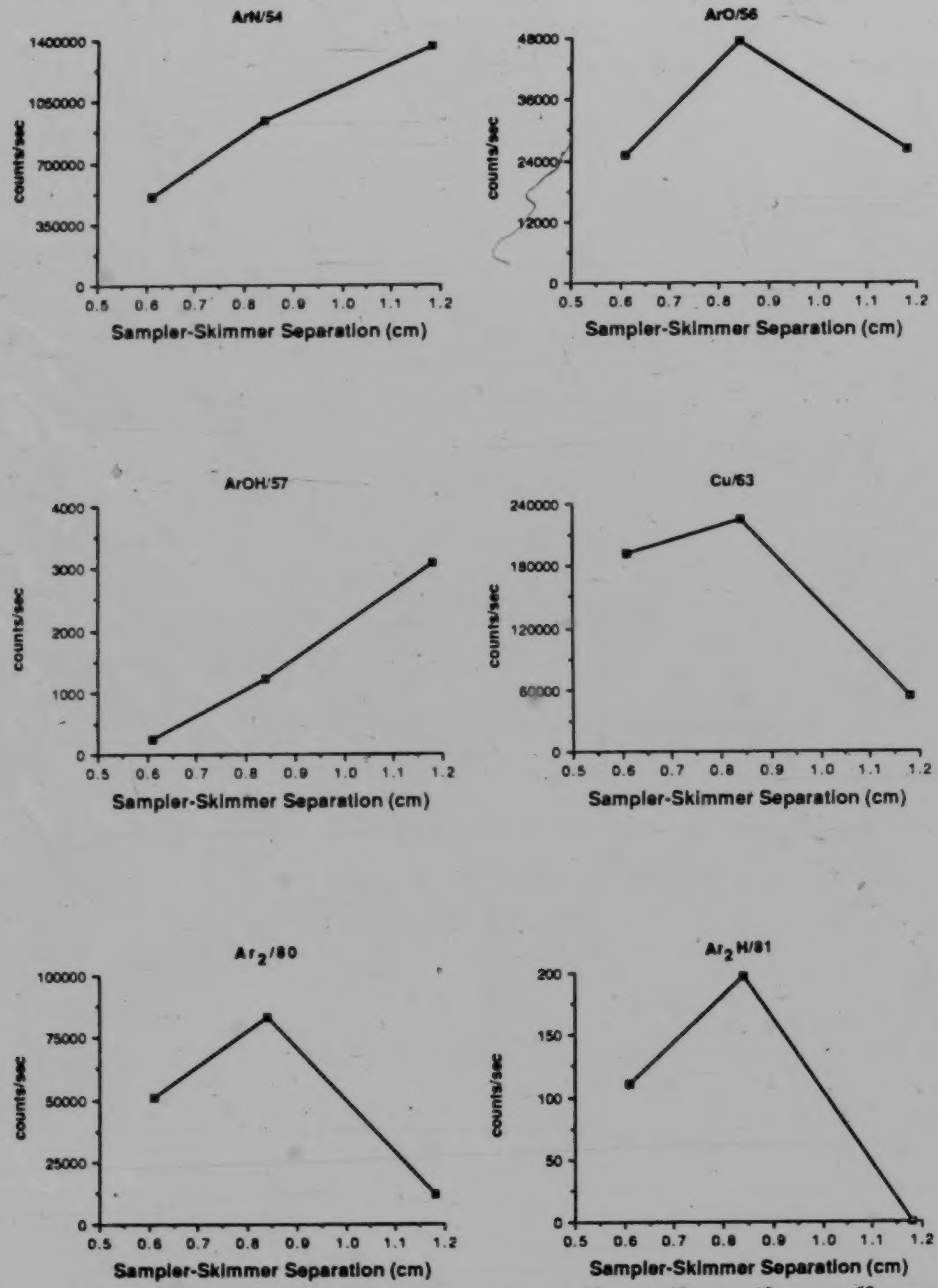

Figure 7-8. Effect of sampler-skimmer separations on peak $^{40}ArN^+$, $^{40}ArO^+$, $^{40}ArOH^+$, $^{63}Cu^+$, $^{40}Ar_2^+$ and $^{40}Ar_2H^+$ ion signals in a 5% nitrogen cooled plasma.

Table 7-4. The normalized signal ratio for ion species at sampler-skimmer separations using 0.23 cm and 0.57 cm spacers. The signals were acquired each at its optimum nebuliser flow rate.

Ionic Species	Normalized Signal (spacer/no spacer)	
	0.23 cm spacer	0.57 cm spacer
ArN	1.86	2.70
ArO	1.88	1.04
ArOH	4.96	13.0
Ar_2	1.64	0.23
Ar_2H	1.78	—
Cu	1.17	0.28

c. Behaviour of Analyte Induced Argon Background Species

In the study of background species in ICP-MS in Chapter 5, it had been concluded that some of the analyte induced background species (Ar-X) cause severe mass spectral interferences for some analyte ions. Since the response of their signals to plasma parameters is similar to normal analyte ions, a simple readjustment of plasma conditions cannot be used to remove the interference from such species. In addition, the use of a nitrogen cooled mixed gas plasma met with only limited success in removing these species. In order to tackle the root of this problem, a better understanding of their formation mechanism is necessary. It has been generally speculated that Ar-X species are an end product of collisions between analyte ions and argon species inside the interface zone. If this perception is correct, then increasing the spacing between the sampler and the skimmer should increase their population density if the molecular beam is not completely "frozen".

The plasma parameters for this study were identical to those in the previous section. In this study, a solution containing a concentration of 1000 ppm sodium in 2% nitric acid was used. The species of interest was Ar-Na with a molecular mass of 63. The signal acquisition was done in the usual way and the data was acquired with the normal configuration and with the 0.23 cm and 0.57 cm spacers. The sampling distance was maintained at 10 mm and the rf power was at 1.50 kW throughout.

The results are presented in Figure 7-9. The signal for Ar-Na increases substantially as the interface spacing is increased. The results can be better illustrated with the optimum ion signals obtained in each condition normalized with respect to the ion counts obtained without the spacer. The final results are plotted as a function of sampler-skimmer separation in Figure 7-10. The data illustrated in the figure reinforce earlier speculation regarding the formation mechanism for Ar-X. The increase in population density for Ar-Na

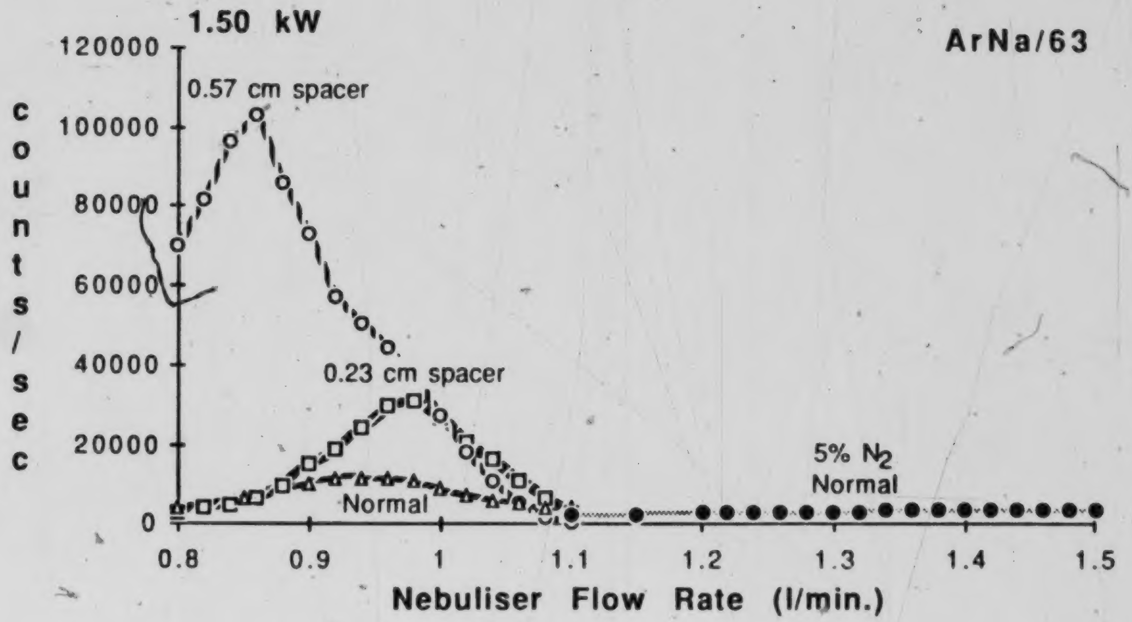

Figure 7-9. Ion signal dependence for Ar-Na on nebuliser flow rate in a 5% nitrogen cooled plasma and its responses to spacer inserts in a pure argon plasma.

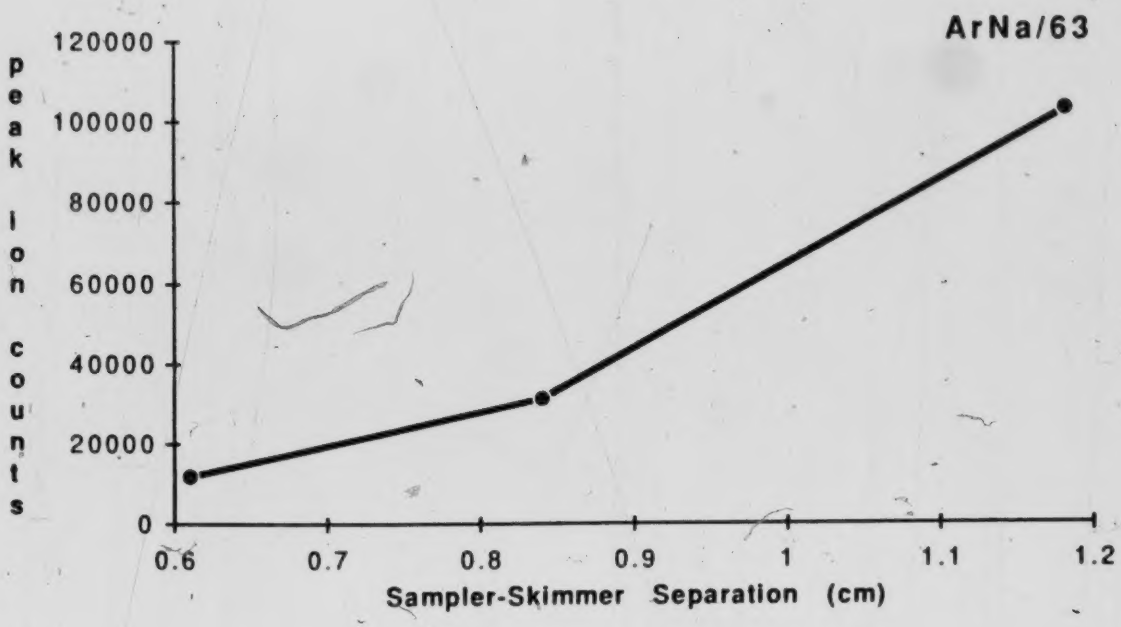

Figure 7-10. Effect of sampler-skimmer separations on peak Ar-Na signals in a pure argon plasma.

at higher sampler-skimmer separation is probably due to the longer residence time for the analyte species inside the interface giving rise to an increased yield of collision products.

E. Effect of Sampler-Skimmer Separation on Analyte Matrix Effects

a. Introduction

The effect of sample matrix on analyses using ICP-MS is extremely complicated. Not only has one to deal with the matrix induced spectral overlap problems documented in Chapter 5 but also serious matrix induced sensitivity changes can occur [14]. During the early development of the technique, the severity of the problems caused by high analyte concentration was not recognized as high analyte concentration would lead to the clogging of the sampling orifice . This was a direct consequence of the use of relatively small sampling orifices (typically < 50 µm in diameter). This problem was alleviated with the use of a larger aperture sampler. The problems caused by matrix effects began to emerge as more practical applications were carried out. Yet, the overall picture was very confusing as both of the commercial ICP-MS manufacturers claimed to observe only low or insignificant interference effects with analyte matrix concentrations at up to 1000 ppm [11, 15-16]. For a more comprehensive review regarding signal suppression matrix effects the article by Tan and Horlick [14] should be consulted.

Recently, most researchers [14, 17-18] have reported that the degree of signal suppression (matrix effect) was related to the mass of the matrix element and they attributed this effect, in part, to Mach number focussing [10] as well as pressure diffusion in the molecular beam at the interface region, caused by lighter molecules diffusing from the centre line of the expanding jet much faster than heavier ones. As a result, the heavier species are concentrated along the central axis. Since the ICP is only about 1% ionized, quantitative comparison to the situation of a molecular beam is valid. Thus, if the above is the main reason for the signal decrease observed using ICP-MS, then the effect of increasing sampler-skimmer separation on matrix effects could clarify the mechanism.

b. Experimental Conditions

The effects of 1000 ppm sodium and uranium on 0.2 ppm of manganese, argon oxide (ArO) and the argon dimer (Ar_2) ions was studied with the use of the 0.23 cm and 0.57 cm spacers. The plasma parameters were the same as before with the rf power at 1.50 kW and a sampling depth at 10 mm through out.

c. Results and Discussion

The effect of matrix elements on ion species was quantified by comparing the optimum ion signal for each of the species without the matrixes to the appropriate signal obtained with the matrix solution at the same nebuliser gas flow rate. The results are presented graphically in Figures 7-11 to 7-13. In each figure, the upper frame consists of the normalized optimal ion signals (without matrix) as a function of sampler-skimmer separations and the middle frame shows the degree of matrix effect caused by uranium while the lower frame illustrates similar data for sodium. In common with all three figures, the ion signal corresponding to each individual species decreased with increasing sampler-skimmer separation while the relative suppression effect caused by the sodium or uranium matrixes decreased with distance. In particular, the lessening of the matrix effect especially at the highest separation distance was more dramatic for uranium than for sodium. Yet, the overall degree of signal suppression was less for sodium than uranium despite the greater molar equivalent concentration of sodium that was introduced. These trends are consistent with the observations of other workers [14, 17]. However, the so called pressure diffusion and Mach number focussing phenomena did not seem to play a major role as the reverse trend would have been observed with the incorporation of the spacers.

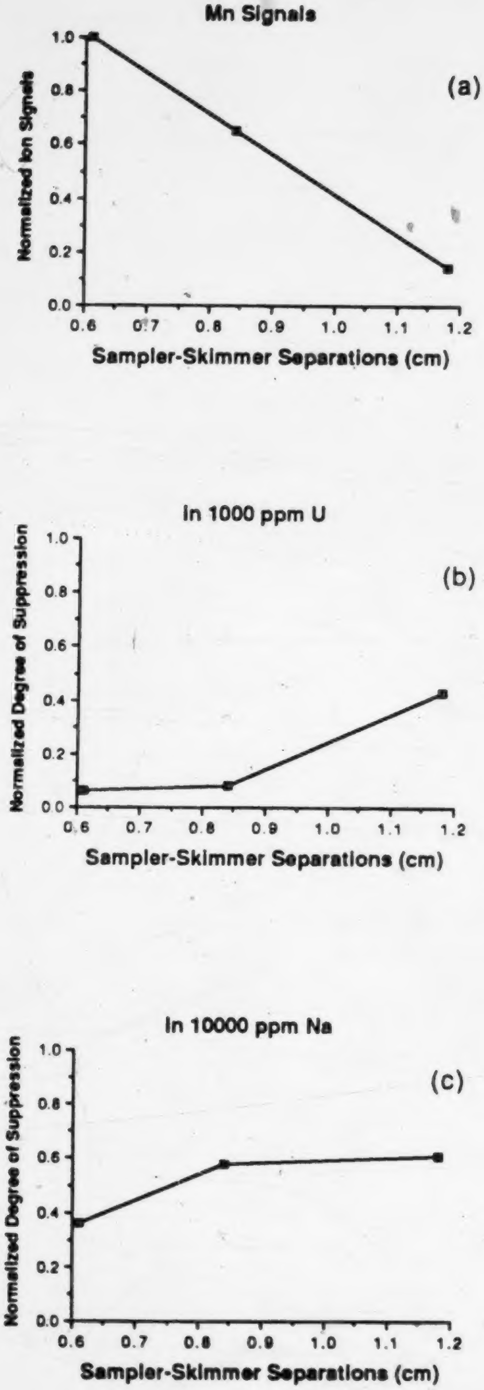

Figure 7-11 a) Effect of sampler-skimmer separations on normalized peak Mn ion signals. b) Degree of signal suppression by 1000 ppm U on peak Mn signal as a function of sampler-skimmer separations. c) Degree of signal suppression by 1000 ppm Na on peak Mn ion signal as a function of sampler-skimmer separations.

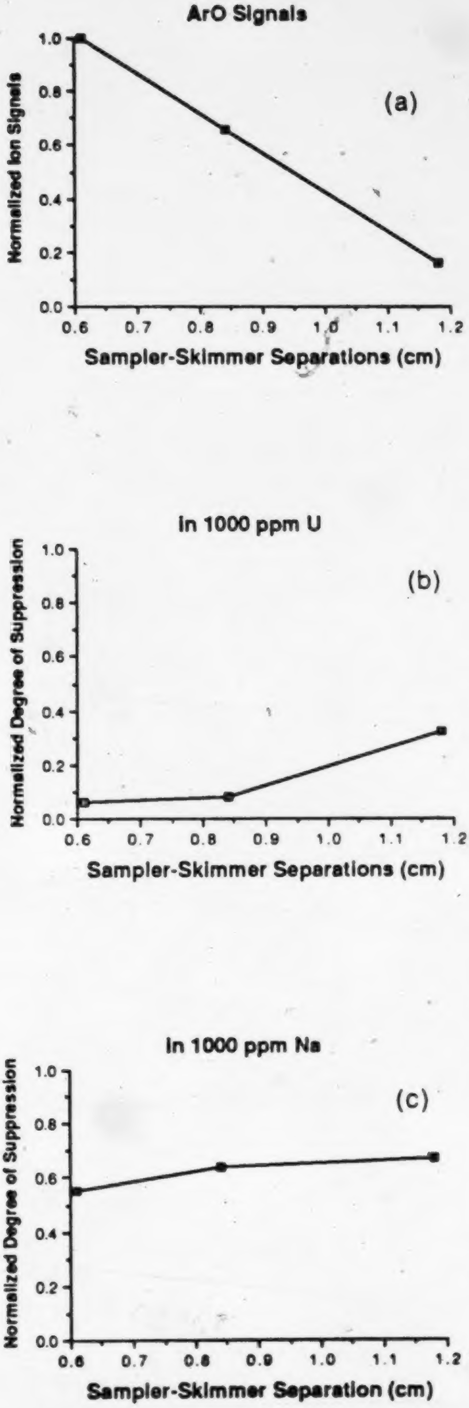

Figure 7-12. a) Effect of sampler-skimmer separations on normalized peak ArO ion signals. b) Degree of signal suppression by 1000 ppm U on peak ArO ion signal as a function of sampler-skimmer separations. c) Degree of signal suppression by 1000 ppm Na on ArO ion signal as a function of sampler-skimmer separations.

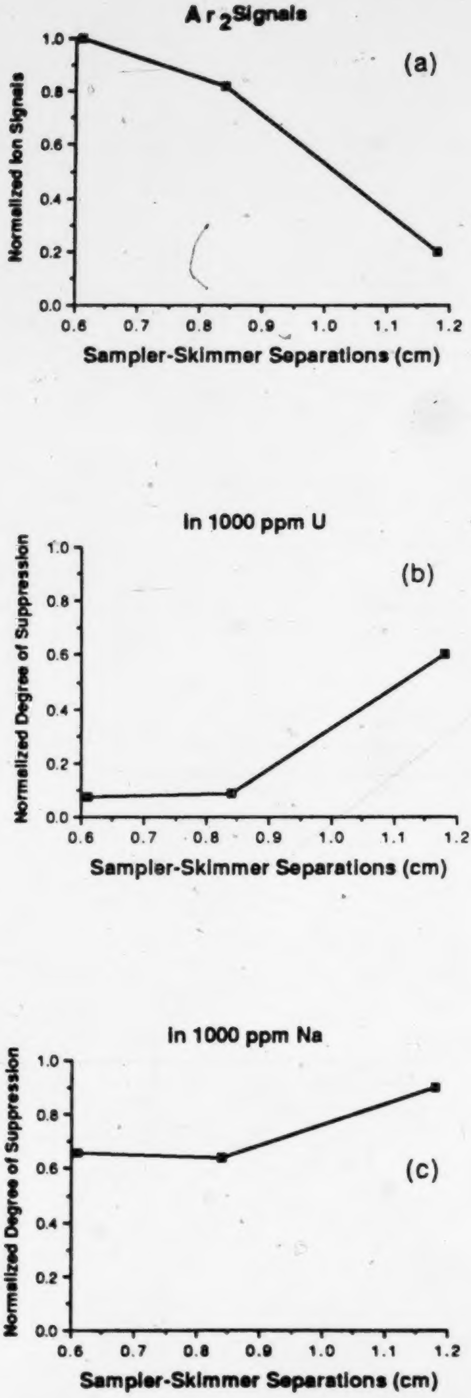

Figure 7-13. a) Effect of sampler-skimmer separations on normalized peak Ar_2 ion signals. b) Degree of signal suppression by 1000 ppm U on peak Ar_2 ion signal as a function of sampler-skimmer separations. c) Degree of signal suppression by 1000 ppm Na on peak Ar_2 ion signal as a function of sampler-skimmer separations.

From the data, the fraction of matrix suppression appears to be inversely related to the level of ion signal transmitted through the skimmer or rather, the amount of material extracted through into the mass spectrometer. This observation, in a way, is similar to the conclusion reached previously by the other researchers [14] that the signal suppression caused by the matrixes could be reduced by dilution of the sample. This suggests that the main cause of the signal suppression by the matrix element originates in the mass spectrometer rather than from the plasma discharge or at the interface region. In addition, this type of signal suppression was not caused by detector fatigue as the SCIEX Elan system was employed in the "peak-hopping" mode. Rather, it is more likely that the increase in the amount of ions extracted through into the mass spectrometer cause an elevation of charge density of the molecular beam through the electrostatic lenses and cause a so called "space-charge defocussing" effect on the lighter component of the ion beam [19]. This, in a way, is similar to a Mach-number focussing effect as the heavier components are concentrated along the flow axis.

Although the above interpretation is speculative, the physical evidence does point toward the mass spectrometer end of the system as the major cause of the observed matrix interference. This speculation also agrees with the observations by Douglas [20]. In his presentation, he also suggested that matrix effects could be minimized by rearrangement of the electrostatic lenses.

F. Conclusions

The preliminary observations on the effect of sampler-skimmer separation appear to be promising from the stand-point of helping to understand the ion behaviour in ICP-MS. Those observations have indicated that analyte oxide percentage can be lowered by fine tuning the sampling distance of the skimmer cone. Although the offered explanations for the above observations are speculative, it is suggested that the oxide species in ICP-MS originate as undissociated molecular species from the discharge. On the other hand, part of the oxide might also be a product of ion molecule interactions via the boundary layer at the edge of the sampler orifice. Further, the results obtained with the nitrogen mixed gas plasma also suggest that the interface region is not entirely inert. Initial results on the effect of sampler-skimmer separation on analyte intensity indicate a higher speciation dependency (i.e. amount of signal decrease is dependent on some analyte properties) as compared to the argon plasma.

In addition, the use of a spacer helps to lower the intense photon background detected, especially when operating in conjunction with a nitrogen mixed gas plasma. This situation can be best demonstrated by the data shown in Figures 7-14 and 7-15 where spectra for a 1 ppm Ce solution in 2% nitric acid were acquired with a 5% nitrogen cooled mixed gas plasma. The spectrum in Figure 7-14 was obtained with the interface set-up in the normal way while the spectrum in Figure 7-15 was acquired with the insertion of a 0.23 cm spacer. In both cases, spectra were obtained at the optimum nebuliser gas flow rate for the analyte ion signal. In both set of figures, the ion intensities were scaled expanded by 10× and 100× in the middle and bottom frames in order to provide a more detailed comparison. It is interesting to point out that while the CeO ion intensity was lowered with the insertion of the spacer, the background continuum signal (bottom frame in both figures) has been reduced rather significantly after the addition of the spacer (background signal dropped from about 1100 counts/sec to 200 counts/sec) without any significant effect on the analyte signal intensity.

Finally, the effect of sampler-skimmer separation on background species is complex. For an argon plasma, depending on the nature of the species, improvement or deterioration of background signals was observed after the addition of spacers. There did not seem to be unique trend for all the species studied and more work is necessary to establish a compromise skimmer position. On the other hand, the insertion of a 0.23 cm spacer

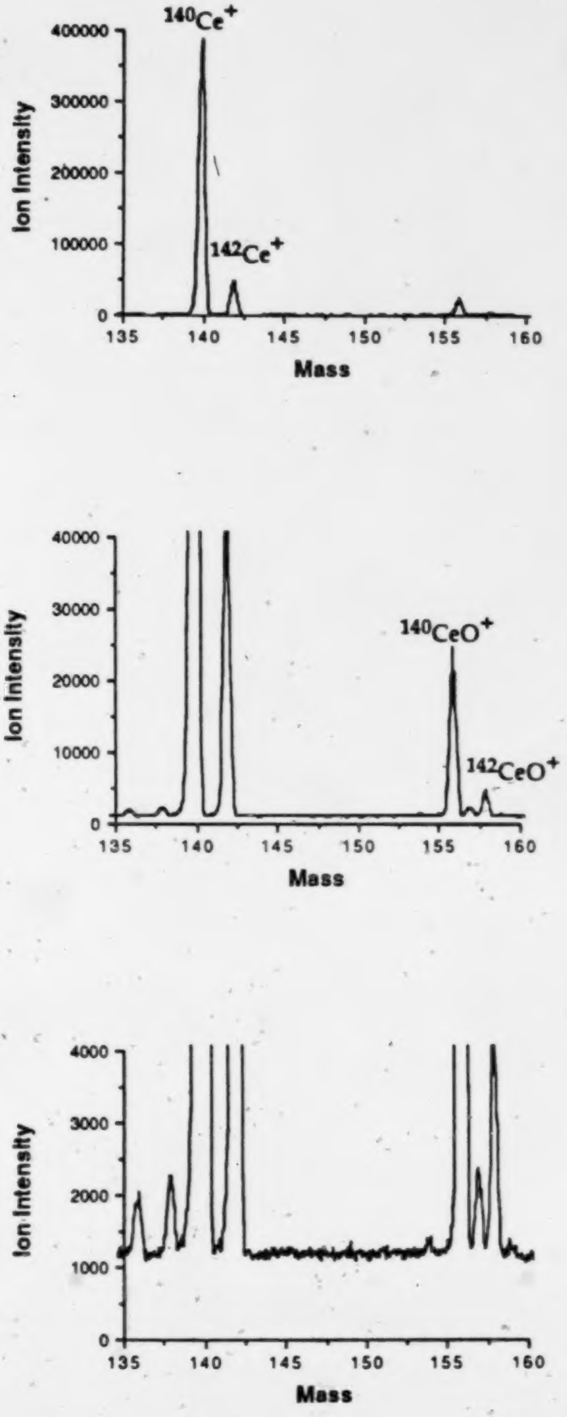

Figure 7-14. Mass spectrum of Ce obtained using a 5% nitrogen cooled plasma.

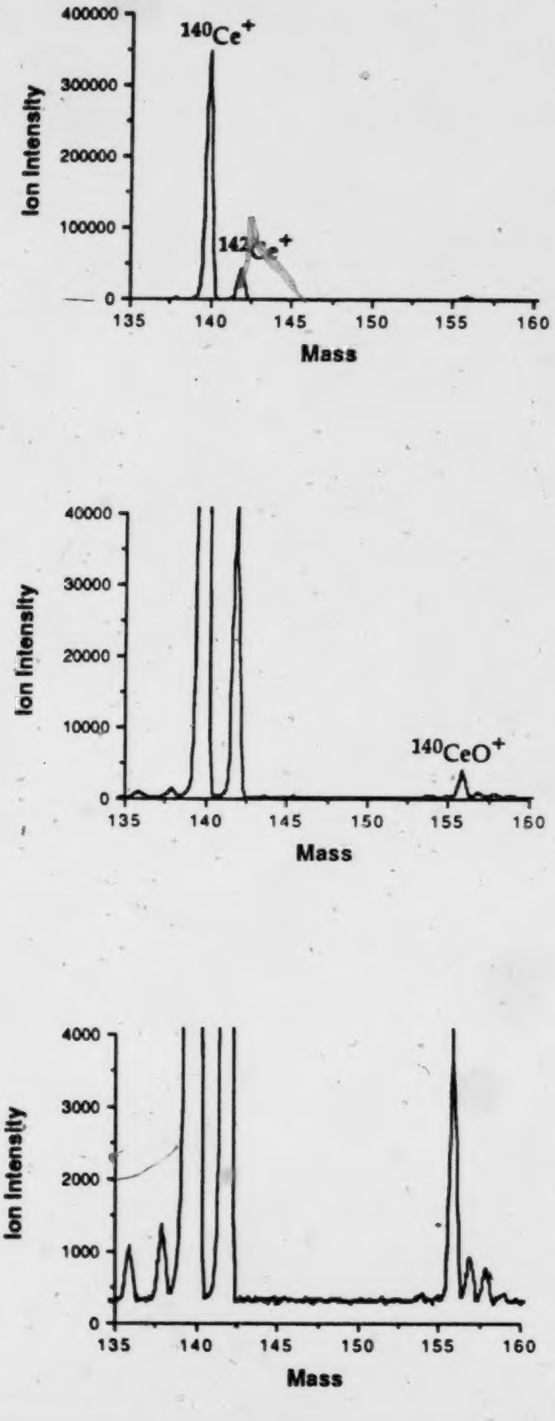

Figure 7-15. Mass spectrum of Ce obtained using a 5% nitrogen cooled plasma with a 0.23 cm spacer insert.

seemed to enhance the population level for all of the background species and for analyte as well when a 5% nitrogen cooled plasma was used. This tended to suggest that the size of the shock barrel might have been altered as a result of the mixed gas plasma. This was probably due to a change in the background pressure in the interface region.

The change in degree of ion signal suppression by the matrix element as a result of increasing sampler-skimmer separating distance also indicated that the major cause of signal suppression by the matrix elements originates from within the mass spectrometer (probably at the electrostatic lenses). However, this did not suggest that the interface would be immune to matrix interference, rather it only indicates that the more efficient approach to tackling the problem of matrix interference would be towards the modification of ion flow inside the mass spectrometer. Based on this speculation, more effort should be spent toward the mass spectrometer end of the instrument in order to better appreciate the problem of matrix effects.

REFERENCES

1. R. S. Houk, V. A. Fassel, G. D. Flesch, H. J. Svec, A. L. Gray and C. E. Taylor, Anal. Chem., 52, 2283 (1980).
2. D. J. Douglas and J. B. French, Anal. Chem., 53, 37 (1981).
3. R. Pertel, Int. J. Mass Spectrom. and Ion Phys., 16, 39 (1975).
4. H. Ashkenas and F. S. Sherman, Rarefied Gas Dynamics, Fourth Symposium, Academic Press Inc., New York, vol. 2, 84 (1966).
5. J. B. Anderson, Am. Instit. Aeron. Astron. J., 10, 112 (1972).
6. José A. Olivares and R. S. Houk, Anal. Chem., 57, 2674 (1985).
7. J. B. Anderson, Molecular Beams and Low Density Gasdynamics, Gasdynamics, vol. 4, Ed. P. P. Wegener, Marcel Dekker, Inc. New York (1974), Chapter 1.
8. D. J. Douglas and J. B. French, 1988 Winter Conference on Plasma Spectrochemistry, San Diego, (1988). Paper no. F1.
9. F. E. Lichte, A. L. Meier and J. G. Crock, Anal. Chem., 59, 1150 (1987).
10. S. Yamazaki, M. Taki and Y. Fujitani, Jap. J. Appl. Phys., 18, 2191 (1979).
11. A. L. Gray and A. R. Date, Analyst, 108, 1033 (1983).
12. H. Helm, T. D. Märk and W. Lindinger, Pure Appl. Chem., 52, 1739 (1980).
13. A. R. Date and A. L. Gray, Spectrochim. Acta, 38B, 29 (1983).
14. S. H. Tan and G. Horlick, J. Anal. At. Spectrom., 2, 745 (1987).
15. D. J. Douglas, E. S. K. Quan and R. G. Smith, Spectrochim. Acta, 38B, 39 (1983).
16. A. R. Date and A. L. Gray, Analyst, 108, 159 (1983).
17. H. Kawaguchi, T. Tanaka, T. Nakamura, M. Morishita and A. Mizuiki, Anal. Sci., 3, 305 (1987).
18. R. S. Houk, XXV Colloquium Spectroscopicum Internationale, Toronto, Canada (1987). Paper no. E 1.1.

19. G. R. Gillson, D. J. Douglas, J. E. Fulford, K. W. Halligan and S. D. Tanner, 1988 Winter Conference on Plasma Spectrochemistry, San Diego, (1988). Paper no. F2.

20. D. J. Douglas, paper presented at ICP-MS Symposium, Muskoka Sands, Canada (1987).

Chapter 8

Conclusion and Further Work

Despite the rapid development of ICP-MS as an analytical tool for trace element analysis, the technique still has plenty of room for improvement. From the results obtained in this study, a number of improvements relating to the basic characteristics of the technique have been achieved. Most importantly, the analytical advantages obtained from a low percentage mixed gas plasma in ICP-MS is consistent with the results observed previously using ICP-AES. For example, better analyte signal sensitivity can be achieved when a small amount of nitrogen is mixed into the outer gas of the plasma and this improvement correlates well with metal oxide bond energy for some refractory elements. Further more, the use of a low percentage nitrogen mixed gas plasma also helps in the dissociation of some primary background species.

Future work necessary to improve on the performance of the technique includes:-

a) Sample Delivery System

In Chapter 4, it was observed that the role of the aqueous aerosol delivery system (solvent load and aerosol particle size) determined, to a certain extent, the degree of analyte ionization, oxide levels and background features. Experimental data also indicated that the size (diameter) of aerosol particles introduce into the plasma rather than the degree of solvent loading was the more important factor in determining the level of oxide detected. While a lot of attention has been given to the development of the ICP-MS interface, there has been insufficient progress towards developing sample delivery systems specifically for ICP-MS. Recently, water-cooled spray chambers have been used in order to reduce the solvent loading factor. Yet, based on the results presented in this thesis, the use of a water-cooled spray chamber should have little effect. In contrast, the implementation of an ultrasonic nebuliser for sample delivery would produce much finer aerosol droplets. Using a home-built device, preliminary results confirm that a lower level of metal oxide ion can indeed be achieved and warrents further investigation.

In the past few years, thermal spray sample introduction devices have been coupled to ICPs. In some cases, detection limits were improved by more than an order of magnitude [1]. Since the performance of ICP-MS is more susceptible to solvent loading, the coupling of a thermal spray device to ICP-MS could even be more efficient in improving analyte sensitivity than for ICP-AES. In addition, it is better able to transfer heat to the aerosol stream, thus enabling it to generate finer and more uniform aerosol particles. Also in Chapter 4, it was explained that a "Liebig" type water condenser was important for the effective removal of solvent. This condenser, perhaps also cascaded with a liquid nitrogen cold trap, should produce near anhydrous aerosol particles. With such a system, improvements in analyte signal sensitivity and a much lower level of oxide and background interferences are to be expected.

b) Non-Spectroscopic Interelement Interference

The loss of signal sensitivity caused by non-spectroscopic interelement interference (matrix effect) is more severe for ICP-MS than for ICP-AES under comparable analytical conditions. This effect is thought to be a result of ion trajectory modifications cause by a high concentration matrix element [2]. In other words, it appears to be a problem of ion focussing originating from charge repulsion due to a high ion beam density population as a result of the presence of the matrix element. If this is true, then further modification of the ion optics such as the geometry and the electrostatic potential to the ion lenses may be necessary to minimize this type of interference effect.

In a related situation, when a high concentration of a sample matrix (usually about 0.1%) is introduced into the plasma, clogging of the sampler orifice as well as condensation of analyte salt on the surface of the sampling cone (giving rise to long term memory effects and sample contamination) is a problem. Blockage of the sampling orifice has been partially eleviated by increasing the size of the aperture. However, salt built-up on the surface of the sampler can only be removed by cleaning. This reduces sample throughput as the system has to be shut down on a regular basis in order to clean the sampler. Mechanical design of a system similar in principle to nebuliser "tip-wash" system in commercial ICP-AES instrumentations could be engineered to alleviate this problem.

c) Interface Design

Despite repeated assurances from Douglas and French that the interface is not a region rich in ion-molecule chemistry [3], the results observed in Chapter 7 indicate that the relative populations of analyte and background species depend on characteristics of this region. While there is little doubt that the basic design of the interface is adequate for normal ion sampling, fine adjustment of the sampler-skimmer separation is necessary to enhance the performance of the system. Further, it was observed that the oxide percentage can be lowered by adjusting the sampler-skimmer separation without sacrificing the ion signal sensitivity. Also, by applying a small potential to the skimmer, this may lower the oxide level and some spectral background interferences (i.e. analyte-argides). In a different study using a home-built instrument, Kawaguchi and coworkers [4] inserted an extra cone in front of the electrostatic lenses (just behind the skimmer) and they reported an enhancement of signal sensitivity as well as a lowering of interelement interference effects. Gillson et al. [2] also pointed out that the defocussing effect of ions caused an excessive lost of charge particles to the skimmer wall and the ion trajectory may be refocussed by applying a potential at the skimmer.

d) Improvement of the Plasma Source

While a lot of effort has been spent toward the configuration of the interface design between the ICP and the MS, not a great deal of attention has been given to the analyte ionization source (the plasma). This is partly due to the success of the ICP for optical emission and also the plasma source has been well studied. However, when ICP is coupled to an optical spectrometer, the interaction between the source and the spectrometer can be considered as remote and passive. Such is clearly not the case when it is coupled to a mass spectrometer interface. The typical analyte sensitivity obtained in ICP-MS is in the order of 10^6 counts/ppm. While this number seems quite impressive. For a given analyte solution, the average number of species per ppm should be in the order of 10^{10}. Therefore, there could be a sensitivity improvement of about 4 orders of magnitude for each analyte still possible in plasma-MS. In a recent study by Caruso and coworkers [5], they indicated that a micro-wave induced plasma-mass spectrometry (MIP-MS) provides a typical analyte sensitivity of $\sim 10^8$ counts/ppm. Their results suggest that a MIP may be a better source to couple to a MS than an ICP source and/or there is an excessive lost of analyte ion between the ICP and the MS. In a recent article by Gillson et al. [2], they also indicated that there was a lost of over 99% of the Ar^+ ion through the skimmer. The reason for this behaviour is not understood at this time but it is obvious that the interface region of the ICP-MS is very complicated indeed.

In the regime of aerosol introduction into the plasma discharge, it is necessary to contain the aerosol stream along the central axis of the plasma as this makes optical focussing and signal detection more sensitive when an optical spectrometer is used. However, in ICP-MS, ions are transmitted through the interface into the mass spectrometer and only a fraction of the plasma is sampled through into the interface. Therefore, the design of the plasma torch should be reconfigured in order to maximize the "analyte-plasma-interface" interaction. Adaptation of a mini-torch to ICP-MS seems reasonable. Also, it might not be necessary to contain the aerosol in the central channel of the plasma discharge as the plasma and thus the ions are physically extracted into the mass spectrometer. Rather, aerosol could be introduced into the the plasma via the flow stream of the plasma gas or the auxiliary gas. This should provide a longer resident time for the aerosol inside the plasma without affecting the condition inside the interface and thus allowing better analyte-plasma interaction. The ionized species will then be carried to the tip of the plasma and traverse through to the mass spectrometer.

In conclusion, some of the suggestions above may appear to be complex if not totally impractical, but they are problem areas worth getting into in order that the real potential of the technique can be fully utilized.

REFERENCES

1. K. Vermeiren, R. Dams and R. Gent, 1988 Winter Conference on Plasma Spectrochemistry, San Diego, (1988). Paper no. M10.
2. G. R. Gillson, D. J. Douglas, J. E. Fulford, K. W. Halligan and S. D. Tanner, 1988 Winter Conference on Plasma Spectrochemistry, San Diego, (1988). Paper no. F2.
3. D. J. Douglas and J. B. French, 1988 Winter Conference on Plasma Spectrochemistry, San Diego, (1988). Paper no. F1.
4. H. Kawaguchi, T. Tanaka, T. Nakarmura and M. Morishita, Analytical Sciences, 3, 305 (1987).
5. P. G. Brown, T. M. Davidson and J. A. Caruso, 1988 Winter Conference on Plasma Spectrochemistry, San Diego, (1988). Paper no. F8.